

**Evaluation of Single-Use Bioreactors for Rapid Development of Industrial
Fermentation Processes**

Submitted by

James David Rutley

to University College London

as a thesis for the degree of Doctor of Engineering in Biochemical Engineering

in April 2019

Declaration

I, James David Rutley, confirm that the work presented in this thesis is my own. Where information has been derived from other sources, I confirm that this has been indicated in the thesis.

Signed:

Acknowledgements

I would like to express my deepest thanks to the people who have helped me on this journey. Without them it would most likely never have come to fruition.

To Professor Gary Lye, you have been a source of wisdom and advice at the times when I have needed it most. Not only during this doctoral program, but as my tutor during my entire academic career. You have provided me with guidance and assistance for over a decade and that is something for which I will be eternally grateful. More broadly to UCL and to the Department of Biochemical Engineering, which has been my academic home since my very first day at university and has helped me to develop into the person with the enthusiasm and belief in this field that I am.

To my family, your faith in me has kept me going when I would otherwise not have felt capable. I hope I have done you proud.

To Synthace, first my sponsor, but for over four years now my employer. You have shown great trust in me and my potential and I am grateful to be part of what you are doing. A special mention must go to Craig & Markus Gershater, who have aided in ensuring that I get to this stage.

To the countless other people, of which there are too many to mention, who have helped me in some way to reach this point, without doubt my greatest achievement to date.

I would also like to thank the EPSRC for funding this research.

Abstract

Microbial fermentation and whole cell biocatalysis have long been used in an industrial context for the generation of commercially valuable biomolecules. There is significant further potential if they can be made as economically attractive as competing chemical process routes. Improvements in genetic engineering techniques such as those pioneered in the area of synthetic biology, have provided access to novel products including therapeutic proteins and enzymes. In order to capitalise on these advances, there remains a requirement for rapid bioprocess development and scale up. Here, single use bioreactors are of interest due to the advantages over traditional stainless steel technologies. These include reduced need for validation and turnaround times, a reduction in capital expenditure and increased facility flexibility. To date, however, they have not been thoroughly investigated for use with microbial expression systems.

The aim of this thesis is to; (i) evaluate the oxygen transfer capabilities of different single-use bioreactors with a view to determining suitability for microbial fermentation, and (ii) to define appropriate scale-up bases from high throughput microwell to laboratory and pilot scale bioreactors. Initial work focused on the characterisation, optimisation and scale-up of a whole cell P450 monooxygenase bioconversion in *Escherichia coli*. Three rounds of optimisation using a Design of Experiments (DoE) methodology resulted in a 3.3 fold increase in the bioconversion of 7-ethoxycoumarin to 7-hydroxycoumarin. Results from the 96 deep square well (DSW) plates were then scaled-up to a traditional, pilot scale stirred tank bioreactor, increasing titres 25 times over a 3000-fold scale increase. Peak oxygen demands of 25.8 mmolL⁻¹min⁻¹ were shown, with clear differences in oxygen consumption as a result of feeding and bioconversion during fermentation. The inability of microwell systems to support high biomass concentrations and oxidative bioconversion was also demonstrated.

In addition, these studies helped provide fundamental insights into the mechanism for oxygen utilisation during microbial whole cell bioconversions. Prioritisation of oxygen utilisation for biomass accumulation over supplementary cellular activities such as bioconversion was seen in all cases. In some cases, oxygen demand as a result of growth was approximately 4 times greater than other contributions. This had previously been hypothesised in literature but not demonstrated.

In order to better characterise oxygen mass transfer in microwell plate geometries, an improved method for quantification of the volumetric oxygen mass transfer coefficient ($k_{L,a}$) and oxygen uptake rate (OUR), based on the dynamic gassing out method, was subsequently

developed. This method determines oxygen mass transfer parameters (k_{La} and OUR) during a fermentation to provide more representative values for OUR. Models for OUR and k_{La} were built in 24 DSW plates with maximum values of over $600 \text{ mgO}_2\text{L}^{-1}\text{h}^{-1}$ and 103.5 h^{-1} respectively. The established models enable equivalent operating conditions for the different plate geometries to be determined.

The applicability of two commercially available single use bioreactors (the Ambr[®]250 and the XDR-10) for microbial fermentation was evaluated, using a traditional pilot scale STR for comparison. This included building models which consider a number of factors likely to influence oxygen mass transfer simultaneously, as opposed to the empirical correlations which have been developed traditionally. The Ambr[®]250 was demonstrated as having similar oxygen mass transfer capability to the STR across the majority of the experimental ranges, reaching maximum k_{La} values of $> 600 \text{ h}^{-1}$. Analysis of a large number of industrial microbial fermentations (approximately 300) demonstrated that the Ambr[®]250 is capable of supporting microbial fermentation and bioconversion (or recombinant protein expression) in each, where the XDR-10 would not be suitable.

After demonstrating the applicability of the Ambr[®]250 system for industrial microbial fermentation, a modelling tool was developed in the Python programming language capable of evaluating the cost and resource requirements of an Ambr[®]250 bioprocess development run. Preliminary sensitivity analysis highlights labour as the main influence on cost, followed by the replacement of single use bioreactors, each responsible for more than one third of the total run cost.

Overall this work has established original, quantitative insights into oxygen utilisation in microbial expression systems and established engineering criteria for the selection and use of single-use bioreactor technologies for microbial cultivation. The methodologies developed here are considered generic and applicable to other expression systems with high specific oxygen demands such as yeast and heterotrophically cultured microalgae.

Impact Statement

This thesis has focused on the characterisation of small and pilot scale single use bioreactor systems and their application in the culturing of microbial expression systems, particularly those undertaking whole cell oxidative bioconversions. As such, in an attempt to further understanding in industry and academia alike: a whole cell oxidative bioconversion has been optimised and characterised enabling greater understanding of oxygen utilisation; methods have been developed for more accurate quantification of oxygen mass transfer capabilities in single use bioreactor technologies; the applicability of commercially available single use bioreactor technologies to microbial fermentation has been evaluated; and a computational tool for the economic evaluation of the Ambr[®]250 system developed.

Optimisation and scale up of a microbial whole cell oxidative bioconversion from microwells to a pilot scale bioreactor quantified the peak demand for oxygen during culture, offered novel insights into the utilisation of oxygen in microbial expression systems and demonstrated the need for small scale culturing systems with enhanced oxygen mass transfer capabilities.

Methodologies developed for the quantification of oxygen mass transfer coefficients, both in small and pilot scale single use culture systems offer potential improvements to the traditional techniques used. This offers a means of quantifying the oxygen demand of a microbial expression system during culture and therefore a more representative way for academia to understand the responses of an aerobic fermentation to the environment, and for industry to develop culturing technologies to meet the demands of microbial expression systems.

Use of a multifactorial approach has offered novel insights into quantification of oxygen mass transfer in commercially available single use bioreactors. The need for characterisation using DoE methods was highlighted by a number of observations wherein key influences on mass transfer were a result of interactions which would not have been observed using other methods.

Finally, an economic evaluation tool has been developed in the Python programming language for determining the cost and resource demands of bioprocess runs undertaken in the Ambr[®]250 system. This tool has already been implemented in an industrial setting for project costing, and the remit has been expanded to include resource allocation, reporting and project scheduling.

In summary, the research undertaken in this thesis provides novel insight into oxygen mass transfer and the methodologies for its characterisation including where, on the basis of oxygen mass transfer, single use bioreactors can be applied to the highly lucrative field of microbial fermentation.

Contents

Chapter 1: Introduction and Literature Review	(1-47)
1.1. Context of the Research	1
1.2. Literature Review	2
1.2.1. Biocatalysis	2
1.2.2. Cytochrome P450s	8
1.2.3. Oxygen Supply to Oxidoreductive Enzymes	15
1.2.4. Criticality of Oxygen Supply to Microbial Fermentations	17
1.2.5. Oxygen Mass Transfer	18
1.2.6. Factors Influencing Oxygen Mass Transfer	21
1.2.7. Oxygen Mass Transfer in Small Scale and Single Use Systems	26
1.2.8. Common Correlations for Oxygen Mass Transfer	37
1.2.9. Techniques for O ₂ Mass Transfer Quantification	38
1.2.10. Design of Experiments (DoE)	42
1.3. Aims and Objectives	44
Chapter 2: Materials and Methods	(48-76)
2.1. Introduction	48
2.2. Materials	48
2.2.1. Chemicals	48
2.2.2. Microorganisms	48
2.3. Equipment	49
2.3.1. Bioreactors	49
2.3.2. Additional Culture Vessels and Equipment	51
2.4. General Methods	56
2.4.1. Preparation of Fermentation Media	56
2.4.2. Preparation of Cell Banks (Master and Working Stock Generation)	56
2.4.3. Multifactorial Experimental Design Methods	57
2.5. Methods for Optimisation and Scale Up of a Whole Cell Oxidative Bioconversion	58

2.5.1. Screening Investigation (DoE 1)	58
2.5.2. Refinement Investigation (DoE 2)	60
2.5.3. Optimisation Time Course (DoE 3)	62
2.5.4. Scale Up Fermentation	63
2.6. Methods for Developing Accurate Oxygen Mass Transfer Characterisation in High Throughput, 24 Microwell Plates	65
2.6.1. Inoculum Preparation	66
2.6.2. Fermentation in 24DSW PreSens Plates for Establishing the Baseline Model	66
2.6.3. Fermentation in 96 and 24DSW PreSens Plates for Developing an Improved Quantification Method for Oxygen Mass Transfer	66
2.6.4. Determination of OUR and k_{La} from online DOT Profiles	67
2.7. Methods for Characterisation of Oxygen Mass Transfer Coefficients (k_{La}) in Commercially Relevant Single Use Bioreactors (SUBs)	70
2.7.1. New Brunswick BioFlo310	70
2.7.2. Ambr [®] 250	73
2.7.3. XDR-10	73
2.8. Analytical Equipment and Techniques	73
2.8.1. Analytical Equipment	73
2.8.2. Quantification of Biomass Concentration	74
2.8.3. Quantification of Bioconversion Substrate and Product Concentrations	75
2.8.4. Quantification of Free Glycerol Concentration	76

Chapter 3: Quantification of Oxygen Utilisation for a Microbial P450 Oxidative Bioconversion (77-104)

3.1. Context and Aim	77
3.1.1. Aims	78
3.2. Optimisation of P450 Bioconversion	79
3.2.1. Screening	81
3.2.2. Refinement	86
3.2.3. Bioconversion Kinetics Under Optimised Conditions	87

3.2.4. Scale Up to Pilot Fermentation Scale	92
3.2.5. Pilot Scale Culture Strategy Comparison	95
3.2.6. Oxygen Demand Quantification at Pilot Scale	96
3.2.7. Identifying Oxygen Requirements and Prioritisation	99
3.2.8. Summary	103

Chapter 4: Accurate Quantification of Oxygen Mass Transfer Rates in High Throughput Scale Down Systems (105-147)

4.1. Context and Aim	105
4.1.1. Aims	107
4.2. Initial Screening Models for k_{La} and OUR in 24 Deep Square Well Plates	110
4.2.1. Building the Design	110
4.2.2. k_{La} Determination in 24DSW (Dynamic Gassing-Out Method)	111
4.2.3. OUR Determination in 24DSW (Dynamic Gassing-Out Method)	115
4.3. Establishing a New Method for Oxygen Mass Transfer Quantification During Microbial Fermentation in Microwell Plates	117
4.3.1. Building the Design	117
4.3.2. Determination of OUR and Q_{O_2} During Culture Using the New Method	121
4.3.3. Modelling OUR in 24DSW Plates Using the New Dynamic Gassing Out Method	123
4.4. Comparing the Initial Screening Model and the Culture Model	127
4.5. Relationship Between Biomass Growth and Oxygen Availability	132
4.6. Relationship Between Recombinant Protein Expression and Oxygen Availability	135
4.7. Modelling Overlaps in Aeration Environment Between 24 and 96 DSW Plates	141
4.7.1. Equating O_2 Mass Transfer Conditions in 24DSW to 96DSW Using Biomass Accretion	143
4.7.2. Equating O_2 Mass Transfer Conditions in 24DSW to 96DSW Using Recombinant Protein Expression	146
4.8. Summary	146

Chapter 5: Oxygen Mass Transfer Characterisation of Laboratory Scale Single Use Bioreactors (148-196)

5.1.	Context and Aim	148
5.1.1.	Aims	148
5.2.	Oxygen Mass Transfer in a Conventional Stirred Tank Bioreactor (New Brunswick BioFlo 310)	149
5.2.1.	Building the Experimental Design	149
5.2.2.	Fixed Factors	151
5.2.3.	Run Ordering	152
5.2.4.	Modelling Oxygen Mass Transfer in a Pilot Scale Stirred Tank Bioreactor	152
5.3.	Xcellerex Disposable Bioreactor-10 (XDR-10)	162
5.3.1.	Building the Experimental Design	163
5.3.2.	Fixed Factors	165
5.3.3.	Modelling Oxygen Mass Transfer Coefficient in a Single Use Bioreactor (XDR-10)	166
5.4.	Ambr®250 Single Use Bioreactor	172
5.4.1.	Preliminary Determination of k_La	173
5.4.2.	Experimental Design for Modelling Oxygen Mass Transfer Coefficient (k_La) in an Ambr®250 SUB	175
5.4.3.	Establishing a Protocol to Automate an O_2 Mass Transfer Investigation in a SUB	176
5.4.4.	Modelling Oxygen Mass Transfer Coefficient in an Ambr®250	177
5.5.	Comparison of Oxygen Mass Transfer in Different Bioreactor Types	185
5.5.1.	Comparison of Models for Three Different Bioreactors	187
5.5.2.	Comparison of k_La Models with Literature Correlations	188
5.6.	Applicability of Single Use Bioreactors to Microbial Fermentation	190
5.6.1.	Comparison of Oxygen Demands Determined in this Thesis and Oxygen Mass Transfer Capabilities of Three Different Bioreactors	190

5.6.2. Comparison of Oxygen Demands Determined in Industrial Microbial Fermentations and Oxygen Mass Transfer Capabilities of Three Different Bioreactors	192
5.6.3. Comparison of Oxygen Mass Transfer Coefficients in SUBs and Microwell Plates	192
5.7. Summary	194

Chapter 6: An Economic Evaluation Tool for Bioprocess Development using the Ambr®250 System (197-219)

6.1. Context and Aim	197
6.1.1. Aims	198
6.2. Ambr®250 Resourcing and Costing (ARC) Tool - Version 1.0 (Microsoft Excel)	199
6.3. Ambr®250 Resourcing and Costing (ARC) Tool - Version 2.0 (Jupyter Notebooks)	202
6.3.1. Summary of Developments	207
6.4. Case Studies	207
6.4.1. Total Bioreactors	212
6.4.2. Bioprocess Run Structure and Duration	214
6.4.3. Supplier Discount	215
6.4.4. Sample Regime During Production Stage Culture	215
6.5. Summary	216
6.6. Future Developments	218

Chapter 7: Conclusions and Future Work (220-225)

7.1. Conclusions	220
7.2. Future Work	223

References 226

Appendices 249

Nomenclature

List of abbreviations:

ALA	- 5-aminolevulonic acid
ANOVA	- Analysis of variance
ARC	- Ambr®250 resourcing and costing
C^*	- Saturation concentration of oxygen
CCF	- Central composite facing design (in DoE)
CCR	- Carbon catabolite repression
CIP	- Clean in place
C_n/C_L	- Oxygen concentration in the first order system
CYP	- Cytochrome P450
D_i	- Diameter of impeller
D_v	- Diameter of vessel
DoE	- Design of experiments
DOT	- Dissolved oxygen tension
DSW	- Deep square well (referring to microwell plate format)
GFP	- Green fluorescent protein
HPLC	- High performance liquid chromatography
I-B	- Induced batch culture
I-FB	- Induced fed batch culture
IPTG	- Isopropyl- β -D-1-thiogalactoside
ISPR	- in-situ product removal
k_{La}	- Volumetric oxygen mass transfer coefficient (measured in h^{-1} , min^{-1} , s^{-1})
LB	- Luria-Bertani broth
N-IB	- Non-induced batch culture
O_2	- Oxygen
OD_{600}	- Optical density measured at a wavelength of 600nm
OFAT	- One factor at a time
OTR	- Oxygen transfer rate
OTR_{max}	- Maximum oxygen transfer rate
OUR	- Oxygen uptake rate
p-value	- a measure of the statistical significance that can be held in the model

P450	- Cytochrome P450
PBS	- Phosphate buffered saline
PC	- Polycarbonate
P_g	- Gassed power consumption
P_i	- Total pressure at air inlet
P_o	- Total pressure at air outlet
PPG	- Polypropylene glycol
PRT	- Probe response time
Q_i	- Volumetric air flowrate at air inlet
Q_o	- Volumetric air flowrate at air outlet
Q_{O_2}	- Specific respiration rate or specific oxygen consumption rate
RSM	- Response surface methodology

R-squared or R^2 - a measure of how well a model or trend fits with experimentally determined data

SIP	- Sterilise in place
SOP	- Standard operating procedure
STR	- Stirred tank bioreactor
SUB	- Single use bioreactor
TB	- Terrific broth
T_i	- Temperature of gas at air inlet
T_o	- Temperature of gas at air outlet
TFA	- Trifluoroacetic acid
URS	- User requirement specification
V_L	- Volume of liquid
V_s	- Superficial gas velocity
v/v	- volume by volume
vvm	- volume by volume per minute
XDR	- Xcellerex disposable reactor
Y_i	- Mole fraction of oxygen at air inlet
Y_o	- Mole fraction of oxygen at air outlet
Y_{XO}	- Yield coefficient of biomass on oxygen

List of Figures

Figure 1.1. Ribbon structures of P450s 3A4 and 2C8

Figure 1.2. Diagrammatic representations of the four main classes of cytochrome P450

Figure 1.3. Suggested improvements to P450s for commercial biotechnological application

Figure 1.4. Steps in the transfer of oxygen from gas bubble to cell

Figure 1.5. Effect on K_{La} in a mechanically agitated bioreactor as a result of changing airflow rate

Figure 1.6. Geometries of common microwell formats

Figure 1.7. Maximum OTRs and k_{Las} in 96 well microtitre plates at different shaking diameters and frequencies

Figure 1.8. Examples of commercially available single use bioreactor bags

Figure 1.9. Examples of plots used in the determination of the volumetric oxygen mass transfer coefficient

Figure 1.10. Diagrammatic comparison of OFAT and DoE experimental approaches

Figure 2.1. Mechanical drawing of New Brunswick BioFlo310 stirred tank bioreactor

Figure 2.2. Mechanical drawing of tank liner for the Xcellerex XDR-10 single use bioreactor

Figure 2.3. Mechanical drawing of Ambr[®]250 single use bioreactor

Figure 2.4. Diagrammatic representation of the rearranged off gas measurement set up in the UCL Advanced Centre for Biochemical Engineering

Figure 2.5. Diagrammatic representation of the set up for online dissolved oxygen measurement in 24 deep square well Oxodish plates

Figure 2.6. Example DOT profile showing the method for quantification of OUR and k_{La}

Figure 2.7. Representative example experimental DOT profiles used for analysis

Figure 2.8. Representative example experimental plots used in the quantification of k_{La}

Figure 3.1. Half normal plot highlighting factors and interactions of significant statistical effect in the screening round of multifactorial optimisation

Figure 3.2. Parity plot to highlight the influence of shaker speed on product concentration in the screening round of multifactorial optimisation

Figure 3.3. Three factor interaction between post induction time, substrate concentration and pre induction time in the screening round of multifactorial optimisation

Figure 3.4. Two factor interactions observed during the screening and refinement rounds of multifactorial optimisation

Figure 3.5. Half normal plot highlighting the factors and interactions of significant statistical effect in the refinement round of multifactorial optimisation

Figure 3.6. Effect plot, showing potential 14 times increase in final product concentration across the post induction temperature range

Figure 3.7. Comparison of growth and bioconversion kinetics between optimised microtitre plate and pilot scale bioreactor scale cultures

Figure 3.8. Comparison of three pilot scale fermentation strategies with respect to growth and bioconversion kinetics

Figure 3.9. Relationship between bioconversion kinetics, volumetric productivity with respect to biomass accumulation and oxygen uptake rate in three fermentation strategies

Figure 3.10. Oxygen uptake rate comparison during each of the pilot scale fermentation modes

Figure 3.11. Breakdown of maximum oxygen uptake rates observed during three pilot scale fermentation modes

Figure 4.1. Overview of the experimental strategy for determining accurate oxygen mass transfer in microwell plates

Figure 4.2. Example DOT profiles at low, medium and high k_{La} values

Figure 4.3. k_{La} s and OURs observed across the experimental landscape during building of a baseline model for O_2 mass transfer in 24 DSW plates

Figure 4.4. Example DOT values at low, medium and high OUR values

Figure 4.5. Main effects on the linear baseline model for k_{La} in 24 DSW plates

Figure 4.6. Main effects on the linear baseline model of OUR in 24 DSW plates

Figure 4.7. Parity plots for modelled k_{La} and OUR in 24 DSW plates

Figure 4.8. Example DOT profiles during culture at low, medium and high k_{La} values

Figure 4.9. Effect profiles for the four factors of influence on the model for OUR in 24 DSW plates

Figure 4.10. Diagnostic plots for the linear model built to describe OUR during 24 DSW culturing

Figure 4.11. Response surface for the model of OUR in 24 DSW plate culture

Figure 4.12. Example raw and modelled biomass concentration profiles during microwell culture

Figure 4.13. Relationship between OUR and volumetric productivity at a range of k_{La} s in 24 DSW culture

Figure 4.14. Effect profiles for the factors of influence on the model for biomass accumulation in 24 and 96 DSW culture

Figure 4.15. Parity plots for the models of biomass accretion in 24 and 96 DSW culturing

Figure 4.16. Representative examples of culture fluorescence profiles at low, medium and high k_{La}

Figure 4.17. Maximum biomass concentration and recombinant protein expression at high, medium and low oxygen availabilities

Figure 4.18. Effect profiles for the factors included in the multifactorial design to evaluate the relationship between recombinant protein expression and oxygen availability in 24 and 96 deep square well plates

Figure 4.19. Parity plots for the models of recombinant protein expression in 24 and 96 deep square well plates

Figure 4.20. Representative examples of the relationship between oxygen availability and protein expression

Figure 5.1. Main effect plots for factors of significance in the model of oxygen mass transfer coefficient in the New Brunswick BioFlo310 stirred tank bioreactor

Figure 5.2. Three-dimensional surface plot showing the impact on oxygen mass transfer of the interaction between agitation speed and aeration rate

Figure 5.3. Interaction plot to show the impact on oxygen mass transfer of the interaction between viscosity and aeration rate

Figure 5.4. Three-dimensional surface plot for the effect on k_{La} of the interaction between viscosity and temperature

Figure 5.5. Contour plot showing the relationship between temperature and aeration rate and the effect on oxygen mass transfer coefficient

Figure 5.6. The effect on k_{La} of the two factor interaction between antifoam concentration and agitation rate

Figure 5.7. The effect on oxygen mass transfer coefficient of the two factor interaction between antifoam concentration and temperature

Figure 5.8. Diagnostic plots for the model of oxygen mass transfer coefficient in a benchtop STR (BioFlo 310)

Figure 5.9. Main effect plot for the impact of agitation rate on the model of oxygen mass transfer coefficient in the XDR-10 SUB

Figure 5.10. Main effect plot for the quadratic relationship observed as a result of temperature on the model of oxygen mass transfer coefficient in the XDR-10 SUB

Figure 5.11. The effect on oxygen mass transfer coefficient of the interaction between temperature and agitation rate

Figure 5.12. Diagnostic plots for the model of oxygen mass transfer coefficient in a tank liner type SUB (XDR-10)

Figure 5.13. Oxygen mass transfer coefficient as determined in Ambr®250 bioreactors under a range of set conditions

Figure 5.14. Profiles of $k_{L,a}$ as a result of each of the factors in the model for oxygen mass transfer coefficient in the Ambr®250.

Figure 5.15. Effect on oxygen mass transfer in an Ambr®250 bioreactor of the interaction between agitation and aeration rates

Figure 5.16. Contour plot for the two factor interaction between antifoam concentration and temperature, and the effect on $k_{L,a}$ in an Ambr®250 bioreactor

Figure 5.17. Overall model for $k_{L,a}$ in an Ambr®250 bioreactor as represented using a 3D response surface and a contour plot

Figure 5.18. Diagnostic plots for the quadratic model built to describe $k_{L,a}$ in an Ambr®250 bioreactor system

Figure 5.19. Parity plots to determine the correlation between experimentally determined $k_{L,a}$ values and those calculated using literature correlation for the BioFlo 310 and Ambr®250 bioreactors

Figure 5.20. Representative example traces of oxygen uptake and biomass concentration profiles from an industrial E. coli fermentation

Figure 6.1. Basic structure for estimation of the resource demands for a given bioprocess development run in the Ambr®250 bioreactor

Figure 6.2. Illustration of the inputs and code in Microsoft Excel cells in order to determine the total number of samples taken during a bioprocess run.

Figure 6.3. Example of the Inputs page from the Version 1.0 of the ARC tool in Microsoft Excel 2013

Figure 6.4. Example of the Outputs page from Version 1.0 of the ARC tool in Microsoft Excel 2013

Figure 6.5. Basic structure for estimation of the resource demands for a given bioprocess development run in the Ambr®250 using Version 2.0 of the ARC tool in Python using Jupyter Notebooks

Figure 6.6. Illustration of the code in Jupyter Notebooks to determine the number of samples taken during the primary seed stage of a bioprocess run

Figure 6.7. Example of the dynamic properties of the ARC tool built in the Jupyter notebook

Figure 6.8. Example of the first part of the Inputs Notebook for the ARC tool built in Jupyter Notebooks using the Python programming language

Figure 6.9. Example of the second part of the Inputs Notebook for the ARC tool built in Jupyter Notebooks using the Python programming language

Figure 6.10. Example of the Resource Estimates Notebook for the ARC tool built in Jupyter Notebooks using the Python programming language

Figure 6.11. Effect of changing the number of production stage bioreactors used on the cost of a bioprocess run in the Ambr[®]250 system

Figure 6.12. Effect of changing the duration of each of the stages of the bioprocess run on the cost of a bioprocess run in the Ambr[®]250 system

Figure 6.13. Effect of increasing the supplier discount on consumables on the cost of a bioprocess run in the Ambr[®]250 system

Figure 6.14. Effect of changing sampling regime on the cost of a bioprocess run in the Ambr[®]250 system

List of Tables

Table 1.1. Examples of industrial application of biocatalysis

Table 1.2. Examples of products manufactured in the chemical and pharmaceutical industries using biocatalysis

Table 1.3. Functions of cytochrome P450 enzymes by host organism

Table 1.4. Actions of selected P450s in the body on therapeutic drugs

Table 1.5. Observed oxygen demands for a range of P450 bioconversions

Table 1.6. Measured oxygen uptake rate values for different microorganisms

Table 1.7. Specific oxygen uptake rate values for different microorganisms

Table 1.8. A brief overview of factors that affect $k_{L,a}$

Table 1.9. Summary of empirical description for avoiding flooding in a stirred bioreactor

Table 1.10. Effect of changing well size and shaking diameter on oxygen mass transfer in microwell plates

Table 1.11. Examples of maximum measured $k_{L,a}$ s in a range of microwell formats

Table 1.12. Examples of oxygen mass transfer values determined for shaken Erlenmeyer flasks

Table 1.13. Configuration and oxygen mass transfer capabilities of commercially available single use bioreactors in literature

Table 1.14. Commonly reported correlations for $K_{L,a}$ in stirred tank bioreactors

Table 1.15. Overview of methods for measurement of oxygen mass transfer coefficient and their advantages and disadvantages

Table 2.1. Properties and geometries of three bioreactors to be investigated

Table 2.2. Summary of experimental designs for the three stages of multifactorial optimisation for a whole cell oxidative bioconversion

Table 2.3. Experimental design for oxygen mass transfer determination in 24 deep square well microtitre plates

Table 2.4. Experimental design for building a model of oxygen mass transfer during culturing in 24 DSW and 96 DSW plates

Table 2.5. Component volumes for preparation of free glycerol assay reaction mixture

Table 3.1. Factors and ranges for each of the iterative rounds in the multifactorial optimisation of a whole cell P450 bioconversion in microwells

Table 3.2. Summary table of statistically significant effects and interactions on end point 7-hydroxycoumarin yield during the first two rounds of multifactorial optimisation

Table 3.3. Analysis of variance for multifactorial landscapes generated to model 7-hydroxycoumarin yield during the first two rounds of multifactorial optimisation

Table 3.4. Calculated gains in biomass accumulation, product concentration and specific product concentration compared with previous work

Table 3.5. Optimised set points and starting conditions for pilot scale culturing

Table 3.6. Effect of fermentation mode on the biomass accumulation and bioconversion productivity for the bioconversion of 7-ethoxycoumarin to 7-hydroxycoumarin

Table 3.7. Contribution to peak oxygen uptake rate of each of the three major components

Table 4.1. Experimental design for determination of k_{La} and OUR in 24 DSW plates when building initial screening models

Table 4.2. k_{La} s observed within the experimental landscape grouped by fill volumes and shaker speeds

Table 4.3. Comparison of k_{La} values reported in this work with literature values of maximum k_{La} values for a range of microwell geometries.

Table 4.4. Factors and parameter value estimates for the initial screening model of k_{La} in 24 DSW plates

Table 4.5. Estimates of parameter coefficients for each of the significant factors in the initial screening model of OUR in 24 DSW plates

Table 4.6. Comparison of analysis of variance for the linear models of k_{La} and OUR in 24 DSW microwell plates.

Table 4.7. Experimental design for OUR quantification in 24 DSW plates during culturing

Table 4.8. Experimental design for OUR quantification in 96 DSW plates during culturing

Table 4.9. Estimates of model coefficients and statistical analysis for each of the significant factors and interactions in the quadratic model of OUR in 24 DSW plates

Table 4.10. Comparison of OURs between the traditional dynamic gassing out method and the new dynamic gassing out method during culturing

Table 4.11. ANOVA statistical diagnostics for the modelled biomass accretion as a result of the aeration environment in 96 and 24 DSW plates

Table 4.12. ANOVA statistical diagnostics for the models of recombinant protein expression in 24 and 96 DSW plates

Table 4.13. Centripetal forces and linear velocities under the range of fill volumes and rotational speeds investigated in 24 and 96 DSW plates

Table 4.14. Parameter coefficients from the models for oxygen mass transfer with respect to biomass accumulation in 24 and 96 DSW plates.

Table 5.1. Factors and ranges for generating the model of oxygen mass transfer in a New Brunswick BioFlo 310 bench top STR

Table 5.2. Summary of the ANOVA statistics for the model of oxygen mass transfer in a BioFlo 310 stirred tank bioreactor

Table 5.3. ANOVA for the terms contained within the quadratic model for $k_{L,a}$ in a BioFlo 310 stirred tank bioreactor

Table 5.4. Factors and ranges for the investigation into oxygen mass transfer in a tank liner style SUB.

Table 5.5. Example $k_{L,a}$ and PRT corrected $k_{L,a}$ data from across the experimental design in an XDR-10 single use bioreactor bag

Table 5.6. Summary of the ANOVA statistics for the model of oxygen mass transfer in a XDR-10 disposable bioreactor

Table 5.7. ANOVA for the terms contained within the quadratic model for oxygen mass transfer coefficient in a XDR-10 SUB

Table 5.8. Set points for the preliminary investigation of $k_{L,a}$ in Ambr[®]250 bioreactor.

Table 5.9. Factors and ranges for the investigation into oxygen mass transfer in an Ambr[®]250 bioreactor.

Table 5.10. Coefficient values and statistical analysis for each of the terms in the model for oxygen mass transfer coefficient in the Ambr[®]250.

Table 5.11. Summary of the statistical diagnostics for the overall model of $k_{L,a}$ in an Ambr[®]250 bioreactor system.

Table 5.12. Maximum $k_{L,a}$ values and significant main effects observed in models of $k_{L,a}$ for each bioreactor type investigated

Table 5.13. Observed oxygen uptake rates and maximum biomass concentrations for a number of industrial microbial fermentations using different expression systems under different modes of operation.

Table 5.14. $k_{L,a}$ values and estimated equivalent oxygen transfer rates determined for a range of commercially available single use bioreactors

Table 6.1. Bioprocess train sequences and durations investigated for their effect on cost of a bioprocess run in the Ambr[®]250 system

1. Introduction and Literature Review

1.1. Context of the Research

Engineered biological systems have been used over the years to process chemicals, produce energy and food, construct materials and even to aid in the improvement of health or the environment (Endy 2005). In the late 1970s Szybalski & Skalka, (1978), highlighted that molecular biology was in a state whereby recombinant DNA could be easily constructed, making it a powerful tool in enhancing biological potential. More recently, the limitations of these traditional techniques has been realised and so new technologies have been developed, such as synthetic biology, which to date has been applied in the production of novel antibiotics and biofuels (Weber et al. 2011), vaccines (Wimmer et al. 2009) and the generation of a minimal free living cell (Hutchison et al. 2016). In short, synthetic biology aims to apply robust engineering principles and characterisation to genetic engineering with a strong focus on the biological context (Andrianantoandro et al. 2006).

From a Biochemical Engineering standpoint, the major commercially applicable outputs are more productive expression systems (thus far particularly microbial), or indeed completely new molecules (Khalil & Collins 2010). This results in lower process cost and a large variety of enzymes being expressed. Significant challenges remain though as a result of greater oxygen demand, process characterisation at small scale and the issue of scaling up expression systems which place an increased burden on the culture environment (Cheng & Lu 2012).

In addition, there is increased use of single use bioreactor (SUB) technologies in the biotechnology sector, particularly for mammalian bioprocessing, due to the advantages they offer with regards to flexibility, environmental impact, capital expenditure and turnaround times (Eibl et al. 2010; Galliher 2008). There is however, a lack of investigation and development for microbial SUBs, a disconnect which needs to be addressed.

In this first chapter, a review of the literature is undertaken in order to gain an appreciation of the current state of the industry, with a particular focus on biocatalysis, oxygen utilisation by microbial microorganisms, and available bioreactor technologies and their ability for oxygen mass transfer.

1.2. Literature Review

1.2.1. Biocatalysis

Biocatalysis is the use of enzymes to perform chemical syntheses. Enzymes undertake highly specific transformation of a 'substrate' to a 'product' and enhance the rate at which a conversion takes place (Beilen & Li 2002). Enzymes are often highly substrate, product and reaction specific, and capable of replacing multiple steps from the manufacture of a given molecule (Pollard & Woodley 2007), particularly if the current process uses traditional chemical catalysts (Woodley 2008). Biocatalysts are capable of regio- and enantio- selective modifications, which may not be possible by chemical means and can be used to generate industrially relevant products with high efficiency and minimal by-product formation (Osbon & Kumar 2019, Nikolova & Ward 1993).

Biocatalysts therefore have the potential to be beneficial to a manufacturing process, particularly in terms of its economics and sustainability (Gavrilescu & Chisti 2005; Wohlgemuth 2010; Thomas et al. 2002; Castro & Knubovets 2003). It is worth noting that there are many factors associated with biocatalysis that can impact on performance and suitability for a given process (Hatti-Kaul et al. 2007).

The major disadvantages of biocatalysis, particularly compared with chemical synthesis, is the lack of understanding relative to traditional chemical process techniques and the time and cost of developing and manufacturing an enzyme (Thomas et al. 2002), although these costs are continually decreasing.

1.2.1.1. Biocatalyst Forms

Biocatalysts may be used as isolated enzymes (often immobilised) or contained within a whole cell. Each has its own advantages and disadvantages and areas of application which are explored below.

Isolated enzymes are amenable to shorter development timelines, and are simpler to implementation than their whole cell counterparts (Cao 2005). Also, very few, if any side reactions take place during the bioconversion as there are no other enzymes present (Nikolova & Ward 1993). This makes the conversion process much more predictable (Ishige et al. 2005). If necessary, immobilisation of the enzyme onto or within a solid support can be used in order to enable reuse (Gupta et al. 2011). Isolated

enzymes though, have much higher upstream costs, even when used in small quantities (Gillera et al. 2010) due to the economic burden of their manufacture and purification. This necessitates enzyme reuse in order to maintain manageable costs (Cao 2005). It has been noted though that due to increasingly efficient enzyme manufacture, using recombinant organisms, these costs are and will continue to decline (Lima-Ramos et al 2014).

Whole cell biocatalysts are cheap to implement upstream as they do not require for processing and isolation (Pollard & Woodley 2007), with an additional benefit due to a lack of requirement for cofactor addition (Nikolova & Ward 1993). Whole cells also have the capacity to contain multiple enzymes, allowing for complex, multistep transformations to take place in a single process step (Leon et al. 1998). However, a potential difficulty resulting from this is the generation of unwanted side products (de Carvalho 2011). A major advantage of whole cell biocatalysis is the relative ease of process scale up due to the ability to use, well characterised fermentation technologies (Fukuda et al. 2008). Additionally, if fermentation and bioconversion steps are separated, then alterations to media and catalyst concentrations can optimise reaction conditions and simplify downstream processing (Wachtmeister & Rother 2016, Park & Geng 1992).

Disadvantages of whole cell biocatalysis include the need for expensive fermentation facilities (Pollard & Woodley 2007), especially if these facilities are required on a large scale. Also, whole cells are generally subject to substrate and product inhibition (Edwards 1970), with concentrations greater than 1gL^{-1} noted as being potentially detrimental. Limited use of whole cells with organic solvents and ionic liquids has also been reported (Roberts et al. 1995). In addition, when compared with isolated enzyme, greater mass transfer resistances due to the need to transport substrates and products across the cell membrane result in overall reaction rates being up to two orders of magnitude slower (Ni & Chen 2004); if whole cells are immobilised then these already high resistances are increased further (Leon et al. 1998).

1.2.1.2. Industrial Relevance and Application of Biocatalysis

Biocatalysis has been applied in industry for around two centuries, beginning with the use of immobilised whole cells for the formation of acetic acid in 1815 (Wandrey et al. 2000). Isolated enzymes have been applied in industry since the late 1960s,

beginning with the industrial resolution of amino acids in Japan, 1969 (Chibata & Tosa 1977).

The majority of success for industrial biocatalysis to date has been seen in the areas of fine chemicals and pharmaceuticals (Choi et al. 2015). Increasing interest in the use of biocatalysts is being seen, with more than 100 industrial biotransformations in the fine chemicals industry in the early 2000s (Straathof et al. 2002). Since then, it has also been reported that around 10% of all drug synthesis is reliant on biocatalysis (Patel 2008).

Biocatalysis is employed in large-scale processes in a number of industrial sectors, including those shown in Table 1.1. The industrial enzyme market in 2009 was estimated at \$5.1 billion, and was predicted to reach \$6.9 billion in 2017 (Sanchez & Demain 2016). This rise can be attributed to the increase in applications in various markets (including cosmetics, paper and detergents), growth in the bulk chemical industry and the increased performance and competition within the enzymes market (van Beilen & Li 2002). Some examples of commercial scale products in the chemical and pharmaceutical industries are semi-synthetic penicillins (Boesten et al. 1996) and acrylamide. Additionally, many industries are under increasing pressure to become more environmentally responsible, with biocatalysts a practical route to achieving this (Saibi et al. 2012). This suggests a shift towards biocatalysis in these large and lucrative markets (the chemicals market alone is projected to be worth in excess of \$5 trillion in 2020) (Clomberg et al, 2018).

1.2.1.2.1. Pharmaceuticals

More than half of all commercial scale processes which apply industrial biotransformations are in the pharmaceutical field (Straathof et al. 2002), though none are considered 'bulk' processes (>20,000 tons per annum). Examples include the manufacture of an anti-HIV agent (3TC, Lamiduvine by Glaxo) (Mahmoudian et al. 1993), intermediates of Omapatrilat, an antihypertensive medication (Patel 2001) and semi synthetic penicillins using penicillin amidase (Boesten et al. 1996). In addition, it was recently reported that biocatalytic processes are used in the manufacture of some of the world's highest grossing pharmaceutical products, including Simvastatin (Zocor®) (Xie & Tang 2007) and Atorvastatin (Lipitor®) (Greenberg et al. 2004), with these two products alone achieving annual sales of around \$20 billion (Tao & Xu 2009).

Table 1.1. Examples of the industrial application of enzymes (adapted from van Beilen & Li, 2002).

Industry	Field of Application	Examples/Comments
Agriculture	Feed additives	Positive effects on environment, animal health and efficiency
	Heterologous enzyme production	Laccase and trypsin production in plants
Chemicals	Biocatalysis	Preparative biotransformations
	Polymers	Polymer synthesis by enzyme catalysis
	Bulk organic compounds	Via pathway engineering
Cleaning	New detergent enzymes	Results in lower prices and increased competition
Energy	Fuel alcohol from biomass	Genencor and Novozymes work on conversion of biomass-to-ethanol
Food	Enzymes used in food	Variety of new enzymes in food preparation
	Nutraceuticals	Increased carotene in tomato
Pharma	Chiral compounds	Enantioselective biocatalysis
	Glycoprotein engineering	<i>In vitro</i> protein glycosylation
	Enzymes as pharmaceutical targets	Numerous target examples
Materials	Paper, textile, leather	New enzymes from extremophiles
	Biosteel (silk)	Heterologous expression of spider silk

Taxol®, an anti-cancer therapeutic involves the use of a lipase catalysed step (Liese et al. 2000).

1.2.1.2.2. Chemicals

There is a gradual move towards selective catalysis within the chemical industry (Straathof et al. 2002). Peroxidases are used in the synthesis of phenolic resins

(Pokora & Cyrus 1987), while ChiPros™, a group of chiral intermediates are manufactured by BASF in Germany (Hieber & Ditrich 2001). Arguably though, the most notable commodity manufactured using biocatalysis is the production of acrylamide using nitrile hydratase (Liese & Filho 1999). Although examples remain rare, some companies have switched from a chemical process to a biocatalytic one for manufacture of a product (e.g. β -lactam antibiotic cephalexin by DSM) (Van De Sandt & De Vroom 2000). Examples of products manufactured in the chemical and pharmaceutical industries using biocatalysis are shown in Table 1.2.

1.2.1.2.3. Additional Industrial Sectors

Enzymes employed in the food industry are many and diverse, including the production of high fructose corn syrup using xylose isomerase (Jensen & Rugh 1987) as well as cheese flavouring (lipases) and use in the baking of biscuits (proteases) (Kirk et al. 2002).

In the textiles industry laccases are used for bleaching materials, and there is a substantial market in pulp and paper, where enzymes are used for bleaching, pitch control and de-inking (Kirk et al. 2002). Also, enzymes are used widely to generate feed additives for agriculture and in detergents such as biological washing powder (DiCosimo et al 2013, Bhat 2000). Examples from additional industries are shown in Table 1.1.

1.2.1.3. Challenges to Adoption of Industrial Biocatalysis

There remain a number of challenges to adoption of biocatalysis for industrial application. For example, due to increased processing times at industrial scale, degradation of the catalyst, substrate or product can result in significantly affected activities, titres and product quality (Pollard & Woodley 2007). Strategies have been developed though, which require either the continual removal of product (*in situ* product removal – ISPR) (Lye & Woodley 1999), or controlled supply of substrate to the bioconversion process. The majority of commercially available enzymes are expensive for their application, meaning that a number of alternative technologies for enzyme production have had to be developed (Lagemaat & Pyle 2001; Fotheringham et al. 2006). Rapid development timelines are essential in the pharmaceutical industry so as to maximize on patent life (Straathof et al. 2002). Thus, inclusion of any biocatalytic steps at an early stage is key for adoption.

Straathof *et al* (2002) discuss the criteria for a successful chemical process as having greater than 80% yield, a minimum final product concentration of 50gL⁻¹, but typically in excess of 100gL⁻¹, and a volumetric productivity from 1gL⁻¹h⁻¹ (with examples reported up to 130gL⁻¹h⁻¹). This highlights the challenge for biocatalysis to be incorporated into an industrial process, and this must be achievable at a commercial scale.

There are industries which have achieved this and integrated biocatalysis as previously shown in Table 1.1. However, challenges remain including ease of scale up, when and where to incorporate biocatalysis and the mode of enzyme. The impact of biocatalysis in these industries is growing and there is little to suggest that this will cease. With the value of biotechnology measured in the hundreds of billions of dollars, the financial potential of this market is not to be underestimated.

Oxidative bioconversions (including cytochrome P450s) are a valuable but challenging subset of biocatalysts (Burton 2003), with widespread application (Gillam 2008; Hasler *et al.* 1999). Thus, P450s are discussed here as a potential model system for investigating oxidative bioconversions of industrial relevance.

Table 1.2. Examples of products manufactured in the chemical and pharmaceutical industries using biocatalysis (adapted from Schmid *et al.*, 2001. Leise *et al.*, 2000 and Ishige *et al.*, 2005).

Product	Enzyme	Scale (tons per yr)	Company
Enantiopure Alcohols	Lipase	Thousands	BASF
R-amide; S-amide	Lipase	Hundreds	BASF
L-Aspartic acid	Ammonia Lyase	Thousands	DSM
Semisynthetic Penicillins	Acylase	Low Hundreds	DSM
6-Hydroxy-S-nicotine	Hydroxylase	Low (Development)	Lonza
Taxol	Lipase	-	Bristol Myers Squibb
L-Tyrosine	Aminoacylase	-	Degussa
Vitamin B3	Nitrile hydratase	-	Lonza
Acrylamide	Nitrile hydratase	-	Mitsubishi Rayon
L-DOPA	Tyrosine phenol lyase	-	Ajinomoto
Pravastatin sodium	P450	-	Sankyo

1.2.2. Cytochrome P450s

The literature indicates that P450s are a widely investigated and promising group of enzymes, capable of a number of highly specific bioconversions of significant industrial potential (Burton 2003), and so they are investigated in this thesis. Cytochrome P450s (CYP) are a super family of heme-proteins which are responsible for catalysing mainly oxidative bioconversions (Shakunthala 2010). Most interestingly from a Biochemical Engineering standpoint are those of pharmacological and toxicological significance.

Many P450s are characterised as monooxygenases, while others are capable of hydroxylations, dealkylations and oxidations (Gillam 2008) with the potential substrates measured in the thousands (Hasler et al. 1999). This breadth is unsurprising when the number of organisms acting as sources of P450s is considered, from mammalian to bacterial and plant species (Baboo 2012).

The advent of recombinant DNA technology and increased titres in heterologous expression systems allowed the determination of high resolution structures of P450s involved in drug metabolism including P450s 3A4 and 2C8 (Yano et al. 2004) (Figure 1.1.), P450 2C9 (Wester et al. 2004), P450 2D6 (Rowland et al. 2006) and P450 2A13 (Smith et al. 2007), present in the lung and associated with causation of lung cancer. Additional important developments include the role of P450s in the metabolism of drugs and other xenobiotics (Zanger & Schwab 2013, Cooper et al. 1965), and the first separation and purification of P450 enzymes (Guengerich 2008).

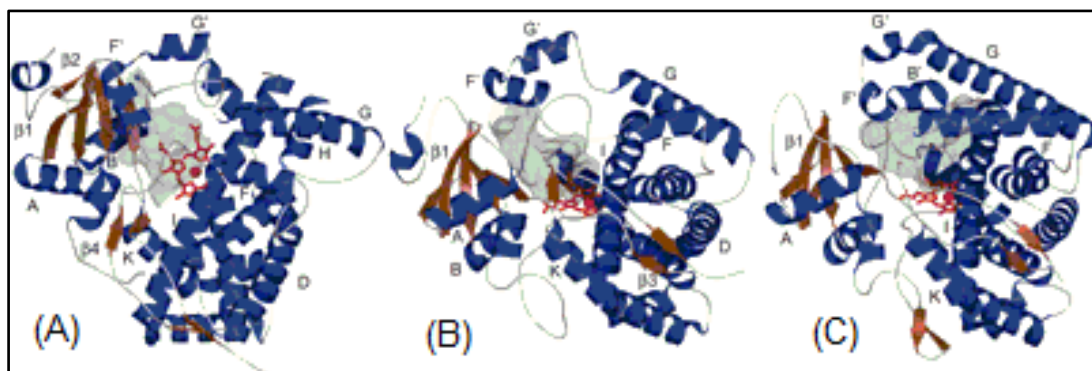


Figure 1.1. Ribbon structures of P450s 3A4 (A and B) and 2C8 (C) (adapted from Yano et al, 2004), showing that the structure in CYPs, even those of different classes, is highly conserved.

1.2.2.1. P450 Classifications

The grouping of cytochrome P450 monooxygenase systems is based on the number of protein components they contain (Degtyarenko & Archakov 1993), with three well established classes, plus a less explored fourth class (Roberts et al. 2002). Diagrammatic representations of these are shown in Figure 1.2 and the details of each are briefly discussed.

Class I P450 monooxygenases are three component systems (Figure 1.2.A). To date the majority of P450 systems characterised are Class I. They are found commonly in bacteria and mammalian mitochondrial cells (Bell et al. 2010). When found in bacteria, Class I systems have a number of uses, including production of secondary metabolites and xenobiotic metabolism (Bernhardt 2006). When found in mammalian mitochondria, the P450 is involved in steroid metabolism (Fulco 1991). Class I systems do not have a P450 reductase (Munro et al. 2007), meaning they are incapable of achieving commercially viable activities without addition of this reductase (Arinc et al. 1999).

Class II P450 monooxygenases are two component systems as shown in Figure 1.2.B. When found in mammalian systems, Class II P450s have been shown to be responsible for the oxidative metabolism of steroids, fatty acids and prostaglandins (Hasler et al. 1999). In plants, they are known to be responsible for the synthesis of cutin and lignin barriers (Bak et al. 2011).

Class III P450 monooxygenases are single component systems (Figure 1.2.C). Found in a variety of prokaryotes and eukaryotes, Class III systems are involved in the synthesis of signalling molecules including prostaglandins (in mammals) and jasmonate (in plants) (Werck-Reichart & Feyereisen 2000). Comparatively high catalytic activity as a result of utilising O₂ containing substrates makes Class III P450s good candidates for industrial application.

Class IV P450 systems are composed of three bound elements similar to those in Classes I to III but used differently (Roberts et al. 2002) as shown in Figure 1.2.D. P450RhF, is a self-sufficient monooxygenase system (Nodate et al. 2006) and has been cloned into *E.coli* where it is capable of carrying out the oxidative bioconversion of 7-ethoxycoumarin to 7-hydroxycoumarin (umbelliferone) (Roberts et al. 2002).

Fusing constitutive parts of a P450 system to enhance the stability or activity is a concept that has been worked on since the late 1980's (Murakami et al. 1987). Hussain and Ward (2003 a; 2003 b), worked on the generation of P450SU1 and P450SU2, which are self-sufficient, single polypeptide systems. These studies in particular are highlighted as the *E.coli* BL21 Star strain, into which these systems were cloned at UCL, are the subject of the work in Chapter 3. Unfortunately, catalytic rates with fusion enzymes, while often greater than those achieved by reconstitution of isolated enzymes, remain suboptimal (Gillam 2008).

Advantages offered by self-sufficient, single polypeptide P450 systems (Class III, IV and fused), may provide a route to P450s being applied more readily to the commercial bioconversion opportunities in the near future. As yet though, there are several obstacles to be overcome before P450s can reach their unrealised industrial potential (discussed in Section 1.2.2.5).

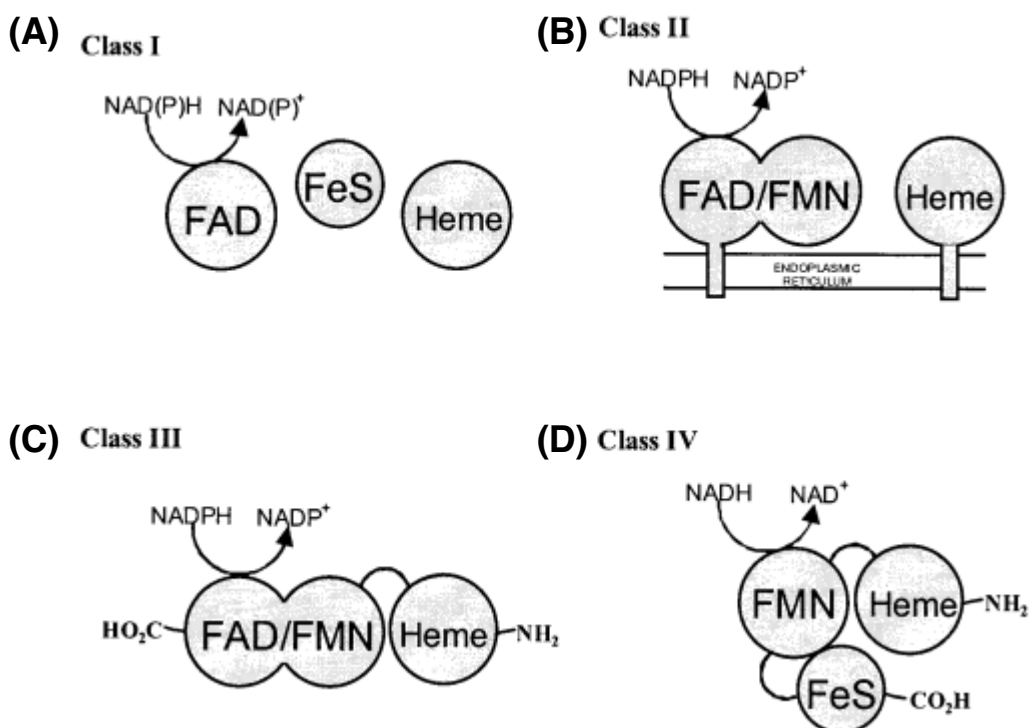


Figure 1.2. Diagrammatic representation of the four main classes of cytochrome P450, classes I to IV (A to D respectively) (taken from Roberts et al, 2002), illustrating key structural and compositional differences. In this diagram, Heme represents the P450 enzyme, FAD flavin adenine dinucleotide, FMN flavin mononucleotide and FeS ferredoxin.

1.2.2.2. Mechanism

Cytochrome P450s use energy from the conversion of NADPH to NADP⁺ and the transport of the resulting electron to perform bioconversions (Baboo 2012), including hydroxylations, oxidations, dealkylations and oxidative C-C bond cleavage (Sono et al. 1996). P450s though, are most commonly monooxygenases, which means that they incorporate a single atom of oxygen into a substrate (Guengerich 2002). This is shown in the following reaction scheme where R represents the conserved region of the substrate undergoing bioconversion (Loew et al. 1981):

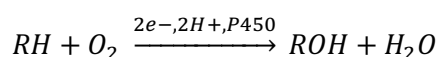


Table 1.3. Functions of cytochrome P450 enzymes by host organism (adapted from Baboo, 2012. and Bernhardt, 2006).

Host Organism	Function of P450
Prokaryotes	detoxify xenobiotics, synthesise antibiotics, fatty acid metabolism
Plants	synthesis of fatty acids and cutins
Fungi	synthesis of membrane sterols and mycotoxins
Bacteria	degradation of natural substrates
Animals	biosynthesis of steroids and hormones, detoxification

1.2.2.3. Functions of P450s

The roles of naturally occurring P450 enzymes are diverse and vary depending on the host organism. These roles in non-human organisms are summarised in Table 1.3.

In humans, P450s perform a number of roles including the metabolism of drugs, biosynthesis of steroids, oxidation of unsaturated fatty acids and stereo- and regio-specific metabolism of fat soluble vitamins (Hasler et al. 1999). In the body, some P450s act on therapeutics, preventing major side effects. It has been reported that P450 enzymes act on the majority of drugs available on the market (Sridhar et al. 2012). Examples are given in Table 1.4. Considerable research is also addressing P450s as drug targets (Guengerich 2002), due to links with production of erythropoietin (Epo) (Fandrey et al. 1990) and the onset of Chron's disease (Corcos et al. 2012).

Table 1.4. Action of selected P450s in the body on therapeutic drugs demonstrating the diversity of functions that P450s naturally undertake within the body (adapted from Wiseman 2005).

CYP	Drug (Substrate)	Action
2E1	Ethanol	Conversion to Ethanal
2C9	Warfarin	Anti-coagulant biotransformation
3A4	Saquinavir	HIV protease inhibitor biotransformation
19	Anastrozole	Aromatisation
19	4-Imidazolyl-flavans	Aromatisation
2C8	Morphine	Morphine N-demethylation
2D6	Tamoxifen	Aromatic hydroxylation

1.2.2.4. Industrial applications of P450s

There is significant commercial interest in P450s from industries including food, pharmaceuticals and cosmetics (Sakaki 2012), with the majority of research focusing on the use of P450s in developing drugs (Nettleton & Einolf 2011). In addition, predicting how cytochrome P450s will interact with drugs in the body has been a significant area of research (Zhang et al. 2009).

1.2.2.4.1. Pharmaceuticals

Early examples of P450s in commercial drug manufacturing is the production of the steroid, cortisone from progesterone in bacterial fermentation (*Rhizopus arrhizus* and *Rhizopus nigricans*) (Peterson et al. 1952), and in immobilised *Curvularia lunata* (a fungus) for the manufacture of hydrocortisone (Suzuki et al. 1993). Arguably the most successful example of industrial scale P450 bioconversion is the production of the statin pravastatin by CYP105A3 (Watanabe et al. 1995), with millions of patients treated in more than 100 countries for high cholesterol related ailments (Tsuji et al. 1997). It should be noted that some of the biggest selling blockbuster therapeutics are statins, including Lipitor®, which has cumulative sales of over \$140 Billion through 2012 (forbes.com), highlighting the potential commercial applicability of CYPs.

Additional examples include conversion of Vitamin D3 to 1 α ,25-dihydroxyvitamin D3 (Rocaltrol for treatment of hypothyroidism, osteoporosis and chronic renal failure) (Sakakis et al. 1992), and the production of leukotoxin B, indicated in a number of pathophysiologic responses in humans (Falck et al. 2001).

The full commercial potential of P450s has not yet been exploited (Kaluzna et al. 2015, Sakaki & Inouye 2000). There are a number of areas including antibiotics such as erythromycin (Shafiee & Hutchinson 1988) and tetracenomycin (Shen & Hutchinson 1994), and anti-cancer therapies, for example Taxol® (Cragg & Newman 2005; Jennewein & Croteau 2001; Croteau et al. 2006; Kirby & Keasling 2009), currently produced by culturing P450 synthesising plant cells (Roberts 2007), where P450s are being explored for industrial application (Guengerich 2002).

1.2.2.4.2. Additional Industries

There are a number of P450 bioconversions used in the manufacture of compounds for the food industry. Astaxanthin is highly valued as a colourant and food supplement synthesised by the cytochrome P450 CrtS (Alcaíno et al. 2012). Catalysis of β -carotene into xanthophylls by CYP175A1 (Urlacher & Eiben 2006) and production of the flavourant trans-carveol by CYP71D18 (Wüst & Croteau 2002) are also successful examples.

Hydroxylation of terpenes by P450s are important processes in the flavour and fragrance industries (Sakaki 2012), such as the conversion of (+)-valencene from (+)-nootkatone, a high value compound traditionally extracted from grapefruit (Girhard et al. 2009). Production of compounds for the cosmetic industry such as oxygenated fatty acids and diacids (aliphatic α,ω -dicarboxylic acids) are produced using microbial P450s (Li & Beisson 2009). One such example is the production of azelaic acid, an FDA approved treatment for rosacea and acne (Gupta & Gover 2007).

An additional application of P450s is their use in the production of transgenic plants, particularly the production of blue roses (Gillam & Guengerich 2001; Katsumoto et al. 2007) and multi-colored carnations using CYP75A (de Vetten et al. 1999; Fukui et al. 2003) both of which have been commercialised.

Cytochrome P450s have practical application in biodegradation (Guengerich 1995), notably of PCDDs (polychlorinated dibenzo-p-dioxins) and PAHs (polycyclic aromatic hydrocarbons), by-products of forest fires and various processes in the oil industry (Kumar 2010).

1.2.2.5. Challenges with use of P450s

Despite examples where P450s are employed in an industrial context (Section 1.2.2.4), there are undoubtedly issues that need to be resolved in order for P450s to reach their potential. Figure 1.3. summarises a number of suggested improvements to P450 systems needed for their successful uptake in the biotechnology sector. In particular process related issues, such as a tolerance to solvents and issues associated with oxygen demand and mass transfer when using whole cells (Wiseman 2003), which are investigated in this thesis.

Widely reported issues include enzyme instability (short half-life), complexity and low catalytic activities, as well as a common dependence on co-factors (Sakaki 2012) although research is on-going to improve the stability of P450 systems expressed in heterologous organisms (Wiseman et al. 2000).

Oxygen transfer and substrate mass transfer rates can hinder the potential for P450 application in commercial bioconversions (van Beilen et al. 2003a). Interestingly, work has been carried out whereby reduced levels of dissolved oxygen in the medium resulted in increased expression of cytochrome P450s (but importantly not activity) in both *E.coli* (Vail et al. 2005) and yeast species (Stansfield et al. 1991). Thus, technologies to facilitate rapid determination of optimal conditions for the P450 systems (production and bioconversion) would be an important advancement.

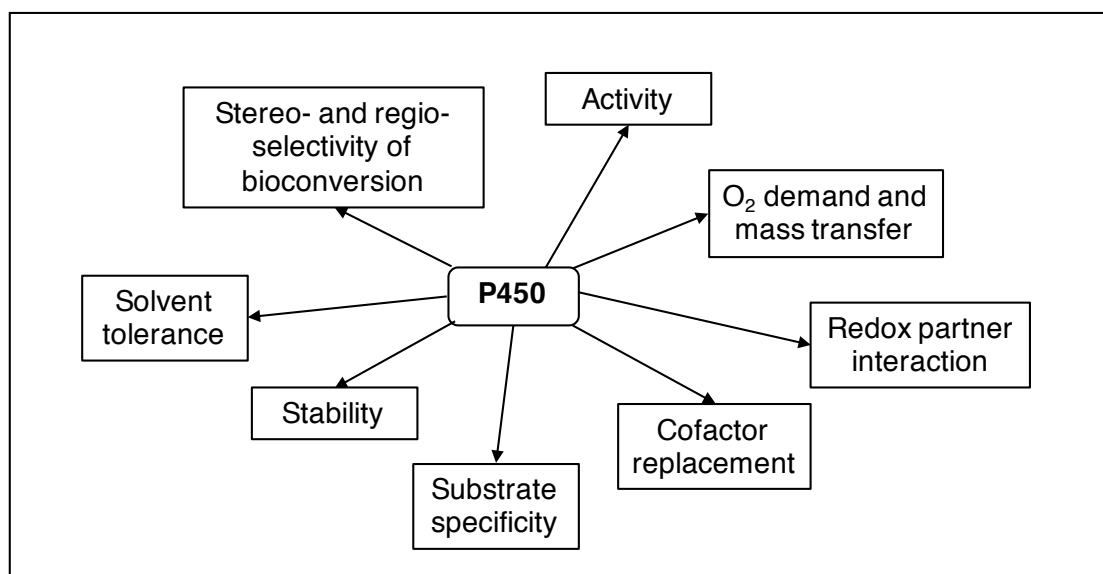


Figure 1.3. Suggested improvements to P450s to make them more suitable for commercial biotechnological application (adapted from Bernhardt, 2006).

1.2.3. Oxygen Supply to Oxidoreductive Enzymes

Sections 1.2.1.3. and 1.2.2.5. highlight a number of the key issues with biocatalysis and the use of P450s in particular. It has already been noted that whole cell systems are the preferred way to undertake P450 bioconversions, and that these have not been well characterised. One of the major limitations is oxygen mass transfer, particularly in whole cell systems due to the oxygen demand of both the organism and the bioconversion. Due to the mechanism of bioconversion, using oxygen as a substrate as well as for metabolism, oxidoreductive enzymes typically have a greater oxygen demand than equivalent microorganisms which are not undertaking these biocatalytic steps (van Beilen et al. 2003b).

1.2.3.1. Observed Oxygen Demands for Cytochrome P450s

Table 1.5. shows the oxygen demand reported for a number of P450 oxidative bioconversions. From this, conclusions can be drawn regarding the criticality of oxygen supply to CYP enzymes.

In general, it appears that hydroxylations require up to three times greater amounts of oxygen than deethylations. In addition, it can be seen that mutations in the enzyme result in differing rates of oxygen and NADPH consumption. It seems that oxygen consumption rates are generally greater than the reaction stoichiometry would suggest. This is most apparent where mutants of a single P450 are compared (Fang et al. 1997; Mayuzumi et al. 1993).

No effect is observed when comparing prokaryotic and eukaryotic host strains. Oxygen demand of a whole cell P450 biocatalyst though is significantly greater than that of a purified enzyme due to the oxygen demand for metabolism in the cell in addition to the requirement for bioconversion (Li et al., 2002). This lends further weight to the argument that these systems require more extensive characterisation. No discernible pattern is seen as a result of P450 class (I and II). Fang et al (1997) demonstrate data of particular interest as the bioconversion of 7-ethoxycoumarin to 7-hydroxycoumarin is studied in Chapter 3 of this thesis.

Limitation of oxygen supply is a serious issue associated with scale-up of oxidative bioconversions in fermentation processes (Schmidt 2005). At one time this was considered the greatest barrier to cell culture at an industrial scale (Glacken et al.

1983), however it should be noted that the issue of oxygen supply in a stirred tank bioreactor (STR) is largely considered to be resolved (Chu & Robinson 2001). Understanding oxygen demand, however, still aids with improving knowledge of the metabolism of the organism, especially critical when the importance of oxygen availability for whole cell P450 bioconversions is considered (van Beilen et al. 2003).

The oxygen transfer rate, commonly represented in the form of the combined oxygen mass transfer coefficient (k_{La}) is an important metric used during bioprocess scale up (Pessoa et al. 1996). For many years, it has been the key constant used for the scaling of fermentation processes (Marques et al. 2010, Fuchs et al. 1971), and maintaining a sufficiently high k_{La} poses a significant challenge in larger volume reactors (hundreds of m^3) (Bliem & Katinger 1988).

Table 1.5. Observed oxygen demands for a range of P450 bioconversions.

P450	Mutation	Host	Measurement Condition	O ₂ demand during bioconversion ($\mu\text{molL}^{-1}\text{min}^{-1}$)		Source
				deethylation	hydroxylation	
P450 1A2	wild type	Produced in Yeast	Purified Protein	7.5	10.2	Mayuzumi et al. 1993
	Lys99Glu			2.01	2.16	
	Arg137Leu			6.6	8.4	
	Lys401Glu			5.1	15.6	
	Lys453Glu			2.37	2.37	
	Arg455Glu			3.3	3.3	
P450 2C9	-	No info (bought purified)	Purified Protein	3.55 to 21.6	dependent on substrate and activator	Hutzler et al. 2003
P450 2B4	-	No info (bought purified)	Immobilised Purified Protein	0.96 ± 0.08	no substrate	Rudakov et al. 2008
				3.88 ± 0.12	substrate	
P450 2B1	wild type	Produced in <i>E.coli</i>	Purified Protein	3.4 ± 0.09		Fang et al. 1997
	Ile114Val			1.91 ± 0.1		
	Phe206Leu			1.04 ± 0.12		
	Val363Ala			1.18 ± 0.05		
	Val363Leu			3.54 ± 0.7		
	Gly478Ser		1.09 ± 0.15			
P450 2E1		HepG2 (Human liver carcinoma)	Whole Cell	11.7 to 48		Sakurai & Cederbaum 1998
CYP21		<i>Schizosaccharo myces pombe</i> (fission yeast)	Whole Cell	6 to 8		Dragan et al. 2006

1.2.4. Criticality of Oxygen Supply to Microbial Fermentations

The majority of the key requirements for a microbial fermentation (primary energy source, temperature and sufficient mixing for example) can be easily provided, monitored and regulated in a standard bioreactor (Schuler & Kargi 2002). However, this is significantly more difficult when using small scales (mLs and below) and high throughput bioreactor technologies. Until recently, sub optimal performance was tolerated (Duetz et al. 2000) rather than overcome.

In addition, as previously noted, oxygen demand for an organism undertaking an oxidative biotransformation is greater than for one which is not (van Beilen et al. 2003a). The extent of this difference is dependent upon the organism, the enzyme and likely also the substrate used (Mayuzumi et al. 1993). A model is suggested by Baldwin and Woodley (2006) for the oxidative bioconversion of a ketone by cyclohexanone monooxygenase (CHMO), which indicates the preferential utilisation of oxygen for oxidative phosphorylation in cellular metabolism, before use in an oxidative bioconversion. The model hypothesises the increased demand of an oxygenase containing expression system and that, with increasing concentration of enzyme, greater oxygen supply is needed to increase reaction rate.

Table 1.6. shows examples of measured Oxygen Uptake Rates (OURs) for a range of microorganisms undertaking different production processes including an *E.coli* strain which relatively speaking would appear to have a high OUR (Çalik et al. 2004). In addition, it is interesting to note the difference in OUR as a result of the production process being carried out. For example, the difference between *Pseudomonas putida* generating toluene cis-glycol (Carragher et al. 2001) and that carrying out a desulphurisation process (Gomez et al. 2006b), with the latter almost four times greater.

Table 1.7 shows the specific oxygen uptake rates, as well as the oxygen required for maintenance for a number of different expression systems. Oxygen required for maintenance is seen to vary by up to an order of magnitude for a number of these organisms including *E.coli* and *Bacillus sp.* Interestingly, a similar relationship is seen with respect to the specific OUR, and it can be speculated that this may be as a result of the environment i.e. available oxygen and nutrients as well as the resultant metabolic activity and productivity of the biomass (as indicated by the widely variation in values for yield coefficient of biomass on oxygen).

Table 1.6. Measured OUR values of different microorganisms from a range of investigations.

Organism	Product	Max. OUR observed (mmolO ₂ L ⁻¹ h ⁻¹)	Reference
<i>Escherichia coli</i>	Benzaldehyde lyase	13.0	Çalik et al. 2004
<i>Xanthomonas campestris</i>	Xanthan	4.3	Garcia-Ochoa et al. 2000
<i>Pseudomonas putida</i>	Toluene cis-glycol	3.4	Carragher et al. 2001
<i>Rhodococcus erythropolis</i>	Biodesulphurisation process	1.8-2.5	Gomez et al. 2006
<i>Pseudomonas putida</i>	Biodesulphurisation process	13.0	Gomez et al. 2006b
<i>Rhodococcus erythropolis</i>	Biodesulphurisation process	2.7	Santos et al. 2006

1.2.5. Oxygen Mass Transfer

Aerobic respiration is undertaken in most fermentation processes and so provision of sufficient oxygen is critical. In aerobic respiration, oxygen is used to convert glucose into water, carbon dioxide and energy in the form of adenosine triphosphate (ATP).

As previously noted, oxygen is regarded as the limiting substrate in many fermentations (Baldwin & Woodley 2006). Provision of enough oxygen is also necessary for efficient oxygen mass transfer from gas, to liquid to cell.

1.2.5.1. Mechanism of Oxygen Mass Transfer

Resistances to oxygen mass transfer before the molecules can be used by a cell are summarised in Figure 1.4. The two-film theory of gas absorption explains that the rate of gas absorption is controlled by the rate of diffusion through surface films on the gas-liquid boundary, a gas film surrounding the liquid, and a liquid film at the surface of the liquid (Whitman 1924). Practically speaking, in the case of a bubble with a liquid, the liquid film is controlling (Danckwerts 1951).

Table 1.7. Specific oxygen uptake rate values and associated parameters from a number of investigation in different microorganisms (microbes and yeast).

Organism	qO ₂ (molO ₂ kg X ⁻¹ h ⁻¹)	mO ₂ (molO ₂ kg X ⁻¹ h ⁻¹)	Y _{xo} (kgX molO ₂ ⁻¹)	Primary energy source (carbon)	Reference
<i>Bacillus thuringiensis (kurstaki)</i>	2-15.5	0.9	17.2	Glucose	Rowe et al. 2003
<i>Escherichia coli K12</i>	0.9-23	2.4-6.4	12.5-520	Glucose	Çalik et al. 2006
<i>Escherichia coli K12</i>	0.9-17.2	0.4-7.2	0.01-13.6	Glucose	Çalik et al. 2004
<i>Xanthomomas campestris</i>	2-15	1.0	0.6	Sucrose	García-Ochoa et al. 2000
<i>Bacillus acidocaldarius</i>	3.1-31.2	2.2-16.6	0.3-43.8	Fructose	Kocabaş et al. 2006
<i>Rhodococcus erythropolis</i>	0.2-4.3	0.8	16.4-20	Glucose, glutamic acid & citrate	Gomez et al. 2006
<i>Pseudomonas putida</i>	2-18	1.9	52.6	Glucose, glutamic acid & citrate	Gomez et al. 2006b
<i>Trigonopsis variabilis</i>	2-3	0.03	13-16	Glucose	Montes et al. 1997
<i>Phaffia rhodozyma</i>	1.9	-	-	Glucose	Liu et al. 2006
<i>Candida bombicola</i>	0.3-1	0.01	4.4	Glucose	Casas 1996
<i>Hansenula anomala</i>	0.8	-	-	Glucose	Djelal et al. 2012
Biomass molecular formula (CH_{1.79}O_{0.5}N_{0.2})	-	1.0	20.3	Glucose	Heijnen & Roels 1981

1.2.5.2. Volumetric Mass Transfer Coefficient ($k_L a$)

The volumetric mass transfer coefficient, $k_L a$ is the product of ' k_L ', the liquid-phase mass transfer coefficient, and ' a ' the specific gas-liquid interfacial area, which individually are very difficult to measure. Gas bubbles are generated in different sizes and with different properties as a result of several factors including thickness of the liquid, which in turn varies depending on hydrodynamic conditions. This results in widely differing ' k_L ' and ' a ' values for each bubble. As such, the combined term $k_L a$ is determined empirically (Andrew 1982).

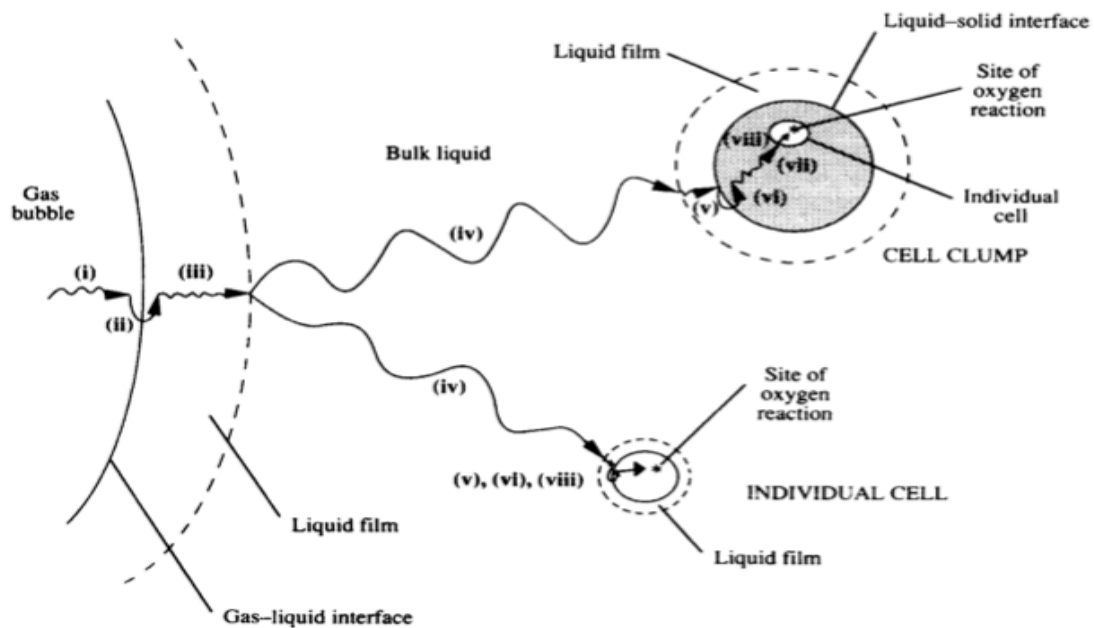


Figure 1.4. Steps for transfer of oxygen from gas bubbles to cell (reproduced from Doran, 1995). The stages are represented as (i) transfer of oxygen molecules from inside the bubble to the gas-liquid interface, (ii) transfer across the gas-liquid interface, (iii) diffusion through the liquid film around the gas bubble (iv) oxygen transfer through the bulk liquid, (v) diffusion through the liquid film surrounding cells, (vi) transfer across the liquid-cell interface, (vii) diffusion through the solid mass to the cell (if cells are in a clump or solid particles), (viii) finally, transport across the cytoplasm for utilisation at the site of reaction.

The rate of oxygen transfer can be calculated using Equation 1.1. (Doran 1995):

$$\frac{dC_L}{dt} = OTR = k_L a \cdot (C^* - C_L) \quad \text{Equation 1.1.}$$

Where, OTR is the rate of oxygen transfer ($\text{mmolL}^{-1}\text{h}^{-1}$), $k_L a$ is the volumetric mass transfer coefficient (h^{-1}), C^* is the saturated dissolved oxygen concentration (mmolL^{-1}), C_L is the dissolved oxygen concentration in the liquid (mmolL^{-1}).

1.2.6. Factors Influencing Oxygen Mass Transfer

There are a large number of factors that influence $k_{L,a}$ in a stirred bioreactor. These factors are physical, operational and equipment specific, including volumetric gas flow rate, agitation, composition of medium, bubble size, temperature, foaming and antifoams. These are regarded as the factors of greatest influence and so are discussed more extensively in this section and summarised in Table 1.8. Furthermore, each of the factors are considered individually and little comment is made as to how they impact on one and other.

1.2.6.1. Supply of Gas

1.2.6.1.1. Volumetric Gas Flowrate

Figure 1.5 shows the typical relationship between air flow rate and $k_{L,a}$. $k_{L,a}$ increases rapidly to begin with but the magnitude of the rise decreases until around 1.0 vvm. After this point, and up to 1.5 vvm good $k_{L,a}$ values are seen as a result of high levels of available oxygen (Stanbury et al. 1995). Beyond this (>1.5 vvm), $k_{L,a}$ tends to decrease as excessive air flow rate results in flooding of the impeller region, meaning that the impellers are unable to disperse the bubbles efficiently.

Several works have endeavoured to generate empirical descriptions for avoiding flooding of the impeller region, and these are summarised in Table 1.9.

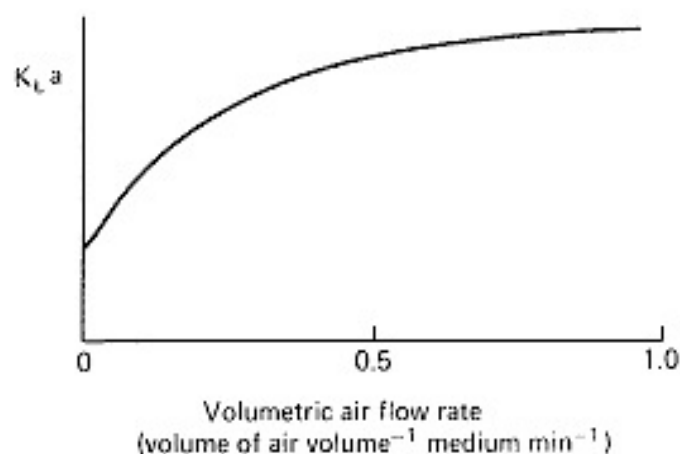


Figure 1.5 Effect on $k_{L,a}$ in a mechanically agitated bioreactor as a result of changing airflow rate (Stanbury, Whitaker and Hall, 1995).

Table 1.8. A brief overview of factors that affect $k_{L,a}$.

Factors affecting $k_{L,a}$	Increase $k_{L,a}$	Decrease $k_{L,a}$
Volumetric airflow rate	Up to 1.5 vvm, $k_{L,a}$ increases, due to increased levels of oxygen. Optimum $k_{L,a}$ s are achieved with agitation speed at maximum level before flooding impeller region	>1.5 vvm leads to flooding of the impeller region, which hinders bubble dispersion and break-up
Agitation	Improved bubble breakdown and dispersion as well as reduced bubble thickness, all improve $k_{L,a}$.	In extreme cases can lead to foaming, requiring antifoam, which reduces $k_{L,a}$.
Composition of medium	Decreasing viscosity increases $k_{L,a}$, due to thinner film around bubbles and improved mixing, Salts in media reduces bubble coalescing, increasing interfacial surface area and gas hold up	Increase viscosity traps small bubbles, increases bubble film thickness and reduces oxygen availability. High salt concentrations may cause bubbles to become detrimentally small
Bubble size	Small bubbles have large interfacial surface areas and long gas hold-up time, increasing $k_{L,a}$.	Bubbles smaller than 3 mm are very rigid reducing k_L . When smaller than 1 mm, oxygen concentration equilibrates rapidly and bubbles become lodged in viscous systems.
Temperature	Between 10-40°C, diffusivity of oxygen increases with rising temperature.	Above 40°C, solubility decreases dramatically, decreasing $k_{L,a}$.
Foaming and antifoam		Adding antifoam reduces $k_{L,a}$ due to its mechanism as a surfactant, foaming traps bubbles and has an overall worse effect on the bioprocess
Pressure	Increased pressure increases the saturation concentration of oxygen in water and hence increases the mass transfer driving force and therefore $k_{L,a}$.	Increasing pressure increases the solubility of all gases, including CO ₂ , that at high levels may be toxic to cells.

1.2.6.1.2. Bubble Size

Bubble size is also affected by agitation, and this will be commented on in section 1.2.6.2. Bubble size directly affects interfacial surface area and therefore the area available for oxygen transfer. Hence it is one of the key factors influencing k_La . Smaller gas bubbles have a larger interfacial surface area, which usually results in a higher k_La . Bubbles with diameters below 1mm become problematic as they rapidly become depleted of oxygen, removing any relationship between gas hold up and oxygen transfer (McGinnis & Little 2002, Heijnen & Roels 1981). Gas hold up refers to the time a bubble will spend in the bulk fluid, hence slow rising velocity increases time available for oxygen transfer (Doran 1995). In bubbles less than 3mm in diameter, it is noted that surface tension is the dominant influencer on the behaviour of the bubble, meaning that bubbles have little to no internal gas circulation. This directly results in a detrimental effect on k_L , reducing overall k_La (Doran 1995).

A change in gas composition to anything above 21% (atmospheric) will change the partial pressure and therefore increase the driving force which causes O_2 mass transfer (Garcia-Ochoa & Gomez 2009).

1.2.6.2. Hydrodynamics

Typically, greater agitation rates result in larger k_La values. This was demonstrated by Yagi and Yoshida (1975) and further commented on by Doran (1995).

Stanbury *et al* (1995) highlighted a number of reasons for this relationship. Most significantly, agitation disrupts bubbles, increasing the number of bubbles in the medium and decreasing their mean size, resulting in larger interfacial surface area for oxygen transfer. In addition, greater agitation hinders gas bubbles in their passage from sparger to the surface of the liquid, hence a greater residence time and therefore more time available for oxygen transfer to occur. Furthermore, gas bubbles are prevented from coalescing as a result of agitation of the liquid. This acts to prevent the k_La from decreasing due to decreasing interfacial surface area, rather than actively increasing it. Finally, agitation creates a turbulent hydrodynamic environment in the culture liquid. As a result, the liquid film at the gas-liquid interface becomes thinner, which leads to a reduced diffusion distance for oxygen transfer, hence greater k_La values.

Table 1.9. Summary of research into empirical descriptors for avoiding flooding of the impeller region in a stirred bioreactor.

Reference	Criteria
Westerterp et al. 1963	Apply minimum impeller tip speed between 1.5-2.5ms ⁻¹
Biesecker 1972	Maintain energy dissipated by the gas flow rate below that dissipated by the impeller
Van't Riet & Tramper 1991	As above but only applied to lower section of bioreactor where gas dispersion is affected
Feijen et al. 1987	Flooding avoided if: $F_s/ND^3 < (0.3)N^2D/g$ where F_s is the volumetric flow rate (m ³ .s ⁻¹), N is the impeller rotational speed (s ⁻¹) and D is the impeller diameter

1.2.6.3. Medium Composition

A number of medium-related factors also affect k_La and hence OTR. The starting composition of the media affects rheology e.g. with the inclusion of viscous components, but also the changing properties of the fermentation culture as it progresses. During culture, increasing biomass concentration as well as the formation and secretion of extracellular molecules result in a change in the broth properties, including the rheology. Values of k_La therefore vary significantly between fermentations (Stanbury et al. 1995). Although the exact effect of rheology on individual fermentation would require specific experimentation, the general effect of rheology on k_La is known.

Newtonian fluids have negligible effects on oxygen transfer, however non-Newtonian fluids (which is more often the case in fermentation processes at high cell densities) can influence oxygen transfer significantly. The result of a viscous culture on k_La values will be detrimental, due to the reduced availability of oxygen and the increased resistance to oxygen transfer because of the thick layer surrounding the gas bubbles (Doran 1995). The relationship between k_La and viscosity in a fermentation, was reported by Buckland *et al* (1988) to be inversely proportional to the square root of the viscosity, as shown in Equation 1.3. This is supported by Steel and Maxon(1966)

as well as Wang and Fewkes (1977), who concluded that oxygen was not efficiently transferred in viscous fluids.

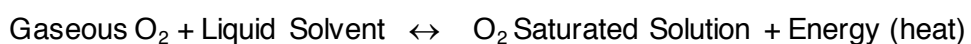
$$k_L a \propto \frac{1}{\sqrt{\text{Viscosity}}} \quad \text{Equation 1.3.}$$

The electrolyte concentration of the medium also has an impact on the solubility of oxygen, and therefore a significant influence on oxygen mass transfer (Maier & Büchs 2001). Higher concentrations of ionic compounds result in reduced oxygen solubility (Weisenberger et al. 1996) and lower mass transfer coefficients (Zieminski & Whittemore 1970). In providing the necessary media components and supplements for cell growth and bioconversion, a negative effect can be impacted upon the oxygen transfer capabilities.

Foam formation is common in mechanically agitated fermentation systems. Excessive foaming can result in longer bubble residence times, depleting the oxygen in bubbles, detrimentally affecting their ability to transfer oxygen (Hall 1973). Chemical surfactants are most commonly used for reducing foam build up, however due to the mechanism of action of most surfactants (reducing the mobility of the gas liquid interface), these commonly have a negative effect on $k_L a$. (Hall 1973). Interestingly, van't Riet and van Sonsberg (1992) showed that although antifoams cause the break up of bubbles, they favour coalescence, meaning that the interfacial surface area of the bubbles decrease, reducing $k_L a$. However, both result in a detrimental effect on oxygen transfer.

1.2.6.4. Temperature

Temperature affects both the oxygen solubility and diffusivity, each of which affect mass transfer in opposite ways. As temperature increases, the solubility of oxygen in solution tends to decrease. The enthalpy of solutions can be used to demonstrate why increasing temperature is detrimental to the solubility of oxygen (Kotz et al. 2014). With energy added, there is a tendency towards gaseous O_2 i.e. reduced level of oxygen in solution as shown. This in turn reduces the $k_L a$ value.



←—————
Energy added, equilibrium tends

The diffusivity of oxygen though increases as temperature rises in the range of 10-40°C. Up to this point, the effect is usually greater than that of oxygen solubility, increasing the overall k_La . However, above 40°C, the solubility of oxygen drops dramatically, overcoming the positive diffusive effect and adversely effecting mass transfer in the system (Doran, 1995).

The influences of each of these factors on oxygen mass transfer has been discussed and due to the fact that they would all appear to be capable of significantly impacting on k_La it would be pertinent to investigate more extensively the interrelationships between these factors, and how they may effect fermentation systems. These relationships are studied in Chapters 4 and 5.

1.2.7. Oxygen Mass Transfer in Small Scale and Single Use Systems

The use of microliter scale technologies has increased in recent years particularly in early stage bioprocess development and strain screening (Marques et al. 2009), mainly due to the advantages offered in terms of low reagent volumes, reduced cost and increasing speed of process design and development (Lye et al. 2003). Availability of oxygen to the microorganism is a major limitation for microbial fermentations at all scales (Baldwin & Woodley 2006). This issue is greater if the expression system is also performing an oxidative bioconversion. This is due to oxygen being needed as a substrate for the enzymatic conversion process (e.g. that studied in Section 3 of this thesis) in addition to its growth and maintenance (Li et al. 2002). Thus, understanding oxygen mass transfer capabilities of scale down systems is of critical importance.

1.2.7.1. Microtiter Plates Types and Geometries

Achieving suitable hydrodynamics within shaken microwells is vital for ensuring a homogeneous environment suitable for growth and biotransformation. However this can be difficult in miniaturised culture vessels (Weiss et al. 2002). This section will draw reference to the demands of an organism carrying out an oxidative bioconversion (Section 1.2.3.), the conditions in various types of microwell and the factors influencing these. Furthermore, whether the available oxygen transfer rates are suitable for the purpose of microbial growth and biotransformation using an oxygenase enzyme is assessed.

Microwell plates come in a range of sizes, geometries and materials. Numbers of wells per plate range from 6 to 1536 (Kumar et al. 2004); commonly used configurations include the 96 and 24 deep square well (DSW) formats, the 24 round well format and the 96 round well format. The geometries of wells in some of these layouts is shown in Figure 1.6. Also included are the maximum well volumes and the cross sectional area, corresponding to the area in contact with the environment and available for oxygen transfer while the microtitre well is stationary i.e. the minimum area available for gas-liquid mass transfer.

The maximum Oxygen Transfer Rate (OTR_{max}) in round microwells is dependent primarily on the specific mass transfer area available (a), a product of the shaking intensity and dimensions of the well (Hermann et al. 2003), but mass transfer coefficient (k_L) remains at a constant value regardless of the shaking intensity. Round wells also result in oxygen transfer rates of between 25 and 50% of those in square vessels with similar diameters, depending on shaking amplitude (Duetz & Witholt 2004). The corners of square wells act with similar effect to baffles, causing a significant increase in oxygen transfer rate and $k_L a$ values (Hermann et al. 2003).

The effect of changing well size and shaking diameter is shown in Table 1.10. Square deep wells, of either 18mm or 50mm squared, have been shown to generate oxygen transfer rates of approximately $40-60 \text{ mmolO}_2\text{L}^{-1}\text{h}^{-1}$. From Tables 1.6. and 1.7. it can be suggested that this would be sufficient for undertaking oxidative bioconversions, but could not maintain a culture of high biomass concentration.

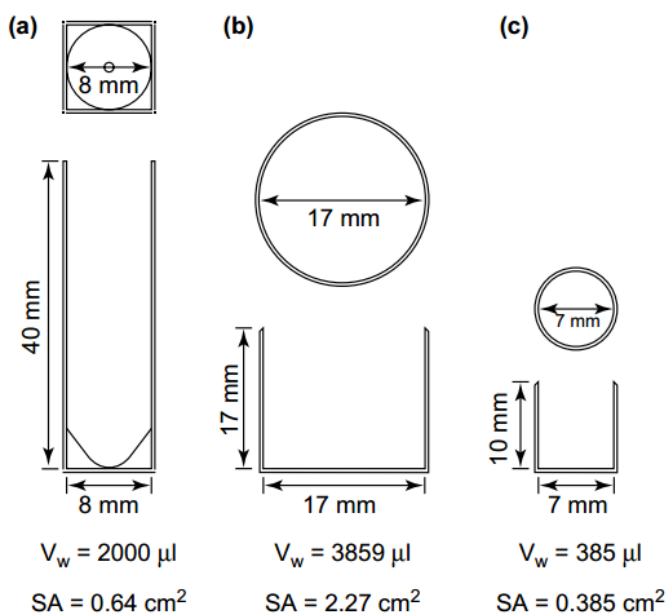


Figure 1.6. Geometries of some common microwell formats including maximum well volumes and surface areas when stationary. 96 DSW (a), 24 round well flat bottom (b) and 96 shallow round well flat bottom (c) geometries are included. Interestingly, surface area to volume ratios are not consistent, although this is implicated as an important indicator of available gas-liquid oxygen mass transfer (adapted from Doig et al, 2002).

It can also be seen that miniaturisation of the wells beyond the 96 DSW format results in a 25-56% reduction in the achievable OTR. It is suggested that this is a result of the increased adhesive and capillary forces acting on the liquid, when compared with larger vessels. Doig *et al* (2005) also suggested that this is due to the air-liquid surface area (and therefore the area available for oxygen mass transfer) being greatly diminished. Work is ongoing into novel well designs (e.g. flower shaped cross sectional area) (Funke et al, 2010), with some suggestion that the flower shaped wells provided greatest oxygen mass transfer rates.

1.2.7.1.1. Factors Influencing Mass Transfer in Microwells

The predominant factors available for influencing mass transfer at microscales are the shaking frequency, the shaking diameter and the fill volume (Maier & Büchs 2001). Shaking frequency in particular has a threshold (critical shaking frequency) which must be overcome in order to achieve effective O₂ mass transfer. It has been shown that, particularly in round microtiter wells, surface tension of the liquid is the parameter which affects the gas-liquid oxygen transfer and hydrodynamics most (Hermann et al. 2003).

Equipment to equipment variation is inherent to bioprocesses at all scales (as yet there is little standardisation), and this influences a number of important parameters (Shivhare & McCreath 2010). The apparatus used in shaking for example will influence the diameter of the shaker orbit, and therefore the hydrodynamics and the efficiency of mass and heat transfer (Schäpper et al. 2009). Schäpper *et al*, also noted that temperature control within the microtiter environment can be challenging, due to large surface area to volume ratios. Additionally, materials of construction used in the production of microtiter plates can affect the oxygen saturation and transfer characteristics (Vogelaar et al. 2000). This results from the impact on the superficial tension of the culture medium (Hermann et al. 2003).

Gas liquid mass transfer has been demonstrated to increase with greater shaking diameter and frequency (Henzler & Schedel 1991). This is because the culture can overcome the critical shaking frequency and increase the maximum oxygen transfer rate. Table 1.10. highlights this, showing that a 50mm orbit compared with 25mm, results in potentially quadrupling OTR.

Well fill volume was shown to influence oxygen transfer rate for growth and oxidative bioconversion (Baboo et al. 2012), with higher fill volumes being shown to have a potentially detrimental effect on achievable biomass concentration. The use of a seal is often employed in order to protect against evaporation and prevent cross well contamination (Ferreira-Torres 2008), with potential for reducing O₂ availability a concern.

1.2.7.1.2. Observed Oxygen Mass Transfers in Microwells

A number of studies have been undertaken to characterise the k_La for these systems under some of the conditions discussed in section 1.2.7.1.1. Examples of are summarised in Tables 1.10. and 1.11. In addition, Figure 1.7. shows the results of a study into the effect of shaking diameter and agitation rates in 96 deep square well plates (Hermann et al. 2003).

The data highlight a reasonably good agreement between studies as to the oxygen mass transfer capabilities of microwell plates. These are maximum observed values and they do not match the values that traditional stirred bioreactors and even a number of single use bioreactors are capable of (Table 1.13).

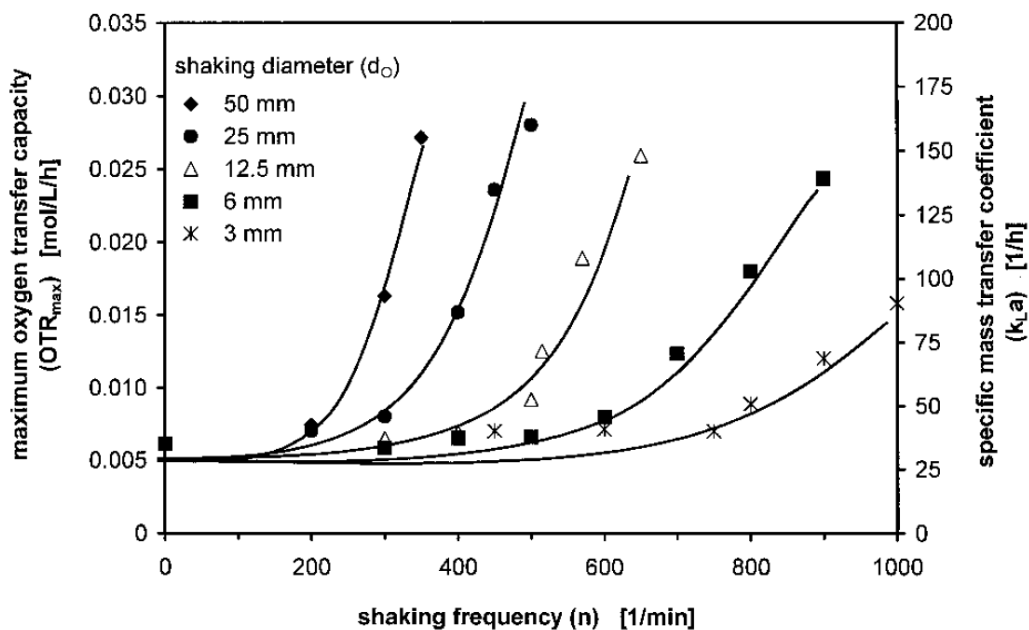


Figure 1.7. Maximum oxygen transfer rate and oxygen mass transfer coefficient in 96 deep square well microtiter plates at different shaking diameters and frequencies. Taken from Hermann et al (2003).

Table 1.10. The effect of changing well size and shaking diameter on oxygen transfer rate during orbital shaking at 25°C and 300rpm. (^a shaking diameter) (adapted from Duetz & Witholt, 2004).

Well Size (mm x mm)	Volume (mL)	Oxygen Transfer Rates (mmolO ₂ L ⁻¹ h ⁻¹)	
		25mm ^a	50mm ^a
Square Wells			
4 x 4	0.125	6.7	25.4 ± 5.9
8 x 8	0.5	15.2 ± 2.4	33.6 ± 4.4
18 x 18	2.5	39.3	50.5 ± 3.5
50 x 50	19.5	47.7	58.1
Round Wells			
6.6 (diameter)	0.26	5.0	16.4

Table 1.11. Examples of maximum measured k_{La} values in different microwell formats using a number of methods of oxygen mass transfer determination.

Plate Format	k_{La} determination method	Max. k_{La} observed (s^{-1})	Reference
24DSW	fluorescent sensors and gassing out method	0.096	Marques <i>et al</i> , 2009
96DSW	oxygen limited growth	0.052	Doig <i>et al</i> , 2005
24DSW	fluorescent sensor and dynamic gassing out	0.068	Islam <i>et al</i> , 2008
24DSW	fluorescent sensor and oxygen balancing	0.069	Kensy <i>et al</i> , 2005
96DSW	optical sensor and static gassing out	0.1	Zhang <i>et al</i> , 2008
24DSW	optical sensor and static gassing out	0.028	Zhang <i>et al</i> , 2008

1.2.7.2. Erlenmeyer Flasks

Shake flasks are, and for many years have been, widely used in bioprocess development (Erlenmeyer 1860), particularly for generation of seed material and screening evaluation of large numbers of genetic constructs and media compositions (Klöckner & Büchs 2012; Gaden 1962). Oxygen mass transfer in shake flasks is widely regarded to be poor, with the inclusion of baffles (sometimes referred to as denting) an example of one step taken to overcome this (Peter *et al* 2006; Mcdaniel *et al*. 1965; Smith & Johnson 1954). However until recently it has been difficult to monitor oxygen levels and therefore gain a robust understanding of oxygen mass transfer (Section 1.2.8).

The development of non-invasive optical sensors by companies such as PreSens GmBH and Fluorometrix (Stow, MA) have meant that similarly to traditional polarographic probes in stirred bioreactors, oxygen can now be monitored online during culture in shaken Erlenmeyer flasks and microwells, with this data used for determination of oxygen mass transfer coefficients. Gupta and Rao (2003) showed k_{La} values of $0.0086 s^{-1}$ and $0.0164 s^{-1}$ in non-baffled and baffled 250mL flasks respectively. They also demonstrated that this could be matched by limiting the capabilities of a bench top STR and similar growth kinetics observed. Some

additionally determined k_{La} values in shake flasks are highlighted in Table 1.12. These values are approximately equivalent to the higher values seen in microtiter plates.

1.2.7.3. Additional and Supplementary Technologies

Until recently, stirring and sparging in miniaturised bioreactors was considered impractical, with the improvement of oxidative conditions focused on the optimisation of orbital shaking parameters and well geometries for microtiter plates (Duetz 2007). In the last decade though, a number of alternative technologies have been developed and are either nearing, or have recently reached commercial availability.

Examples include the Micro24 system from Pall Corporation (based on a 24 round well geometry) which offers sparged gas supply controlled to individual wells, as well as online monitoring and control of dissolved oxygen (DO), pH and temperature. This platform has been demonstrated as an accurate scale down mimic of a 2L stirred tank bioreactor (Chen et al. 2009). Additionally, the M2P Biolector system, which also offers pH, DO and temperature monitoring has been characterised (Funke et al. 2010).

In addition, the RAMOS (respiratory activity monitoring system) is available for the online measurement and analysis of respiratory gases, enabling real time measurement of oxygen transfer and carbon-dioxide evolution rates. The system has been demonstrated to work with microbial and mammalian expression systems (Anderlei et al, 2004)

Table 1.12. Examples of oxygen mass transfer values determined for shaken Erlenmeyer flasks in the literature.

Erlenmeyer flask geometry	Method	Max. k_{La} observed		Reference
		(s^{-1})	(h^{-1})	
500mL	Sulphite oxidation	0.040	144	Henzler & Schedel 1991
500mL	Sulphite oxidation	0.027	97.2	Veljkovic et al. 1995
500mL	Dynamic gassing out (polarographic probe)	0.020	72.0	Suijdam et al. 1978
250mL Baffled	Non-invasive sensors	0.016	59.2	Gupta & Rao 2003
250mL Unbaffled	Non-invasive sensors	0.009	30.8	Gupta & Rao 2003

The Ambr[®]250 system from Sartorius Stedim Biotech, operating automated single use fermentation cultures up to 250ml. A Rushton turbine impeller, feed addition ports, gassing and monitoring capabilities provide a mimic of a production scale bioreactor (Hart 2013). This system is noted to be capable of a k_{La} up to $500h^{-1}$ (Bareither et al. 2013). Interestingly, many of the developments of note in recent times have concentrated on the monitoring and provision of oxygen and adequate hydrodynamics in the culture media, an indicator of how important these parameters are as drivers for improvements in fermentation development. Major advances in culturing technologies (e.g. Micro24 and Ambr[®]250 systems) have removed the issue of surface moderated oxygen transfer.

1.2.7.4. Single Use Bioreactors (SUBs)

The use of SUBs is becoming more prevalent in industry for use in pre-clinical, clinical and production scale manufacturing in biotechnology (Eibl et al. 2010). SUBs are being used as alternatives to traditional stainless steel bioreactors as the benefits of doing so are significant, including operation without the need for clean in place (CIP) and sterilise in place (SIP) steps, reducing turnaround times, resources, waste generation, validation, space and cost of goods as well as capital expenditure (Gallagher 2007).

However, there are also limitations with single use bioreactor systems including scalability (beyond 2000L), materials compatibility (most notably the concern over extractables and leachables), availability of specialised components and regulatory and validation concerns (Whitford 2010). Although less significant an issue in some reactor designs, oxygen transfer is commonly poor and prediction of k_{La} is unreliable. Enhancing oxygen transfer and prediction of k_{La} is highly desirable in industry, hence SUB designs mimicking traditional STRs as closely as possible are being developed and becoming increasingly prevalent.

Increasing interest and adoption has meant a rise in the number of SUBs in development. These differ with regards to the scale of the container, the design geometry, the instrumentation and the power input (Eibl et al. 2010). There are three main categories of SUBs; non-mechanically agitated bag (such as the Wave[™] bioreactor), mechanically agitated bag (such as the Xcellerex Disposable Reactor (XDR) and rigidly moulded bioreactors that closely mimic STRs, such as the Ambr[®]250 system. Each will be looked at briefly here for their advantages and disadvantages, as

well as exploring what is currently commercially available. Additionally, the mechanically agitated and moulded SUBs will be used in this thesis (Section 5), as non-mechanically agitated bioreactors are beyond the scope of this research.

1.2.7.4.1. Single Use Bags

There are two categories of single use bag. The 'pillow' type, such as the Wave™ bioreactor, which is held in place on a rocking platform (Figure 1.8A), responsible for generating the mixing and therefore the oxygen mass transfer (Shukla & Gottschalk 2013). Achievable oxygen mass transfer was initially seen to be poor, with neither the 2 or the 20L bags exceeding a k_{La} of 4 hr^{-1} (Singh 1999). Though this is satisfactory for early stage mammalian culture, it would not be sufficient for microbial expression systems. Recently, Oosterhuis *et al* (2013) have noted that they were able to achieve k_{La} values of up to 300 h^{-1} using the CELLtainer system with a two-dimensional rocking motion. This would be more appropriate for microbial fermentation.

The alternative form of single use bag is based on a bag, fitted into a frame or cage, inflated before filling and then mixed with mechanical agitation, typically an impeller driven either by a motor or magnetically (Figure 1.8B). There are numerous examples of these bioreactors commercially available including the BioStat Cultibag (Sartorius Stedim), the Appliflex (Applicon), the XDR system (Xcellerex) and the Hyclone SUB STR (ThermoFisher). Studies have highlighted the ability of these SUBs to match the performance of traditional cell culture bioreactors (Werner *et al.* 2010; Brecht 2009), Again there is little investigation for microbial fermentation, but to say that Dreher *et al* (Dreher *et al.* 2013) demonstrated the potential for using the BioStat Cultibag STR system for *E.coli* fermentation, however this did require highly adapted feeding and gassing strategies.

1.2.7.4.2. Single Use Bioreactors of Rigid Construction

Single use bioreactor geometries are becoming increasingly similar to traditional stirred tank bioreactors. Initially this was with the transition from one and two-dimensional rocking bags to mechanical agitation of cylindrical bags within a rigid frame. The next stage was the introduction of single use bioreactors of rigid construction which would hold a number of advantages for microbial fermentation. The potential for increased airflow rates due to higher pressures in the vessel, and

improvement in sensing technologies (Isett et al. 2007; Diehl et al. 2015) would both be beneficial.

An early commercially available SUB STR of rigid construction was the Mobius CellReady, which operates a marine impeller within a 3L vessel and is capable of oxygen mass transfer coefficients in the region of 70h^{-1} (Nienow et al. 2013). Additional data including maximum achievable impeller tip speeds of $<0.5\text{ms}^{-1}$ (Millipore, 2009 technical data sheet) indicates suitability for mammalian processing, but not microbial expression systems.

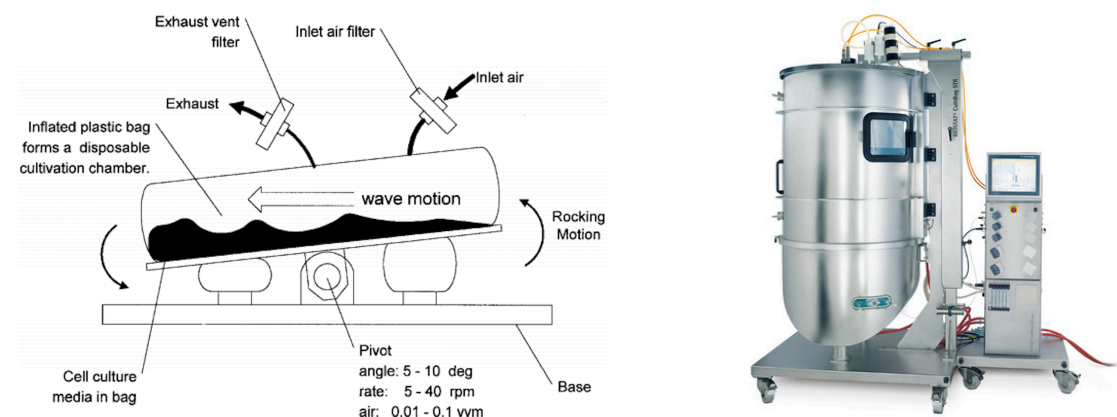


Figure 1.8. WAVE Bioreactor (A) and BioStat Cultibag STR (B). Images courtesy of Singh, 1999. and Sartorius.com respectively.

The original Ambr[®]15 system is a small (15mL) 24 or 48-way parallel bioreactor system designed specifically for mammalian processing, achievable k_La values of less than 20h^{-1} (Nienow et al. 2013). More recently, Sartorius have developed a fermentation version of the Ambr[®]15 which uses a Rushton style impeller and implements feeding and pH control pumping (Stedim 2016). The Ambr[®]250 is the larger scale (up to 250mL working volume) offering, and is geometrically similar to larger scale STRs (Grebe et al. 2014) with a high oxygen mass transfer coefficient (up to 500h^{-1}) (Bareither et al. 2013). Two configurations are available, one of which is specifically designed for microbial fermentation (two, six-blade Rushton turbine impeller), with the system itself designed for 12 or 24 parallel fermentations with automated sampling.

1.2.7.4.3. Observed Oxygen Mass Transfers in SUBs

Table 1.13. summarises the range of commercially available SUB technologies and their capabilities. Most importantly it highlights that some of the recently available SUBs are able to provide sufficient OTRs to support microbial fermentation including an oxidative bioconversion.

Table 1.13. Configuration and oxygen mass transfer capabilities of commercially available single use bioreactors in literature.

Reactor	Working Vol. (L)	Bag type	Mixing type	k_{La} (h ⁻¹)
Wave Bioreactor™	1-200	Pillow	Rocking	<10
CELL-tainer®-20	0.2-2.5	Pillow or Square	2D Rocking	>400
CELL-tainer®-200	5-200	Pillow or Square	2D Rocking	>400
BIOSTAT Cultibag	50-200	Tankliner	Stirred	>150
HyPerforma SUB	30-300	Tankliner	Stirred	>600
XDR SUB (mamm.)	10-2000	Tankliner	Stirred	<20
Mobius® Cell Ready	50-200	Tankliner	Stirred	<70
Ambr®15	0.01-0.015	Moulded PC STR	Stirred	<20
Ambr®250	0.1-0.25	Moulded PC STR	Stirred	≤500

Table adapted from Oosterhuis *et al*, 2013. Bareither *et al*, 2013. Nienow *et al*, 2013 and Jones 2015. PC STR – Polycarbonate Stirred Tank Bioreactor. This table is expanded upon in Chapter 5 based on the findings of the work in this section.

1.2.8. Common Correlations for Oxygen Mass Transfer

A number of correlations have been empirically developed for the relationship between $k_L a$, power consumption and superficial gas velocity. The equation can be generally expressed as:

$$k_L a = C \cdot (P_g/V)^\alpha \cdot V_s^\beta \quad \text{Equation 1.4.}$$

Where, P_g is the gassed power consumption (W), V_s is the superficial gas velocity ($\text{m}\cdot\text{s}^{-1}$) and C , α and β are empirical factors specific to the system under investigation

Over the last 40 years, a number of studies have determined the coefficients of the correlation, however there is significant disagreement between reports (as shown in Table 1.14.). Bartholomew (1950) demonstrated that the correlation is dependent on the scale of the reactor, which accounts for some of the differences between values, but as already discussed (Section 1.2.6.) there are a number of factors which affect $k_L a$ which these correlations do not take into account.

After evaluation of similar experiments and their correlations, Van't Riet (1983) concluded that for coalescing air-water dispersion systems, the values fall within 20-40% when $C = 0.026$, $\alpha = 0.4$ and $\beta = 0.5$. Therefore, the empirical correlation proposed was:

$$k_L a = 0.026 \cdot (P_g/V)^{0.4} \cdot V_s^{0.5} \quad \text{Equation 1.5.}$$

Table 1.14. Some commonly reported correlations for $k_L a$ in stirred tank reactors (2-2600 L).

Investigated fluid	Correlation with coefficients	Reference
Air-water with ions	$k_L a = 0.224(P_g/V)^{0.35} V_s^{0.52}$	Gill et al. 2008
Air-water with ions	$k_L a = 0.002(P_g/V)^{0.7} V_s^{0.2}$	Van't Riet 1979
Air-water-sulphite solution	$k_L a = 0.007(P_g/V)^{0.94} V_s^{0.65}$	Vilaça et al. 2000
Air-water	$k_L a = 0.01(P_g/V)^{0.699} V_s^{0.581}$	Linek et al. 2004
Air-water	$k_L a = 0.01(P_g/V)^{0.475} V_s^{0.4}$	Smith 1977
Air-water	$k_L a = 0.031(P_g/V)^{0.4} V_s^{0.5}$	Zhu et al. 2001
Yeast suspension	$k_L a = 1.645(P_g/V)^{0.5} V_s^{0.64}$	Ni et al. 1995

Van't Riet (1983) went on to describe the correlation of a non-coalescing (salt/ions containing) air-water system (Equation 1.6.), though this solution is more comparable to fermentation media, the properties are such that the correlation could not be directly applied:

$$k_L a = 0.002 \cdot (P_g/V)^{0.7} \cdot V_S^{0.2} \quad \text{Equation 1.6.}$$

From these correlations, it can be seen that $k_L a$ is larger for water without salt/ion. However, $k_L a$ tends to be larger in actual fermentation broth. This can be attributed to the concentration of salt, the non-Newtonian behaviour of cultures and the presence of antifoams, cells and nutrients, none of which are taken into account here. As a result, empirical correlations give a misleading representation of $k_L a$ in a vessel. Nevertheless, the correlations are sufficient for use as a guide prior to experimental determination (Stanbury et al. 1995). There is a need for modelling of oxygen mass transfer landscapes which can be applied to a broad range of experimental conditions, and ideally bioreactor types and scales. This is investigated experimentally in Chapter 5.

1.2.9. Techniques for O₂ Mass Transfer Quantification

Experimental methods have been developed over time to try and accurately quantify oxygen mass transfer in bioreactors of all scales and geometries. Some of the most commonly used are gassing out techniques, gas analysis, sulphite oxidation and oxygen limited growth. Each is discussed here, and summarised in Table 1.15.

1.2.9.1. Static Gassing Out

Gassing-out techniques involve the measurement of change in dissolved oxygen tension (DOT) in a solution during aeration and agitation at known rates (Estrada et al 2014, Stanbury et al. 1995). During static gassing out, the solution is stripped of oxygen by applying nitrogen gas. The liquid is then aerated and agitated and the increase in DOT measured using a probe (Wise 1951).

The following equation describes the increase in DO concentration (C_L):

$$dC_L/dt = k_L a \cdot (C^* - C_L) \quad \text{Equation 1.7.}$$

which, when integrated gives:

$$\ln(C^* - C_L) = -k_L a \cdot t \quad \text{Equation 1.8.}$$

where C^* is the saturation concentration of dissolved oxygen. As such, $\ln(C^* - C_L)$ can be plotted against time such that the gradient is equal to $-k_L a$, as shown in Figure 1.9A.

1.2.9.2. Dynamic Gassing Out

In the dynamic gassing out method the fermentation broth is deoxygenated using the respiratory activity of respiring organisms. A linear decrease in DO concentration is achieved. Once the fermentation broth reaches a sufficiently low oxygen threshold (typically <5%) the bioreactor is aerated and rise in DO concentration is measured as in the static gassing out method (Bandyopadhyay et al. 1967).

The increase in DO concentration over the period BC, shown in Figure 1.9B, is the difference between oxygen transfer into the solution and the uptake of oxygen by the respiring culture (Stanbury et al. 1995). This change is expressed by the following equation:

$$\frac{dC_L}{dt} = k_L a \cdot (C^* - C_L) - xQ_{O_2} \quad \text{Equation 1.9.}$$

where, x is the concentration of biomass and Q_{O_2} is the specific respiration rate (moles of oxygen kg^{-1} biomass s^{-1}). The value of xQ_{O_2} is obtained from the gradient of line AB in Figure 1.9B. $k_L a$ can be found as the negative reciprocal of the gradient, on the plot shown in Figure 1.9C.

1.2.9.3. Gas Analysis

The amount of oxygen transferred into the solution (difference between oxygen in and oxygen out) is directly measured during fermentation. OTR is then determined directly using the following equation (Wang et al. 1979):

$$OTR = (7.32 \times 10^5 / V_L) \cdot (Q_i \cdot P_i \cdot Y_i / T_i - Q_o \cdot P_o \cdot Y_o / T_o) \quad \text{Equation 1.10.}$$

where V_L represents the broth volume in the vessel (in dm^3), Q_i and Q_o volumetric airflow rates at air inlet and outlet respectively ($\text{dm}^3 \cdot \text{min}^{-1}$), P_i and P_o the total pressure at the air inlet and outlet (in atm), T_i and T_o the temperature of the gases at air inlet and outlet (in K) and Y_i and Y_o the mole fraction of oxygen at the inlet and outlet.

k_{La} is then calculated using the equation:

$$k_{La} = OTR / (C^* - C_L) \quad \text{Equation 1.11.}$$

Although monitoring the living culture directly, there are a number of limitations to this method. Firstly, invasive probes are needed as well as large volumes and gas flows. Additionally, measurements can only be made when cells are actively consuming oxygen and the measurements themselves are limited by the oxygen analyser equipment used (Garcia-Ochoa & Gomez 2009).

1.2.9.4. Sulphite Oxidation

The sulphite oxidation method, originally described by Cooper *et al* (1944) is based on the reaction of sodium sulphite with dissolved oxygen in the presence of a catalyst (typically a copper or cobalt cation). The basic reaction is shown in Equation 1.12. The reaction is limited by the rate of oxygen mass transfer, and therefore by sampling the reaction and monitoring the rate, the rate of oxygen mass transfer can be calculated using a plot of sulphite concentration over time and the Equation 1.13.



$$-dC_{Na_2SO_3} / dt = 2 k_{La} \cdot C^* \quad \text{Equation 1.13.}$$

Although used in a large number of experimental determinations of oxygen mass transfer (Dussap *et al.* 1985; Ogut & Hatch 1988; Thibault *et al.* 1990; Yang & Wang 1992; Benadda *et al.* 1997; Garcia-Ochoa & Gomez 1998; Liu *et al.* 2006), there is a significant limitation in that the physicochemical properties of the liquids used are fixed and differ greatly from fermentation broths, resulting in differences (particularly bubble size) which lead to unrealistically high k_{La} values (Van't Riet, 1979). It was noted by Maier *et al* (2001) that an update on this method was needed and that the assumption that the concentration of oxygen in the sulphite solution is zero is in fact incorrect and leads to a significant underestimation in the k_{La} . A simple adjustment of data to account for one or the other would therefore not be sufficient to correct for these errors.

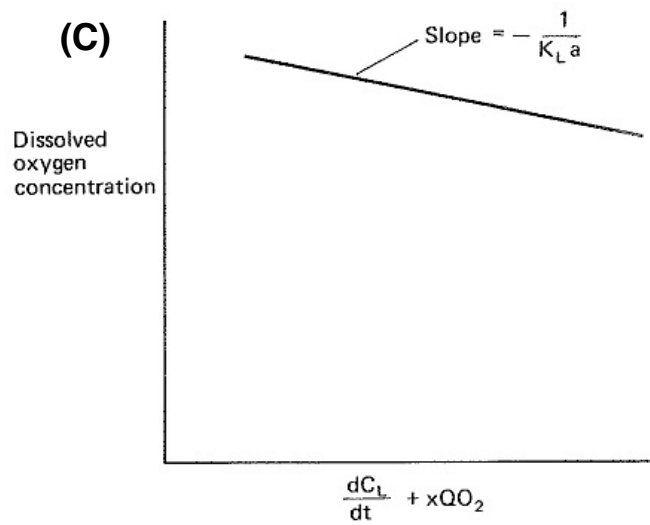
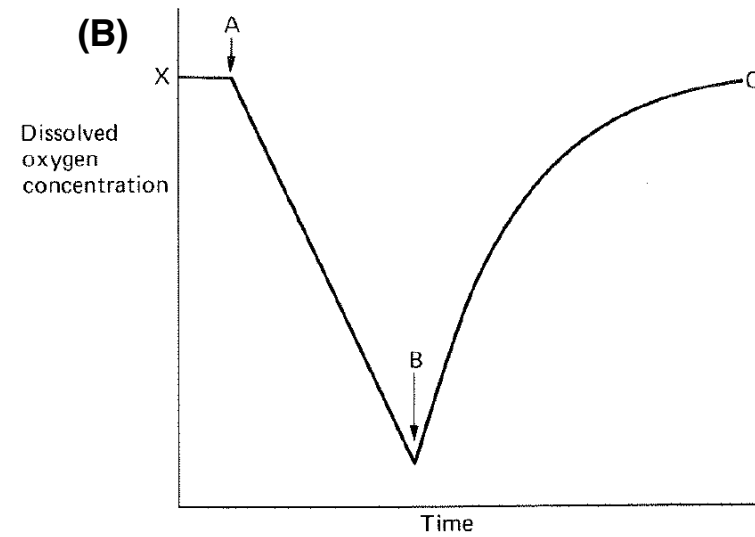
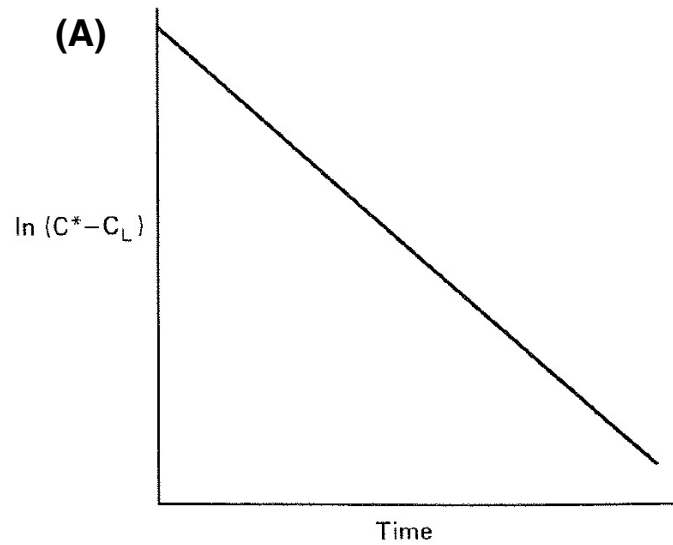


Figure 1.9. Plot of $\ln(C^* - C_L)$ vs. time (A), where the gradient is equal to $-k_L a$. %DOT vs. time (B), as generated during the dynamic gassing-out method, aeration was ceased at point A and then pumped back in from point B. Finally, a plot of C_L against $dC_L/dt + xQO_2$ (C) produced by taking the tangent from figure 1.9B BC at given values of C_L . This gives a straight line with a gradient of $-1/k_L a$.

1.2.9.5. Oxygen Limited Growth

Using a strict aerobic microorganism (i.e. one that cannot respire anaerobically), the oxygen mass transfer coefficient can be determined using the growth profile of the culture. Duetz *et al* (2000) demonstrated this in 96 deep square well microtiter plates using *P. putida* and observed k_{La} values of up to $188h^{-1}$. The growth rate during oxygen limited growth is determined and a conversion factor applied in order to calculate OTR (equal to k_{La} in this oxygen limited environment).

Although this method has the advantage of measuring the oxygen mass transfer directly during culture, making it more likely to provide representative values, there are a number of limitations. It is experimentally laborious in comparison with other techniques, but the greater issue is that significant assumptions about growth kinetics are required e.g. that the growth rate under oxygen limited conditions remains constant during the measurement period.

1.2.10. Design of Experiments (DoE)

A Design of Experiments (DoE) approach to experimentation will be used throughout this work and so it is important to introduce the basic concepts here. These will be expanded on at appropriate points later in the thesis.

Traditional experimentation is based around a 'one-factor-at-a-time' (OFAT) approach, where all but a single factor are fixed while an optimal level for the factor under investigation is determined (Czitrom 1999). There are a number of drawbacks to this approach including a high number of experimental runs and resource demand for a limited gain in terms of understanding the system, potential experimental bias based on legacy information influencing experimental factors and levels, and no guarantee that the best value for each individual factor will result in the optimum set of conditions for the system as a whole due to a failure to consider interactions (Montgomery 2017; Lendrem et al. 2015).

The multifactorial approach however, interrogates the entirety of the experimental space without bias, investigating factors and levels in parallel in order to determine, through iteration, a true optimum. DoE is a structured approach for determining cause and effect relationships which can be applied to any process with measurable inputs and outputs (Anderson & Whitcomb 2007). Additional advantages include a reduction in cost and resource demand for an experimental campaign (Barker & Milivojevic 2016). Figure 1.10. highlights the difference in approach between the OFAT and DoE methodologies for a simple three-factor investigation,

including a summary of the experimental demands.

Although employed in many industries, in particular the process industries for many years (Anderson & Whitcomb 2007), use of DoE in biology is less established. This is surprising considering the complexity of biological systems, and the advantages that DoE offers in terms of identifying the influence of interacting factors.

Depending on the objective of the experiment, different types of experimental design are available which offer distinct advantages and disadvantages of their own. Specific design and model approaches will be discussed and justified in the chapters where they are applied.

Table 1.15. Brief overview of the different methods for measurement of the oxygen mass transfer coefficient and their advantages and disadvantages for determination of k_{La} .

Method	Advantages	Disadvantages	References
Static gassing-out	Quick, can be used with actual fermentation media	Delay in probe response time causes error which needs to be adjusted for, method is limited to reactors with height <1 m, point sampling	Van't Riet (1979) and Rodriguez, <i>et al.</i> , (2014)
Dynamic gassing-out	Quick, low cost, k_{La} measured with live cells, OUR of cells can be determined	All of those seen for static method, limited range for DO measurement (due to respiring cells), not simple to operate	Van't Riet and Tramper (1991) and Doran (1995)
Oxygen balancing	Steady-state oxygen conc. measured, so probe response time is not an issue, simple operation and data available online	Oxygen solubility must be known (accurately, and conversion to engineering units), point sampling, only suitable for small-scale	Wang, <i>et al.</i> , (1979) and Doran (2013)
Sulphite Oxidation	Simple to operate, long established and well understood	Physiochemical properties of the solutions results in misleading values, assumptions may also result in misleading k_{La} values	Van't Riet (1979), Maier <i>et al</i> (2001)
Oxygen limited growth	Applied to live culture	Laborious and significant kinetic assumptions required	Duetz <i>et al</i> (2000)

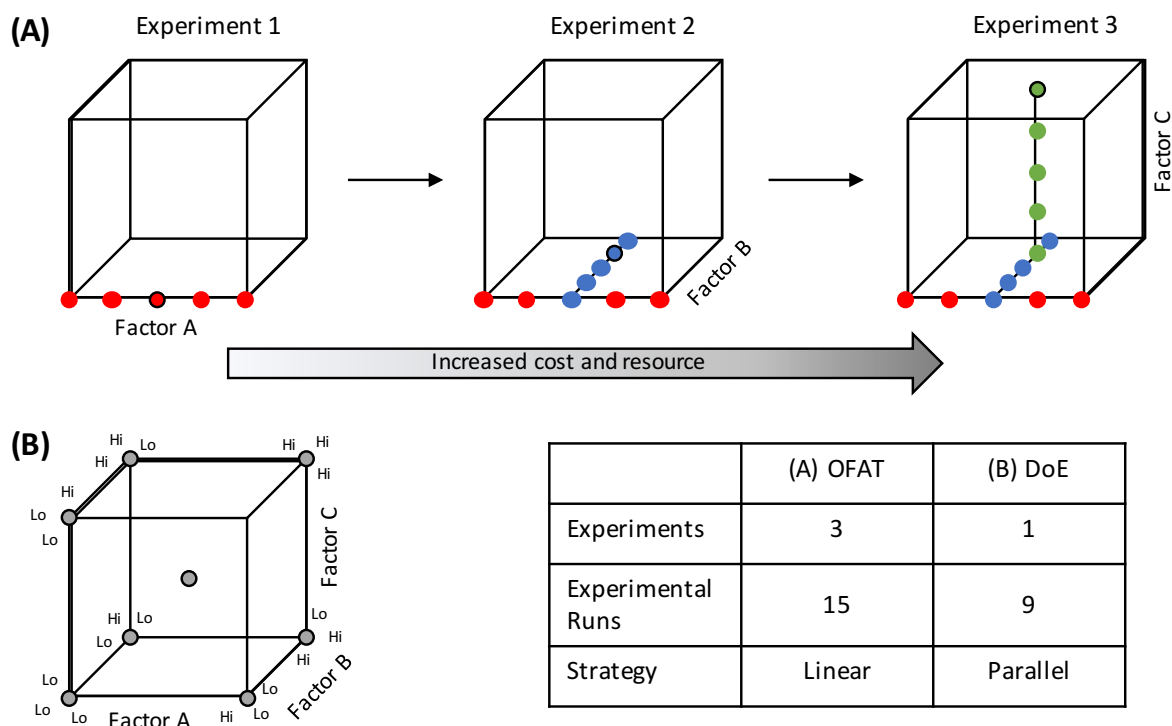


Figure 1.10. Comparing one-factor-at-a-time (OFAT) (A) and Design of Experiments (DoE) (B) experimental approaches in a simple experiment in which three-factors are investigated.

1.3. Aims and Objectives

Biocatalysis is a field that holds considerable potential within biotechnology. It is currently implemented in a broad range of industrial manufacturing processes, but with a market size and applications which are growing rapidly (Section 1.2.1).

With the advancement of genetic engineering techniques and the emergence of areas such as synthetic biology (Section 1.1), the range of enzymes that can be expressed using microbial organisms is constantly expanding. Combined with the fact that microbes are relatively cheap and simple to grow (Section 1.2.4.), fermentation is a potential route to the manufacture of high value products which until recently had not been available. Expression and bioconversion using oxidative biocatalysts in particular appear to be an area of great potential, with a broad range of industrial processes either employing or trialling these already (Sections 1.2.1.2 and 1.2.2.4).

Oxygen is the terminal electron acceptor in aerobic metabolism, meaning it plays a crucial role in growth and generation of secondary metabolites and recombinant molecules. The oxygen demand of microbial expression systems (Section 1.2.4), not only due to their fast doubling times, is significantly higher than most other cell types, meaning that the demand placed on a fermentation system during culturing is somewhat greater than for alternative expression systems (e.g. mammalian cells).

Oxygen mass transfer is a complex and multi-faceted issue. There are a broad range of factors that have been demonstrated to have an influence on mass transfer, including bioreactor hydrodynamics, fluid rheology, the composition of supplied gas and environmental factors such as temperature (Section 1.2.6). The effect that these have changes greatly relative to one and other, however research to date has focused on using an OFAT approach, testing parameters independently. Understanding these factors and how they impact upon oxygen mass transfer, both individually and in combination with one and other, is critical in determining which bioreactor technologies are appropriate for culturing microbial expression systems, and to what extent they can be expected to scale (up or down) to other technologies. As such, this thesis will use a multi-factorial approach (Section 1.2.10.), investigating factors simultaneously in order to quantify potential interactions.

There have been a number of techniques developed for the determination of oxygen mass transfer coefficients (Section 1.2.9). These include gassing out methods (both static and dynamic), sulphite oxidation and oxygen limited growth, all of which have significant limitations, and so improved quantification methods are needed. In addition, a number of empirical correlations have been developed over the past 40 years using these methods. These correlate oxygen mass transfer capabilities with specific bioreactor types and geometries, under highly specific conditions. This specificity makes it extremely difficult to ascertain the capacity of a system for oxygen mass transfer without experimental determination for a particular explicit configuration. Development of multifactorial models, which have been rigorously examined for their statistical validity, provide a means by which this can be overcome.

High throughput scale down systems (in particular microtitre plates) are of critical importance for early stage bioprocess development and strain screening (Section 1.2.7). However, little work has been undertaken on accurate quantification of the oxygen mass transfer capabilities of these systems, meaning they are potentially underutilised and their use as an accurate scale up mimic is currently limited.

Single use bioreactors are gaining momentum in industrial bioprocessing due to their versatility, reduced turnaround times and minimisation of validation requirements for steps such as cleaning (Section 1.2.7.4). There are a range of different geometries and configurations commercially available depending on the demands of the process. However, few of these technologies are available at micro- to millilitre scales, with recent advancements such as the Ambr®250 one of a limited number of systems capable of providing an environment akin to that of a traditional STR. As such it is vital that cheaper, more widely adopted technologies are evaluated for their applicability to microbial fermentation. In addition to a lack of characterisation with respect to oxygen transfer capabilities, an additional limitation on single use bioreactor technologies is cost, and evaluating the resource demand of a disposable system. This is significantly more complex than with a traditional bioreactor system as, not only are there a large number of consumables to be replaced after each run, but each fermentation could conceivably be completely different to its predecessor.

Multifactorial methods such as design of experiments (DoE) have been applied in a number of industries including chemical manufacture for decades, however to date they are underutilised in biocatalysis. This is a surprising scenario, as the investigation of multiple factors simultaneously would seem ideally suited to a field as complex as biology, where there is a large amount of interdependence and in many ways a lack of understanding with regards to the biology itself.

The overall **aim** of this thesis therefore will be to determine the applicability of commercially available SUB technologies for microbial fermentation, particularly those undertaking oxidative bioconversions. This will involve evaluation of some widely used scale down technologies as well as of some larger, pilot scale single use bioreactors in order to determine their applicability with regard to microbial fermentation. All work will be undertaken using multifactorial DoE methodologies with a number of different modelling strategies (e.g. optimisation, predictive landscapes) in order to comprehensively characterise the experimental space and determine the validity of the models developed and conclusions drawn.

- The initial objective was to establish a multifactorial methodology and strategy to optimise microbial fermentation in terms of growth and (oxidative) biocatalytic productivity in microwells. This optimised process would then be scaled into bench top stirred tank bioreactors so as to experimentally determine the maximum oxygen demand under different operating strategies. A whole cell P450 monooxygenase (P450SU2) in *E.coli* was used as a model system due to the potential commercial

applicability, challenges regarding provision of sufficient oxygen and the previous work done with this enzyme (Section 1.2.2). These findings could then be used to evaluate the relative rates of oxygen utilisation for cell maintenance, growth and bioconversion. The results of this work are described in Chapter 3.

- The second objective is to improve the current level of understanding and to improve the accuracy of oxygen mass transfer rate quantification in microwell plates. An improvement on the traditional dynamic gassing out method will be developed based on the limitations observed in the literature (Section 1.2.9.). This will improve understanding of the mechanism of oxygen mass transfer in plates by evaluating the truly dynamic nature of the fermentation culture, and endeavour to capture the change in environment across a multifactorial experimental design, rather than under a selection of individual, idealised scenarios. Additionally, an attempt will be made to achieve equivalent culture performance across different plate formats (from 96 to 24 DSWs) using the methodology developed here. The results of this work are presented and discussed in Chapter 4.
- Subsequently, it will be necessary to evaluate the oxygen transfer capabilities of several commercially available SUB systems to undertake microbial fermentation by interrogating their oxygen mass transfer capabilities. The SUBs will be characterised in comparison with a traditional bench top STR, across multifactorial experimental landscapes which will comprise a range of widely used fermentation conditions, both in terms of the mechanical process parameters, but also the commonly overlooked media aspects. The results of this work are elaborated in Chapter 5.
- Once the validity of using a single use bioreactor system for microbial fermentation was established, the final objective was to develop a tool for evaluation of the economic feasibility and sensitivity. This tool will approximate the consumables and resource commitment for a single fermentation run and estimate the associated cost, allowing it to be used for project costing and a rapid cost benefit analysis of a given fermentation investigation against the anticipated outputs. The results of this work are deliberated in Chapter 6.

In addition to the above, Chapter 2 describes the materials, equipment and experimental methods used during this work; in particular operation and control of a number of fermentation systems, including the Ambr[®]250 high throughput and the New Brunswick BioFlo 310. Methodologies developed throughout the work are included in Chapters 3 to 7. Conclusions and suggestions for future work building on these studies are discussed in Chapter 7.

2. Materials and Methods

2.1. Introduction

The chapter describes the materials and methodologies used in this research. Section 2.2. outlines the materials used, while Section 2.3. describes the equipment used, with a focus on the bioreactors investigated. Section 2.4. outlines the general experimental methods including preparation of fermentation media both for culturing and oxygen mass transfer investigation and establishing master and working cell banks. Section 2.5. covers the experimental methods used for optimisation and scale up of a whole cell oxidative bioconversion using multifactorial methods, while Section 2.6. outlines the methods used for developing an accurate oxygen mass transfer characterisation methodology. Section 2.7. describes the methods used for oxygen mass transfer characterisation in single use bioreactors. Finally, Section 2.8. details the analytical equipment and methods used throughout this thesis.

2.2. Materials

2.2.1. Chemicals

7-ethoxycoumarin (99.45%), 7-hydroxycoumarin ($\geq 98\%$), yeast extract (premium grade), tryptone, glycerol ($\geq 99\%$), glycerol solution (84-89%), ampicillin sodium salts ($> 91\%$), 5-aminolevulonic acid (ALA) ($\sim 98\%$), iron III chloride (FeCl_3) (97%), isopropyl- β -D-1-thiogalactoside (IPTG) ($\geq 99\%$), polypropylene glycol (PPG), potassium phosphate monobasic (KH_2PO_4) ($\geq 98\%$), potassium phosphate dibasic (K_2HPO_4) ($\geq 98\%$), poly-propylene glycol, acetonitrile and trifluoroacetic acid (TFA) (99%) were obtained from Sigma-Aldrich Company Ltd (Poole, UK). Chloramphenicol ($\geq 99\%$) was obtained from Fluka (Poole, UK). Sodium chloride (general purpose grade) was obtained from Fischer Scientific (Loughborough, UK).

2.2.2. Microorganisms

E. coli BL21 Star (DE3) pLysS [pQR368] expressing the cytochrome P450 monooxygenase P450SU2 were generously provided by J.Baboo (Department of Biochemical Engineering, University College London, UK), having been described previously by Hussain and Ward (2003).

E. coli Top10 expressing CometGFP from DNA2.0 was kindly provided by Synthace Ltd. (London, UK).

2.3. Equipment

2.3.1. Bioreactors

Three stirred tank bioreactors are used during this work: a BioFlo 310 from New Brunswick (Eppendorf, Germany), an XDR-10 single use bioreactor from Xcellerex (GE Healthcare, USA) and an Ambr[®]250 bioreactor system from TAP biosystems (now Sartorius-Stedim Biotech, GmbH, Goettingen, Germany). Table 2.1 highlights the key properties of the three bioreactors. The major engineering characteristics of the reactor types, with regard to oxygen mass transfer, are compared in the following sections.

2.3.1.1. Gas Supply

One of the most important factors for oxygen mass transfer in terms of reactor design is the supply of gas, and the main source of this is through sparging (Kaster et al. 1990). Each of the bioreactors interrogated have different sparger types which influence the gassing capabilities, including flowrates, bubble size and residence times (Bareither et al. 2013, Minow et al. 2014, New Brunswick Scientific, 2008).

The BioFlo 310 has a perforated ring sparger which enables a wide range of gas flowrates (up to 10Lmin⁻¹) and supplies gas directly to the impeller region resulting in good bubble breakup and distribution. For maximising oxygen mass transfer this would be the preferred arrangement. The Ambr[®]250 has an open tube sparger, meaning that bubble size at the sparger tip is more strongly controlled by gas flow rate, and breakup of bubbles and their distribution is reliant on having a well-mixed environment. The XDR differs again, with four frit spargers positioned directly below the impeller, this allows the control of flowrate and bubble size from the gas inlets (as any combination of the four spargers can be used).

2.3.1.2. Geometries

The XDR and the BioFlo have similar reactor geometries (aspect ratios of 1.47 and 1.46 respectively), while the Ambr[®]250 has a higher ratio at 2.0. The impeller ratios (D_i/D_v) of the two reactors containing Rushton impellers are similar, 0.29 for the BioFlo and 0.33 for the Ambr[®]250, which is close to the figure classically seen for STRs employing Rushton turbines (Chisti & Moo-Young 2001). The pitch blade impeller however has a higher ratio (0.41), most likely to try and gain optimal mixing and gas distribution with the less shear intensive impeller design.

2.3.1.3. Impeller Configurations

Both the BioFlo and the Ambr[®]250 are fitted with dual, six blade Rushton turbine impellers, highly effective at energy input and dissipation (and therefore bubble distribution) and more common in microbial bioreactors where shear stress is not such a concern and oxygen demands are higher. The pitch blade impeller used in the XDR is much less effective at bubble breakup however the positioning directly over the impellers and the use of different pore sizes on the frit spargers should aid in overcoming this.

2.3.1.4. Probe Type and Data Recording

The determination of oxygen mass transfer rates rely heavily on the sensors used to measure dissolved oxygen (Najafpour 2015). As such it is important to comment on the type of probes used in each reactor type and how this information is recorded. Both the XDR and the BioFlo use traditional polarographic probes, while the Ambr[®]250 employs a DO sensor spot (PreSens Precision Sensing GmbH, Germany) and optical sensor, and although probe response time is taken into consideration for calculations, to directly compare, ideally this would not change between reactors.

Additionally, each of the reactor types uses proprietary software whereby the interrogation of the data requires exporting in different file formats and use of an additional software package to compile structured data tables which can then be analysed. The recording of dissolved oxygen tension is carried out at different frequencies (every 12 seconds for the Ambr, up to 8 seconds for the BioFlo). This arrangement also requires significant reworking of the raw data.

2.3.1.5. Bioreactor Configurations

Each of the reactor types have different configurations with respect to their physical and engineering characteristics. Although some properties are shared, each of the bioreactors differs in terms of either their geometry or the gassing and mixing set up. Based on these arrangements, the limitations of the system set up (including agitation speed and gas flow restrictions), and using literature information and prior knowledge, the oxygen mass transfer capabilities of each of the reactors relative to one and other can be hypothesised.

The BioFlo 310 is likely to provide the greatest $k_L a$. It is configured with the preferred combination of features for oxygen mass transfer with Rushton impellers, perforated ring

sparger and the polarographic probe. It is also reasonable to expect that the Ambr[®]250 will provide good oxygen mass transfer with the impeller type and ratio similar to that of the BioFlo and the potential for high agitation and airflow rates. The main properties which may restrict the k_{La} are the open tube sparger and the optical probe, although good mixing and repeat readings to give confidence in the data should limit the effect of these.




The XDR10 however, has an inferior impeller type, limitations on the airflow rates (due to the plastic bag construction and maximum pressure), and agitation rates, and although the frit sparger has the potential for ensuring small bubbles at entry to the culture this is unlikely to overcome the other restrictions and so the rate of oxygen mass transfer is likely to be low (relative to the BioFlo and the Ambr).

2.3.2. Additional Culture Vessels and Equipment

100 and 500mL glass Erlenmeyer flasks (unbaffled) and 100 and 500mL polycarbonate Erlenmeyer flasks (baffled and unbaffled) were supplied by Corning (NY, USA). A Kuhner Shaker X Orbital shaker (Kuhner, Basel, Switzerland) and Thermomixer Comfort (Eppendorf, Hamburg, Germany) were used for orbital shaking of culture vessels. 1.5 and 2.0mL sterile Eppendorf tubes, 96 Deep Square Well (DSW) plates and 24 Deep Square Well (DSW) plates were obtained from Starlab (UK) Ltd (Milton Keynes, UK). 24 Deep Square Well Oxodish Plates were supplied by PreSens.

Analytical equipment is described in Section 2.8.

Table 2.1. Properties and geometries of the three bioreactors in which oxygen mass transfer rates are investigated. Images courtesy of New Brunswick BioFlo310 Guide to operations, Bareither et al, 2013 and GE life science XDR-10 data sheet.

Bioreactor Image	Properties	
 <p data-bbox="204 887 344 913">BioFlo 310</p>	Total volume (L)	7.5
	Diameter (vessel): D_v (m)	0.23
	Height (vessel): H_v (m)	0.41
	Diameter (impeller): D_i (m)	0.08
	Aspect ratio: (H_v/D_v)	1.46
	Impeller ratio: (D_i/D_v)	0.29
	Impeller type	2 x 6-blade Rushton turbine
	Sparger type	Perforated ring
 <p data-bbox="204 1379 312 1406">XDR-10</p>	Total volume (L)	10
	Diameter (vessel): D_v (m)	0.32
	Height (vessel): H_v (m)	0.47
	Diameter (impeller): D_i (m)	0.13
	Aspect ratio: (H_v/D_v)	1.47
	Impeller ratio: (D_i/D_v)	0.41
	Impeller type	Single, base mounted 4x pitch blade
	Sparger type	4x frit sparger of 2x pore size
 <p data-bbox="204 1821 344 1848">Ambr[®]250</p>	Total volume (L)	0.25
	Diameter (vessel): D_v (m)	0.06 (at base)
	Height (vessel): H_v (m)	0.12
	Diameter (impeller): D_i (m)	0.02
	Aspect ratio: (H_v/D_v)	2.0
	Impeller ratio: (D_i/D_v)	0.33
	Impeller type	2 x 6-blade Rushton turbine
	Sparger type	Open tube

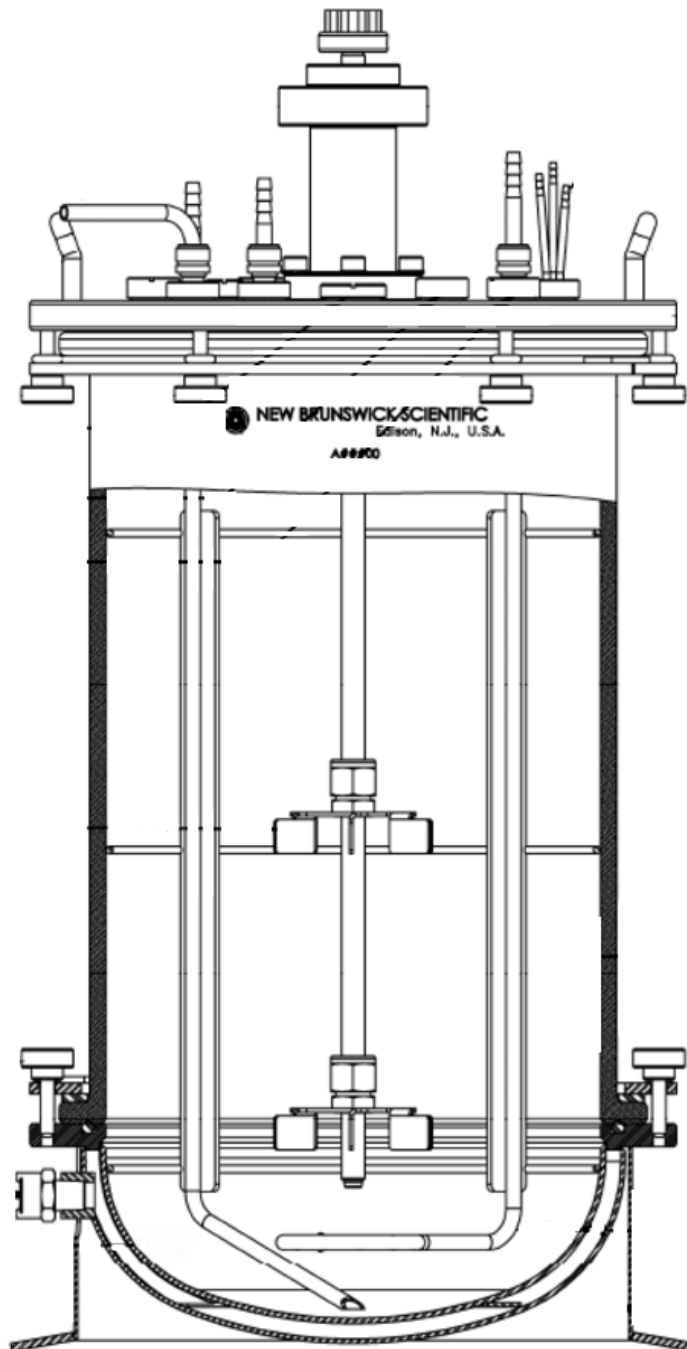


Figure 2.1. Mechanical drawing of New Brunswick BioFlo310 stirred tank bioreactor. Additional information on dimensions and configuration of the bioreactor can be found in Table 2.1. (image courtesy of the New Brunswick BioFlo310 guide to operations).

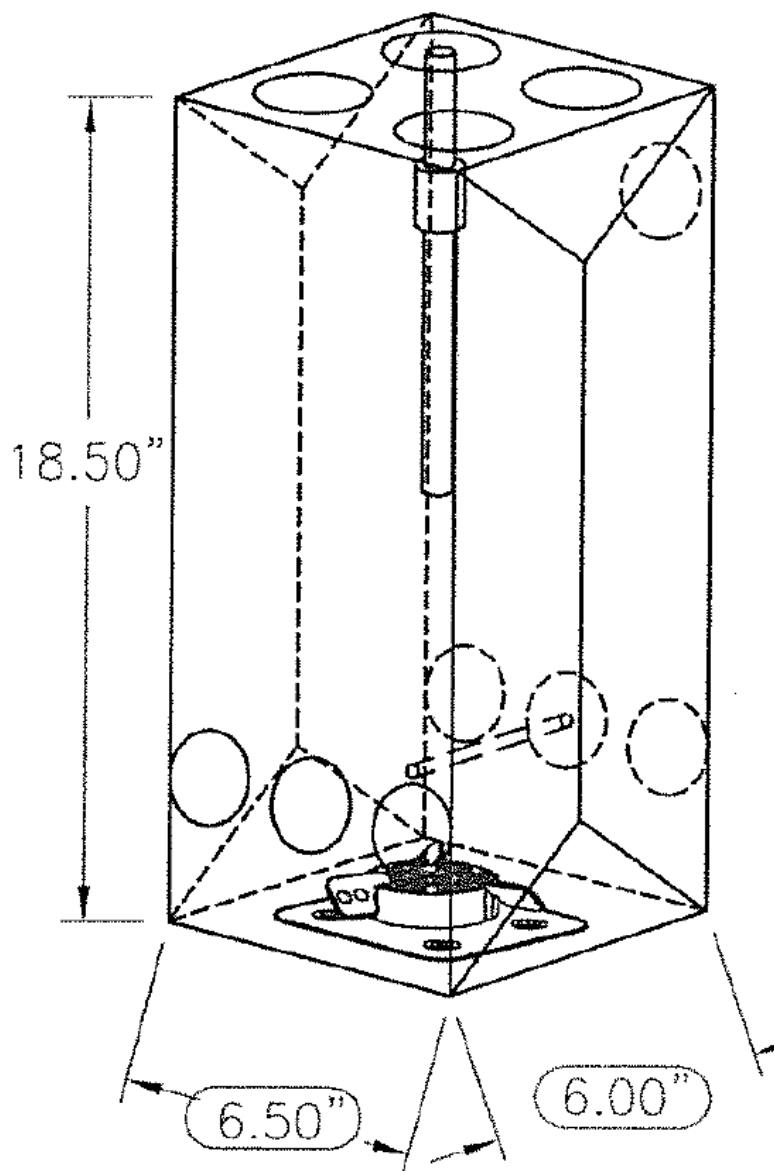


Figure 2.2. Mechanical drawing of tank liner for the Xcellerex XDR-10 single use bioreactor. Dimensions shown are in inches. Additional information on dimensions and configuration of the bioreactor can be found in Table 2.1. (image courtesy of the GE life science XDR-10 data sheet).

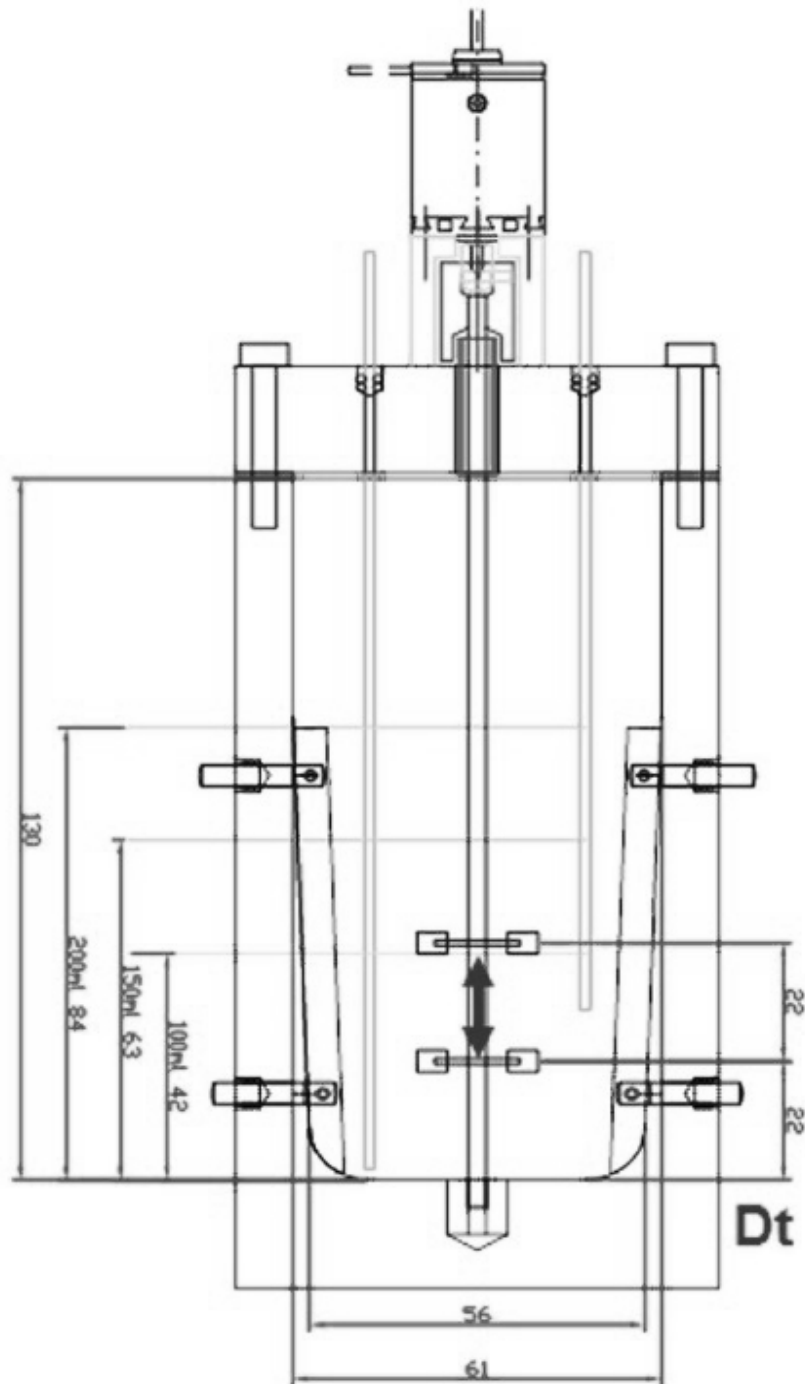


Figure 2.3. Mechanical drawing of Ambr®250 single use bioreactor. Dimensions shown are in millimetres. Additional information on dimensions and configuration of the bioreactor can be found in Table 2.1. (image modified from Bareither et al, 2013).

2.4. General Methods

2.4.1. Preparation of Fermentation Media

Growth media both for fermentation and oxygen mass transfer investigations was prepared as follows, with additional media requirements commented on when relevant. Typical fermentation media prepared were as follows:

- Luria-Bertani (LB) Growth Media – 10gL⁻¹ tryptone, 10gL⁻¹ sodium chloride, 5gL⁻¹ yeast extract, 10mgL⁻¹ chloramphenicol (pre-dissolved in ethanol) and 100mgL⁻¹ ampicillin (antibiotics added after media sterilisation)
- Terrific Broth (TB) – 12gL⁻¹ tryptone, 24gL⁻¹ yeast extract, 4mL.L⁻¹ glycerol, 10mgL⁻¹ chloramphenicol (pre-dissolved in ethanol) and 100mg.L⁻¹ ampicillin (antibiotics added after media sterilisation)
- 40% v/v glycerol solution – 40mL glycerol, 60mL ddH₂O, mixed and 0.2 micron sterile filtered
- Additional media were prepared in accordance with DoE designs generated throughout the thesis (e.g. in Chapter 3). Further details will be provided where relevant, while the method for preparation remains the same as for standard media.

Once prepared, all growth media were autoclaved on a liquid cycle to 121°C and held for 20 minutes in order to ensure sterility.

2.4.2. Preparation of Cell Banks (Master and Working Stock Generation)

Generation of master and working cell banks in order to secure the strains used is essential to ensure consistency in the biology and so that work can continue on the organisms beyond this thesis.

2.4.2.1. *E. coli* [pQR368]

A 1mL frozen stock of *E. coli* [pQR368] was inoculated into a 100mL baffled shake flask containing 19mL LB growth media with chloramphenicol and ampicillin under sterile conditions. The shake flask was incubated for 16 hours overnight at 200rpm and 37°C in an orbital shaker. 40 % v/v glycerol solution was added to the overnight culture in a 1:1 ratio (20

% v/v final glycerol concentration) and 1mL aliquots were aseptically transferred to sterile Eppendorf tubes before storage in a -80°C freezer.

2.4.2.2. *E. coli* Top10 expressing CometGFP

A 1mL frozen stock of *E. coli* Top10 CometGFP was inoculated into a 500mL baffled shake flask containing 99mL LB growth media with kanamycin under sterile conditions. The shake flask was incubated for 16 hours overnight at 200rpm and 37°C in an orbital shaker. Stocks were then prepared as outlined in Section 2.4.2.1.

2.4.3. Multifactorial Experimental Design Methods (DoE)

Of critical importance to all investigations undertaken in this thesis is the use of multifactorial, design of experiment methodologies (Tabora & Domagalski 2017). Characterisation of many systems, be they biological or physical has traditionally been undertaken using a 'one factor at a time' approach which does not take into consideration interactions between factors affecting the system and as such may lead to inaccurate optimisation for a desired response (Lendrem et al. 2015).

2.4.3.1. Selection of Factors

Throughout this thesis, factors and experimental ranges for multifactorial designs are selected on the basis of the objective of the experiments, the factors themselves and the limitations of the apparatus used. Additional detail on the selection of particular factors and ranges is included where relevant throughout the thesis.

2.4.3.2. Analysis and Influence on Subsequent Design

Analysis of DoE designs and models throughout this thesis is carried out using JMP versions 10 to 13 (SAS Institute, North Carolina, USA) or Design Expert version 8 or 9 (Statease, Minneapolis, USA). The basic mathematics and statistical analysis underpinning each is the same, and both provide the opportunity to examine the statistics and analysis of variance (ANOVA) in order to explore the validity of parameters and models as a whole.

2.4.3.3. Design Ethos and Progression

2.4.3.3.1. Screening

In an initial screening design, many factors are included and the ranges set as wide as possible in order to determine which of the factors and combinations of factors have a statistically relevant effect. The large number of factors are used to construct a relatively sparse design as the objective is to find any response away from the normal distribution. In this work initial screening designs employed up to 10 factors.

2.4.3.3.2. Refinement

A reduced number of factors and refined ranges are used in order to explore a different area of design space based on the outputs of the screening experiment (in this case between 5 and 7 factors). This should help in the progression towards an optimum.

2.4.3.3.3. Optimisation

In order to determine the local optimum, the number of factors are reduced again and the ranges set around where the optimum is perceived to be from the first two stages (screening and refinement). The design will often include axial, face residing and centre points in order to look for curvature in the response surface (Box et al. 2005). Potential design types include Response Surface Method (RSM), Definitive Screening Design (DSD) or composite designs (Tabora & Domagalski 2017; Candiotti et al. 2014). The number of factors included in optimisation designs ranged from 3 to 4.

2.5. Methods for Optimisation and Scale Up of a Whole Cell Oxidative Bioconversion

Multifactorial experimental designs for the studies outlined in Sections 2.5.1. to 2.5.3. are summarised in Table 2.2.

2.5.1. Screening Investigation (DoE 1)

2.5.1.1. Additional Materials

Additional materials required for DoE 1 are described here. Four media of differing compositions (A-D) were investigated, based on the initial composition of TB medium (Section 2.4.1). Media A comprised 12gL⁻¹ tryptone, 10gL⁻¹ yeast extract, 4mLL⁻¹ glycerol, 10% v/v

Phosphate Buffer Solution (pre-sterilised using a 0.2 μ m filter) 10mgL⁻¹ chloramphenicol (pre-dissolved in ethanol) and 100mgL⁻¹ ampicillin (antibiotics added after media sterilisation). Media B was made up of 12gL⁻¹ tryptone, 10gL⁻¹ yeast extract, 4mLL⁻¹ glycerol, 10mgL⁻¹ chloramphenicol (pre-dissolved in ethanol) and 100mgL⁻¹ ampicillin (antibiotics added after media sterilisation). Media C was composed of 12gL⁻¹ tryptone, 30gL⁻¹ yeast extract, 4mLL⁻¹ glycerol, 10% v/v Phosphate Buffer Solution (pre-sterilised using 0.2 μ m filter) 10mgL⁻¹ chloramphenicol (pre-dissolved in ethanol) and 100mgL⁻¹ ampicillin (antibiotics added after media sterilisation). Media D comprised of 12gL⁻¹ tryptone, 30gL⁻¹ yeast extract, 4mLL⁻¹ glycerol, 10mgL⁻¹ chloramphenicol (pre-dissolved in ethanol) and 100mgL⁻¹ ampicillin (antibiotics added after media sterilisation).

2.5.1.2. Inoculum Preparation

Preparation of fermentation inoculum for all microwell fermentations was as described in Section 2.4.2. However, TB media was used instead of LB media.

2.5.1.3. Microwell Fermentation

A nine-factor design of experiments investigation with 64 runs was designed using Design Expert 8[®] software. The layout of the design can be seen in Appendix 1.1. additional figures will be used to aid in the explanation of the experimental method.

To begin, 500 μ L of the appropriate media (A-D) was added to each of 96 wells across four 96 DSW plates; into the remaining wells, 500 μ L of sterile water was added to reduce heat loss during the process. The layout of media in each well can be seen in Appendix 1.2. The plate was covered during the process with a breathable, hydrophobic rayon seal (Starlab (UK) Ltd) in order to minimise evaporation. 5 μ L of the overnight inoculum was added to each of the wells containing media and shaken at 37°C and 300 or 1100rpm in an Eppendorf Thermomixer Comfort. The arrangement is displayed in Appendix 1.2. After 2 hours, the temperature in two of the thermomixers was reduced to 25°C, after which 1mM ALA and 0.5mM FeCl₃ was added to half of the cultures. The same wells were then induced using 1mM IPTG and after 10 minutes 0.1 or 1mM 7-ethoxycoumarin (pre-dissolved in ethanol) was added to half of the induced cultures (as shown in Appendix 1.1. for wells). One half of the wells were then increased to a volume of 1mL using inoculated culture in additional wells. After a further hour, 0.1 or 1mM 7-ethoxycoumarin (pre-dissolved in ethanol) was added to the other induced wells. The remaining wells were induced after an additional two hours, and the timing pattern of volume increase and substrate addition is repeated for these wells. Eight hours after their

induction, half of the cultures were harvested, the OD recorded as a measure of culture growth (as described in Section 2.8.2.1) using a Cecil Aquarius Spectrophotometer (Cecil Instrument, Cambridge, UK), and the product of the bioconversion (7-hydroxycoumarin) measured using a Dionex HPLC system as described in Section 2.8.3. The remaining wells are harvested 65 hours after induction and the same measurements of OD and product concentration measured.

2.5.2. Refinement Investigation (DoE 2)

2.5.2.1. Additional Materials

Four media of differing composition for investigation, based on the outputs of the first round of investigation (Section 3.2.1.) were required. Media A was made up of 12gL⁻¹ tryptone, 25 gL⁻¹ yeast extract, 4mLL⁻¹ glycerol, 10mgL⁻¹ chloramphenicol (pre-dissolved in ethanol) and 100mgL⁻¹ ampicillin (antibiotics added after media sterilisation). Media B was composed of 12gL⁻¹ tryptone, 25gL⁻¹ yeast extract, 4mLL⁻¹ glycerol, 10% v/v Phosphate Buffer Solution (pre-sterilised using 0.2µm filter) 10mgL⁻¹ chloramphenicol (pre-dissolved in ethanol) and 100mgL⁻¹ ampicillin (antibiotics added after media sterilisation). Media C comprised 12gL⁻¹ tryptone, 40 gL⁻¹ yeast extract, 4mLL⁻¹ glycerol, 10mgL⁻¹ chloramphenicol (pre-dissolved in ethanol) and 100mgL⁻¹ ampicillin (antibiotics added after media sterilisation). Media D was made up of 12gL⁻¹ tryptone, 40gL⁻¹ yeast extract, 4mLL⁻¹ glycerol, 10% v/v Phosphate Buffer Solution (pre-sterilised using 0.2µm filter) 10mgL⁻¹ chloramphenicol (pre-dissolved in ethanol) and 100mgL⁻¹ ampicillin (antibiotics added after media sterilisation).

2.5.2.2. Microwell Fermentation

A seven-factor design of experiments investigation with 64 runs was designed using Design Expert 8[®] software. The layout of the design is shown in Appendix 1.3.

The method for the experiment is similar to that in Section 2.5.1. but was carried out in two 96 DSW plates. After 50 hours half of the wells are harvested, the OD recorded as a measure of growth (as described in Section 2.8.2.1.) using a spectrophotometer and the product of the bioconversion (7-hydroxycoumarin) measured using HPLC as described in Section 2.8.3. After a further 25 hours the remaining wells are harvested and the same OD₆₀₀ and product concentration measurements taken.

Table 2.2. Experimental designs used for multifactorial optimisation of a P450 whole cell oxidative bioconversion in microwells. This table summarises experiments performed in three stages (1: Screening, 2: Refinement, 3: Optimisation).

DoE Round	Factor	Factor Name	Unit	Range		
				Low	High	Change
1	A	Post Induction Time	hr	8	65	-
	B	Substrate Concentration	mM	0.1	1.0	-
	C	Post Induction Volume	mL	0.5	1.0	-
	D	Pre-Induction Time	hr	2	5	-
	E	Bioconversion Temperature	°C	25	37	-
	F	Substrate Addition Time (Post Induction)	hr	0.17	1.0	-
	G	Yeast Extract Concentration	gL ⁻¹	25	40	-
	H	Buffered Media	-	No	Yes	-
	J	Orbital Shaking Speed	rpm	300	1100	-
	2	A	Post Induction Time	hr	50	75
B		Substrate Concentration	mM	0.75	1.25	Higher
C		Post Induction Volume	mL	0.5	1.0	No change
D		Pre-Induction Time	hr	2	5	No change
E		Yeast Extract Concentration	gL ⁻¹	25	40	Higher
F		Bioconversion Temperature	°C	22	30	Lower
G		Buffered Media	-	No	Yes	No change
3	A	Substrate Concentration	mM	0.75	1.0	Lower
	B	Yeast Extract Concentration	gL ⁻¹	40	50	Higher
	C	(Post Induction Time)	hr	0	75	Continuous time course

2.5.3. Optimisation Time course (DoE 3)

2.5.3.1. Additional Materials

Three media of differing composition were required, Media A was made up of 12gL⁻¹ tryptone, 50gL⁻¹ yeast extract, 4mLL⁻¹ glycerol, 10% v/v Phosphate Buffer Solution (pre sterilised using 0.2µm filter) 10mgL⁻¹ chloramphenicol (pre-dissolved in ethanol) and 100mgL⁻¹ ampicillin (antibiotics added after media sterilisation). Media B was composed of 12gL⁻¹ tryptone, 40gL⁻¹ yeast extract, 4mLL⁻¹ glycerol, 10% v/v Phosphate Buffer Solution (pre sterilised using 0.2µm filter) 10mgL⁻¹ chloramphenicol (pre-dissolved in ethanol) and 100mgL⁻¹ ampicillin (antibiotics added after media sterilisation). Media C comprised of 12gL⁻¹ tryptone, 45gL⁻¹ yeast extract, 4mLL⁻¹ glycerol, 10% v/v Phosphate Buffer Solution (pre-sterilised using 0.2µm filter) 10mgL⁻¹ chloramphenicol (pre-dissolved in ethanol) and 100mgL⁻¹ ampicillin (antibiotics added after media sterilisation).

2.5.3.2. Microwell Fermentation

A two-factor central composite face-centred (CCF) DoE investigation with four centre points (eight runs total) was designed using Design Expert 8® software. The experiment was also designed to run over a 75 hour time course, with harvesting at selected time points using the sacrificial well approach. The layout and arrangement of the design can be seen Appendix 1.4.

To begin, 1 mL of the appropriate media (A-C) was added to each of 96 wells across a 96 DSW plate. Microwell experiments were then performed as described in Section 2.5.1. with the following modifications. After 2 hours, the temperature was reduced to 30°C, after which 1mM ALA and 0.5mM FeCl₃ were added. The cultures were then induced using 1mM IPTG and after 10 minutes 0.75, 0.88 or 1mM 7-ethoxycoumarin (pre-dissolved in ethanol) was added to the induced cultures. After 5 hours, the first column of wells was harvested (see Appendix 1.5.), the OD recorded as a measure of culture growth (as described in Section 2.8.2.1.) using a spectrophotometer, and the product of the bioconversion (7-hydroxycoumarin) measured using HPLC as described in Section 2.8.3. Additionally, samples were taken and prepared for a free glycerol assay as described in Section 2.8.4.

2.5.4. Scale Up Fermentation

2.5.4.1. Overnight Inoculum

In order to ensure continuity of the fermentation inoculum, the inoculum preparation process described in 2.5.1.2. was also used for 7.5L scale up fermentation inoculum preparation. However, in order to secure sufficient material for the inoculation of the stirred tank reactors, a 500mL flask was used containing 99mL of TB.

2.5.4.2. 7.5L Fermenter Operation

For the scale up fermentation, a 7.5L (New Brunswick Scientific Co, New Jersey, USA) 0.18m internal diameter bioreactor with aspect ratio (H_v/D_v) and impeller ratios (D_i/D_v) of 1.6 and 0.3 respectively was used. This bioreactor is geometrically and operationally similar to the BioFlo310 described in Section 2.3.1. Agitation was provided by two six-blade Rushton turbine impellers connected to a top-driven impeller shaft. The bioreactor was filled with an optimised TB medium (with 40gL^{-1} yeast extract instead of the standard 24gL^{-1}) containing 10% v/v phosphate buffer solution (starting volume 3 L) and 0.5mLL^{-1} PPG.

The dissolved oxygen tension (DOT) probe was calibrated between 0% in pure nitrogen, and 100% in gaseous air. The pH probes were calibrated using standard pH 4 and 7 buffers. The probes were installed into their respective ports and the whole vessel was sterilised by autoclaving at 121°C for 20 minutes. After removal from the autoclave and cooling, 100mgL^{-1} ampicillin (0.2 micron filtered) and 10mgL^{-1} chloramphenicol (pre-dissolved in ethanol) were added to the vessel. 12.5% ammonia solution and 10% phosphoric acid were transferred to the base and acid addition bottles respectively, for control of pH as necessary. The pH probe underwent an offline check of the media pH, and the DOT probe a final review, and both were recalibrated as appropriate if necessary. The conditions of the bioreactor were set to 37°C , 750rpm, pH7.0 and 1vvm (in this case 3Lmin^{-1}) air addition.

The vessel was inoculated with 1% v/v of the working volume of the reactor from the overnight inoculum culture. The operating conditions were selected based on a Reynolds number (Re) number in the turbulent region, and are consistent with those selected for work previously carried out with this cell line (Baboo, 2012). The pH was both monitored and controlled, as previously direct comparison with the microwell has been carried out and the purpose of this experiment was both to attempt to demonstrate scalability from microwells, whilst also determining if this bioconversion would be enhanced by utilising some of the

features that are offered by the scale up fermenter. 2 hours after inoculation, the temperature was reduced to 30°C and the agitation rate to 600rpm as the conditions for enzyme expression and bioconversion. Once the temperature had reduced, 1mM ALA and 0.5mM FeCl₃ were added to the reactor as components which have been shown to enhance the P450 expression and the bioconversion. After this, the culture was induced using 1mM IPTG and after 10 minutes 1mM 7-ethoxycoumarin (pre-dissolved in ethanol) was added as the bioconversion substrate. The culture was then run for a total of 28 hours with samples taken periodically for OD readings as a measure of culture growth as described in Section 2.8.2.1. and 500µL aliquots taken for offline bioconversion product quantification by HPLC as described in Section 2.8.3.

2.5.4.3. Quantification of Bioreactor Inlet and Outlet Gas Compositions

Quantification of bioreactor inlet and outlet gases during fermentation in the 7.5L New Brunswick bioreactors required reconfiguration of the gassing set up in the Advanced Centre for Biochemical Engineering (ACBE, University College London) fermentation facility. The new set up is as shown in Figure 2.4. The accurate quantification of inlet and outlet gas compositions was crucial for determining oxygen uptake rates under different fermentation conditions (Garcia-Ochoa et al, 2009), and as such understanding the demands of the expression system on the culture environment.

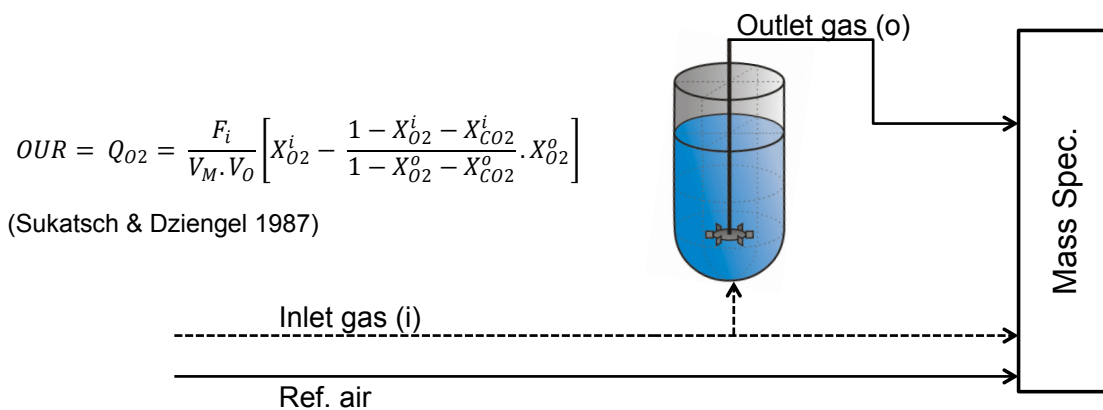


Figure 2.4. Diagrammatic representation of the rearranged gas measurement set up in the UCL ACBE fermentation suite to allow accurate quantification of inlet and outlet gas compositions from the bench top STR.

Table 2.3: Experimental design for oxygen mass transfer rate determination in 24 deep square well microtitre plates (Section 2.6.2.).

Factor				
	Fill volume (mL)	Agitation rate (rpm)	Culture Temp. (°C)	OD ₆₀₀
Lo	1.6	200	30	0,1,5,10,20,50
Hi	3.2	250	37	

2.6. Methods for Developing Accurate Oxygen Mass Transfer Characterisation in High Throughput, 24 Microwell Plates

For measuring online dissolved oxygen tension in microwell plates, the PreSens Oxodish system was used, with the set up as shown in Figure 2.5. The Duetz clamp system (Duetz et al. 2000) was also used in order to hold the Sensordish® Reader with the Oxodish placed on top and the microwell plate held in position above that. Where possible during microwell determination of k_{La} , experiments were carried out in duplicate in order to ensure that data was representative.

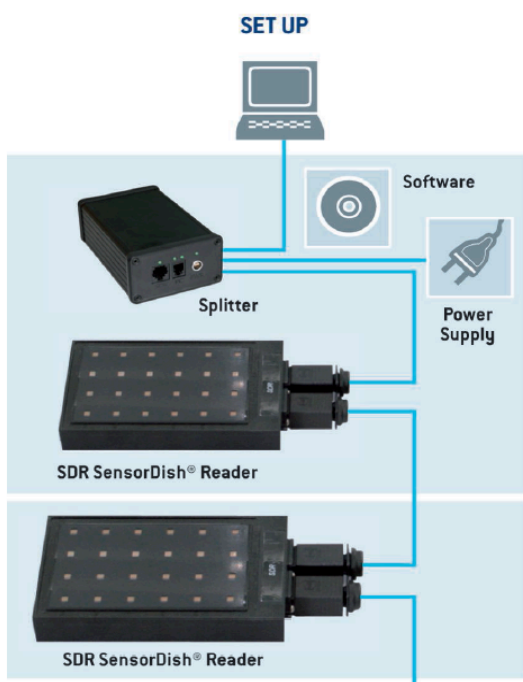


Figure 2.5. Diagrammatic representation of the set up for online dissolved oxygen measurement in 24 DSW Oxodish plates (image courtesy of PreSens GmbH)

2.6.1. Inoculum Preparation

As with previous experiments, the inoculum is generated as described in Section 2.5.1.2.

2.6.2. Fermentation in 24DSW PreSens Plates for Establishing the Baseline Model

When building the initial linear model for k_{La} , a four factor, two level, full factorial design was used, with the design blocked for each biomass concentration, with the intention of generating a linear model. The design can be seen in Table 2.3. Each design point was replicated in the plate.

The evening prior to inoculation, wells of a 24 Deep Square Well Oxodish were filled with the appropriate volume of media, covered with a breathable seal, a rubber seal with holes above the location of each well to allow gas exchange and a metal lid also with holes above the well locations, before being incubated overnight in a floor standing shaking incubator in order to ensure sterility prior to inoculation. During this time the online DOT recording is also started in order to allow readings to stabilise prior to calibration. Each well was inoculated with overnight culture grown for 16 hours (as described in Section 2.5.1.2.), and the microtitre plates incubated at the temperatures and agitation rates according to the experimental design (Table 2.3.). Starting biomass concentrations were achieved by measuring the OD_{600} of the overnight culture and calculating the required proportional volume to give a desired OD_{600} . In the case of higher ODs, concentration of the culture using bench top centrifugation was required before resuspension in media at a higher concentration, followed by immediate inoculation into the wells. Three hours post inoculation, the culture is induced with 2mM L-Rhamnose for the expression of CometGFP (from DNA 2.0). The culture was then continued for a further 27 hours with online readings recorded.

2.6.3. Fermentation in 96 and 24DSW PreSens Plates for Developing an Improved Quantification Method for Oxygen Mass Transfer

E. coli cultures in 24DSW plates for establishing an oxygen mass transfer model were carried out as described in Section 2.6.2. with the exception of the factors and ranges as part of the experimental design. These are highlighted in Table 2.4.

Fermentations in 96 DSW plates for comparison with the larger scale 24 DSWs were also undertaken as described in Section 2.6.2. with the exception of the orbital shaker (a Thermomixer comfort) and the corresponding agitation rates. Proportional differences are also

made in the set up and experimental design, in line with the difference in well volume. The experimental design is outlined in Table 2.4. Further information regarding how the experimental data generated was processed and analysed for building the model of oxygen mass transfer in 24 DSW plates is covered in Chapter 4.

2.6.4. Determination of OUR and k_La from online DOT Profiles

In order to quantify OUR and k_La using the online dissolved oxygen measurements, the following analysis was undertaken.

Once the DoE experiments were performed (Section 4.3.) and the DOT profiles extracted from the PreSens monitoring software, the raw DOT profiles were normalized to 100% saturation, before being converted to engineering units ($\text{mgO}_2\text{L}^{-1}$) using the appropriate saturation concentration of oxygen for the corresponding temperature at that point in design space (Rice et al. 2012).

OUR is calculated during the time at which the mixing of the system has been stopped and therefore it is assumed that there is zero mass transfer of oxygen into the liquid (i.e. $k_La = 0$) and therefore Equation 2.1. can be simplified such that $\text{OUR} = dC_L/dt$ (see (A) in Figure 2.6.). k_La is then determined during the phase where mixing has been restarted in the system (see (B) in Figure 2.6.) and therefore oxygenation of the system is also returned. By plotting C_L against $dC_L/dt + \text{OUR}$, k_La is determined from the gradient of the slope.

These values can then be used in order to determine factors that influence the oxygen mass transfer rate and generate baseline models for both OUR and k_La .

$$\text{OUR} = k_La(C^* - C_L) + \frac{dC_L}{dt} \quad \text{Equation 2.1.}$$

$$k_La = \frac{\left(\text{OUR} - \left(\frac{dC_L}{dt}\right)\right)}{(C^* - C_L)} \quad \text{Equation 2.2.}$$

Where C^* is the saturation concentration of O_2 , C_L is the oxygen concentration in the first order system at a given time, $d(C_L)/dt$ represents the first derivative of oxygen concentration with respect to time.

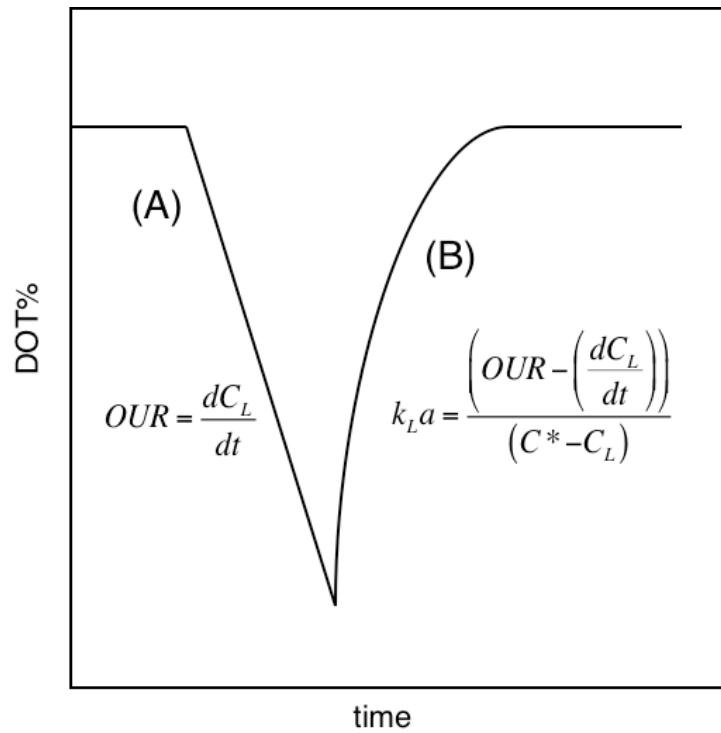


Figure 2.6. Example DOT profile demonstrating the effect of ceasing aeration (A) and restarting it (B) during the dynamic gassing out method. Figure 2.6. also illustrates how OUR and $k_L a$ are calculated respectively.

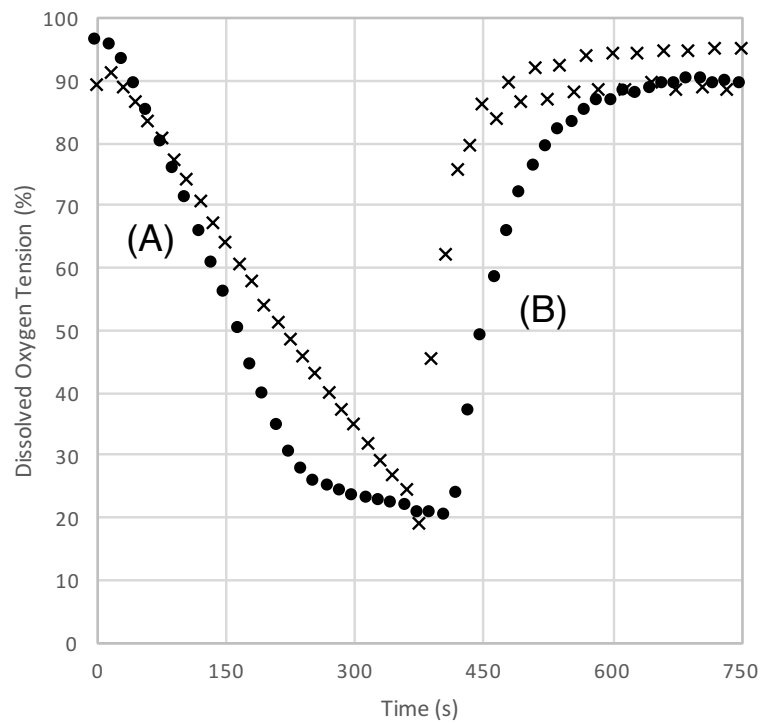


Figure 2.7. Representative example experimental DOT profiles used for analysis. (A) shows the period after cessation of aeration and (B) after restarting aeration.

Table 2.4. Experimental design for building a model for oxygen mass transfer during *E. coli* fermentation in 24DSW PreSens Oxodish plates, and 96DSW microwell plates.

Plate type	Factor	Unit	Range		
			Lo	Hi	
24 Deep Square Well PreSens	A	Fill Volume	μL	1600	3200
	B	Agitation Speed	rpm	200	400
	C	Post Induction Temp.	$^{\circ}\text{C}$	30	37
	D	% Inoculum	%	1	5
	E	Log hour time points	hr	PreInd (t0), Post Ind (t8), t24, t32, t48, t56	
96 Deep Square Well	A	Fill Volume	μL	400	800
	B	Agitation Speed	rpm	600	1100
	C	Post Induction Temp.	$^{\circ}\text{C}$	30	37
	D	% Inoculum	%	1	5
	E	Log hour time points	hr	PreInd (t0), Post Ind (t8), t24, t32, t48, t56	

2.7. Methods for Characterisation of Oxygen Mass Transfer Coefficients (k_{La}) in Commercially Relevant Single Use Bioreactors (SUBs)

Quantification of oxygen mass transfer coefficients is central to the main aim of this thesis (Section 1.3.), and as such it is crucial to understand the methodologies used, and notably the differences which were required due to the constraints of the different vessels and measurement systems. Experimentally, the static gassing out method was used for k_{La} determination as described by Garcia-Ochoa et al, 2009. Where appropriate measurements were made in triplicate.

2.7.1. New Brunswick BioFlo310

2.7.1.1. Run Order

Run ordering was a key experimental consideration and although randomisation of run order would have been ideal, this was not practical. The reasoning and remedial actions are discussed in the relevant sections of Chapter 5.

2.7.1.2. Quantification of k_{La} Values

Before building a model for the oxygen mass transfer, the k_{La} under each set of conditions must be quantified. Firstly, the dissolved oxygen tension is plotted against time (see Figure 2.8A) in order to identify the period of the experiment over which there is an exponential change in DOT, as this is the region from which k_{La} can be calculated. For this data, Equation 2.3. can be rearranged and applied to each data point used to calculate a value for $\ln(C^*/C^* - C_L)$ (Equation 2.4.), with the output then plotted against time (Figure 2.8B). The gradient of this plot is then equal to the k_{La} . It must be noted that this method does not take into account probe response time (PRT), which, in such a rapidly changing system is needed, and so this data is used for the preliminary indication of trends across the experimental landscape, and for validation of the k_{La} values calculated with PRT taken into account. Subsequent multifactorial analysis was carried out as described in Section 2.4.4.2.

$$\frac{dC_L}{dt} = k_{La} \cdot (C^* - C_L) \quad \text{Equation 2.3.}$$

$$\ln(C^*/C^* - C_L) = k_{La} \cdot t \quad \text{Equation 2.4.}$$

2.7.1.2.1. Adjusting for Probe Response Time

Due to there being a delay between the change in environment and the recording of this change by the probe, it is crucial to account for this in the calculation of k_{La} (Tribe et al. 1995). First the readings should be normalised using Equation 2.5 where Y_L is the normalised oxygen concentration.

$$Y_L = (C^* - C_L)/C^* \quad \text{Equation 2.5.}$$

It is then necessary to calculate the normalised probe response using Equation 2.6. Here R_1 is the reciprocal of k_{La} and R_2 is the mean measured probe response time (in the case of the BioFlo 310 this is 34.8 seconds from $n=5$ measurements). Y_p is the normalised oxygen concentration allowing for probe response.

$$Y_p = \left[R_1 \cdot e\left(-\frac{t}{R_1}\right) - R_2 \cdot e\left(-\frac{t}{R_2}\right) \right] / (R_1 - R_2) \quad \text{Equation 2.6.}$$

Following this, the squared error is calculated using Equation 2.7., and from this the sum of the errors for the desired data set can be determined. The data set used is the same as when calculating k_{La} without PRT, highlighting the exponential range, which should cover at least 66% of the complete DOT range measured.

$$Error = (Y_L - Y_p)^2 \quad \text{Equation 2.7.}$$

In order to determine k_{La} from this, the value of R_1 is adjusted in Equation 2.6. so as to minimise the sum of the square errors over the experimental range. This can be achieved either manually or, more practically, using a computer program e.g. Microsoft Excel's solver function. k_{La} is then found by calculating the reciprocal of the R_1 value which gives the minimised sum of square errors. Table 5.5., highlights the difference in k_{La} values when calculated with and without taking probe response time into consideration.

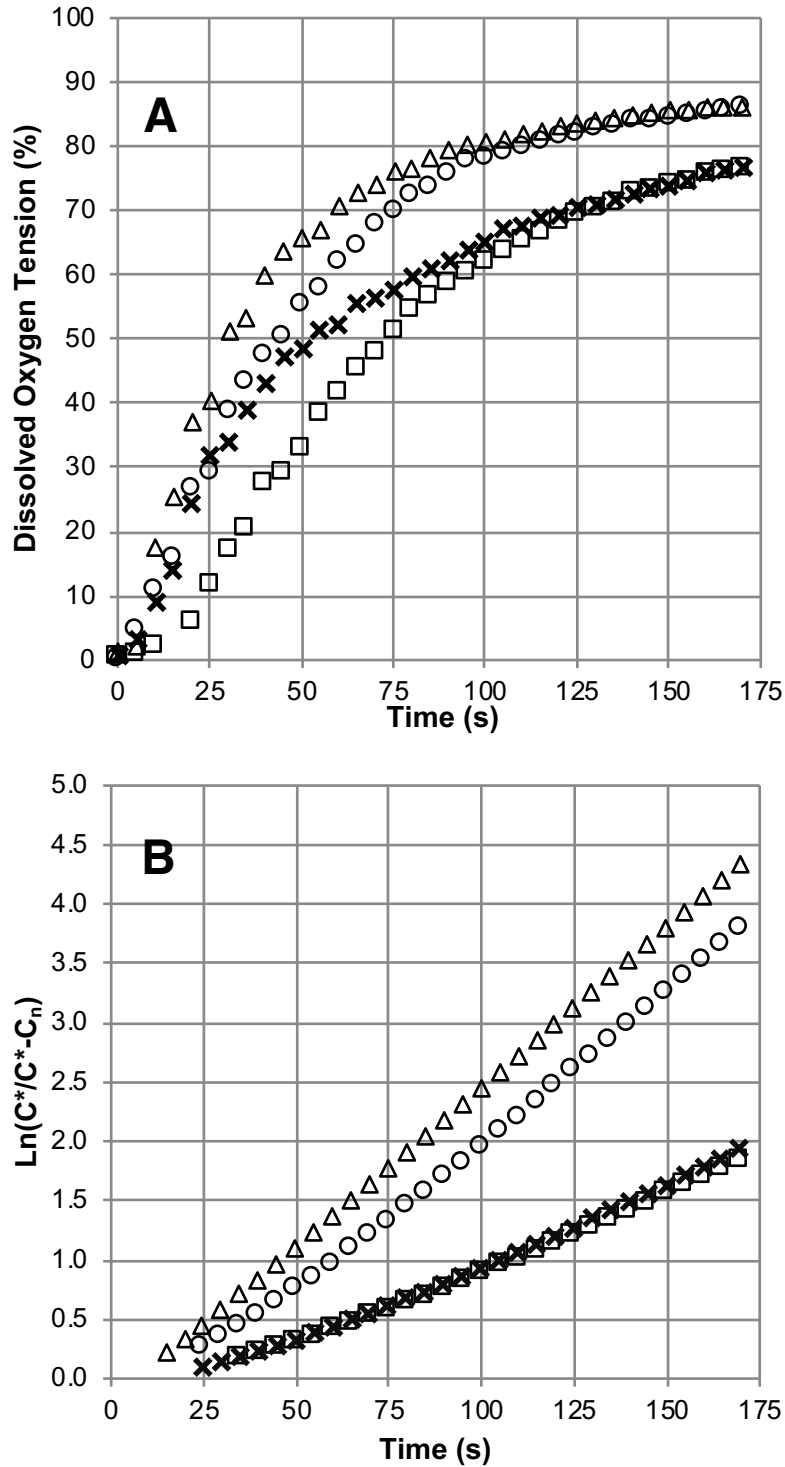


Figure 2.8 Plots of dissolved oxygen tension (A) and $\ln(C^*/C^* - C_L)$ (B) against time for calculating k_{La} in the New Brunswick BioFlo 310 reactor. \square represents 0.43vvm and 419rpm, \times 0.43vvm and 881rpm, \circ 1.07vvm and 419rpm and Δ 1.07vvm and 881rpm. Both plots use the same representative sample from the data set generated in the BioFlo 310 STR.

2.7.2. Ambr®250

The method for quantification of the oxygen mass transfer coefficient is as outlined in Section 2.7.1.

The protocol for quantification of k_{La} in the Ambr®250 was based on that in Section 2.7.1. The protocol was automated using the Ambr's Pegasus software. The progress in design and development of this protocol are detailed in Section 5.4. Appendix 4.8. shows the software protocol.

2.7.3. XDR10

Execution and analysis of the output data streams, the method is as described in Section 2.7.1.

2.8. Analytical Equipment and Techniques

2.8.1. Analytical Equipment

The HPLC System used was a Dionex Thermostatted Column Compartment TCC-100 with Dionex P680 Pump, Dionex UVD 170U UV-Vis Detector and LC Packings Famos Autosampler (Dionex, California, USA). A Cecil Aquarius spectrophotometer (Cecil Instruments, Cambridge, UK) was used for OD_{600} measurements, a CLARIOstar plate reader (BMG Labtech GmbH, Germany) and a Tecan Geneios Plate reader (Tecan, Switzerland) were used for absorbance and fluorescence measurements. Clear and black 96 well flat bottom microtitre plates were supplied by Starlab (Milton Keynes, UK). A Prima δ B mass spectroscopy gas analyser (from Thermo Scientific, Waltham, MA, USA) was used for offline gas analysis and quantification during scale up fermentation. Measurement of glycerol was done using a Free Glycerol Assay Kit (Colorimetric) (Cell Biolabs, California, USA) and DNA purification and quantification used a QIAminiprep® kit (Qiagen®, Hilden, Germany). Manual handling of samples and reagents was using P1000, P100, P20 Gilson pipettes (Middleton, WI, USA) and 1mL, 200 μ L and 20 μ L sterile pipette tips (supplied by Starlab, Milton Keynes, UK). An Eppendorf microfuge (Eppendorf, Germany) was used for centrifugation of samples. A Nanodrop 2000c was used for quantification of purified DNA concentration.

2.8.2. Quantification of Biomass Concentration

2.8.2.1. At Line Quantification of Biomass Concentration

The Optical Density (OD_{600}) of fermentation samples was measured using a Cecil Aquarius spectrophotometer or Clariostar plate reader at 600 nm for shake flask, microwell and bioreactor fermentations. During shake flask and bioreactor fermentations, triplicate readings were taken. During the Design of Experiments rounds in microwells, duplicates were measured where possible, but replication of samples was not necessary as the way in which the experiments are designed ensures that replicates are inherent within the design (Tabora & Domagalski, 2017). For all measurements, samples were prepared in a Class II biosafety cabinet.

Composition of media was included in experiments throughout the thesis, and each affected the optical density at 600 nm. Thus, in order to ensure accuracy of readings, each sample was measured after blanking with the fermentation medium. Dilutions were also done using the fermentation media.

2.8.2.2. Off Line Quantification of Biomass Concentration

A calibration curve for biomass concentration against OD_{600} was generated from a number of fermentations in the benchtop stirred tank bioreactor (New Brunswick 7.5L). Fermentation samples were collected in triplicate and their OD_{600} recorded. 1 mL of sample were then placed into pre-weighed 2 mL Eppendorf tubes before being centrifuged at 13,000 rpm ($\sim 18,000 \times g$) and having the supernatant carefully removed. Samples were then washed with phosphate buffered saline, before being centrifuged again and having the supernatant removed. Samples were then weighed again and the difference between this and the initial weight of the tube taken as the wet cell weight per mL of culture (converted to gL^{-1} by multiplying by 1000). The tubes were then left in an oven to dry for a minimum of 16 hours, and after being allowed to cool were weighed and again, the difference from the initial weight taken as the dry cell weight per mL of culture (converted to gL^{-1} by multiplying by 1000). The calibration curve obtained was then used to convert OD_{600} measurements into wet cell weight per litre of culture ($g_{WCW}L^{-1}$) or dry cell weight per litre of culture ($g_{DCW}L^{-1}$). A change in OD_{600} of one corresponded to a WCW of $1.55 gL^{-1}$ and a DCW of $0.34 gL^{-1}$.

2.8.3. Quantification of Bioconversion Substrate and Product Concentrations

2.8.3.1. High Performance Liquid Chromatography (HPLC)

2.8.3.1.1. Sample Preparation

Aqueous samples from bioconversions were prepared by mixing a 500 μ L sample with 500 μ L methanol. Where a 500 μ L sample was not available, as large a sample as possible was taken and mixed in a 1:1 ratio with methanol. The sample with methanol was vortex mixed for 15 seconds and then centrifuged at 13,000 rpm for 5 minutes. 150 μ L of the solvent layer was then transferred to an HPLC vial, sealed, and analysed using HPLC as described in Section 2.8.3.1.2. The UV-Vis detector response to the samples was measured as an integrated peak area. 7-ethoxycoumarin was used for substrate standards and 7-hydroxycoumarin (umbelliferone) was used for the product standards. Sample calibration curves for 7-ethoxycoumarin and 7-hydroxycoumarin can be seen in Appendix 1.6.

2.8.3.1.2. HPLC Operation and Quantification

A Dionex HPLC system (Dionex, California, USA), fitted with an ACE 5 C18 column (ACE, Aberdeen, UK) with guard column, was used to analyse the conversion of 7-ethoxycoumarin to 7-hydroxycoumarin. The mobile phases used were B: Acetonitrile and C: 0.1% Trifluoroacetic acid (TFA) in water. The column was equilibrated for 30 minutes prior to the sample analysis with 10% mobile phase B and 90% mobile phase C flowing at 1mLmin⁻¹. The column was maintained at a temperature of 30°C and 20 μ L samples were injected into the column, also at a flow rate of 1mL/min. A ten minute programme was used at this flow rate. Product and substrate were detected at a wavelength of 325 nm (see Appendix 1.7.) using the UV-Vis detector.

2.8.3.2. Quantification of Green Fluorescent Protein expression

Fermentation samples were vortex mixed for 30 seconds before being diluted 1 in 20 with phosphate buffered saline (PBS) solution as the diluent, and 200 μ L transferred into 96 round well, flat bottom black microtitre plates. Triplicate samples were prepared and blanks containing 200 μ L of PBS distributed in the plate. Determinations of fluorescence were made using a CLARIOstar plate reader, from the top, at excitation and emission wavelengths of 395 and 509 nm respectively. The mean of the three sample readings was taken and the background (mean of the three blank samples) subtracted.

2.8.4. Quantification of Free Glycerol Concentration

2.8.4.1. Sample Preparation

A Free Glycerol Assay Kit from Cell Biolabs (California, USA) was used to measure the consumption of glycerol from the media throughout the bioconversion. 250 μ L sample of the fermentation broth was collected and transferred to an Eppendorf tube. This was centrifuged at 5000 rpm and 4°C for 10 minutes. The supernatant was collected without disturbing the cell pellet and vortex mixed for 10 seconds. Each sample was then stored at -80°C until all were ready to be assayed.

2.8.4.2. Assay Protocol

All samples and materials were maintained on ice for the duration of the assay preparation. Samples were thawed on ice and then vortex mixed for 10 seconds each. At the beginning of each assay set, a freshly prepared standard curve was prepared (see Appendix 1.8.).

10 μ L of diluted glycerol standards (at 0, 6.25, 12.5, 25, 50, 100, 200 and 400 μ M) and samples added to a 96 well plate. The reaction mixture was prepared using the volumes shown in Table 2.5, mixing well after the addition of each of the components. 90 μ L of this reaction mixture was added to each of the 10 μ L samples. The plate was covered with foil and incubated for 15 minutes at 25°C in an orbital shaker. The absorbance was then read on a Tecan Geneios plate reader at 570nm. The standard curve generated was then used to calculate the glycerol concentration in each of the samples. A sample calibration curve can be found in Appendix 1.8.

Table 2.5. Component volumes for makeup of Glycerol Assay reaction mixture.

Deionised Water (mL)	10X Assay Buffer (mL)	5X Enzyme Mixture (mL)	200X Colorimetric Probe (μ L)	Total Reaction mixture volume (mL)	No. tests available
5.95	1	2	50	9	100

3. Quantification of Oxygen Utilisation for a Microbial P450 Oxidative Bioconversion

3.1 Context and Aim

Oxidative bioconversions are currently applied in a number of industrial processes (Section 1.2.1.). These include the manufacture of Pravastatin by Daiichi-Sankyo (Watanabe et al. 1995), Rocaltrol from Vitamin D3 by Roche (Sakakis et al. 1992) and Leukotoxin B for pathophysiological responses in humans (Falck et al. 2001). There is considerable future potential to apply oxidative conversions in the manufacture of antibiotics (Shafiee & Hutchinson 1988; Anzai et al. 2012; Tian et al. 2013) and pharmaceuticals including the chemotherapeutic Taxol® (Kirby & Keasling 2009). Additional applications can be found in the fragrances and cosmetics (Sakaki 2012) and food and pigments (Gillam et al. 2000) industries. Despite industrial application for almost two centuries, when production of acetic acid from ethanol began in the early 1800s (Wandrey et al. 2000), oxidative bioconversions have seldom been fully characterised.

P450s, as described in Section 1.2.2, are a family of haem-proteins, responsible for catalysing mainly oxidative bioconversions. When expressed in microbial hosts they have the potential for application in a wide range of industrial processes generating high value products. There are however, a number of significant issues associated with their use. These include instability, complexity (Sakaki 2012), limited oxygen transfer rates (van Beilen et al. 2003) and insufficient yields when compared with those traditionally required for a successful chemical process (Straathof et al. 2002).

In order to be able to properly quantify factors contributing to the oxygen demand of P450 bioconversions, expression levels of the enzyme need to be increased to easily quantifiable levels. Multifactorial optimisation using a DoE methodology provides a potential solution to this with significant advantages over a traditional OFAT approach (Section 1.2.10) (Zhang et al. 2006; Adinarayana & Ellaiyah 2002). In particular it is possible to determine a 'true optimum' set of parameters based on a desired output, such as enzyme activity (Islam et al. 2007; Shivhare & McCreath 2010). DoE is a tool widely used in chemistry, but greatly underutilised with biological systems (Jansen 2003). Employing a set of DoE principles and experimental procedures, may aid in overcoming some of the issues associated with whole cell P450 bioconversions,

particularly the problem of industrially inadequate expression levels and hence product titres.

Microorganisms have a particularly high metabolic requirement for oxygen, especially when compared with alternative expression systems such as mammalian cells (Micheletti & Lye 2006; Fleishaker & Sinskey 1981). This is an established challenge for culturing microbial expression systems, particularly in vessel designs which are known to have oxygen transfer limitations, including microwells (Eibl et al. 2010). It is important therefore that when assessing the needs of an organism carrying out an oxidative bioconversion, where O₂ is a substrate both for metabolism and a biocatalytic process, that the maximum O₂ demands are determined.

At present, there is little understanding in the literature of the balance between metabolism and bioconversion with regard to total oxygen demand during whole cell bioconversions. By distinguishing between the O₂ required for metabolism and the O₂ required for bioconversion, understanding of O₂ utilisation will be significantly improved. The limited previously published work has concluded that the extent of the requirement differs depending on organism, enzyme and substrate used (Mayuzumi et al. 1993). In addition there has been a suggestion that a P450 bioconversion in *E.coli* is responsible for just 1.5% of the total oxygen utilised (Shet et al. 1997), however this was concerned with only millilitre scale experiments. This lack of knowledge is a major shortcoming from a bioprocessing standpoint, as a thorough understanding of the demands of the system on the culture environment is imperative when developing commercially relevant strains and processes.

3.1.1. Aims

The aim of this chapter is to establish the methodologies which can be used for effectively optimising, and accurately quantifying OUR for a microbial expression system under optimised conditions. In order to achieve this, a number of objectives can be identified:

- Multifactorial DoE methods will be used to optimise the oxidative bioconversion of a P450 monooxygenase expressed in *E.coli*, such that the productivity, growth and therefore oxygen demand of the expression system is maximised.

- A 3000-fold scale up to a 7.5L stirred tank bioreactor will be carried out, including reconfiguring of a mass spectrometer set up for accurate oxygen mass transfer quantification.
- Comparison of three cultivation strategies (non-induced batch, induced batch and induced fed-batch, denoted as NI-B, I-B and I-FB respectively) will then be used to examine the preferred conditions for carrying out a whole cell P450 bioconversion and the demands on the culture environment. This will also support the better elucidation of oxygen demands for metabolism and bioconversion.

3.2. Optimisation of P450 Bioconversion

A multifactorial Design of Experiments (DoE) methodology was employed in order to optimise the expression of the P450 expressed in *E. coli* and the subsequent bioconversion of 7-ethoxycoumarin to 7-hydroxycoumarin (Section 2.4.5). This would establish a set of conditions which maximise the activity of the bioconversion, making the OURs more easy to measure once transferred into pilot scale bioreactors, as well as providing an insight into the kinetics of the culture and bioconversion at the microwell scale.

This process was carried out in three stages. First, an initial 'Screening' round was conducted (Section 3.2.1) to identify factors and interactions which have a significant impact on bioconversion product titre and therefore require further investigation. Second, a 'Refinement' round was undertaken (Section 3.2.2) which took those factors identified as being of interest and refined the ranges based on the outputs of the screening round in order to move closer to an optimal set of conditions. Finally, an 'Optimisation time course' was performed (Section 3.2.3) in order to refine a set of parameters and ranges to investigate the kinetics of the culture and bioconversion at the microwell scale. The changes in the factors and set points of the experimental stages is shown in Table 3.1.

Table 3.1. Factors and ranges for each of the rounds of multifactorial optimisation for the bioconversion of 7-ethoxycoumarin to 7-hydroxycoumarin by *E. coli* PQR368. Experiments performed as described in Section 2.4.5. Factors and ranges selected as discussed in Section 3.2. Change indicates variation in factor range compared to previous round of DoE experiments.

DoE Round	Factor	Unit	Range		Change
			Low	High	
1 (Screening)	A Post Induction Time	hr	8	65	-
	B Substrate Concentration	mM	0.1	1.0	-
	C Post Induction Volume	mL	0.5	1.0	-
	D Pre Induction Time	hr	2	5	-
	E Bioconversion Temperature	°C	25	37	-
	F Substrate Addition Time (Post Induction)	hr	0.17	1.0	-
	G Yeast Extract Concentration	gL ⁻¹	25	40	-
	H Buffered Media	-	No	Yes	-
	J Orbital Shaking Speed	rpm	300	1100	-
2 (Refinement)	A Post Induction Time	hr	50	75	Higher
	B Substrate Concentration	mM	0.75	1.25	Higher
	C Post Induction Volume	mL	0.5	1.0	No change
	D Pre Induction Time	hr	2	5	No change
	E Yeast Extract Concentration	gL ⁻¹	25	40	Higher
	F Bioconversion Temperature	°C	22	30	Lower
	G Buffered Media	-	No	Yes	No change
3 (Optimisation Time course)	A Substrate Concentration	mM	0.75	1.0	Lower
	B Yeast Extract Concentration	gL ⁻¹	40	50	Higher
	C (Post Induction Time)	hr	0	75	Continuous time course

3.2.1. Screening

A 10 factor, 128 run experiment (split into two blocks of 64 run experiments) was constructed in a resolution IV fractional factorial design (Whitcomb & Anderson 2004). This means that two factor interactions may be aliased with other two factor interactions, and three factor interactions with main effects (Goos & Jones 2011). The design was split into two blocks since two different shaking speeds could not be achieved simultaneously. It therefore allowed the determination of whether this was a significant factor in the context of the current design.

Figure 3.1. shows the half normal plot generated through analysis of the experimental data using Design Expert 8™ software. The half normal plot indicates factors or combinations of factors which lead to outputs which do not fit within the normal distribution (represented by the orange line on Figure 3.1.) and therefore have a statistically significant impact on the system.

Factors were selected on the basis of prior knowledge and literature data (Section 1.2.2.), in order to choose those which would appear to have the greatest chance of influencing productivity and growth. Ranges were selected on the same basis and spread wide enough that if there was an effect to be seen, it would become apparent. The design set points for this screening stage can be seen in Table 3.1 as DoE Round 1 (Screening). The experimental design complete with experimental data can be seen in Appendix 2.1.

A number of effects are evident (Figure 3.1.) including three main effects (post induction time - A, substrate concentration - B and buffering of the media - H), three two-factor interactions and a single three-factor interaction. Shaker speed is also a highly influential main effect (Figure 3.2.) not seen on the half normal plot as the design was broken down into two blocks around this factor. Figure 3.2. demonstrates the clear influence of shaking speed on productivity of the expression system, with the parity plot showing all experiments at a greater shaking speed result in higher 7-hydroxycoumarin concentration. As discussed previously (Sections 1.2.2. to 1.2.4.) oxygen availability is a crucial factor in the metabolism of microbial organisms, and for use as a substrate in P450 bioconversions. It would therefore be expected that there would be a significant positive influence of increasing shaking speed, which in turn increases oxygen mass transfer into the culture (Hermann et al. 2003).

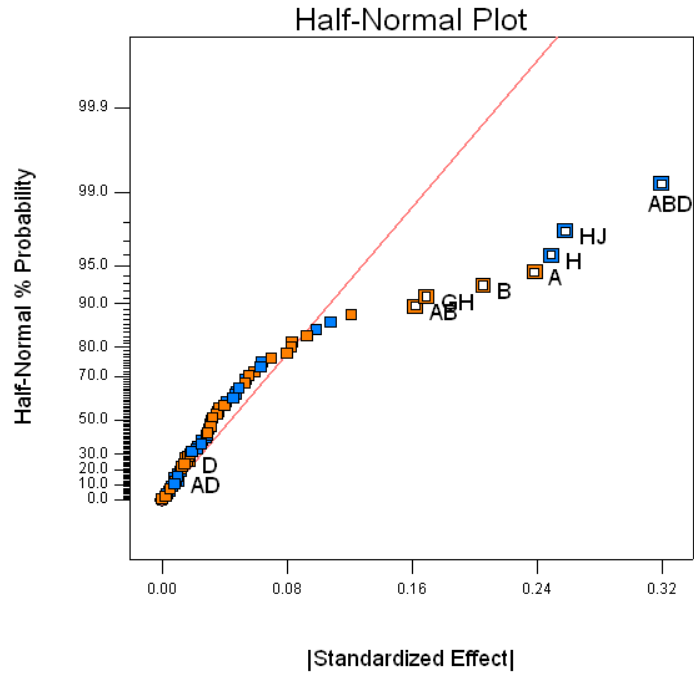


Figure 3.1. Half Normal Plot highlighting those factors with a statistically significant effect. Three main effects can be seen (A, H and B), as well as three two-factor interactions (AB, GH and HJ) and a single three factor interaction (ABD). Factors D and AD are included in order to ensure that the model is hierarchical. Experiments performed as described in Section 2.5.1. Factors and ranges defined in Table 3.1.

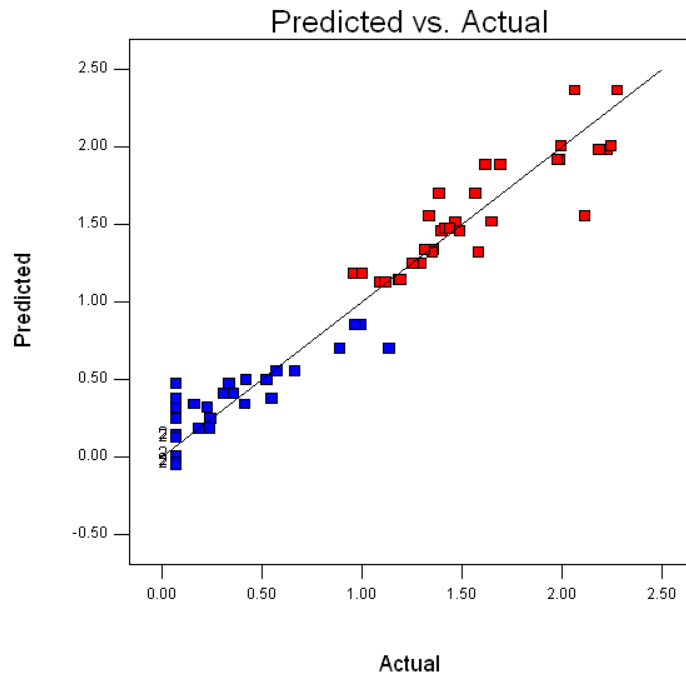


Figure 3.2. Parity plot for the P450 optimisation screening experiments. A clear influence of shaker speed on product concentration is seen. At greater shaker speed (red symbols) greater product concentration is seen when compared with lower shaker speed (blue symbols), irrespective of all other factors investigated. Experimental data generated as described in Section 2.5.1. Model generated using Design Expert 8 software.

As may be expected, increased substrate concentration and a longer post induction time result in increased final product concentrations. This indicates that over the ranges investigated there is no inhibition to the bioconversion seen as a result of substrate toxicity, nor that degradation of the product occurs such that it is no longer detected above noise.

The sole three factor interaction (post induction time, substrate concentration and pre-induction time) also incorporates one of the two factor interactions seen (between post induction time and substrate concentration). The influence of this interaction can be seen in Figure 3.3. It should be noted that the identification of multi-factor interactions such as this is one of the major advantages of using a DoE methodology. Three factor interactions are particularly difficult to decipher, but it can be seen that at the higher substrate concentration, increasing post induction time and lowering pre-induction time results in a greater product concentration, with an approximately four-fold increase in product titre. At low substrate concentration however, having both the post- and pre-induction times greater, results in increased product concentration. It is clear though that lower substrate concentrations result in lower product concentrations compared with those seen at higher substrate concentrations. The experimental against predicted data is an excellent fit (close to $y=x$), as shown in Figure 3.2., indicating that the model is highly representative of the system.

Additional two factor interactions are seen between yeast extract concentration and buffered media, and shaker speed and buffered media. The former indicates that when the media is buffered, increasing yeast extract concentration results in greater product concentration. Conversely, when the media is not buffered, increasing yeast extract concentration results in a reduced product concentration. This effect can be seen in Figure 3.4A, and is most likely as a result of the inability of the culture to maintain a favourable pH when the components of the complex media are broken down and used as an energy source upon depletion of the primary available carbon. The latter interaction highlights that at a higher shaker speed, buffering of the media results in reduced final product concentration, while at a lower shaker speed, the difference in product concentration between buffered and unbuffered media is negligible (Figure 3.4B).

The outputs of this stage of the investigation were used as the basis of the next round to inform factor and range selection as indicated in Table 3.1.

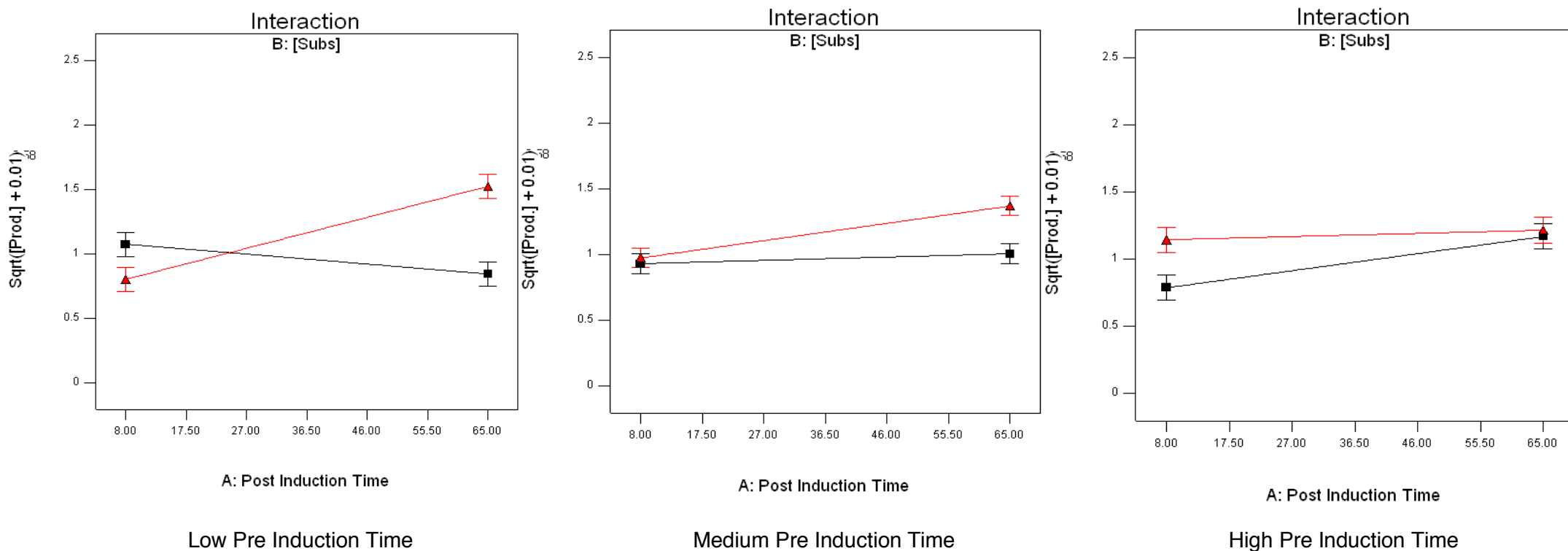


Figure 3.3. Three factor interaction between post induction time, substrate concentration and pre-induction time showing the effect on bioconversion of 7-ethoxycoumarin to 7-hydroxycoumarin. Black lines represent trends at low substrate concentration (0.1mM), while red lines represent high substrate concentrations (1.0mM). Experiments performed as described in Section 2.5.1. Model generated using Design Expert 8 software. Error bars represent one standard deviation about the mean.

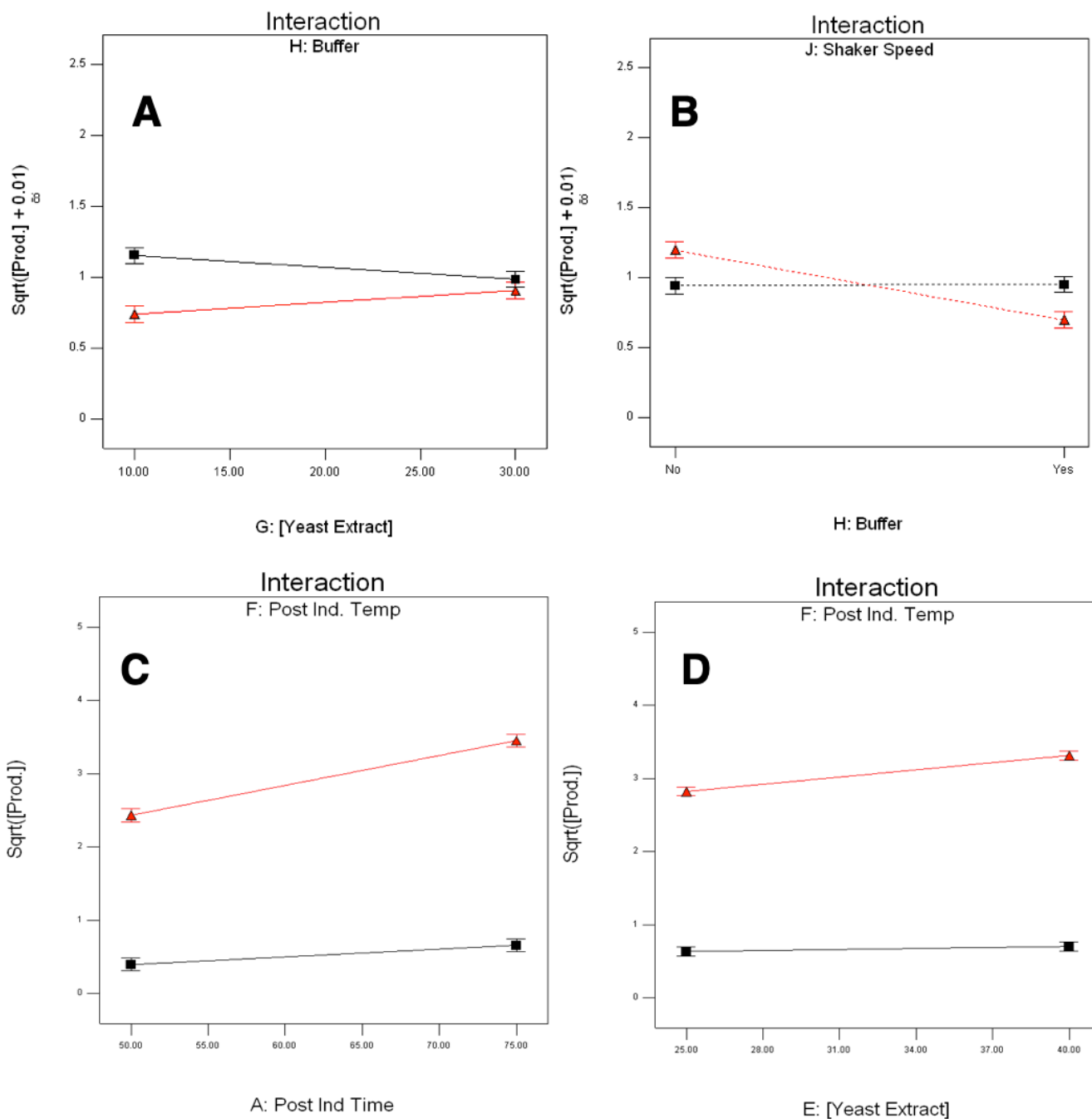


Figure 3.4. Two factor interactions observed during screening and refinement of the bioconversion of 7-ethoxycoumarin to 7-hydroxycoumarin by *E. coli* PQR368. A) Two factor interaction between yeast extract concentration and buffering of the media. Red line represents buffered media, while the black line represents unbuffered. B) Two factor interaction between shaker speed and buffering of the growth media. Red line represents buffered media, while the black line is unbuffered. C) Two factor interaction between post induction time and post induction temperature. Red line represents high post induction temperature (30°C), while black line represents low post induction temperature (22°C). D) Two factor interaction between yeast extract concentration and post induction temperature. Red line represents high post induction temperature (30°C), while black line represents low post induction temperature (22°C). Experiments performed as described in Section 2.5.2. Factors and ranges defined in Table 3.1.

3.2.2. Refinement

For the refinement stage, a seven factor, 64 run experiment was constructed in a resolution VII fractional factorial design (Whitcomb & Anderson, 2004). In this case, three factor interactions are aliased with four factor interactions, and notionally, five factor interactions with two factor interactions (Goos & Jones, 2011). 7-hydroxycoumarin concentration, resulting from the bioconversion of 7-ethoxycoumarin was again measured as the response. Figure 3.5. shows the half normal plot to highlight the factors and interactions of significant effect.

Four main effects (post induction time, substrate concentration, yeast extract concentration and post induction temperature) were identified using the half normal plot. At the higher substrate concentration used, a negative effect was observed, meaning that final product concentration is reduced with increasing substrate concentration. Combined with observations from the first round, it can be concluded that concentrations of substrate exceeding 1.0mM are likely to be inhibitory, and that the optimum is in the range of 0.75 to 1.0mM. The greatest impact seen is as a result of post induction temperature, with the increase from 22 to 30°C resulting in a 14-fold increase in final product concentration (Figure 3.6.).

The presence of two, two-factor interactions is also indicated (Figure 3.4 C&D). These both include post induction temperature, interacting with post induction time and yeast extract concentration independently. The first of these relationships shows that when post induction temperature is higher, increasing post induction time results in increased final product concentration, with all product titres significantly greater than those seen with lower post induction temperature. The interaction with yeast extract concentration is similar, with greater post induction temperature resulting in a positive relationship with increasing yeast extract concentration with respect to final product concentration. However, at the lower temperature the effect of yeast extract concentration can be considered negligible.

Finally, a single three factor interaction is identified between post induction time, post induction temperature and substrate concentration. For both high and low substrate concentrations, increasing post induction time and temperature results in greater product accumulation. Also, at high substrate concentration, increasing post induction time and temperature results in a more significant increase in final product concentration.

It can be seen that certain factors appear to show an effect repeatedly. Post induction time for example, suggesting that even under non-optimal conditions, the bioconversion will continue, however slowly, without inhibiting itself or creating a scarcity in key resources e.g. notably with cofactors. Additionally, post induction temperature is seen repeatedly as a positive effect, highlighting the requirement for energy input to the system to aid the progression of the oxidative bioconversion.

3.2.3. Bioconversion Kinetics Under Optimised Conditions

The optimisation time course incorporated two factors (substrate and yeast extract concentrations) investigated over a post induction time course. A sacrificial sampling method as described in Doig et al. (2002) was used to generate the time course of the bioconversion in microwells and a central composite facing (CCF) design, allowing for the determination of curvature within the ranges of the remaining variables. The design was constructed with four centre points.

This optimisation stage, highlighted the detrimental influence of substrate concentration (within the optimised band) on growth i.e. greater substrate concentration resulted in reduced biomass concentration.

The time course element showed that at around 20 hours post inoculation, there was a significant deterioration in the rate of biomass accumulation as the primary carbon source was depleted and there was a switch in metabolism to the deamination of yeast extract components (this was confirmed by free glycerol concentration assays and pH change measured over the culture). A similar effect is seen with bioconversion product concentration that plateaus alongside the depletion of the primary carbon source, indicating readily available carbon is crucial for bioconversion productivity, or that in the microwell environment there is a limited specific productivity that the culture can achieve.

From these observations, feeding of additional primary carbon source, as well as online pH monitoring and control is going to be critical during scale up to pilot scale STRs. It should also be noted that little effect was seen on bioconversion product formation as a result of the factor ranges employed, indicating that this is a relatively stable region of design space (Tholudur et al. 2005).

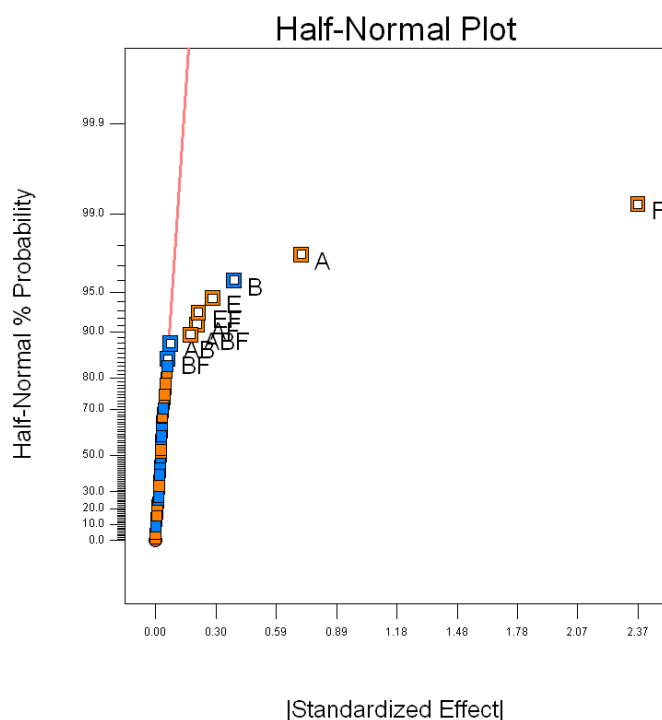


Figure 3.5. Half Normal Plot highlighting those factors of significant statistical effect during refinement of the bioconversion of 7-ethoxycoumarin to 7-hydroxycoumarin by *E. coli* PQR368. Four main effects can be seen (factors F, A, B, E), as well as two, two-factor interactions (EF, AF) and a three factor interaction (ABF) (see main body of text for comments). Factors and ranges defined in Table 3.1.

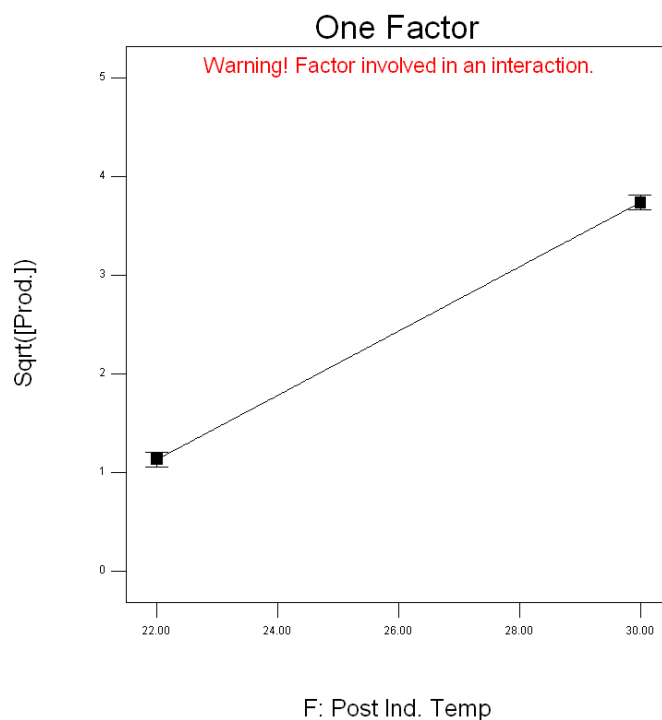


Figure 3.6. One factor effect plot highlighting a potential 14 times increase in final product concentration across the post induction temperature range (22-30°C) during refinement of the bioconversion of 7-ethoxycoumarin to 7-hydroxycoumarin by *E. coli* PQR368.

Table 3.2 provides a summary of the effects and interactions during the first two rounds of optimisation. This highlights several things, firstly an iterative progression towards a multifactorial optimum, a significant dependence on Post Induction Time for the progression of the bioconversion, and in the second stage, as the models become more refined, a significant positive relationship between the productivity of the culture and the post induction temperature (both as a main effect and within interactions).

Table 3.3. uses analysis of variance (ANOVA) to highlight the statistical significance of the models generated in each of the DoE rounds. The p-value indicates a measure of the confidence that can be held in the model, with a value less than 0.05 typically considered significant (Rice 1989). The Cook statistic indicates which of the runs would have the greatest impact on the model if it were removed. If all values are small (<1) then the model can be considered a good representation of the data. The number of outliers in the residuals is the number of experimental runs which do not fit within the normal distribution once the model is applied. A measure of signal to noise has also been included, with ratios of 31.1 and 54.1 to one found in the models for the first two rounds of DoE. This shows that the data is valid and not an artefact of the noise of the system. Additionally, all models are seen to conform to a high degree of statistical certainty as demonstrated by the ANOVA data (Table 3.3.).

Table 3.4. summarises the overall gains in biomass and product accumulation, using the multifactorial optimisation approach, when compared with preliminary work done as part of this research, but also with previous work carried out at UCL on this expression system (Baboo et al. 2012). After three rounds of DoE, 3.3 and 2.0 times increases in bioconversion product and biomass accumulation were seen over preliminary experiments in microwells with respect to product titre and biomass concentration respectively, with a specific product concentration increase of 1.5 times. In addition, as a comparison with previous optimisation work on this expression system (Baboo 2012), there is a 1.1 to 1.4 times increase in the identified responses.

It can be seen that, although successful in increasing the product concentration, the optimisation was not able to considerably increase specific productivity i.e. product generated per unit of biomass (Table 3.4.).

Table 3.2. Summary table of the statistically significant effects and interactions on the yield of 7-hydroxycoumarin during two rounds of multifactorial optimisation on the bioconversion from 7-ethoxycoumarin using *E. coli* PQR368.

DoE Round	Interaction	Factor/s	Units	Range		Effect
				Low	High	+/-
1 (Screening)	Main Effect	Post Induction Time	hr	8	65	+
		Substrate Concentration	mM	0.1	1.0	+
		Shaker Speed	rpm	300	1100	+
		Buffered Media	-	No	Yes	-
	Two Factor Interaction	Post Induction Time, Substrate Concentration	hr, mM	8, 0.1	65, 1.0	+
		Yeast Extract Concentration, Buffered Media	gL ⁻¹ , -	10, No	30, Yes	+
		Buffered Media, Shaker Speed	-, rpm	No, 300	Yes, 1100	-
Three Factor Interaction	Post Induction Time, Substrate Concentration, Pre Induction Time	hr, mM, hr	8, 0.1, 2	65, 1.0, 5	-	
2 (Refinement)	Main Effect	Post Induction Time	hr	50	75	+
		Substrate Concentration	mM	0.75	1.25	-
		Yeast Extract Concentration	gL ⁻¹	25	40	+
		Post Induction Temperature	°C	22	30	+
	Two Factor Interaction	Post Induction Time, Post Induction Temperature	hr, °C	50, 22	75, 30	+
		Post Induction Time, Yeast Extract Concentration	hr, gL ⁻¹	50, 25	75, 40	+
	Three Factor Interaction	Post Induction Time, Post Induction Temperature, Substrate Concentration	hr, °C, mM	50, 22, 0.75	75, 30, 1.25	+

Table 3.3. Analysis of Variance (ANOVA) for the models generated during multifactorial screening and refinement of the bioconversion of 7-ethoxycoumarin to 7-hydroxycoumarin by *E. coli* PQR368.

DoE Round	p-value	Cook statistic. (largest value to model)	No. outliers in residuals	Signal:Noise (x:1)
1	<0.0001	0.209	2/64	31.1
2	<0.0001	0.161	1/64	54.1

Table 3.4. Calculated gains in biomass accumulation, 7-hydroxycoumarin concentration and specific product concentration upon scale up of the whole cell bioconversion of 7-ethoxycoumarin to 7-hydroxycoumarin using *E. coli* PQR368. Table shows significant increases in biomass and bioconversion product compared with preliminary microwell cultures and previous work (Baboo, 2012).

	Biomass gL ⁻¹	[7-Hydroxycoumarin] mgL ⁻¹	Specific [7-Hydroxycoumarin] (x10 ⁻³)
Preliminary Work (μ -well)	2.3	0.8	0.4
Prior Work	4.1	2.0	0.5
After DoE	4.5	2.8	0.6
Increase:			
- vs. prelim. μ -well	2.0x	3.3x	1.5x
- vs. Baboo (2012)	1.1x	1.4x	1.3x

In addition to increased product and biomass concentration, the output of the three rounds of experiments was a set of optimised conditions to be translated to pilot scale. These conditions are shown in Table 3.5. Media compounds and levels were fixed based on the DoE timecourse experiment, while other factors specific to STRs e.g. RPM and DOT set points, were established based on prior knowledge of *E. coli* fermentation and literature precedent.

3.2.4. Scale Up to Pilot Fermentation Scale

3.2.4.1. Initial Scale Up Comparison with Microwells

After optimising the bioconversion of 7-ethoxycoumarin to 7-hydroxycoumarin in *E. coli* PQR368 in microwells, scale up to bench top bioreactors was undertaken in order to: (i) quantify the oxygen demand (using the adapted mass spectrometer configuration as described in Section 2.5.4.), (ii) determine the mechanism of oxygen utilisation and so, (iii) demonstrate the optimised conditions in industrially relevant bioreactors. Without characterisation of the oxygen mass transfer in the microwells, scale up was performed on the basis of providing a turbulent flow environment and literature values appropriate for *E. coli* fermentation. Direct comparison between microwells and stirred tank bioreactors is poorly characterised (as discussed in Section 1.2.7.), and so with the objective to quantify the maximum oxygen demand of the optimised system, the decision was made to ensure that a turbulent flow environment was achieved to ensure effective oxygen mass transfer.

Table 3.5. Set points and starting conditions for all pilot scale STR cultures of whole cell bioconversion of 7-ethoxycoumarin to 7-hydroxycoumarin using *E. coli* PQR368.

Factor	Set point	Unit
Media:		
• Yeast Extract	40	gL ⁻¹
• Tryptone	12	gL ⁻¹
• Glycerol	4	mLL ⁻¹
• Phosphate Buffer	10	%v/v
• PPG	0.5	mLL ⁻¹
DOT	40	%
pH	7	-
Agitation	750	rpm
Temperature		
• Pre Induction	37	°C
• Post Induction	30	°C
Pre Induction Time	2	hr
Post Induction Time	28	hr
Substrate	1	mM
Starting Volume	3	L

The basic trends from the scale up comparison can be seen in Figure 3.7. In microwells, biomass concentration increases to $2.0 \text{ g}_{\text{DCW}}\text{L}^{-1}$ after 20 hours, and shows a characteristic growth curve. In parallel, product concentration increases to a maximum of 0.05mgL^{-1} between 20 and 25 hours after inoculation, with the accumulation rate closely aligned to the increase in biomass concentration. In STRs under induced, batch conditions the rate of biomass accumulation is greater, reaching approximately $5.0 \text{ g}_{\text{DCW}}\text{L}^{-1}$ after 20 hours. As with the microwells, product accumulation is closely aligned with the increase in biomass concentration, reaching a maximum of 1.36 mgL^{-1} after 30 hours.

Figure 3.7. shows a positive correlation between biomass concentration and bioconversion product concentration at both microtiter (1mL) and batch pilot bioreactor (3L) scales. However, it can be seen that the product formed per unit biomass is significantly greater in the case of the pilot scale bioreactor. Table 3.6. reinforces this, demonstrating a 10 times greater specific product concentration than could be achieved in microwells. There are a number of reasons for this. Firstly, the pilot scale bioreactor sparges air directly into the culture (Figure 2.1, Section 2.3.1), rather than relying on gas-liquid mass transfer across the surface of the culture. This means greater oxygen mass transfer and therefore more available oxygen for use as a metabolic and bioconversion substrate. Additionally, in the case of the pilot bioreactor more O_2 is made available than can be utilised for growth due to the limited supply of carbon in batch mode. As such, the excess oxygen as represented by the maintenance of DOT values at 40%, is more freely available for use in the P450 bioconversion.

It should also be noted that previous work suggests that a microwell may not be able to sustain the biomass and bioconversion titres achieved in the batch pilot scale fermentation, with maximum achievable OTRs reported to be $150 \text{ mmolL}^{-1}\text{hr}^{-1}$ ($2.5 \text{ mmolL}^{-1}\text{min}^{-1}$) (Hermann et al. 2003). A question is therefore raised over the suitability of microwells to provide an accurate scalable mimic for stirred tank bioreactors when studying oxidative bioconversions. This suggests a requirement for either novel plate designs (Funke et al. 2010) or sparged microwell systems (Betts et al. 2014).

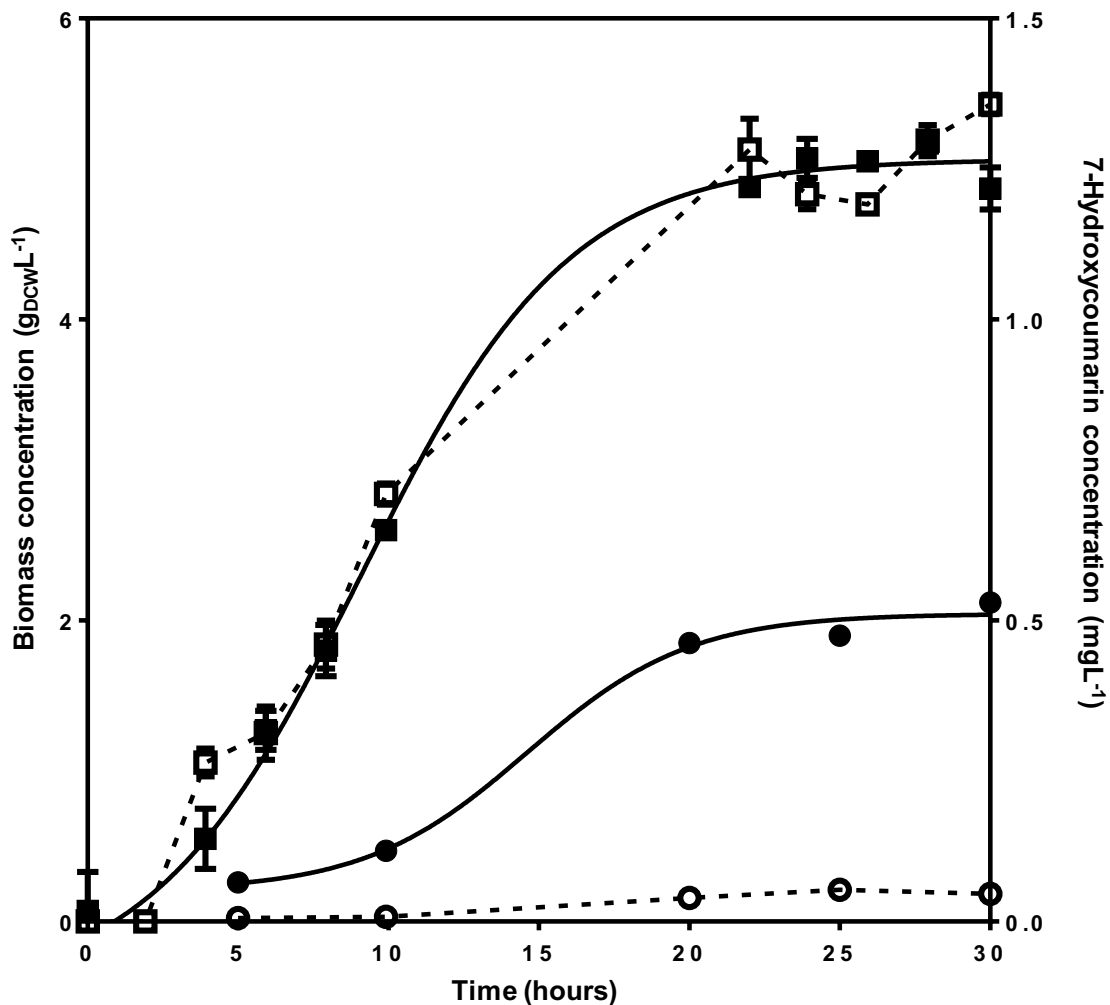


Figure 3.7. Comparison of growth and bioconversion kinetics between optimised microtiter plate and pilot scale bioreactor cultures of *E. coli* PQR368 for the bioconversion of 7-ethoxycoumarin to 7-hydroxycoumarin. Closed symbols and solid lines show the biomass concentration (DCW) in microwells (●) and batch pilot scale bioreactor (■). Open symbols (○, □) and dashed lines show bioconversion product concentration for microwell and bioreactor respectively. Cultures were induced at two hours post inoculation. Growth data has been fitted with a sigmoidal function curve to illustrate growth kinetics. Experiments performed as described in Section 2.5.4. Error bars represent one standard deviation about the mean (n=3).

3.2.5. Pilot Scale Culture Strategy Comparison

In order to further elucidate the oxygen requirements for growth and bioconversion three fermentation strategies were explored; non-induced batch (NI-B), induced batch (I-B) and induced fed batch (I-FB). Comparisons were made in terms of their growth, P450 bioconversion productivity and the resultant demands of the system for oxygen. All fermentations were performed based on the optimised conditions in Table 3.5.

Biomass accumulation across the three fermentation strategies was found to differ greatly. Figure 3.8A and Table 3.6 shows the relationship between biomass concentrations and accumulation rates under each of the three fermentation conditions. As expected, biomass accumulation is greatest in the induced fed batch culture, reaching a peak cell density of over 25gL^{-1} after 28 hours. Interestingly, non-induced batch culture grows significantly better than induced batch, reaching densities of around 15gL^{-1} and 5gL^{-1} respectively after approximately 12 and 25 hours. This is the result of a number of influences. A significant volume of ethanol is introduced to the culture after two hours (used to dissolve bioconversion substrate). The impact of this can be seen between two and eight hours in Figure 3.8A, during which time the non-induced culture enters log phase, rapidly accumulating biomass, while this is delayed in the cultures to which ethanol is added. This is seen in Figure 3.9. also, where the volumetric productivity of induced cultures is impeded.

Additionally, the induced batch culture has an increased demand for energy and oxygen due to the bioconversion (Figure 3.9.). As there is no provision of carbon source during batch mode, the ability of the culture to enter a phase of sustained growth is impeded.

The bioconversion though, proceeds alongside reduced growth. This is most likely due to metabolism having a greater energy requirement than the bioconversion. A large portion of a cells activities involve acquiring and utilising energy for metabolism (Cooper 2000), while the bioconversion is a single enzymatic reaction, and therefore does not have the same amount of energetic demands. This observation relates to the productivity of the induced batch and fed batch cultures also.

Figure 3.8B and Table 3.6 highlight that the priority of the induced fed batch culture, in the carbon rich environment is on growth. Product titres achieved are approximately half that of the batch culture (0.66mgL^{-1} compared with 1.36mgL^{-1} maximum). Figure

3.7. and Figure 3.9. do highlight that there is a correlation between culture growth and bioconversion activity, however it has been demonstrated that the relationship is more complex than this with respect to the titre achieved, as discussed in Section 3.2.3. This is reinforced by the difference in specific product concentration, which is over 10 times greater during batch culturing (Table 3.6.).

3.2.6. Oxygen Demand Quantification at Pilot Scale

Oxygen demands during whole cell oxidative bioconversions must be understood in the context of the individual culture performance, but also in terms of the impact of each of the three fermentation modes. To do this, Figure 3.9 compares the biomass accumulation and bioconversion productivity with the OUR for each of the three fermentation strategies independently, while Figure 3.10 compares the oxygen demands of each of the three fermentation strategies directly. This allows understanding of the mechanism for oxygen utilisation and a clear appreciation of the preferred bioprocess conditions. In order to achieve this, gas lines into, and out of the bioreactor were configured such that they were measured directly by a mass spectrometer. Thus, accurate quantification of the gas stream compositions was possible (Section 2.5.4.3.).

A comparison of the oxygen demand for each of the three fermentation strategies over the 30 hour culture is shown in Figure 3.10. It serves to demonstrate the varying requirement for oxygen throughout the culture, which depends upon the phase of the culture, the mode of operation and the condition of the culture environment. For example, the induced fed batch culture maintains a high OUR, most likely as oxygen is being prioritised for growth, and the maintenance of the culture, and the availability of carbon is making this possible.

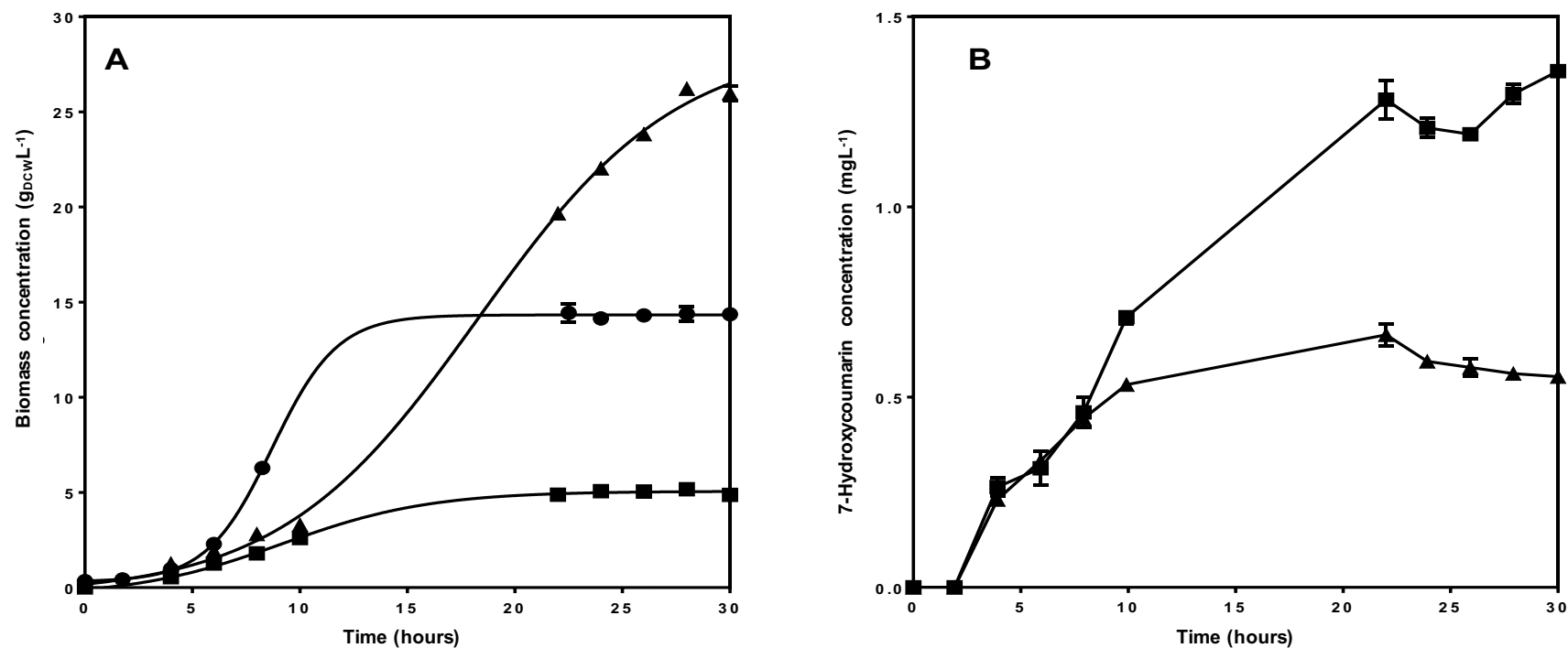


Figure 3.8. Comparison of three pilot scale fermentation strategies with respect to (A) growth of *E. coli* PQR368 strain and (B) kinetics of the bioconversion of 7-ethoxycoumarin to 7-hydroxycoumarin carried out by *E. coli* PQR368. Non-induced batch (●), induced batch (■) and induced fed batch (▲) are shown, with induction and the start of feeding at two and eight hours post inoculation respectively. Errors bars represent one standard deviation about the mean ($n=3$). Growth data has been fitted with a sigmoidal function curve to illustrate growth kinetics. Experiments performed as described in Section 2.5.4.

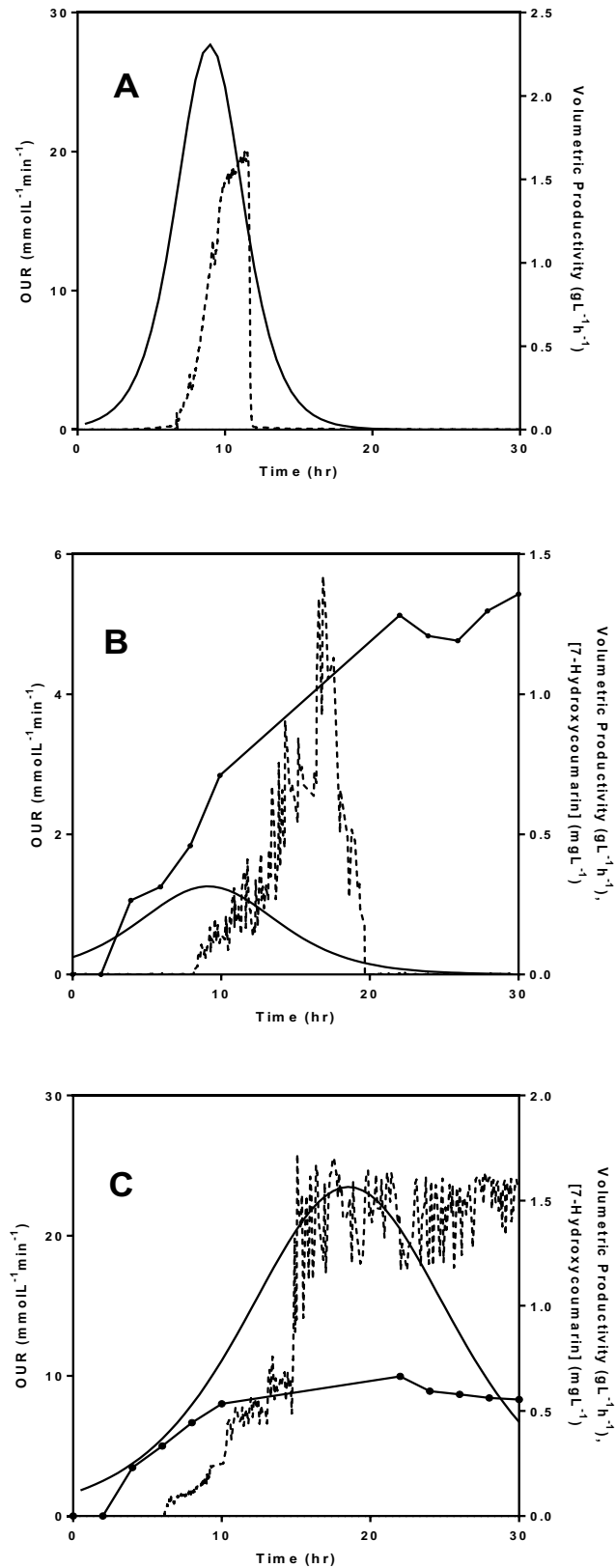


Figure 3.9. Relationship between kinetics of bioconversion of 7-ethoxycoumarin to 7-hydroxycoumarin by *E. coli* PQR368 (●), volumetric productivity with respect to biomass accumulation (solid line), and oxygen uptake rate (dashed line) during non-induced batch (A), induced batch (B) and induced fed batch (C) pilot scale cultures. Induction and start of feeding are at two and eight hours post inoculation respectively. Errors bars represent one standard deviation about the mean ($n=3$). Experiments performed as described in Section 2.5.4.

3.2.7. Identifying Oxygen Requirements and Prioritisation

Figure 3.9. allows interpretation of the mechanism by which each of the culture modes are utilising oxygen and how this impacts on culture outputs. Each of the cultures are plotted on different scales so as to highlight the relationships between variables within each separate culture. Figure 3.9A shows the use of oxygen during the non-induced batch culture, which is exclusively for accumulation of biomass. There is a direct interaction between the transition into log phase and the sharp rise in the uptake of oxygen as the culture enters a period of exponential growth. After this period, when the culture enters stationary phase, the requirement decreases as the biomass concentration in the culture is sustained (stationary phase), rather than increasing (exponential phase).

For induced cultures, OUR begins to rise dramatically when volumetric productivity with respect to biomass accumulation reaches approximately $0.3\text{gL}^{-1}\text{h}^{-1}$ (Figures 3.9B&C). OUR for the NI-B culture however, starts to increase at a much greater volumetric productivity ($\sim 1.3\text{gL}^{-1}\text{h}^{-1}$) (Figure 3.9A). This is most likely due to the additional burden, both in terms of oxygen and energy, of generating the P450 enzyme and carrying out the bioconversion in induced cultures. In addition, for NI-B culture growth has not also been negatively impacted by the introduction of chemical inhibitors (e.g. ethanol for dissolution of substrate). Peak OUR is seen in batch cultures between 1 and 3 hours after peak volumetric productivity as the system attempts to respond to the culture demand. The fall in OUR corresponds with the end of the transition from exponential into stationary phase in all cases. In fed batch culture, where growth is sustained, peak OUR directly coincides with maximum volumetric productivity. This further supports the point made pertaining to the mechanism of oxygen utilisation and its dependence on the condition of the culture. Additionally, the stage of the fermentation can be seen to have a significant impact on the O_2 demand in each of the three fermentation strategies.

In order to better illustrate the differences in OUR demand between the three fermentation strategies, Figure 3.10. shows the oxygen uptake rate for each plotted on the same scale for direct comparison. The maximum oxygen demand seen during fed batch culture is $25.8\text{mmolL}^{-1}\text{min}^{-1}$, which, while greater than that of the non-induced culture, does not correlate directly with the almost doubling in peak biomass concentration. This demonstrates the presence of additional influences on the oxygen demand.

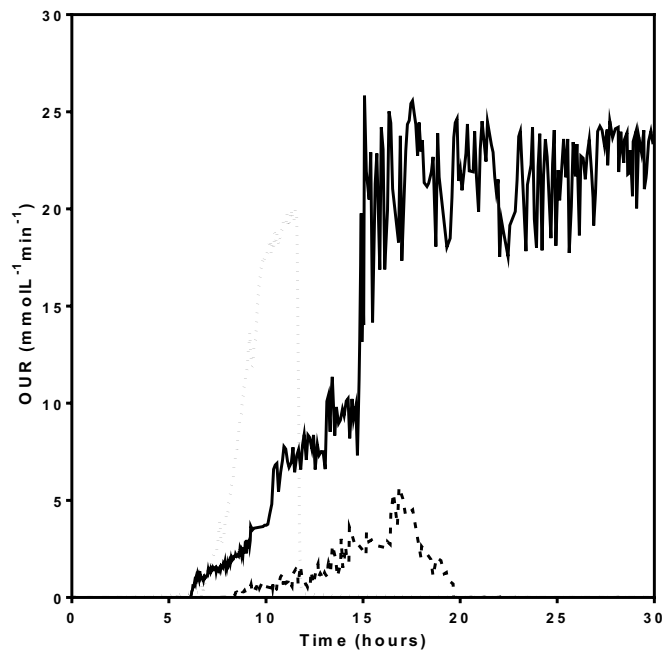


Figure 3.10. Oxygen uptake rate during induced fed batch (solid line), induced batch (dashed line) and non-induced batch (dotted line) pilot scale cultures of *E. coli* PQR368 carrying out the bioconversion of 7-ethoxycoumarin to 7-hydroxycoumarin. Experiments carried out as described in Section 2.5.4.

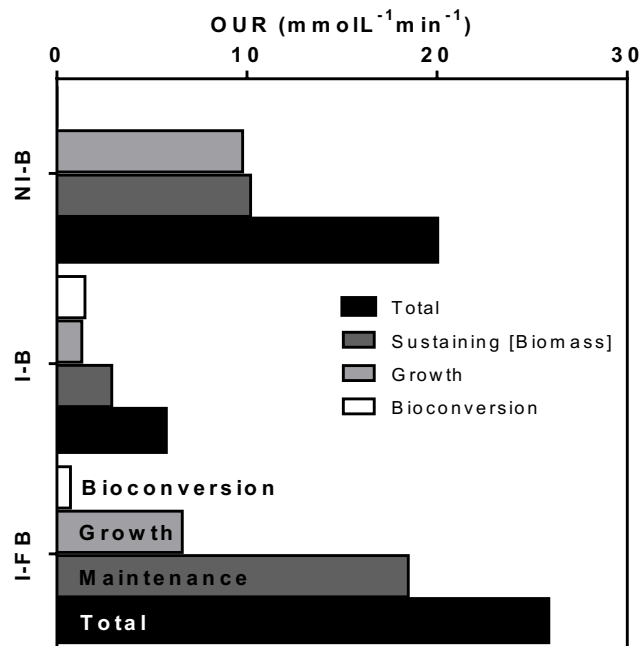


Figure 3.11. Breakdown of maximum oxygen uptake rates observed during non-induced batch, induced batch and induced fed batch pilot scale cultures of *E. coli* PQR368 carrying out the bioconversion of 7-ethoxycoumarin to 7-hydroxycoumarin. Contributions due to bioconversion (white), growth (light grey), maintenance of the biomass concentration (dark grey) are shown as well as peak total OUR (black). Values determined as described in Section 2.5.4.

Table 3.6. Effect of fermentation mode on the biomass accumulation and bioconversion productivity for the bioconversion of 7-ethoxycoumarin to 7-hydroxycoumarin using *E. coli* PQR368 in optimised microwell culture and each of three pilot scale fermentation modes (non-induced batch - NI-B, induced batch - I-B, induced fed batch – I-FB). Experiments performed as described in Section 2.5.4.

	Unit	DSW	NI-B	I-B	I-FB
Peak OUR	mmolL ⁻¹ min ⁻¹	-	19.9	5.68	25.8
Peak DCW	gDCWL ⁻¹	2.12	14.4	4.10	26.2
Peak [7-Hydroxycoumarin]	mgL ⁻¹	0.05	-	1.36	0.66
Peak Volumetric Productivity	gDCWL ⁻¹ h ⁻¹	-	2.31	0.31	1.56
Specific [7-Hydroxycoumarin]	x10 ⁻⁴	0.24	-	3.30	0.25

Figure 3.11. shows the breakdown of the maximum observed oxygen uptake rate during culturing for each of the three fermentation strategies. In addition to maintaining the biomass concentration, the OUR can be attributed to both the oxygen utilised as substrate in the bioconversion and the oxygen required for growth. Batch mode culture demands the lowest peak oxygen uptake rate. The OUR is more than four times lower than that of the fed batch culture, highlighting the dominance that growth has on the required oxygen. In addition, Table 3.6. helps to highlight the influence of fermentation strategy, and the relationship between maximum oxygen demand and productivity.

Table 3.7 shows the contribution of each of the three major influences on culture oxygen demand; sustaining the level of biomass present in the culture at that time, increasing biomass concentration through growth and the P450 bioconversion of 7-ethoxycoumarin to 7-hydroxycoumarin. Thus, the effect on the total OUR of each of these is highlighted. The contributions were derived using simultaneous equations and the data generated during the pilot scale cultures under each of the three different fermentation strategies. By comparing the oxygen demands derived for each of the cultures and their performance in terms of the major influences on oxygen uptake (growth, maintenance and bioconversion), the oxygen requirement which can be attributed to each is calculated as shown in Appendix 2.2. Therefore, based on this investigation, the peak total OUR can be estimated using Equation 3.1.

$$\text{Peak Total OUR} = 0.71 \alpha + 4.23 \beta + 1.09 \gamma \quad \text{Equation 3.1.}$$

Where α represents the maximum biomass concentration during culture ($\text{g}_{\text{DCW}}\text{L}^{-1}$), β the peak volumetric productivity ($\text{gL}^{-1}\text{h}^{-1}$) and γ the maximum 7-hydroxycoumarin concentration (mgL^{-1}).

Table 3.7. Contribution to the peak total OUR for each of the three major components; sustaining the level of biomass present in the culture at that time, increasing biomass concentration through growth and the P450 bioconversion of 7-ethoxycoumarin to 7-hydroxycoumarin. Calculated using simultaneous equations formed from the fermentation data generated for each of the three culture strategies.

Component of total OUR	Contribution (%)
Sustaining current biomass	11.8
Growth	70.1
Bioconversion	18.1

Although the specific oxygen requirement for the bioconversion is much greater than for growth (approximately 250 times), the percentage conversion is very low. As such, in the case of induced batch culture, although bioconversion titre is greater than other cultures, low volumetric productivities and biomass concentrations result in a much lower total OUR. Growth is shown to be a more significant influencer on total OUR proportionally (when compared to maintenance), however, as Figure 3.11. shows, the OUR required for maintaining biomass concentration can outweigh that for growth due to the quantity of biomass.

In order to meet the demands of these high oxygen demand expression systems, there is a need for DOT controlled microwell cultivation systems, particularly for microbial, whole cell oxidative bioconversions. Previous data suggests that oxygen supply to microwells would be insufficient for the demands under the optimal conditions seen in this investigation. This is something which will be investigated in Chapter 4 of this thesis. It has been shown that optimal shaking of the DSWs can provide a maximum OUR of $150 \text{ mmolL}^{-1}\text{hr}^{-1}$ (equating to $2.5 \text{ mmolL}^{-1}\text{min}^{-1}$) (Hermann et al. 2003), with all oxygen delivered through surface gas-liquid mass transfer. It is possible to extrapolate from the OUR relationship in Table 3.7. to suggest that the OUR for the optimised scale down culture (using biomass concentration, bioconversion

product concentration and assuming volumetric productivity equal to the I-B pilot culture) would be approximately $2.9 \text{ mmolL}^{-1}\text{min}^{-1}$, which is close to the oxygen transfer limit identified by Hermann et al (2003), and explains the limitations in achievable cell density and product titre.

3.2.8. Summary

The aim of this chapter was to establish the methodologies for effective optimisation of a whole cell oxidative bioconversion using a microbial expression system at microwell scale, and accurate quantification of OUR for a microbial expression system under the conditions which result in peak oxygen demand.

Two of the greatest obstacles limiting the application of whole cell P450 monooxygenases in industry are insufficient bioconversion yields, and a lack of understanding regarding the demands on the culture environment, particularly in terms of the oxygen requirement of these expression systems.

The bioconversion of 7-ethoxycoumarin to 7-hydroxycoumarin using P450SU2 has been optimised using a multifactorial DoE methodology. Three rounds of DoE (screening, refinement and optimisation) were carried out resulting in a 3.3-fold increase in product titre and a 1.5-fold rise in specific productivity. Despite this, bioconversion yields achieved remain insufficient for commercial application, particularly when compared with what has been stated as necessary to replace a chemical process (Straathof et al. 2002). As such, in this case it appears that the limitations are with the biological system, rather than with the engineering.

Scale up characterisation over a 3000-fold volume increase, under optimised conditions showed that microwells, because of the OTR limitations, do not provide an accurate scale down model in terms of growth rates and yields. In this chapter, investigating microbial oxidative bioconversions, product concentrations achieved were more than 25 times lower at the smaller scale. Scale up characterisation suggests that more advanced, DOT controlled microwell systems would be better suited to providing a direct mimic to a pilot scale bioreactor when culturing a whole cell, oxidative bioconversion. A tenfold greater specific productivity was achieved in the bioreactor and the most likely cause is the limited achievable oxygen supply in microwells.

Batch mode fermentation proved to be the favoured route for increased product generation, with yields achieved (1.36 mgL^{-1}) approximately double that of the fed batch

counterpart. Although a correlation is observed between biomass accumulation and bioconversion product concentration, they are not directly linked. The relationship is more complicated, requiring sufficient oxygen and energy for the bioconversion to take place, but ensuring that which is provided is limiting to growth. Additionally, it has by far the lowest oxygen demand of the three fermentation modes.

Peak oxygen demands derived were in the range of 5.68 to 25.8 mmolL⁻¹min⁻¹, and showed not only that cellular metabolism is the priority for oxygen utilisation, but also confirmed that microwells are incapable of providing sufficient oxygen to match the peak demands of the larger scale cultures they are attempting to replicate.

A relationship was identified between the three main contributors to OUR (maintenance, growth and bioconversion) as indicated in Figure 3.11. Oxygen requirement due to maintenance of the biomass was highlighted as the greatest proportional contributor. The greatest specific demand on oxygen was the bioconversion, however due to low 7-hydroxycoumarin yields it contributes little to the total OUR, with maintenance of accumulated biomass and growth demanding the majority.

The mechanism for oxygen utilisation has been determined, with biomass accumulation the priority, rather than supplementary cellular activities. This corroborates the work of Baldwin & Woodley (2006) and Luedeking & Piret (1959) which hypothesises that metabolism is prioritised over additional cellular activities in the utilisation of oxygen. The relationship between the major influencers on OUR has been determined, further indicating growth as the key driver behind peak OUR.

In the following chapter oxygen mass transfer rates will be quantified in high throughput scale down systems. This will involve the development of an improved method for quantification in microwell plates in order to enhance understanding of oxygen mass transfer during microbial cultivation.

4. Accurate Quantification of Oxygen Mass Transfer Rates in High Throughput Scale Down Systems.

4.1. Context and Aim

In the previous chapter the importance of understanding the relationship between bioreactor oxygen transfer capability and the utilisation of oxygen in an oxidative, whole-cell bioconversion process was demonstrated (Section 3.2.6). That work was performed in a conventional laboratory scale bioreactor equipped with a polarographic dissolved oxygen probe and off-gas mass spectrometry for analysis of inlet and outlet gas compositions (Section 2.5.4.3). Modern approaches to microbial fermentation process development make use of high throughput scale down systems (Bareither et al. 2013; Ellert & Vikstrom 2014) where the challenge of characterising and understanding oxygen mass transfer capabilities is a substantial one. The challenge is confounded by an abundance of commercially available technologies (Section 1.2.7); not only do scales range by up to six orders of magnitude, from microliters to hundreds of millilitres, but geometries, configurations, methods of mixing and gas delivery also differ from system to system. This chapter will focus on oxygen transfer quantification in two of the most commonly used microwell systems (24- and 96-deep square well plates) and the relationship between them.

Single use scale down microwell systems are seeing a year on year increase in uptake, particularly as simple and inexpensive culture vessels for high throughput screening applications and process development before scale up (Büchs 2001; Kensy et al. 2005). Unfortunately, though, due to the dependence of mass transfer on transport across the gas-liquid interface, oxygen, a key substrate for microbial expression systems is often limiting (Marques et al. 2010; Büchs 2001). This growing uptake of microwell culture systems leads to a question of compatibility and comparability with larger laboratory and pilot scale bioreactors such as stainless steel (and increasingly, single use) stirred tank bioreactors. However, this too is difficult to reconcile. There are a range of influences to consider including heat transfer, hydrodynamics, nutritional and process parameters.

Oxygen is the terminal electron acceptor in aerobic metabolism, required for growth, cellular maintenance and the generation of primary and secondary metabolites. Provision of adequate oxygen is arguably the greatest influence on

productivity of a microbial system (van Beilen et al. 2003). This makes it a key factor in what makes transferring between scales extremely challenging (Junker 2004). As such, it is imperative that the oxygen mass transfer capabilities of microwell systems are accurately quantified.

Until recently it has been difficult to measure and characterise oxygen mass transfer in smaller scale bioreactor formats during cultivation. Previously, it has been necessary to rely on methods such as sulphite oxidation (e.g. Linek & Vacek 1981; Hermann et al. 2001; Maier et al. 2001), or calculation of interfacial surface areas (Doig et al. 2005). More recently work has been carried out with a miniature DOT probe inserted into a single well of a microwell plate (Baboo, 2012), but this has its limitations also (Section 1.2.9).

Now however, it is possible to measure DOT online in 24 DSW plates using the SDR SensorDish® system with OxoDish® plates (as described in Section 2.6), which use fluorescent spots and readers to non-invasively quantify the extent of oxygen saturation. This means that DOT profiles can be generated enabling the calculation of oxygen mass transfer in a manner much more akin to larger, process relevant bioreactors using polarographic probes. Indeed, it has been noted by Gupta & Rao (2003) that non-invasive optical sensors are a superior method of determining oxygen mass transfer coefficients than the sulphite oxidation method. A similar technology employing fluorescent chemical compounds was used in microwells for animal cell culture (Deshpande & Heinzle 2004), however, this is simpler as it operates over much longer time periods and with much slower changes in DOT. For a more extensive review of oxygen mass transfer characterisation methodologies see Section 1.2.9.

Use of the SDR system to generate oxygen saturation profiles offers some improvements over the previously mentioned methods. Oxygen mass transfer characterisation using either static (Wise 1951; de Ory et al. 1999; Puthli et al. 2005; Özbek & Gayik 2001 etc.) or dynamic gassing out methods (Bandyopadhyay et al. 1967; Parente et al. 2004; Islam et al. 2008; Ni et al. 1995) is possible, each of which have their limitations, including a need for correction of values due to the response time of sensors (Gupta & Rao 2003) and the assumption that cultures remain unchanged for the duration of the measurements (Garcia-Ochoa et al. 2010), thus not taking into consideration the dynamic properties of a fermentation culture.

There is also significant disparity in bacterial culture between the OURs measured using the traditional dynamic method, and those observed by calculation using online process data (Santos et al. 2006). Additionally, these measurements are commonly taken under a single set of conditions, assuming that the environment will not change. Determination of how the aeration environment changes under the influence of a range of factors is important.

This work focuses on overcoming the obstacles of characterizing oxygen mass transfer rates in small scale culture technologies, translation to commercially relevant process scales and the limitations of traditional measurement methodologies.

4.1.1. Aims

Many scale down systems are unable to meet the maximum oxygen demands determined in the previous chapter (Section 3), the increasing use of microwell technologies for screening and initial process development, and the limitations with current methods for oxygen mass transfer quantification. To this end, the aim of this chapter is to develop a new method for accurate quantification of oxygen mass transfer in two microwell scales, and describe the relationship between them.

Depending on the experimental objective and workflow, both 96 DSW and 24 DSW are highly relevant. 96 DSW geometries are commonly used for high throughput screening applications, while 24 DSWs are capable of providing sufficient material for small scale down stream processing studies. As such it is important to be able to transition between the two geometries and understand the implications of doing so. Specific objectives are to:

- Improve the precision of oxygen mass transfer quantification in two widely used geometries of microtitre plate, developing a new method (Figure 4.1) for OUR characterisation under a range of culture conditions;
- Build statistical models for oxygen mass transfer in 96 and 24 DSW plates and characterise the overlap between the two in terms of oxygen mass transfer capability;
- Provide a mathematical translation between 96 and 24 DSW plates in terms of parameter set points (e.g. shaking speed) to achieve equivalent oxygen mass transfer rates;

- Demonstrate that equivalent culture performance can be achieved in 96 and 24 DSW microwell geometries.

Using the new method, accurate quantification of oxygen mass transfer values (k_{La} , OUR, Q_{O_2}) during small scale cultures will be enabled. As the new method will aim to accurately determine k_{La} using representative experimental conditions with live biomass, it is likely that values will be slightly lower than those previously reported in literature for the same geometries, although they would be expected to follow similar trends. The experimental strategy is summarised in Figure 4.1.

The physiological responses of a microorganism expressing a recombinant protein to changes in the aeration environment are needed for direct comparison of the two plate geometries. The previous chapter highlighted that growth and maintenance of biomass were the major contributors to oxygen demand (Section 3.2.5.), and with the productivity of the P450-containing strain being low, the decision was made to use a similar *E. coli* strain expressing a different, more easily measured protein (green fluorescent protein – GFP).

It is expected that, based on previous observations in lab scale fermentations (Section 3.2.5.), during culture the maximum specific growth rate will coincide with maximum specific oxygen consumption rate (Q_{O_2}). Additionally, it is anticipated that the achievable biomass concentration will be affected by the availability of oxygen and therefore by engineering and physical factors determined to be of influence during the development of the initial screening model. In terms of recombinant protein production, it is expected that oxygen limitation will restrict expression. This is due to the prioritization of essential metabolic activity.

It is also crucial to enhance the achievable online data stream in scale down fermentations to include DOT, biomass concentration, substrate utilization and product accretion profiles as well as preliminary derived data analysis. Without this it is not possible to gain a sufficiently thorough understanding of scale down systems to determine appropriate applications.

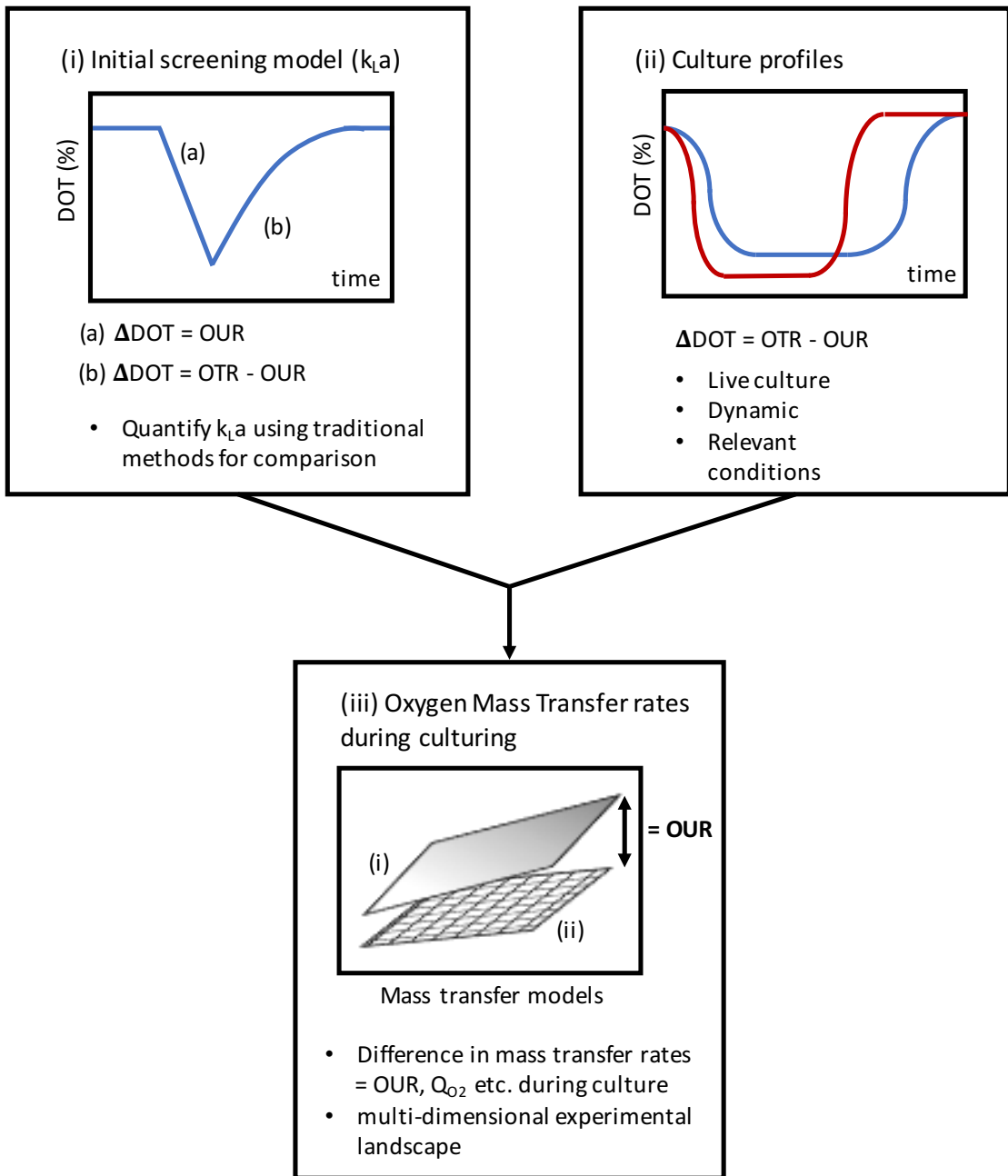


Figure 4.1. Overview of the experimental strategy for determining accurate oxygen mass transfer rates in microwell plate geometries. An initial screening model is used to determine k_La (i) using the traditional dynamic gassing out method, online culture profiles are generated in a multifactorial experimental design (ii) to quantify changes in the culture, and compared with the initial screening model to determine the oxygen demand of the expression system in the microwell environments during culture (iii).

4.2. Initial Screening Models for k_{LA} and OUR in 24 Deep Square Well Plates

4.2.1. Building the Design

A multifactorial DoE approach was used to design an experimental landscape that would enable quantification of k_{LA} and OUR in 24 DSW plates and the subsequent modelling of these responses to provide a baseline for calculation of the same responses during culture.

Factors and ranges were selected through review of the literature (Section 1.2.6) such that they are likely to have an influence on oxygen mass transfer (and therefore oxygen availability) in microwell plates. Also, as this design is to be used in the culture stages, effects on growth and productivity were considered. In addition, being able to build an equivalent design in 96 DSW was important.

A four factor, full factorial design blocked for each of the six biomass concentrations (by OD_{600}) to be used, was built. Table 4.1. shows the design. Design points were replicated in order to ensure that DOT profiles were reproducible and representative. The traditional dynamic gassing out method was used (Section 2.6.2. & 2.6.4.) with a range of biomass concentrations in order to understand the effect on k_{LA} and to what extent there is an impact on OUR.

Table 4.1. Experimental design for determination of k_{LA} and OUR values in 24 DSW plates when building the initial screening models for oxygen mass transfer. Experiments performed as described in Section 2.6.2.

Range	Factor			
	Fill Volume (mL)	Shaker Speed (rpm)	Culture Temp. (°C)	Biomass Conc. (OD_{600})
Low	1.6	200	30	0,1,5,10,20,50
High	3.2	250	37	

4.2.2. k_{La} Determination in 24 DSW (Dynamic Gassing-Out Method)

Examples of raw data are shown in Figure 4.2. and derived k_{La} and OUR values under the range of different parameter set points in Figure 4.3. Additional detail on quantification of k_{La} values can be found in Section 2.6.4. There is a distinct trend seen as k_{La} decreases with increased fill volume and reduced shaking speed, in agreement with literature (Section 1.2.6.) These physical parameters impact upon the available surface area for gas liquid mass transfer and are regarded as being influential to oxygen mass transfer at all culture scales. Table 4.2. further emphasises this as the key relationship for k_{La} . Temperature appears to have little effect on the oxygen mass transfer coefficient under these conditions. In addition, the biomass concentration had no significant effect on k_{La} . This is likely due to a limitation on O_2 in the system.

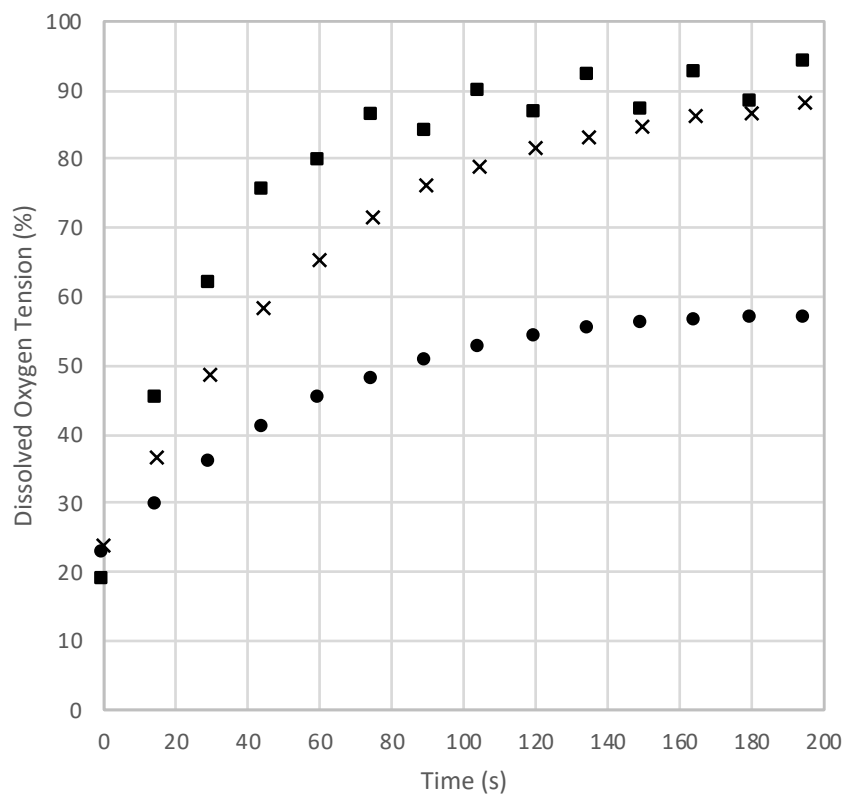


Figure 4.2. Example DOT profiles at low ($31.3h^{-1}$, represented by ●), medium ($65.5h^{-1}$, represented by x) and high ($104.1h^{-1}$, represented by ■) k_{La} values. Experiments performed as described in Section 2.6.

Table 4.2. k_{La} value ranges observed within the experimental landscape by fill volumes and shaker speeds. Experiments performed as described in Section 2.6, analysis as described in Section 2.6.4. Data shown in Figure 4.3.

Fill Volume (mL)	Shaker Speed (rpm)	k_{La} (h⁻¹)
1.6	250	80-120
1.6	200	60-100
3.2	All	<60

Across the experimental landscape, the k_{La} was seen to range between 30.1 and 122.3 h⁻¹. The range of values seen are similar to those previously reported for microwell plates using sulphite oxidation method in 96 well plates (Hermann et al. 2003; Kensy et al. 2009; Kensy et al. 2005a; Kensy et al. 2005b), oxygen limited growth of aerobic microorganisms in 96 well plates (Doig et al, 2005) and optical sensors (Islam et al. 2008; John et al. 2003) (Table 4.3.). Additionally, these values can be compared with k_{La} values observed in other, larger scale, single use bioreactors (Table 1.13.).

The O₂ mass transfer coefficient was also modelled (Figure 4.3. and Table 4.4), such that the statistical model generated can be used to predict k_{La} across the equivalent design space during culture. A linear model was constructed based on data from the full factorial design. Good agreement is seen between the experimental and modelled values (Figure 4.3), and this is confirmed by the low standard error (a measure of the statistical accuracy) for each the model parameters.

Table 4.3. Comparison of k_{La} values reported in this work with literature values of maximum k_{La} values for a range of microwell geometries. Measured k_{La} values taken from Figure 4.2.

Reference:	Plate Geometry*	Method of k_{La} determination	Max. k_{La} (h^{-1})
Hermann et al, 2003	96 RW, FB	Sulphite Oxidation	~160
Kensy et al, 2005a	24 RW, FB	Sulphite Oxidation	~250
Kensy et al, 2005b	48 RW, FB	Sulphite Oxidation	~ 350
Kensy et al, 2009	96 RW, FB	Sulphite Oxidation	~300
Duetz, 2007	96 DW	O ₂ limited growth & Sulphite Oxidation	188
Doig et al, 2005	24 RW, FB	O ₂ limited growth & Sulphite Oxidation	~180
	96 RW, FB		~200
	384 RW, FB		~115
Islam et al, 2008	24 SW, PB	Optical Sensors	~250
	24 SW, RB		~190
	48 RW, FB		~90
John et al, 2003	96 RW, RB	Optical Sensors	~130
This work	24 SW, PB	Optical Sensors	~120

*In plate geometry column, number refers to number of wells in microtitre plate. RW = round wells, SW = square wells, DW = deep wells, FB = flat bottom, RB = round bottom and PB = pyramidal bottom.

Table 4.4. Factors and parameter value estimates for the initial screening model of k_{La} in 24 DSW plates. The resultant model equation can be seen in Equation 4.1. Standard errors were 3.41 for each of the parameters.

Term	Unit	Coefficient Estimate	p-value	t Ratio
Intercept	-	68.7	-	20.1
Fill Volume	mL	-24.3	0.0006	-7.13
Shaker Speed	rpm	10.4	0.007	3.05

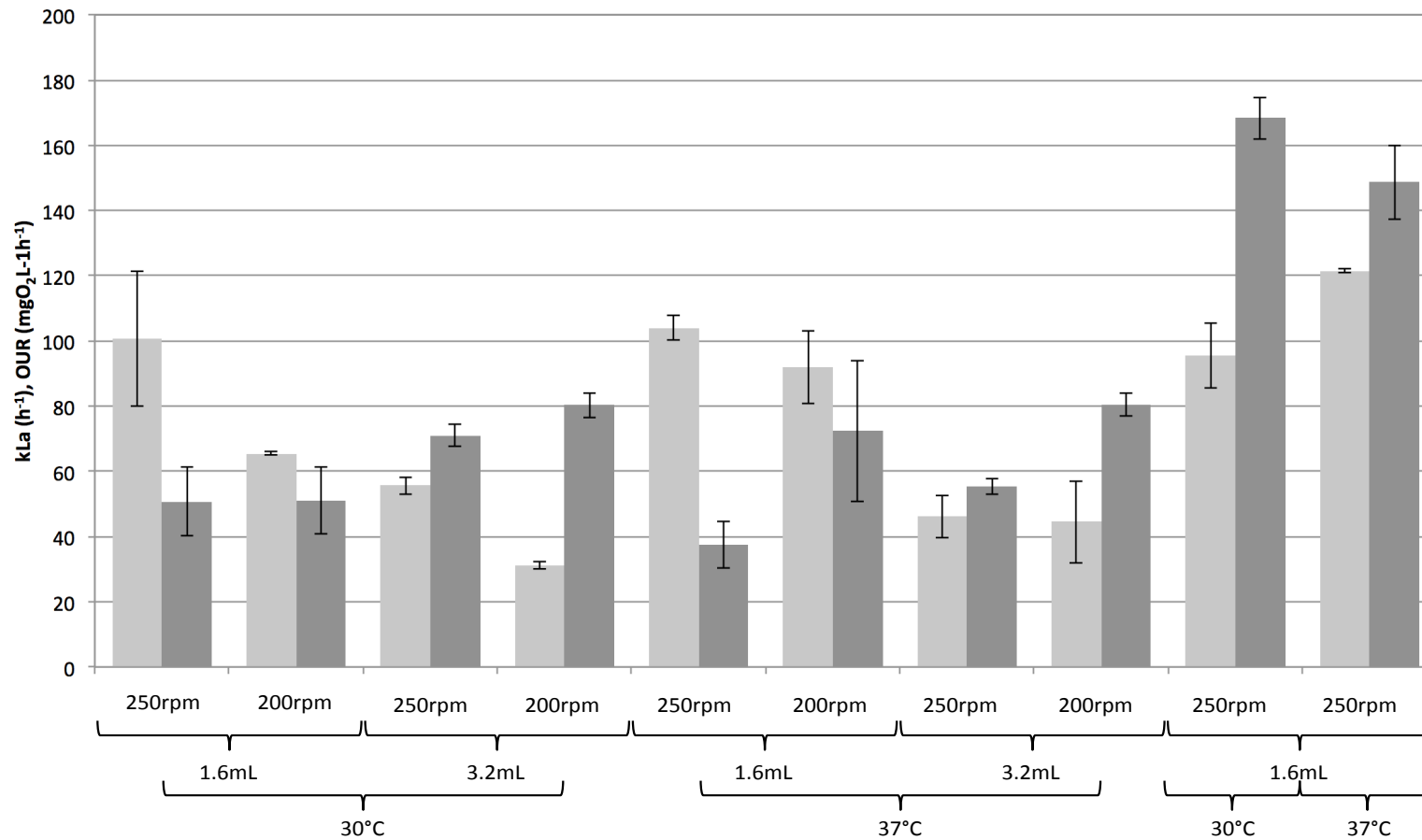


Figure 4.3. $k_L a$ and OUR values determined in 24 DSW microwell formats as a function of shaker speed, well fill volume and temperature. Dark grey bars represent OUR values (in $mgO_2L^{-1}h^{-1}$), while light grey bars show $k_L a$ values. Error bars represent the range of experimental values ($n=2$). Experiments performed as described in Section 2.6. $k_L a$ values determined using Equation 2.2 and OUR values based on Equation 2.1. All data with the exception of the four right hand bars ($1.75 g_{DCW}L^{-1}$) were determined at a biomass concentration of $0.35 g_{DCW}L^{-1}$.

4.2.3. OUR Determination in 24 DSW (Dynamic Gassing-Out Method)

Example raw data profiles for determination of OUR are shown in Figure 4.4. and the derived OUR values at the different parameter set points used are shown in Figure 4.3. Additional detail on the quantification of OUR values can be found in Section 2.6.4. The greatest influence on oxygen uptake rate was biomass concentration. As expected, a greater number of cells resulted in a greater OUR. The oxygen uptake rate appears to follow the opposite trend to $k_{L,a}$, increasing with greater fill volume and reduced shaker speed (Figure 4.3. & 4.6.). This would seem counterintuitive as it would be expected that the greatest oxygen uptake would occur under conditions that would provide the greatest oxygen availability (i.e. highest $k_{L,a}$), however higher shaker speed may result in increased levels of stress, while increased fill volumes and lower shaker speeds result in poorer mixing and therefore less renewal of oxygen at the base of the well, hence OUR appears greater.

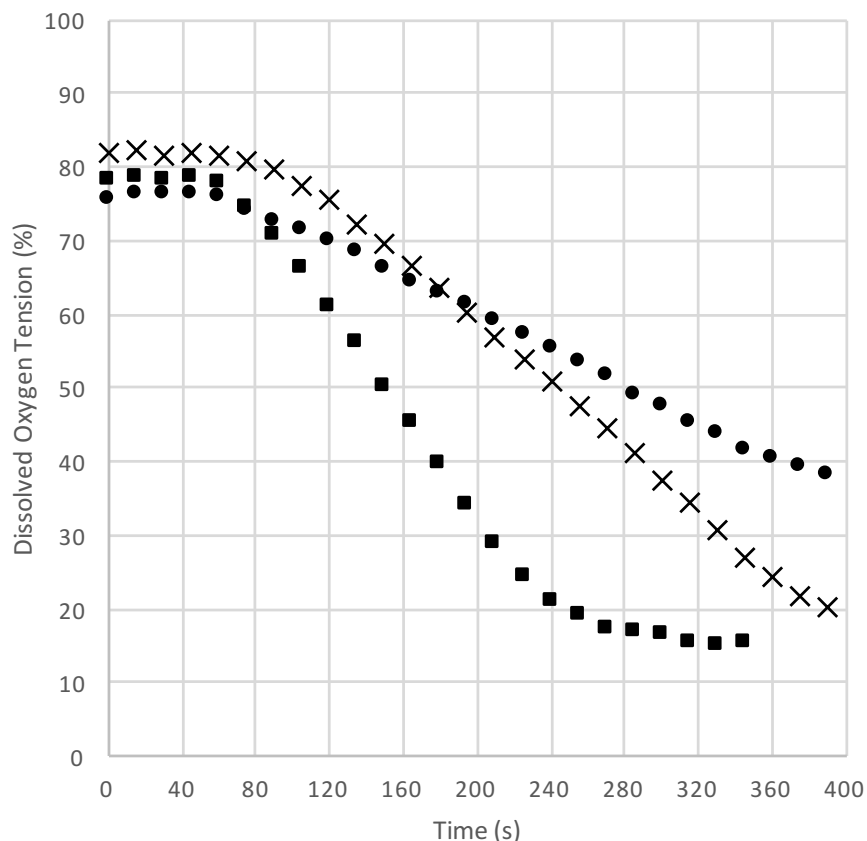


Figure 4.4. Example DOT profiles at low ($32.5 \text{ mgO}_2\text{L}^{-1}\text{h}^{-1}$, represented by ●), medium ($58.4 \text{ mgO}_2\text{L}^{-1}\text{h}^{-1}$, represented by x) and high ($87.6 \text{ mgO}_2\text{L}^{-1}\text{h}^{-1}$, represented by ■) OUR values. Experiments performed as described in Section 2.6.

The relationship between OUR and biomass concentration is not linear, with OUR appearing to be limited by the availability of O₂ into the culture (indicated by k_La and shown in Figure 4.3.). This explains the difficulty in determining k_La at higher biomass concentrations (3.5 g_{DCW}L⁻¹ and higher), where the method requires the depletion of oxygen before attempting to return to 100% of saturation. It is likely that the biomass present instantly demands all of the O₂ made available in the system.

$$k_L a = 68.73 - 24.35 \cdot \frac{(Fill\ Vol. - 2.4)}{0.8} + 10.42 \cdot \frac{(RPM. - 225)}{25} \quad \text{Equation 4.1.}$$

OUR was also modelled. Figure 4.6, Equation 4.2. and Table 4.5. show these effects as part of a linear model, and the magnitude of the coefficients within it. The influence that biomass concentration has is large, while the effect of the physical parameters (shaking speed and fill volume) are proportionally lower, when compared to the model for k_La. Figure 4.7. and Table 4.5. highlight a good agreement between the modelled and experimental data (low p-value, high t ratio), providing confidence in the statistical model generated.

The influence of fill volume and shaker speed on k_La and OUR were inverse to one and other i.e. greater fill volume had a negative effect on k_La, and a positive influence on OUR (Figure 4.5. & 4.6.). This may result from their basic mechanisms, with k_La a measure of oxygen into the culture and OUR its removal by the organism, and the calculation of k_La being dependent on an OUR already determined when using the dynamic gassing out method.

$$OUR = 119.45 + 57.08 \cdot \frac{(Biomass\ Conc. - 3.0)}{2.0} + 9.41 \cdot \frac{(Fill\ Vol. - 2.4)}{0.8} - 8.70 \cdot \frac{(RPM. - 225)}{25}$$

Equation 4.2.

In summary, the models that have been generated provide a good baseline for quantifying and understanding the oxygen mass transfer properties of 24 DSW plates. Both models are linear, due to the use of a full factorial design, meaning curvature cannot be detected. The linear model though is suitable for this purpose. The analysis of variance shown in Table 4.6. and the parity plots for k_La (Figure 4.7. A) and OUR (Figure 4.7. B) demonstrates a high degree of confidence can be had in each model, with good agreement between the model generated and experimental data in both

cases. Root Mean Square Error (RMSE) is included, providing a statistical measure of how concentrated the data is around the line of the model.

4.3. Establishing a New Method for Oxygen Mass Transfer Quantification During Microbial Fermentation in Microwell Plates

4.3.1. Building the Design

The experimental design used to quantify and model the oxygen mass transfer properties of a microbial culture in 24 DSW microwell plates was designed to mimic the experiments run for the building of the initial screening model (Section 4.2.). The experimental design for the 96 DSW used the principle that the ranges should provide the greatest potential for overlap with the 24 well format in terms of the aeration environment.

Table 4.5. Estimates of parameter coefficients for each of the significant factors in the initial screening model of OUR in 24 DSW plates. The resultant model equation can be seen in Equation 4.2.

Term	Unit	Coefficient Estimate	p-value	t Ratio
Intercept	-	119.4	-	30.7
Biomass Concentration	OD ₆₀₀	57.1	<0.0001	14.7
Fill Volume	mL	9.41	0.006	3.20
Shaker Speed	rpm	-8.70	0.009	-2.96

Table 4.6. Comparison of analysis of variance for the linear models of k_{La} and OUR in 24 DSW microwell plates.

	Model	
	k_{La}	OUR
p-value	<0.0001	<0.0001
R-squared	0.80	0.94
RMSE	14.7	11.7

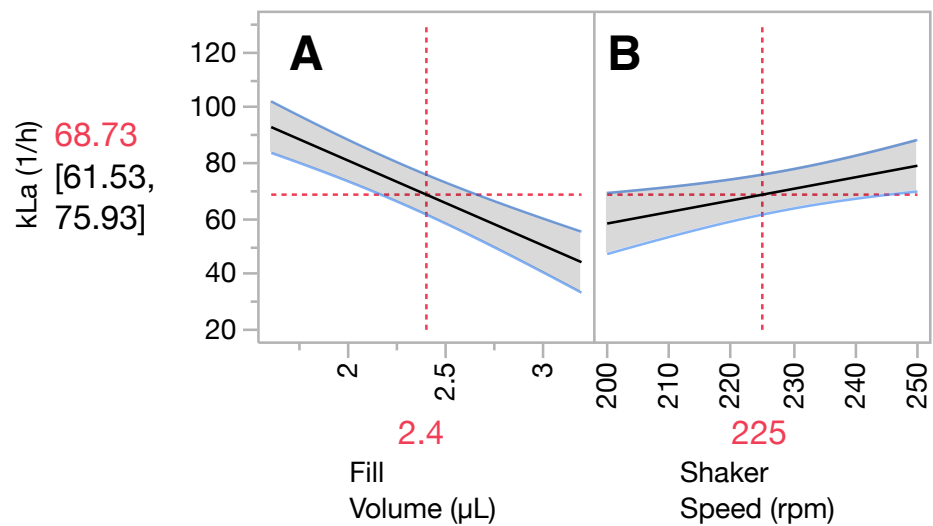


Figure 4.5. Main effects plots of the initial screening model for k_{La} in a 24 DSW plate for shaker speed (A) and fill volume (B) across their respective experimental ranges. Blue lines represent a 95% confidence interval, and red dashed lines highlight the value for k_{La} at the centre point of the experimental range. Raw data can be found in Appendix 3.1.

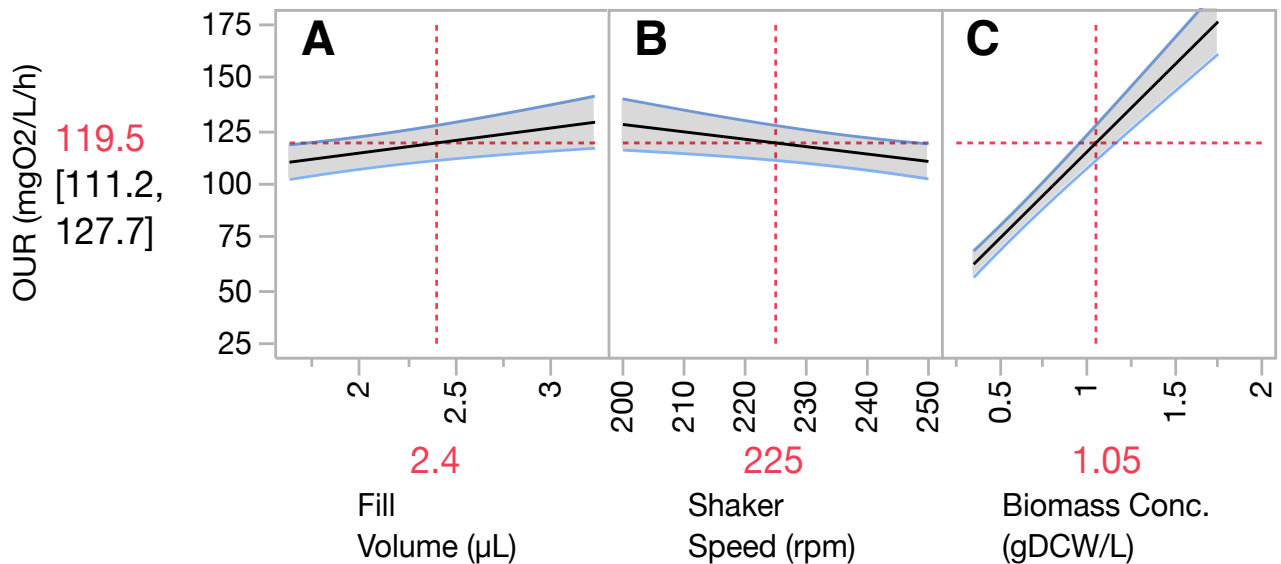


Figure 4.6. Main effects plots of the initial screening model for OUR in a 24 DSW plate for shaker speed (A), fill volume (B) and biomass concentration (C) across their respective experimental ranges. Blue lines represent a 95% confidence interval, and red dashed lines highlight the value for OUR at the centre point of the experimental range. OUR values are in $mgO_2L^{-1}h^{-1}$. Raw data available in Appendix 3.1.

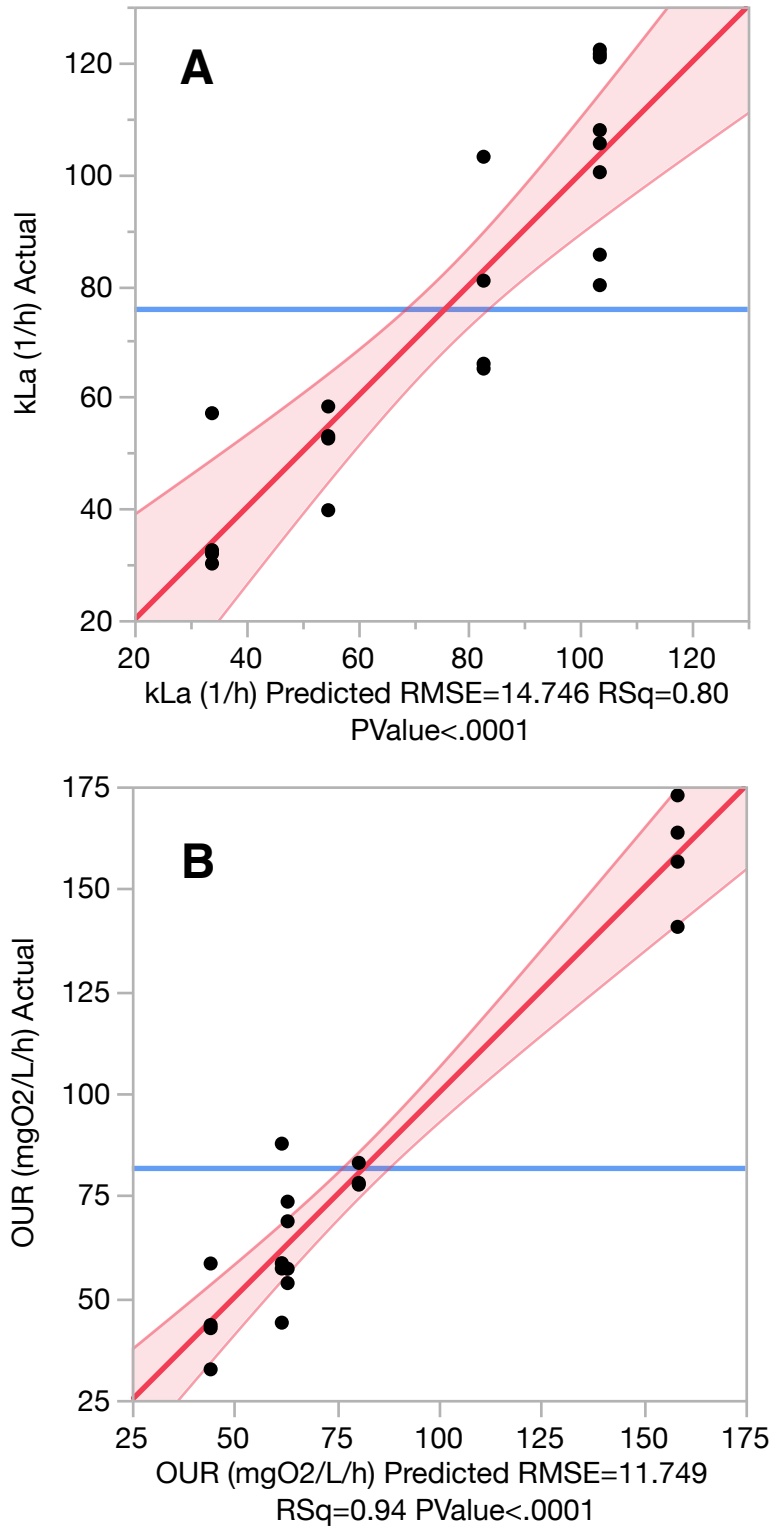


Figure 4.7. Predicted versus experimental values of the statistical models for (A) k_{La} and (B) OUR in 24 DSW plates. k_{La} values are in reciprocal hours, OUR values in $\text{mgO}_2\text{L}^{-1}\text{h}^{-1}$. Black dots represent data points which have been measured experimentally and calculated by the model, the red line indicates a line of parity i.e. $y=x$, and the red shaded area shows the 95% confidence interval. Experiments undertaken as described in Section 2.6. Analysis as described in Section 2.6.4.

In order that the oxygen mass transfer environment be modelled, a multifactorial DoE method was used to construct a five factor, two level, full factorial design for both microwell plate formats using a sacrificial sampling method with six time points (0, 8, 24, 32, 48 and 56 hours post inoculation). The design was blocked for each of the sampling time points. Tables 4.7. and 4.8. show the designs for 24 and 96 DSW plates respectively. Points in the design space were replicated within the same plate in order to ensure that profiles and responses were representative.

Factor and ranges in the design for the 96 DSW plate have been calculated and set either using correlations based on the geometries of the well, such as fill volumes which are set at 0.25 times that of the 24 DSW (maximum fill volume is 2.5mL compared to 10mL) or based on commonly used ranges for corresponding equipment.

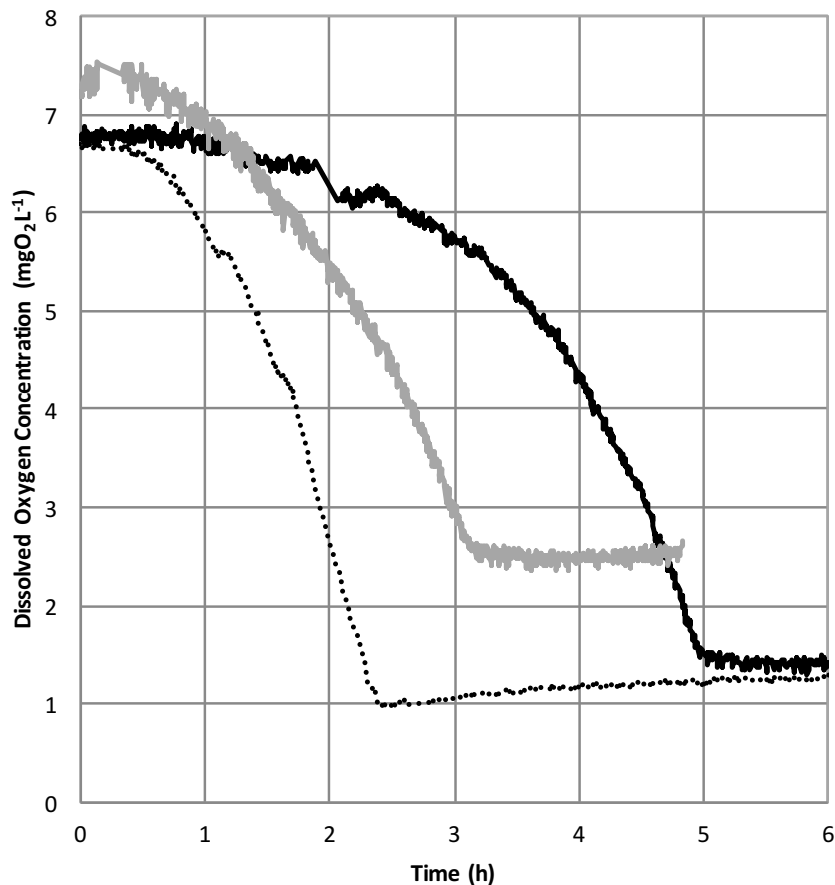


Figure 4.8. Example DOT profiles for six hours after culture inoculation at low (34.0 h^{-1} , dotted line), medium (54.8 h^{-1} , solid grey line) and high (82.7 h^{-1} , solid black line) k_{La} values. Experiments performed as described in Section 2.6. Analysis of profiles for quantification of oxygen mass transfer rates as described in Section 2.6.4.

Table 4.7. Experimental design for OUR quantification in 24 DSW microwell plates during microbial culture by dynamic gassing out methods. The design was intended to mimic the initial screening model (Section 4.2.) as closely as possible.

	Factor	Unit	Range	
			Low	High
A	Fill Volume	mL	1.6	3.2
B	Shaker Speed	rpm	200	250
C	Post Induction Temp.	°C	30	37
D	Inoculum Conc.	%v/v	1	5
E	Log Hour time course	hr	t0, Post Ind(t8), t24, t32, t48, t56	

Table 4.8. Experimental design for OUR quantification in 96 DSW microwell plates during microbial culture. The design is intended to mimic that of the 24 DSW and provide the greatest potential overlap in oxygenation of the culture.

	Factor	Unit	Range	
			Low	High
A	Fill Volume	mL	0.4	0.8
B	Shaker Speed	rpm	600	1100
C	Post Induction Temp.	°C	30	37
D	Inoculum Conc.	%v/v	1	5
E	Log Hour time course	hr	t0, Post Ind(t8), t24, t32, t48, t56	

4.3.2. Determination of OUR and Q_{O_2} During Culture Using the New Method

Due to the issues outlined previously with the use of the traditional dynamic gassing out method (Section 1.2.9. and 4.1.), here the intention was to devise an improved technique for determining responses of the culture to forced differences in oxygen availability using the strategy outlined in Section 4.1. The experimental method differs from traditional dynamic gassing out since it is run continuously as a culture stage (Section 2.6.3.). The interpretation and analysis of the online data traces generated then differs also. This is explored in this section. Example DOT profiles

during culture are shown in Figure 4.8. It is observed that with increased k_{La} , the reduction in DOT to a minimum begins later and is prolonged. As increased k_{La} means greater input of oxygen into the culture, this would seem reasonable.

In order to quantify OUR and Q_{O_2} using online dissolved oxygen measurements during culture, the analysis steps were as follows.

As with analysis of the traditional dynamic method, once the DOT profiles have been obtained, they are normalized to 100% saturation, before being converted to engineering units (mgO_2L^{-1}) using the appropriate saturation concentration for that experiment (Figure 4.8.).

For example, for a solution of pure water at 20°C, the saturation concentration of oxygen is 9.1 mgO_2L^{-1} (Eaton et al. 2005). Therefore at 50% of saturation:

$$O_2 \text{ conc. } (mgO_2L^{-1}h^{-1}) = DOT (\%) \times O_2 \text{ saturation conc.} \quad \text{Equation 4.3.}$$

$$\begin{aligned} C_L &= 0.5 \times 9.1 \\ &= 4.55 \text{ } mgO_2L^{-1}h^{-1} \end{aligned}$$

At this point, the method for quantification differs. The first derivative of C_L with respect to time (dC_L/dt) is calculated over the first 15 hours of culture, every five minutes. This time frame is significantly shorter than the doubling time for *E. coli*, and so it can be assumed that there is no change in the ‘instantaneous’ biomass concentration between calculated points. In addition, the interval is short enough to observe the responses in the traces, but not so short that it increases error due to noise in the profile (e.g. Figure 4.18). Using the derived values and the initial model for k_{La} (Section 4.2), the OUR can then be calculated using Equation 4.4.

$$OUR = k_{La} \cdot (C^* - C_L) - \frac{dC_L}{dt} \quad \text{Equation 4.4.}$$

Where C^* is the saturation concentration of oxygen and C_L is the concentration of oxygen at a given time in the first order system.

Using equation 4.4, OUR is calculated as follows (data from an experiment at 37°C, 400 rpm, 1600 μL fill volume, where k_{La} was determined to be 54.8 h^{-1}):

$$OUR = k_{La} \cdot (C^* - C_L) - \left(\frac{C_L - C_{L,t-5}}{t_L - t_{t-5}} \right)$$

$$OUR = 54.8 \cdot (6.71 - 3.34) - (3.34 - 3.18/0.083)$$

$$OUR = 183.1 \text{ mgO}_2\text{L}^{-1}\text{h}^{-1}$$

The specific oxygen consumption rate can then be calculated using equation 4.5.

$$OUR = xQ_{O_2} \quad \text{Equation 4.5.}$$

Where $C_{L,t-5}$ is the concentration of oxygen in the first order system five minutes prior to the current measurement, t_L is the current time, t_{t-5} is the time 5 minutes prior to the current measurement ($t_L - t_{t-5}$ should therefore remain as 0.083 h using this method). x represents the biomass concentration and Q_{O_2} the specific oxygen consumption rate.

4.3.3. Modelling OUR in 24 DSW Plates Using the New Dynamic Gassing Out Method.

Initially, a model was built using all design factors (Table 4.7. and Figure 4.9.). This highlighted that, as with $k_L a$, fill volume and shaker speed were the most significant factors influencing OUR (Figure 4.9A and 4.9B respectively), with only a small effect due to biomass concentration (Figure 4.9D) and no significant effect due to temperature (Figure 4.9C). The effects of fill volume and shaker speed are opposite, increasing fill volume resulting in a large decrease in OUR, and increase in shaker speed resulting in a rise in the OUR. Table 4.9. highlights the magnitude of each of the parameter coefficients in the model and statistical analysis of the factors of significance, showing that the model can be used with a high degree of confidence.

The high R-squared (0.99) in combination with a low p-value (<0.0001) and RMSE (19.9) indicate that the model is a very good fit for the experimental data. In addition, Figure 4.10. shows the diagnostic plots. The predicted against actual plot (Figure 4.10A) shows no outlying data points, and therefore a good agreement between the experimental data and that generated by the model. The half normal plot (Figure 4.10B) demonstrates the effects and how strong they are, while the plot of residuals against run number (Figure 4.10C) shows no systematic bias in the design or its execution. The model is shown in Figure 4.11. and exhibits the significant impact that the two main effects have, with the range of OURs from around 200 $\text{mgO}_2\text{L}^{-1}\text{h}^{-1}$, approximately quadrupling to 800 $\text{mgO}_2\text{L}^{-1}\text{h}^{-1}$.

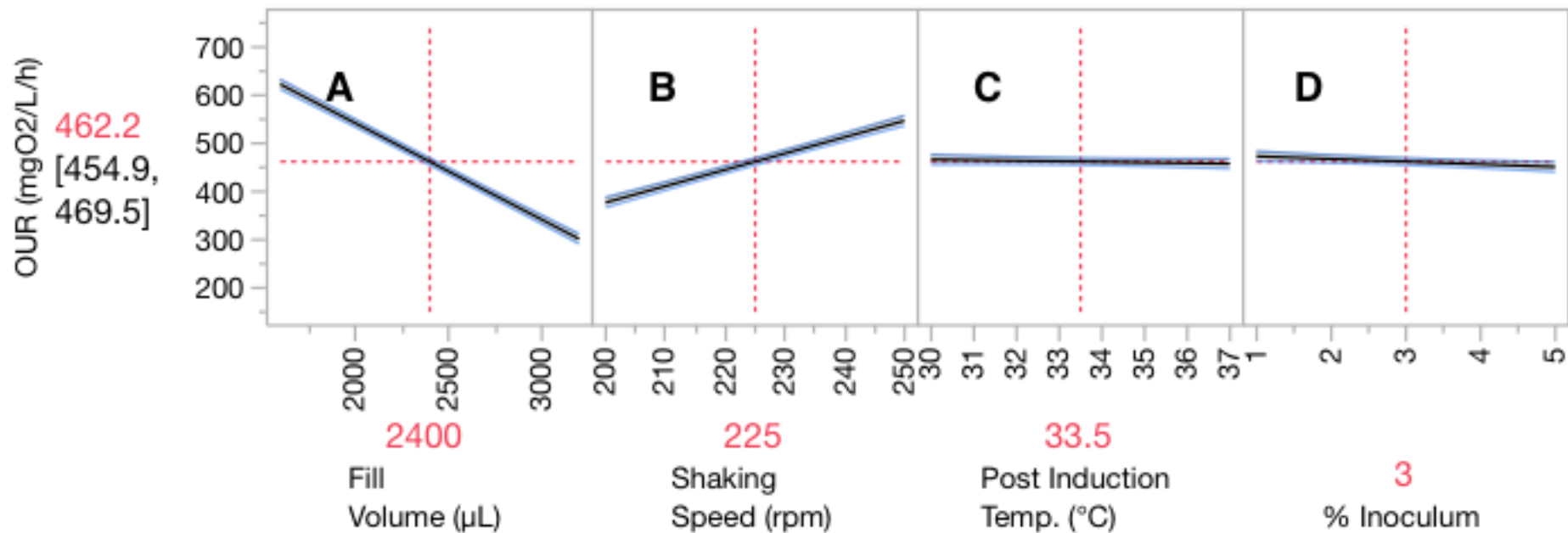


Figure 4.9. Effects plots showing the variation of calculated OUR with well fill volume, shaking speed, post induction temperature and inoculum concentration in 24 DSW microbial culture. Fill Volume (A), shaker speed (B) and inoculum concentration (D) are seen to have a significant effect, while temperature (C) did not. Blue shaded areas represent a 95% confidence interval, while dashed red lines highlight OUR values at the mid-point of the experimental range. Experiments were performed as described in Section 2.6. Analysis as described in Section 2.6.4.

Table 4.9. Estimates of model coefficients and statistical analysis for each of the significant factors and interactions in the quadratic model of OUR in 24 DSW plates using the new dynamic gassing out method during culture. Standard errors are 3.52 for all terms in the model.

Term	Parameter coefficient	p-value
Intercept	462.2	<0.0001
Fill Volume	-160.5	<0.0001
Shaker Speed	84.8	<0.0001
Inoculum Conc.	-11.0	0.005
Fill Vol. – Shaker Speed	-18.0	<0.0001
Shaker Speed – Temp.	17.2	<0.0001

The experimental data was reanalysed using k_{La} as the input factor in place of fill volume and shaker speed, as these were the two factors shown to have the most significant effect on OUR (as well as k_{La} in the initial screening model). This was to determine if there was a correlation to be made between k_{La} and OUR directly, as shown in Section 4.4. k_{La} became the only significant factor in a model with an R-squared value of 0.96 and p-value of <0.0001. The relationship was positive, and further demonstrates the importance that availability of oxygen has on the culture and the ability to utilise it i.e. with the provision of more oxygen (greater k_{La}), the culture responds by using more oxygen (greater OUR). This is highlighted both in Table 4.11. and Figure 4.11. This is in contrast with the relationship seen with non-growing cells during development of the initial screening model (Section 4.2.).

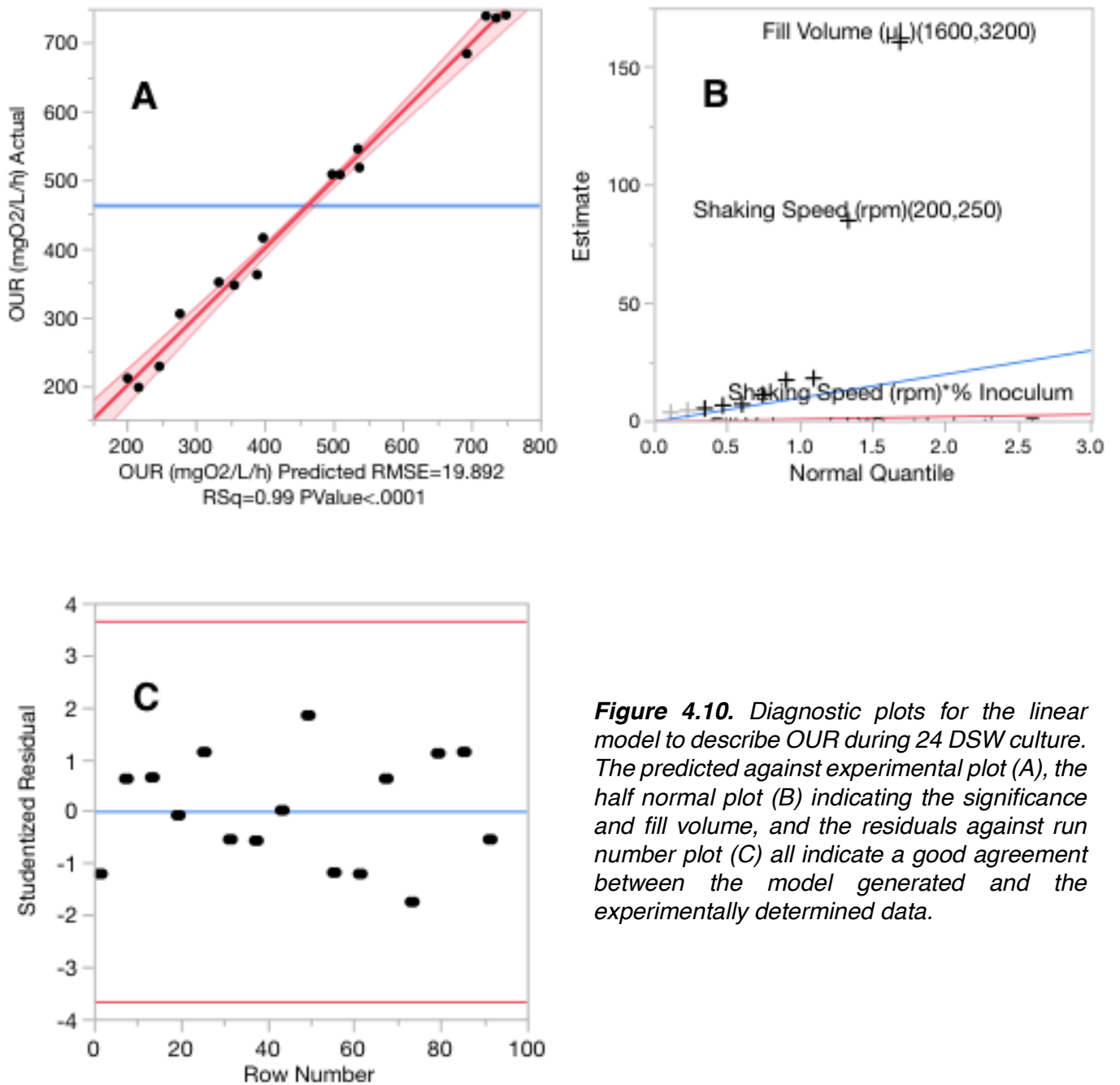


Figure 4.10. Diagnostic plots for the linear model to describe OUR during 24 DSW culture. The predicted against experimental plot (A), the half normal plot (B) indicating the significance and fill volume, and the residuals against run number plot (C) all indicate a good agreement between the model generated and the experimentally determined data.

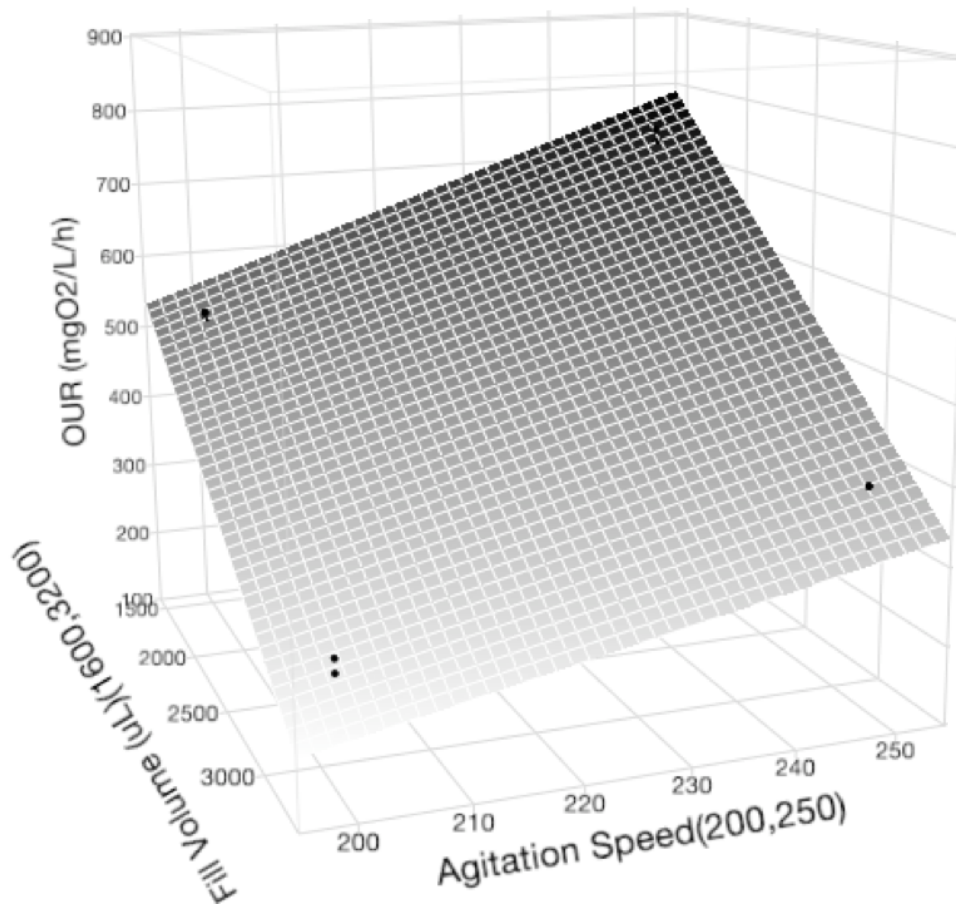


Figure 4.11. Response surface plot for the model of OUR in 24 DSW culture. Light to dark indicates the increase in OUR value, and black dots represent experimental data points. Experiments performed as described in Section 2.6. OUR values calculated as described in Section 2.6.4.

4.4. Comparing the Initial Screening Model and the Culture Model

Although the primary use of the initial screening model was to provide the landscape for k_La which was then the basis for calculations of OUR during culture, the OUR using the traditional dynamic gassing out method can also be calculated. Table 4.10. shows a comparison of the OURs observed using the two measurement methods, with OURs during culture up to over 10 times greater in magnitude. This can be explained as during the traditional method, aeration (in the case of this study by shaking) to provide oxygen is stopped and the calculation is based on the oxygen utilisation of non-growing biomass in a static environment. Whereas during culture, the

cells are being provided with O₂, and so consuming and metabolising it at a much greater rate. This provides insight into oxygen utilisation in microwells which cannot be achieved with the traditional method, and suggests that OURs determined using the traditional dynamic gassing out method, though indicative, are of little quantitative value as they do not accurately represent the demands of the organism to be cultured.

The process of generating modelled biomass concentration data and the calculation of the corresponding volumetric productivity with respect to biomass accumulation is shown in Figure 4.12. The biomass concentration of sacrificial microwell samples is measured (as described in Section 2.8.2.) before a sigmoidal curve fit is applied to the data. The model equation is then used to calculate the estimated biomass concentration at 10 minute intervals. Volumetric productivity can then be calculated as the change in biomass concentration over each of these periods (dX/dt) and plotted.

Table 4.10. Comparison of oxygen uptake rates using the traditional dynamic gassing out method and using the new dynamic gassing out method during culture. OURs are calculated as described in Sections 2.6.4. and 4.4.

k_La (h⁻¹)	OUR (traditional dynamic gassing out) (mgO₂L⁻¹h⁻¹)	OUR (new method) (mgO₂L⁻¹h⁻¹)
34.0	~80	190-220
54.8	55-70	300-350
82.7	50-70	400-530
103.5	40-50	600-650
103.5 (at 1.75 g_{DCW}L⁻¹)	150-170	

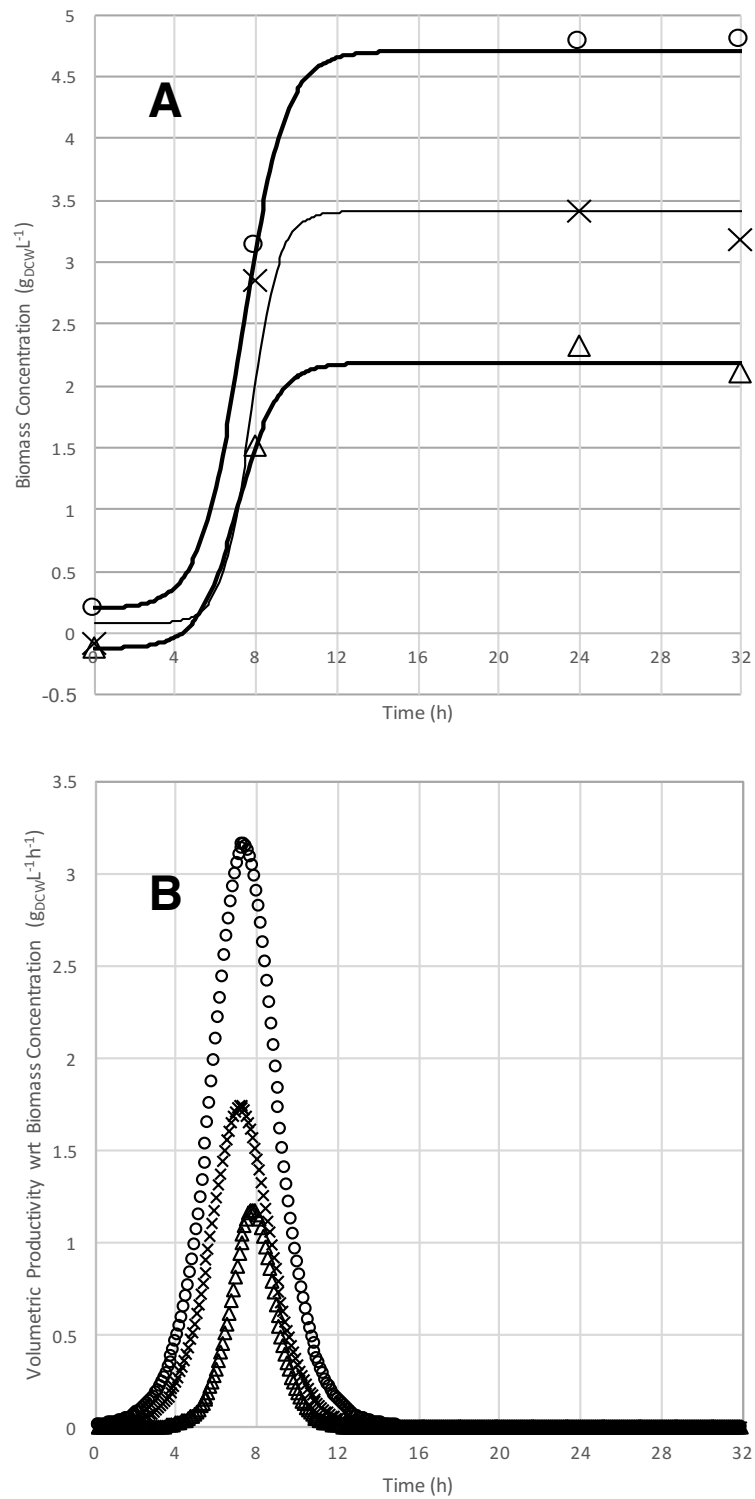


Figure 4.12. Example data (open symbols) and modelled (solid lines) biomass concentration profiles (A), and the corresponding biomass productivity (B). \circ , \times , \triangle represent high, medium and low OURs respectively. Experiments carried out as described in Section 2.6. Analysis as described in Section 2.6.4. and 4.4.

Figure 4.13. then shows the relationship during culture in microwell plates between growth and oxygen uptake. As has been seen previously (Section 3.2.5.), a sharp increase in OUR is followed shortly afterwards by the transition into exponential growth phase and the greatest rate of volumetric productivity. It is interesting to note the clear trend between greater available oxygen (shown here as greater k_{La}), greater OUR (as noted in Sections 4.2. and 4.3.) and a greater rate of biomass accumulation (dX/dt), as this helps to highlight the criticality of oxygen availability for microbial culture, particularly in small scale, high throughput systems. OUR peaks and then plateaus when volumetric productivity (dX/dt) reaches its maximum i.e. during the exponential growth phase. This is yet further evidence for the prioritization of growth in terms of oxygen utilization. OUR is then sustained, indicating that there is significant oxygen demand required for sustaining biomass concentration as suggested in Section 3.2.5.

In summary, the method developed here for accurately quantifying and modelling the oxygen uptake rate of live microbial cells in culture appears to have been effective. The experimental method and analysis, though extensive, result in empirical models for k_{La} and OUR which can be easily reasoned and used with a high degree of confidence. In terms of the experimental method, little variance was seen between replicated profiles for DOT using the PreSens system, again providing a high degree of confidence in this technique, which hopefully is seen as an improvement on the traditional dynamic method as it accounts for the dynamic nature of a fermentation.

In addition, this method has provided valuable insight into culture dynamics and the demands of a microbial expression system on the culture in terms of oxygen. It has also provided further support for the hypotheses in Section 3.2.5. on the prioritisation of oxygen utilisation.

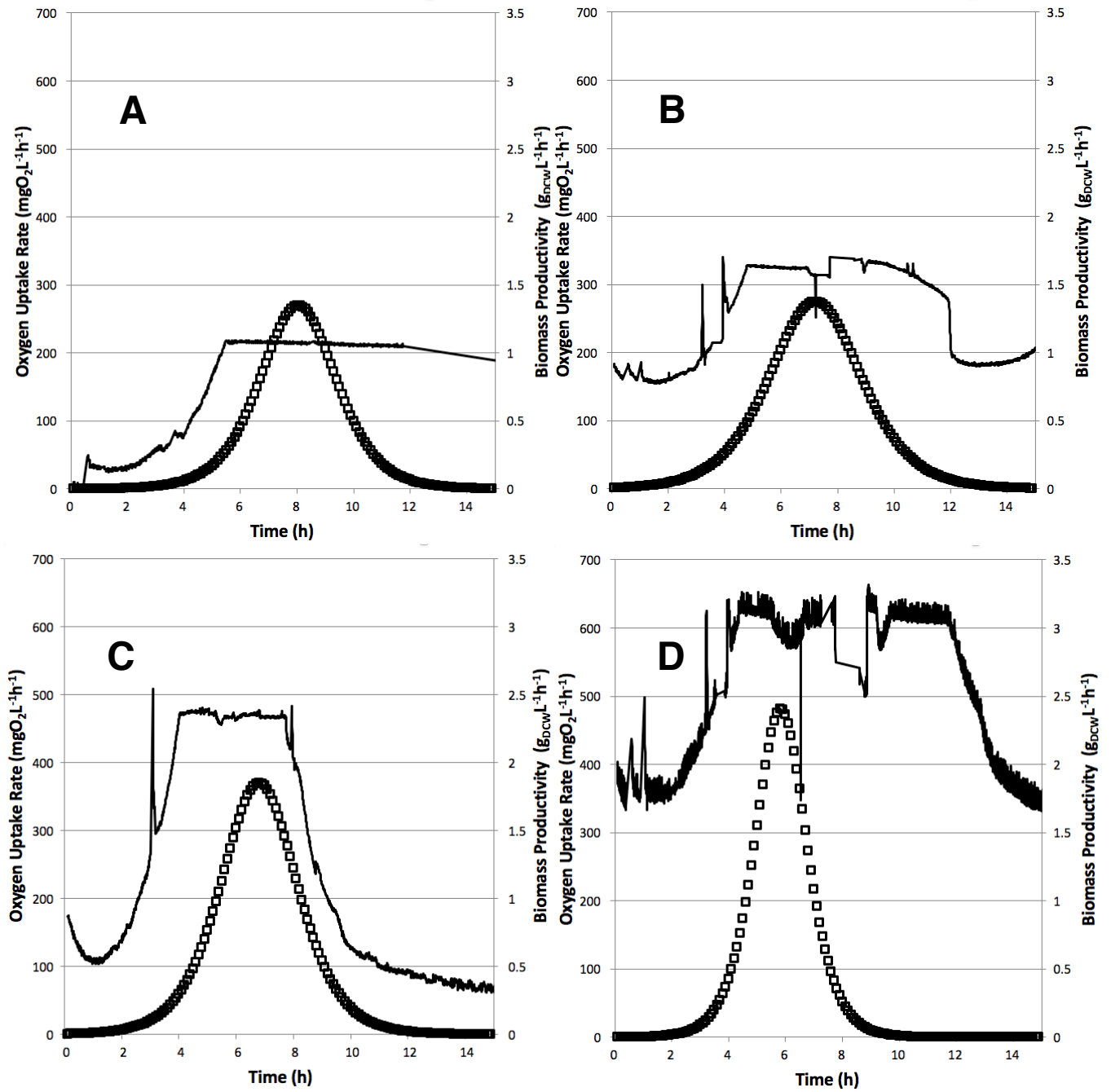


Figure 4.13. Plots of OUR (solid line) and biomass volumetric productivity (\square) at differing oxygen availabilities (by k_La). k_La values represented are $34.0h^{-1}$ (A), $54.8h^{-1}$ (B), $82.7h^{-1}$ (C) and $103.5h^{-1}$ (D). Profiles are a representative example of the trends seen in each of the different aeration environments across the experimental landscape. Experiments performed as described in Section 2.6. Analysis as described in Sections 2.6.4. and 4.4.

4.5. Relationship Between Biomass Growth and Oxygen Availability

Figure 4.13 highlights the relationship between oxygen availability, the rate of oxygen uptake and the dynamics of culture growth, as noted in Section 4.4. However, with oxygen widely regarded as the limiting substrate in microbial fermentation, the interrelationship between the availability of oxygen and the achievable biomass concentration was interrogated. The effects on biomass accumulation were modelled in each of the 24 and 96 deep square well plates. Figure 4.14. shows those factors from the design seen to have a statistically significant effect. It is shown in both cases that fill volume and shaker speed, the two main factors influencing $k_L a$, are significant effects. In addition to this, Figure 4.17 again highlights that oxygen availability in microwells has a major influence on biomass accumulation, and that as previously suggested, it is likely to be limiting, with greater biomass concentrations seen with higher levels of available oxygen.

Analysis of variance was undertaken on the models in order to ensure that these observations were statistically valid. The predicted against experimental plots (Figure 4.15.) and ANOVA statistical diagnostics (Table 4.11.) show that the model of biomass concentration in 24 DSW fits well with the experimental data, and that it can be used with a high degree of confidence. An R-squared of 1.00 and close grouping of the data points around the predicted versus experimental parity line are good indicators. A good fit is also seen in the model for biomass accumulation in 96 DSW, though the R-squared (0.83) and grouping of data points is not quite so good.

Table 4.11. ANOVA statistical diagnostics to show confidence in the models for biomass accumulation as a result of oxygen availability in 24 and 96 DSW plates during culture. Models shown in Figure 4.14. and diagnostics on the model in Figure 4.15.

	Model	
	24 DSW	96 DSW
R-squared	1.00	0.83
p-value	<0.0001	<0.0001
Root Mean Square Error (RMSE)	0.19	0.68

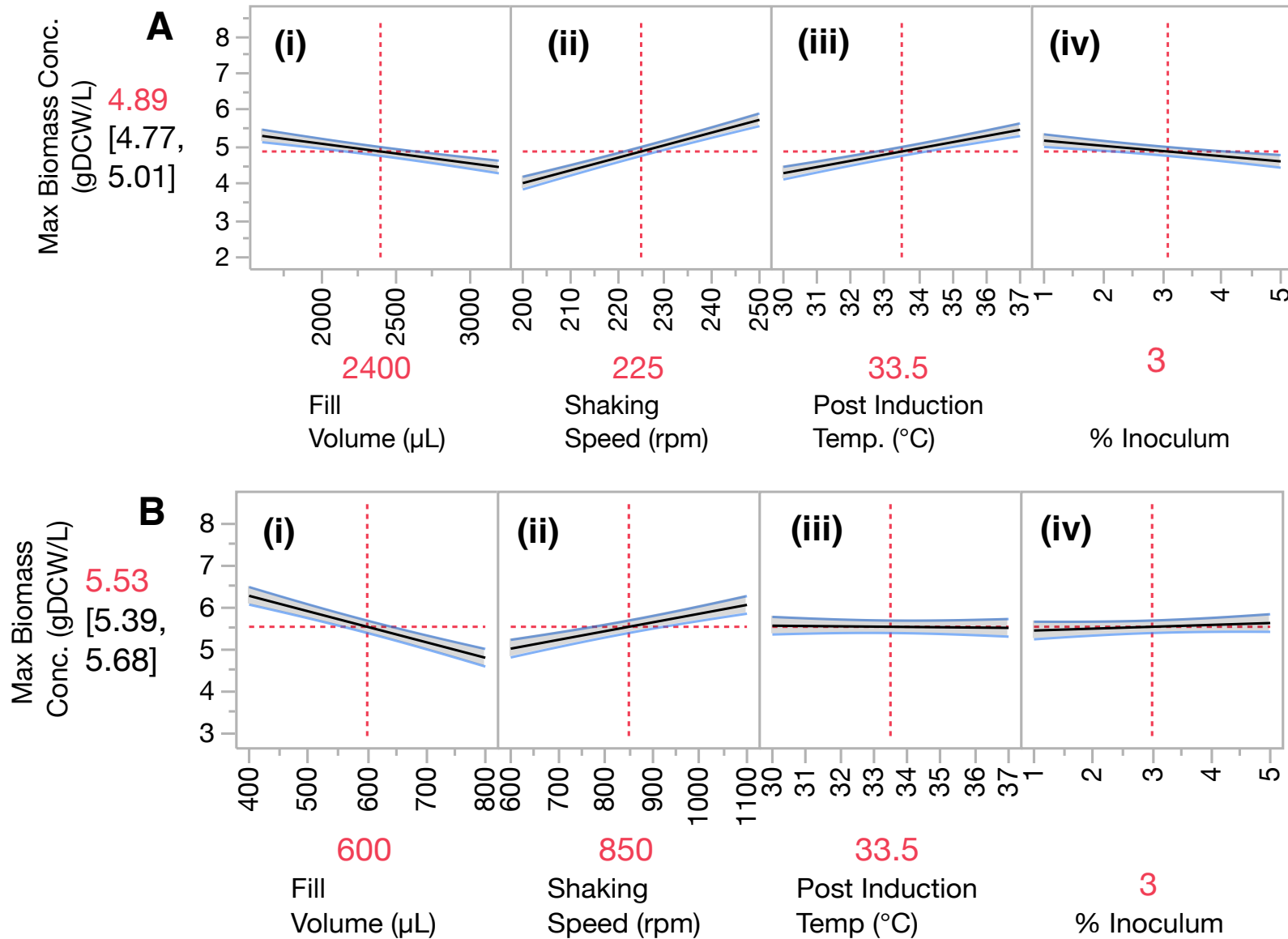


Figure 4.14. Effect profiles for the factors of influence on the model for biomass accumulation 24 DSW culture (A) and 96 DSW culture (B). Fill Volume (i), shaking speed (ii), temperature (iii) and inoculum concentration (iv) are all seen to have a significant effect in both cases. Greater gradients indicate an effect of larger magnitude. Grey shaded areas indicate 95% confidence intervals, while dashed red lines represent the value for biomass concentration at the centre point of the experimental range. Experiments carried out as described in Section 2.6. Analysis as described in Section 2.6.4.

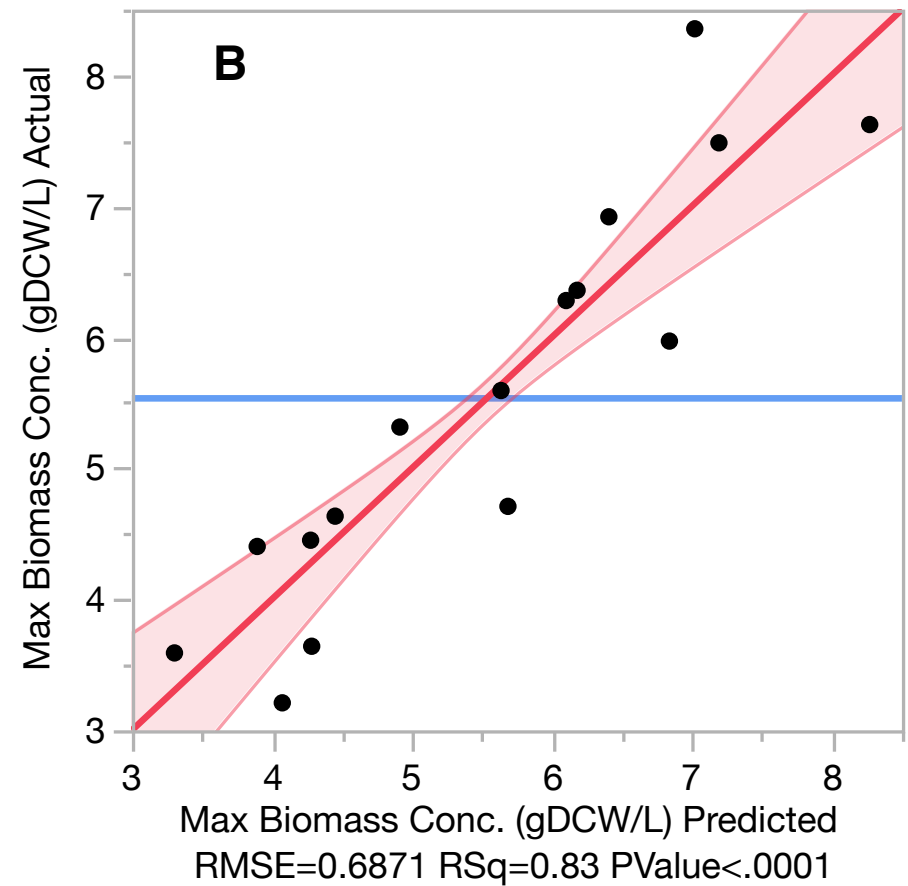
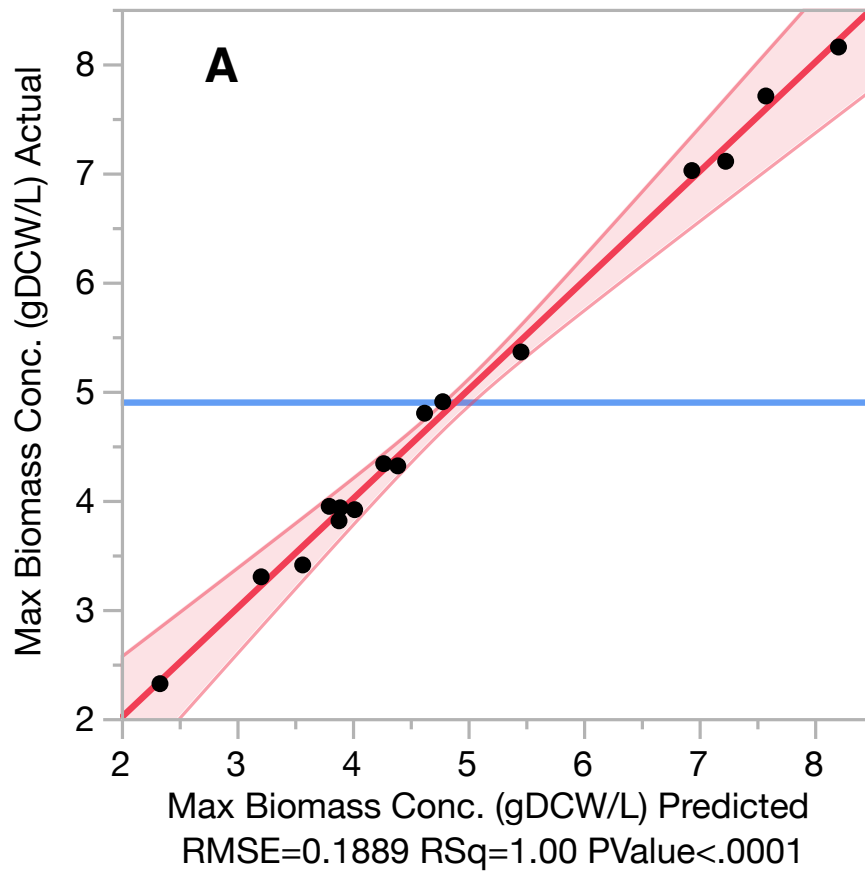


Figure 4.15. Predicted versus experimental plots for the models of biomass accretion in 24 DSW (A) and 96 DSW (B) during culture. Black dots represent data points, the red line the line of parity (i.e. $y=x$) and the shaded red area the 95% confidence interval. Experiments carried out as described in Section 2.6. Analysis as described in Section 2.6.4.

4.6. Relationship Between Recombinant Protein Expression and Oxygen Availability

Oxygen availability is highlighted as a potentially key factor in recombinant protein expression (Section 1.2.3. and 1.2.4.) and so the relationship between factors influencing oxygen mass transfer and the accumulation of protein are looked at in each of the microwell formats. The relationship between oxygen availability and recombinant protein expression appears to be a complex one, and one which is not extensively investigated in literature, which in some cases makes the cause behind responses more difficult to evaluate.

As described in Section 2.5. sacrificial time point samples were taken from microwell cultures and measured for total fluorescence. Figure 4.16. shows representative examples of total fluorescence at different oxygen availabilities. Figure 4.18. shows that there are a number of significant effects on protein expression. Interestingly though, these do not appear to be directly linked to oxygen availability. Although shaking speed and fill volume are significant effects, they are small in magnitude, particularly when compared with the largest effect (time post inoculation). It is also interesting to note that the effect seen for shaking speed is a negative one in both plate formats, the opposite to k_{La} . Additionally, there is little effect seen as a result of changing inoculum concentration. Figure 4.17. also highlights that in the oxygen limited microwell plates, there is no direct correlation between increasing available oxygen and recombinant protein expression.

The most significant positive effect after post inoculation time is temperature of the culture. It is hypothesised that this effect results from increasing biomass concentration and provision of sufficient energy for expression and fluorescence of the recombinant protein. Models for both the 24 and 96 DSW plate formats are similar, as indicated by the responses to factors in Figure 4.18. The effects, have similarly sized parameter coefficients and, as the statistical diagnostics demonstrate (Figure 4.19. and Table 4.12), the validity of the models are both good. The ANOVA undertaken on the models show low p-values and R-squared values in excess of 0.8, which, though not as high as other models seen in this work, are still acceptable for such a complex system and provide a high degree of confidence in the model. In addition, the predicted against experimental plots (Figure 4.19.) show a good agreement between the model and the experimental data, with limited scatter outside of the 95% confidence interval. As such it can be said that these models are a good representation of the system.

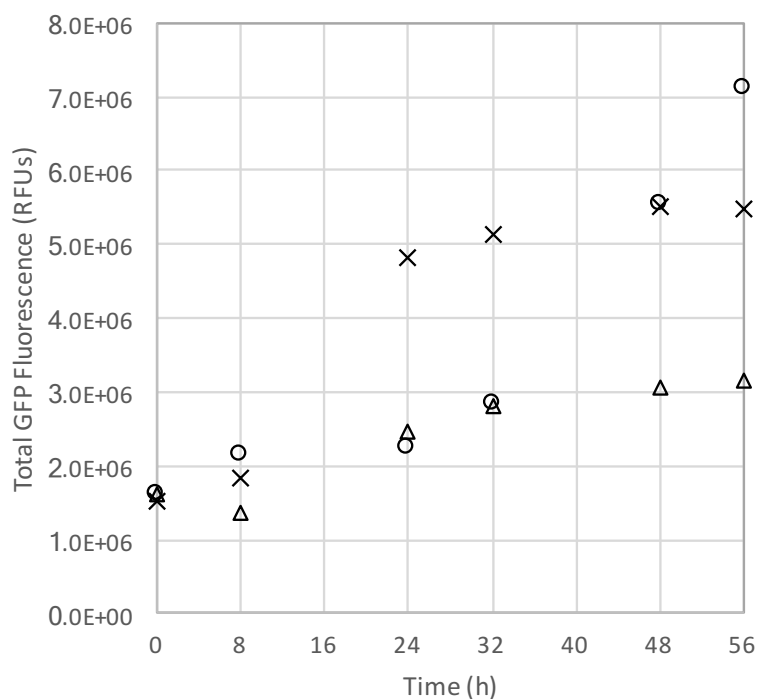


Figure 4.16. Representative examples of culture fluorescence profiles at low (\circ), medium (\times) and high (Δ) $k_L a$. Experiments carried out as described in Section 2.6. Fluorescence measured as described in Section 2.8.

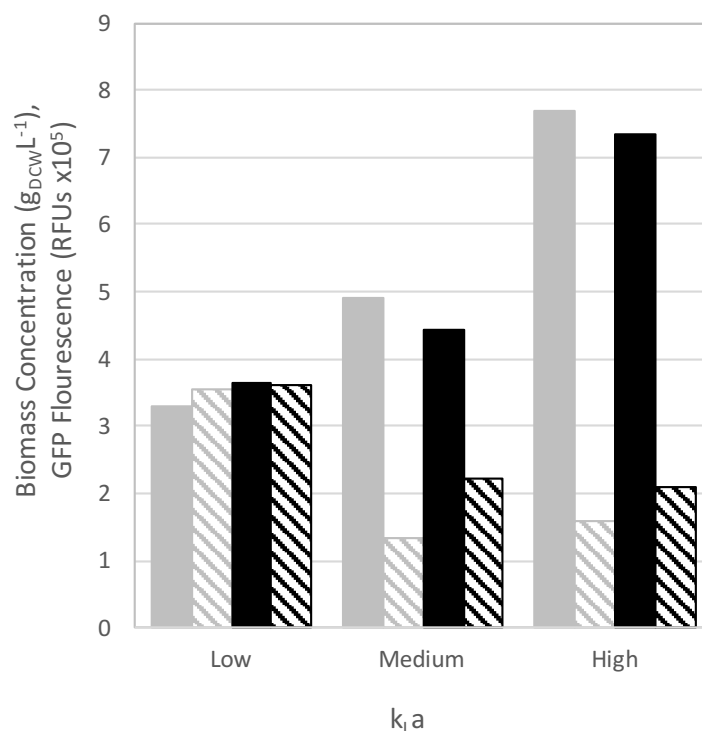


Figure 4.17. Maximum biomass concentration (solid bars) and recombinant protein expression (striped bars) in conditions representative of high, medium and low oxygen availabilities in 24 and 96 DSW plates (grey and black respectively). Experiments carried out as described in Section 2.6. Protein expression determined as described in Section 2.8.3.2.

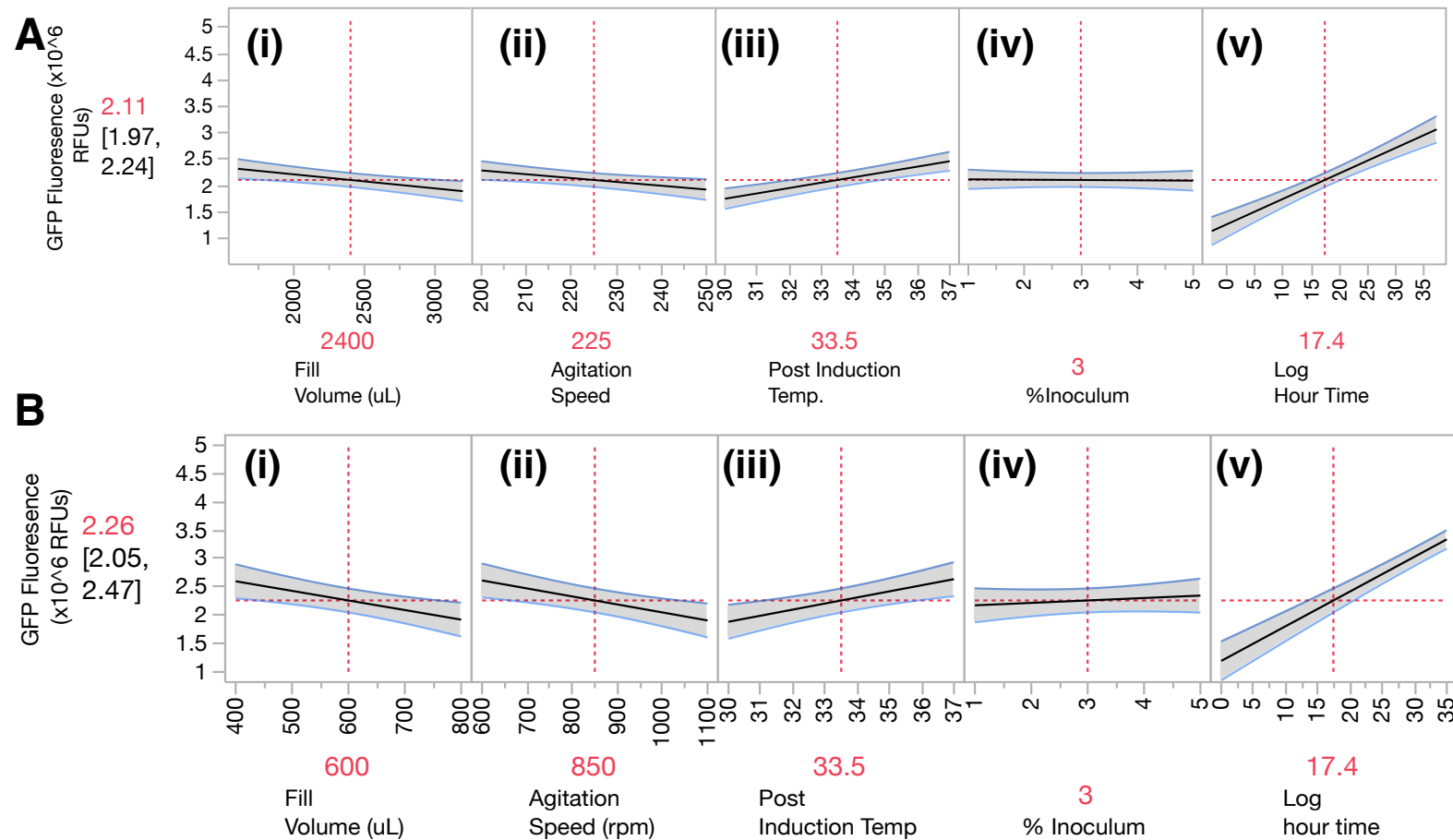


Figure 4.18. Effect profiles for factors included in the multifactorial design evaluating the relationship between recombinant protein expression and oxygen availability in 24 DSW (A) and 96 DSW (B) plates. Fill volume (i), shaking speed (ii), post induction temperature (iii), inoculum concentration (iv) and log hour time post inoculation (v) are all shown. Solid black lines represent the model as a result of the contribution from the individual factor, grey shaded areas indicate 95% confidence intervals, while dashed red lines represent the value for GFP fluorescence at the centre point of the experimental range. Experiments and analysis performed as described in Section 2.6.

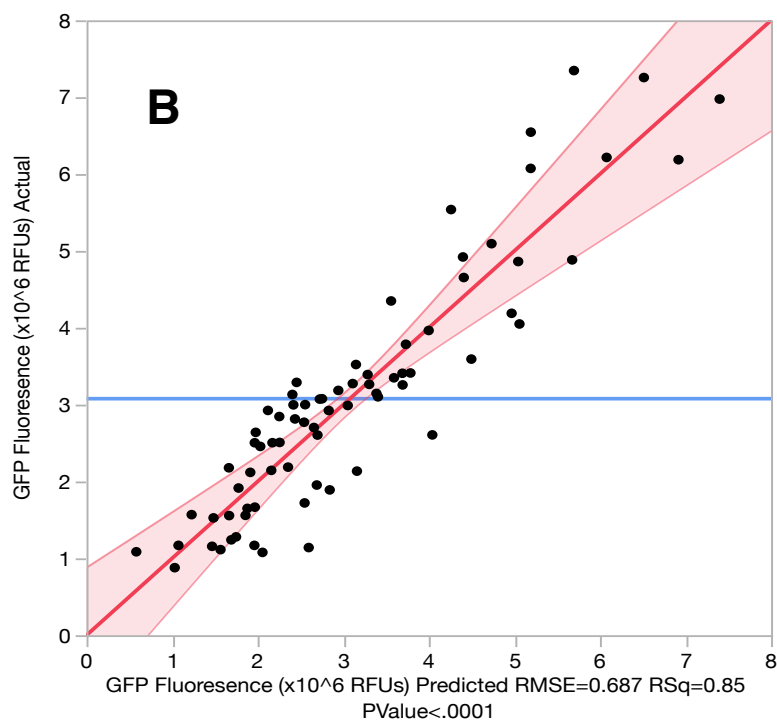
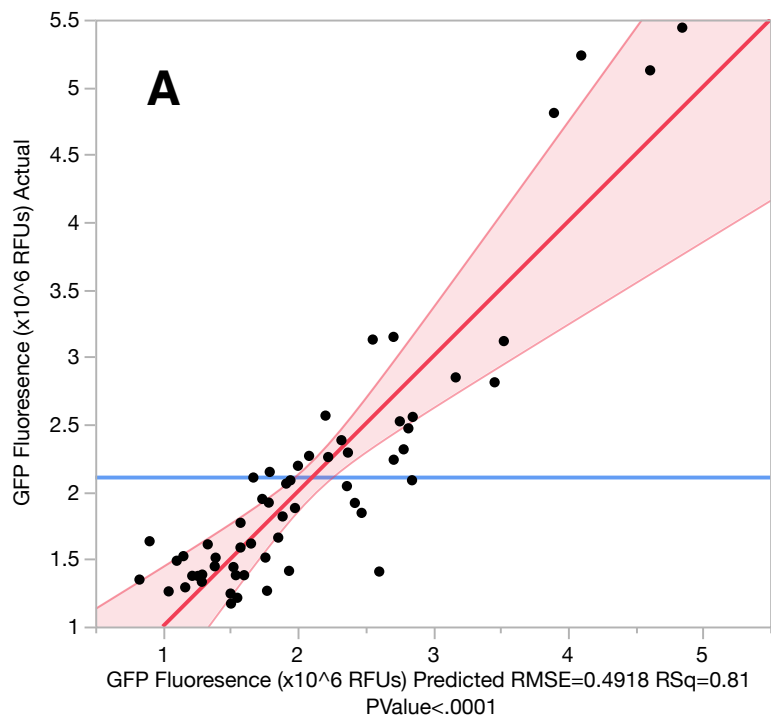


Figure 4.19. Predicted versus experimental parity plots for the models of recombinant GFP expression (by total fluorescence) in 24 DSW (A) and 96 DSW microwell plates (B) during culture. Black dots represent data points, the red line the line of parity (i.e. $y=x$) and the shaded red area the 95% confidence interval. Experiments performed as described in Section 2.6. Analysis as described in Section 2.6.4.

It is therefore interesting to observe that over this scale increase, 96 DSW plates should be a good mimic for the larger 24 DSWs as they give quantitatively similar titres and biomass concentrations, while responses to factors and levels are comparable in response to factors and levels investigated. These observations are needed to further scale up understanding between bioreactor systems and accelerate associated development timelines. It should be highlighted though that these are both oxygen limited environments, and so while this concurrence is good, it does not yet reflect performance in STRs or at commercial scale.

In order to interrogate why there appeared not to be a direct relationship between oxygen availability and recombinant GFP expression. Figure 4.20. shows representative examples of the expression of GFP relative to the online DOT. This highlights that the timing of GFP accumulation, which follows the point at which DOT is minimum, and is approximately correlated with when the culture transitions from exponential growth to stationary phase. This indicates that protein is being produced but not folding completely until oxygen is available (oxygen is required for the maturation of GFP to the fluorescent state), and lends further weight to the argument that oxygen use is prioritised for growth and the generation (and maturation) of a recombinant protein product comes second.

It is also noted that with greater k_{La} , there is an earlier start to product accumulation. In relation to the points previously made about the relationship between growth and productivity, it is likely that this is because with greater available oxygen the exponential phase begins and is exhausted earlier, allowing the culture to transition into stationary phase and protein generation. These plots also confirm that product generation is heavily impacted by culture temperature.

Table 4.12. ANOVA statistical diagnostics to determine confidence in the models for recombinant GFP expression as a result of aeration environment in 24 and 96 DSW plates during culture. Analysis as described in Section 2.6.

	Model	
	24 DSW	96 DSW
R-squared	0.81	0.88
p-value	<0.0001	<0.0001
Root Mean Square Error (RMSE)	0.49	0.49

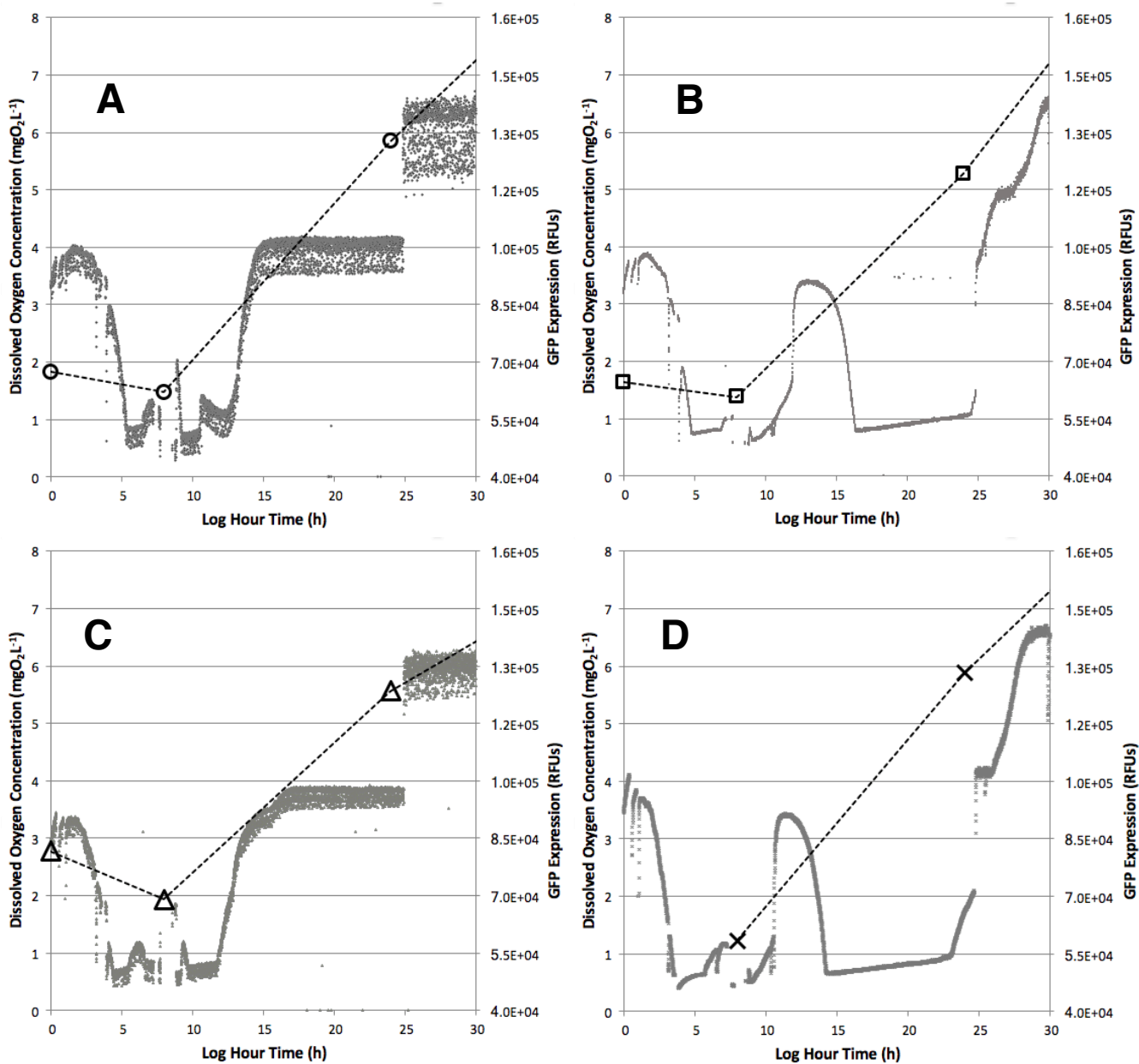


Figure 4.20. Representative examples of dissolved oxygen and protein expression profiles over time. Examples are taken from time courses with a k_{LA} of $\sim 104h^{-1}$. Examples are at $37^{\circ}C$ and 250rpm, fill volumes of 1.6mL (A & C) and 3.2mL (B & D), and inoculum concentration of 1%v/v (A & B) and 5%v/v (C & D). Grey dots represent the DOT trace, while symbols (O, □, Δ, X) show the expression levels of the recombinant protein product by total GFP fluorescence. Experiments were performed as described in Section 2.6. Analysis as described in Section 2.6.4.

It appears that, provided a sufficient threshold of available oxygen, reached when the culture is no longer in growth phase, there is no distinct advantage to increased levels of oxygen with respect to recombinant protein expression. Indeed, given sufficient oxygen the cell will prioritise growth rather than the generation of protein product, and therefore promoting a greater O₂ mass transfer coefficient in microwells would seem to have the potential to be detrimental to productivity in the early stages of culture. This is highlighted in Figure 4.17. also. This is not to say that microwells are providing an ideal environment for microbial growth, but rather that utilisation of oxygen by the cells for protein expression is lower priority. This relationship is hypothesised and discussed also in Section 3.

4.7. Modelling Overlaps in Aeration Environment Between 24 and 96 DSW Plates.

One of the objectives of this work was to develop models for the overlap in aeration environment between 24 and 96 DSW plates using biomass accumulation and protein expression as key responses in each of the plate formats. This assumes oxygen limitation in microwell plates which as discussed in previous sections is a reasonable one. It should then be possible to estimate the set points required to achieve equivalent O₂ mass transfer between plate geometries.

In order to make the models generated in 96 and 24 well plates directly relatable, the parameters related to shaking speed in the orbital shakers have been converted into a linear velocity and a centripetal force. Additionally, to more appropriately correlate the volumes used in the different geometries, a ratio of fill volume to well volume has been calculated.

For example, a 96DSW in an Eppendorf thermomixer comfort with a 3mm throw, running at 1100rpm with an 800µL fill volume and the density of culture assumed to be that of water:

$$\begin{aligned}
 C &= \pi D && \text{Equation 4.6.} \\
 &= 0.003\pi \\
 &= 0.009425m
 \end{aligned}$$

Where C is the circumference and D the diameter of the orbital throw respectively.

$$1100rpm = 1100/60 = 18.33s^{-1}$$

$$\text{Linear velocity} = C \times \omega \quad \text{Equation 4.7.}$$

$$v = 0.009425 \times 18.33 = 0.173ms^{-1}$$

Where ω is the angular velocity.

$$\text{Centripetal force} = \frac{(m \cdot v^2)}{r} \quad \text{Equation 4.8.}$$

$$= 0.0008 \cdot 0.173^2 / 0.0015$$

$$= 0.015962$$

$$= 0.016 \text{ N}$$

Table 4.13. shows the calculated linear velocities and centripetal forces under each of the set of factor set points. There is an approximately 1.5 (with RPM) to 3 (with fill volume) times increase in linear velocity at the low and high ends of the ranges respectively. This translates to an almost 12 times increase from minimum to maximum centripetal force (2.37 to 27.4×10^{-3} N), providing a good breadth which it was expected would impact on oxygen availability and the resultant biomass and protein production.

Table 4.13. Centripetal forces ($\times 10^{-3}$ N) and linear velocities (ms^{-1} in parentheses) for the fill volumes and shaking speed investigated in the 24 and 96 DSW plates. Fill volumes of 400 and 800 μL pertain to the 96 DSW plates, while 1600 and 3200 μL fill volumes were used in 24 DSWs. Similarly, shaking speeds of 200 and 250 rpm refer to set points used with 24 DSW plates, and 600 and 1100 rpm to 96 DSWs. Values calculated as described in Section 4.7.

		Well Fill Volume (μL)			
		400	800	1600	3200
Shaking Speed (rpm)	200	-	-	8.79 (0.262)	17.6 (0.262)
	250	-	-	13.7 (0.327)	27.4 (0.327)
	600	2.37 (0.094)	4.74 (0.094)	-	-
	1100	7.98 (0.173)	16.0 (0.173)	-	-

4.7.1. Equating O₂ Mass Transfer Conditions in 24DSW to 96DSW Using Biomass Accretion

Oxygen availability is assumed to be the factor which is limiting to growth in both 24 and 96 DSW plates. This is based on the work in this thesis, as well as literature precedent. Thus a model can be built based on the measurements of oxygen availability, as well as the input parameters which have already been shown to affect this in 24 deep square well plates, to infer the availability of O₂ in the smaller, 96 deep square wells which cannot be measured directly.

4.7.1.1. Model Generation

Models generated for maximum biomass concentration using JMP (Figure 4.14.) demonstrate that there is an overlap in the factors impacting on oxygen mass transfer in microwells. These include well fill volume, shaking speed (which for the purpose of developing this model has been converted to linear velocity of the well), an interaction between linear velocity and the temperature, and temperature for the 24 DSW plate.

The equivalence is tested using the statistical models generated in this chapter. The models can be generalised as:

$$OD_{96} = A + BV_{96} + CT + DF_{96} + E(V_{96} - V_{96}^*)(T - T_{96}^*) \quad \text{Equation 4.9.}$$

$$OD_{24} = A' + B'V_{24} + C'T + D'F_{24} + E'(V_{24} - V_{24}^*)(T - T_{24}^*) \quad \text{Equation 4.10.}$$

Where V_{96} is the linear velocity of 96 deep square well plate (ms^{-1}), V_{24} the linear velocity of 24 deep square well plate (ms^{-1}), T the temperature ($^{\circ}\text{C}$), F_{96} is the fill volume of 96 deep square well plate (μL) and F_{24} the fill volume of 24 deep square well plate (μL). The mean values of these variables, used for the interaction terms, are indicated using an asterisk (e.g. V_{96}^*)

The constants and coefficients of these terms are defined as: OD_{96} is the maximum OD in 96 deep square well plate using curve fitting; OD_{24} the maximum OD in 24 deep square well plate using curve fitting; A the constant term for 96 deep square well model; A' the constant term for 24 deep square well model (this convention is used also for the following coefficients e.g. B'); B is the coefficient of velocity term; C the coefficient of temperature term; D is the coefficient of volume term and E the coefficient of velocity-temperature interaction.

Here the intention is to determine an equivalent linear velocity for the 96 and 24 well plates. Equating the two generalized models and rearranging so that V_{96} (the desired output) is the subject gives:

$$V_{96} = \frac{\alpha + f(V_{24}, T) + g(T) + h(F_{96}, F_{24})}{d(T)} \quad \text{Equation 4.11.}$$

Where:

$$\alpha = A' - A + E V_{24}^* T_{24}^* - E V_{96}^* T_{96}^*$$

$$f(V_{24}, T) = (E'(T - T_{24}^*) + B)V_{24}V_{24}$$

$$g(T) = (C' - E V_{24}^* - (C - E V_{24}^*))T$$

$$h(F_{96}, F_{24}) = D'F_{24} - DF_{96}$$

$$d(T) = E(T - T_{96}^*) + B$$

Values for constants and coefficients from the models for OD in both 96 and 24 DSW plates can be introduced. The parameter values for each of the models are required. Values are shown in Table 4.14.

From here, an example of equivalence can be considered using two cultures (one from the 96 well plates, one from the 24 wells), which resulted in similar maximum biomass concentrations, in order to demonstrate the intended application of the equivalence model with known data. The set points are as follows:

$$T=37^\circ\text{C}, F_{96} = 400\mu\text{L}, F_{24} = 3200\mu\text{L}, V_{96} = 0.173\text{ms}^{-1}, V_{24} = 0.327\text{ms}^{-1}$$

Incorporating these into the model, gives:

$$\alpha = 161.22$$

$$f(V_{24}, T) = 44.88$$

$$g(T) = -198.73$$

$$h(F_{96}, F_{24}) = -5.2$$

$$d(T) = 96.36$$

Giving a prediction that V_{96} should be 0.178 ms^{-1} in order to generate the same maximum biomass concentration, which is acceptably close to the actual value of 0.173 ms^{-1} used experimentally. Some error can be attributed to the small difference between actual and curve

fit biomass concentration values. Additionally, some to the fact that although good, the model is not a perfect fit.

There are large areas of the design space which overlap in terms of biomass accumulation and therefore oxygen mass transfer in the two different plate geometries. Similar final biomass concentrations can be achieved, modelled and predicted between 96 and 24 deep square well plates using this method, and in turn be used to determine equivalent experimental parameter set points to achieve the same biomass concentration in each format.

In turn, as O_2 is assumed to be limiting, oxygen mass transfer in 96 well plates can be estimated i.e. the set points which achieve equivalent biomass concentrations are providing the same level of available oxygen and therefore have equivalent $k_L a_s$. This is shown in the development of O_2 mass transfer models in Sections 4.4. and 4.5., in which there is shown already to be a high degree of confidence.

Table 4.14. Parameter coefficients from the models for oxygen mass transfer with respect to biomass accumulation in 24 and 96 DSW plates.

Parameter	Term in 24	Value in 24	Term in 96	Value in 96
	DSW Eqn.	DSW model	DSW Eqn.	DSW model
Intercept	A'	-16.12	A	17.22
Coefficient of velocity	B'	66.90	B	28.44
Coefficient of temperature	C'	-0.10	C	0.38
Coefficient of fill volume	D'	-0.001	D	-0.005
Coefficient of velocity-temperature interaction	E'	29.71	E	22.64
Mean velocity	V^*_{24}	0.295	V^*_{96}	0.128
Mean temperature	T^*_{24}	33.5	T^*_{96}	34.0

This in turn acts as a proof of concept for establishing similar relationships at different stages of the scale up paradigm.

4.7.2. Equating O₂ Mass Transfer Conditions in 24DSW to 96DSW Using Recombinant Protein Expression

An initial aim of this section of work was to generate a model to equate recombinant protein expression in 24 and 96 DSW plate formats which would estimate the set points required to provide equal amounts of protein in each case, such as has been done in Section 4.7.1. for biomass accretion.

Although some overlap is seen between the two plate geometries in terms of protein expression, it has also been demonstrated that oxygen does not appear to be the directly limiting factor for generation of this product (Section 4.6.). As such, any model generated in order to try and equate protein production as a result of the oxygen environment would be misleading, and likely unsuccessful.

4.8. Summary

The aim of this chapter was to develop a method to improve the precision of oxygen mass transfer quantification in commonly used microwell plate formats, using statistical models to demonstrate the usefulness of the method and equivalent culture performance in both geometries. Using recent developments in online dissolved oxygen measurement in microwell plates, a new method for quantification of OUR and mass transfer rates has been developed (Section 4.3.) which has a number of advantages compared with traditional gassing out or sulphite oxidation methods. As expected, influencing the physical parameters to which a microwell culture is subjected, impacts on both the available oxygen and the physiological response of the culture (Section 4.4.). Greater available oxygen results in increased biomass accumulation and reduced recombinant protein formation, lending further weight to the hypothesis that oxygen utilisation prioritises growth (Section 3.5.).

Multi-dimensional models for k_{La} (Figure 4.5. and Table 4.4.) and OUR (Figure 4.9. and Table 4.9.) were developed in 24 DSW plates based on the new method, improving the understanding of culture dynamics in microwells, mass transfer of oxygen into the culture and oxygen utilisation by the microbial expression system.

Accumulation of biomass and a recombinant protein product (GFP) were evaluated in a multifactorial landscape (Sections 4.5. and 4.6.), and modelled to determine that oxygen does indeed appear to be the limiting factor in biomass accumulation in microwells but that additional significant factors influence on protein expression.

Similar models were observed in both plate geometries, indicating that 96 DSW plates are a good mimic for protein expression and growth in 24 DSW plates (Figures 4.14. and 4.18.). This allows users to switch between formats enabling flexibility for high throughput screening and expression studies. As many of the limitations of the two plate types are shared this would seem reasonable. This observation was only made available by the use of a DoE landscape in order to understand the influence of interacting factors on the system.

A mathematical model was also built for estimation of equivalent biomass and parameter set points in 96 DSWs using overlaps with 24 DSW maximum biomass concentration and (due to oxygen being the limiting substrate) the aeration environment (Section 4.7.).

In the next chapter the oxygen mass transfer capabilities of a number of commercially available single use bioreactors (SUBs) will be quantified and characterised. This will be used to determine the applicability of SUBs for culturing microbial expression systems, using the characterisation work undertaken in Section 3 as a reference point.

5. Oxygen Mass Transfer Characterisation of Laboratory Scale Single Use Bioreactors

5.1. Context and Aim

This work so far has reviewed the relevance of industrial biocatalysis, with a focus on oxidoreductive enzymes and oxygen utilisation by cytochrome P450 monooxygenases (Section 3), and demonstrated the compatibility of scale down technologies (Section 4) in the form of microtiter plates for culturing microbial expression systems, and producing recombinant proteins of commercial interest. It is now interesting to consider the potential for scale up of microtiter plate results into single use bioreactors (SUBs).

SUBs are increasingly used in industrial bioprocess development and manufacturing, with the largest reactor commercially available for microbial systems being 2m³ total volume. SUBs have a number of advantages including reduction in batch turnaround time and resource requirement for cleaning, but are not without their challenges (Section 1.2.7.). One of the biggest limitations is that SUBs typically have limited oxygen mass transfer capabilities (Table 1.13). Given the overall aim of this work, it is important to demonstrate which technologies are capable of supporting microbial fermentation and whole cell oxidative bioconversions.

SUBs are available in a number of designs, from simple two-dimensional, pillow style bags which require rocking, to three-dimensional bags which require a support frame for stability, and rigid moulded designs which share many of the characteristics of a traditional stainless steel bioreactor. Each of these has differences in their geometry and configuration which will influence oxygen mass transfer capabilities. This was discussed in Section 1.2.7.4.

5.1.1. Aims

As discussed previously in Sections 1.2.9. and 4.1, current methods for characterisation of oxygen mass transfer have significant limitations, two of which are that an idealised liquid is often used (typically water) and that evaluations are done under a specific set of conditions and are not broadly applicable. As such, the objectives for this chapter will focus on evaluating the oxygen mass transfer

capabilities of commercially available SUBs and determining where they can be used for culturing microbial expression systems. Specific objectives are to:

- Quantify oxygen mass transfer capabilities of two commercially available SUBs, and a traditional glass benchtop STR as a benchmark;
- Establish a method for modelling oxygen mass transfer in multifactorial experimental space under a range of widely used experimental conditions. This will aid in understanding which factors interact with one and other, but also which of the factors that influence oxygen mass transfer are common to different reactor geometries,
- Use this method to generate models for oxygen mass transfer in SUBs in order to establish where they can be applied to microbial fermentation.

5.2. Oxygen Mass Transfer in a Conventional Stirred Tank Bioreactor (New Brunswick BioFlo 310)

The New Brunswick BioFlo 310 is a glass, bench top, autoclavable, pilot scale, stirred tank bioreactor. It provides a model system with which to compare the SUBs, having similar total volume and aspect ratio to the XDR-10 (Section 2.3.1. and 2.7.3.) and the rigid construction and impeller type of the Ambr®250 (Section 2.3.1. and 2.7.2.). Additional information on the BioFlo 310 can be found in Section 2.3.1, 2.7.1. and Table 2.1 including configuration and geometries.

The BioFlo 310 uses a polarographic dissolved oxygen probe which must be calibrated outside of the reactor before a range check is undertaken once the probe is installed in the vessel. The data recording software provided has changing frequencies for data recording depending on the rate of change of the parameter (i.e. DOT). As a result, during rapid changes in DOT, data is recorded every five seconds, but this increases when the rate of change is reduced. Therefore, there is a concern over the consistency with which data points are logged.

5.2.1. Building the Experimental Design

The factors and ranges selected for investigation have been informed by prior knowledge of oxygen mass transfer in fermentation, and by evaluation of the available literature (Section 1.2.6.). Additional constraints were placed on the ranges by the limitations of the BioFlo 310 and the associated control software. A multifactorial

response surface methodology (RSM) was applied in order to generate a predictive model for k_{LA} (Section 2.7.). This enables the identification of curvature in the response and a high degree of statistical confidence with respect to how the properties of the environment and process constraints affect mass transfer.

Five factors were selected from a preliminary list of 11. A design containing 50 runs in an RSM framework was constructed. The experimental points were distributed across the range (at 0%, 25-30%, 50%, 70-75% and 100% of the range). The five factors chosen were aeration rate, agitation speed, temperature, viscosity as measured by media concentration of glycerol (henceforth referred to as viscosity) and supplementary antifoam concentration. Selection was of the factors deemed most likely to influence oxygen transfer.

Factors and ranges are summarised in Table 5.1. In addition, the experimental design can be found in Appendix 4.1. Aeration rate is known to influence oxygen mass transfer. However, it has been shown that aeration rates in excess of 1.5vvm can flood the impeller region (Stanbury et al, 1995) and have a detrimental effect on mass transfer. As such 1.5vvm was set as the upper limit, while a preliminary experiment using water indicated that aeration rates less than 0.13 vvm result in the DOT not reaching above 70% of saturation, and so this was set as the minimum. A similar effect was seen for agitation speeds lower than 100rpm, and so this was set as the minimum for this factor. The maximum was dictated by the constraints of the BioFlo 310 motor and control software and was set at 1200rpm.

As discussed in Section 1.2.6.4. temperature effects the solubility and diffusivity of oxygen, and so it was considered a potentially important factor to investigate. The temperature range was defined with a consideration for microbial fermentation which is unlikely to be performed below 15°C. In addition, diffusivity of oxygen dominates mass transfer in the range of 10-40°C (Doran, 1995) while outside of this range solubility of oxygen dominates. Thus, to test both of these mechanisms, a maximum temperature of 50°C was selected. With respect to viscosity, the established approach of using water and glycerol mixtures in order to modify viscosity in a predictable way was used (Sheely 1932; Segur & Oberstar 1951; Özbek & Gayik 2001; González et al. 2011). The minimum would be close to that of water and so no addition of glycerol to the base media was used. 30mLL⁻¹ was selected as the maximum concentration, with

fermentations unlikely to go this high due to a potential for carbon catabolite repression (CCR) and high cost at scale (Brückner & Titgemeyer 2002).

Antifoam (poly-propylene glycol - PPG) concentrations were in the range of 0 to 0.1% v/v, with a concentration of 0.02% v/v commented as being sufficient for suppression of foam in an aqueous media (Sigma-Aldrich 2015).

Table 5.1. Factors and ranges for generating the model of oxygen mass transfer in a New Brunswick BioFlo 310 bench top STR. Experiments performed as described in Section 2.7.

Factor	Unit	Set points				
		Minimum	Low	Centre	High	Maximum
Glycerol Concentration	mL L ⁻¹	0	8.69	15	21.31	30
Aeration Rate	vvm	0.125	0.43	0.75	1.07	1.50
Agitation Speed	rpm	100	419	650	881	1200
Temperature	°C	15	25.1	32.5	39.9	50
Antifoam	%v/v	0.0	0.036	0.055	0.074	0.100

5.2.2. Fixed Factors

In addition to highlighting what was changed, it is important to know what was fixed and why. Compressed air for example was used throughout rather than changing the composition of the inlet gas with respect to oxygen concentration. Although potentially impactful, beyond small pilot scale, pure oxygen is seldom used for microbial fermentation. This is due to cost, and because of the safety issues associated with storing large volumes of compressed oxygen. Instead, alternative means are used such as head pressure to increase the solubility of oxygen.

It has been assumed that the hydrodynamics of the system are sufficient to provide a well-mixed environment (i.e. instantaneous dispersal of oxygen), and so there is no requirement to investigate probe height as a factor. The ionic content of the liquid phase has been shown to influence solubility of oxygen and therefore k_{La} , however this was deemed to be relatively minor, and would have likely required a switch to a

defined medium composition, and so the base media composition was fixed around that of terrific broth (TB).

Finally, the static gassing out method was used (Section 2.7). Use of dynamic gassing out (as demonstrated in Chapter 4) would have been preferred, testing with a range of biomass concentrations. However, this would be impacted by the strain used, again distracting from the desired output of a widely applicable model.

5.2.3. Run Ordering

The order in which experimental runs were undertaken was a critical consideration dictated principally by media composition and temperature factors (Table 2.2.). Ideally, run order would be randomised to minimise the likelihood of any bias or introduction of experimental error into the data, however it was not practical to prepare fresh media for each run. As such, runs were grouped (no more than 6 runs in each group), accommodating increasing antifoam concentration, as it is a physical addition, and so cannot subsequently be removed. Furthermore, in order to avoid any potential adverse effects of high temperature on media properties (e.g. possible degradation of media components), if more than one temperature was grouped, then lower temperature runs were performed first.

5.2.4. Modelling Oxygen Mass Transfer in a Pilot Scale Stirred Tank Bioreactor

Prior to building a model for oxygen mass transfer, the k_{La} under each set of conditions must be quantified. The method for doing this and adjusting for the probe response time (PRT) is described in Section 2.7.1.2. A table of calculated k_{La} values for this investigation can be found in Appendix 4.2. The model equation can be found in Appendix 4.5.

Building the multifactorial model after the initial data processing is a significant undertaking. Decisions regarding the application of particular model fits are required and must be based on the statistical evidence provided by analysis using the DoE software.

The model built was quadratic. Since an RSM design was used and the design space was saturated, it was possible to look for curvature in the responses. The statistics behind the quadratic model were the strongest available (when compared with linear, two factor interaction and cubic options). A sequential p-value of <0.0001

and an R-squared of 0.88, as well as the lowest standard deviation value confirm the quadratic as the preferred choice. This is discussed in more detail in Section 5.2.4.3.

In order to exclude those factors with an insignificant effect, a backward elimination was used, removing those factors and interactions with the smallest effects first and continuing until only significant terms remain as part of the model. The literature which describes the influence of factors investigated here on oxygen mass transfer is discussed in Section 1.2.6. In addition, comparison of the values determined here with those in the literature can be found in Table 5.14.

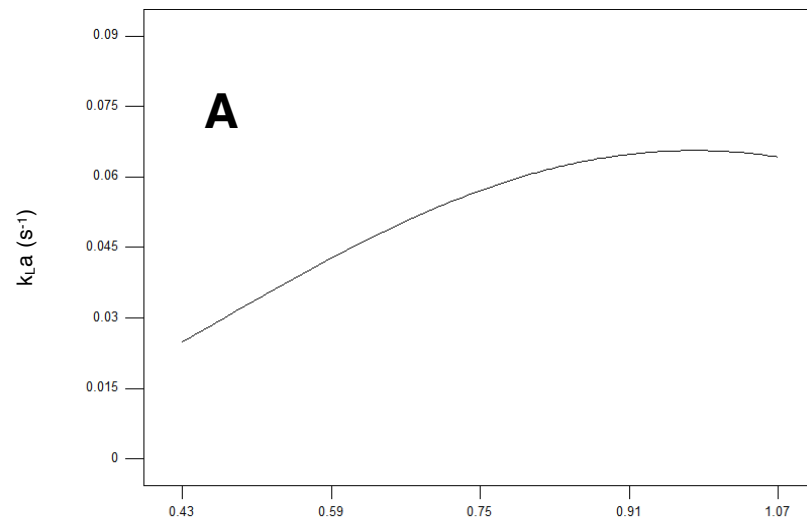
5.2.4.1. Main Effects

The model highlights three main effects on oxygen mass transfer. These are aeration rate, agitation speed and antifoam concentration.

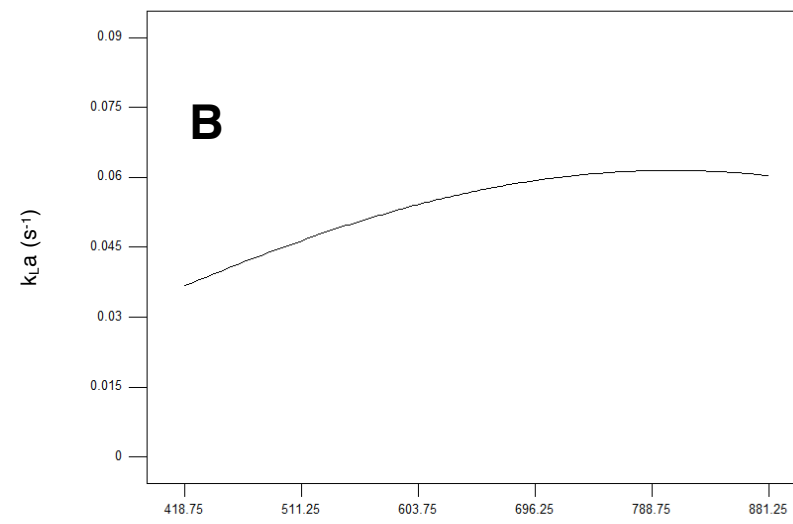
Figure 5.1A. shows the effect of aeration rate on $k_{L,a}$. Up to 1vvm there is a steady increase in $k_{L,a}$ from 0.020 to 0.065s⁻¹. Above 1vvm the $k_{L,a}$ plateaus before beginning to decline. This is most likely due to flooding of the impeller resulting in ineffective dispersion of the gas into the liquid media. In addition, at higher aeration rates, with the fixed hole size of the sparger the bubbles formed become larger, resulting in a smaller surface area to volume ratio which has a negative impact on oxygen mass transfer. Aeration rate is the single greatest main effect.

Agitation speed is the next most influential factor. The relationship between $k_{L,a}$ and agitation speed is shown in Figure 5.1B, and again it is not a linear one. As agitation speed increases, bubbles are broken down, increasing the surface area to volume ratio. This larger interfacial surface area improves the efficiency of oxygen mass transfer into the media (Doran, 1995). Additionally, with increasing agitation speed, there is greater dispersion of the bubbles. These contribute to the increasing $k_{L,a}$ (by ~0.03s⁻¹) up to approximately 0.065s⁻¹ at 800rpm, after which, there is a plateau and decline as with aeration rate. Above 800rpm, the decline in $k_{L,a}$ is most likely due to flooding of the impeller region, in an interaction with aeration rate. This interaction will be discussed in Section 5.2.4.2.

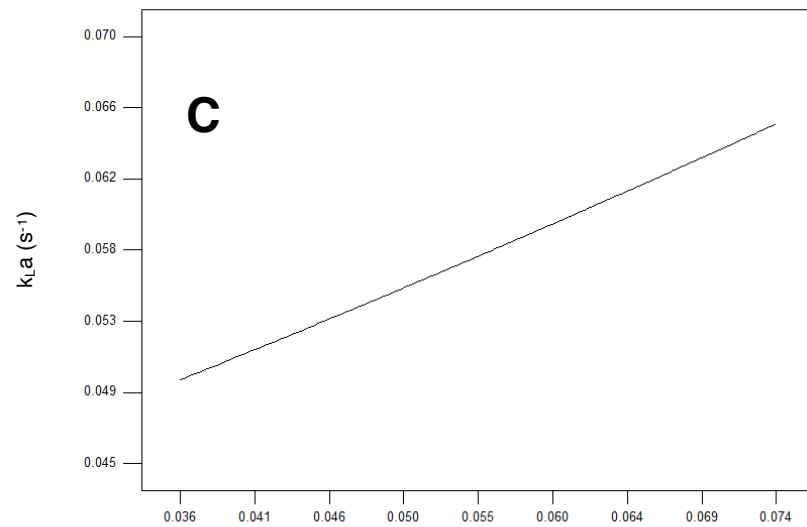
Aeration rate has a greater influence on oxygen mass transfer than agitation speed as a main effect (although they also interact). In Figures 5.1A and 5.1B it can be seen that changes in aeration rate are responsible for a more than three-fold increase in



B: Aeration (vvm)



C: Agitation (rpm)



E: Antifoam (PPG) (%v/v)

Figure 5.1. Plots for the three main effects observed in the model of oxygen mass transfer coefficient in the BioFlo 310 stainless steel stirred tank bioreactor. Effects of aeration rate (A), agitation speed (B) and antifoam concentration (C) are shown. Experiments and analysis performed as described in Section 2.7.

k_{LA} , from 0.02 to 0.065s⁻¹, while the agitation speed causes an increase from 0.035 to 0.065s⁻¹ (a change of 0.03s⁻¹). This is likely due to the aeration rate being responsible for increasing the volume of oxygen in the reactor, while agitation speed is responsible for the breaking down the bubbles. It appears therefore that there is a dependence, the contribution of agitation speed is restricted by aeration. It is reasonable also that these would have the greatest individual effects.

Figure 5.1C shows the influence of antifoam on k_{LA} , which also has a positive effect, increasing k_{LA} from ~0.05 to ~0.065s⁻¹. This positive correlation is contrary to much of the information available from the literature which suggests that, as antifoams are surfactants, they reduce the mobility of the gas-liquid interface and increase the coalescence which in turn adversely affects k_{LA} (Stanbury et al. 1995; Hebrard et al. 2009). However, there are a number of potential explanations for this effect. The first, put forth by Masutani and Stenstrom (1991), is that during unsteady state testing, with an increase in experimental number, there is deterioration in the performance of the antifoam as the same media is reused (Section 2.7.1.1.), resulting in increased k_{LA} . Alternatively, oxygen may accumulate on the antifoam at the interface between the gaseous and liquid phases (Rols et al. 1990). This may result in increased concentrations of oxygen over time. The main effect is not as substantial as aeration or agitation speeds but is still a significant influence.

5.2.4.2. Two Factor Interactions

In addition to the main effects, there are six interactions between factors which have a statistically significant effect on oxygen mass transfer in the BioFlo 310 STR. These are aeration rate and agitation speed, viscosity and aeration rate, viscosity and temperature, aeration rate and temperature, agitation speed and antifoam concentration and antifoam concentration with temperature.

The interaction between aeration rate and agitation speed is the greatest contributing interaction. Figure 5.2. shows a three-dimensional representation of the relationship, highlighting the complexity. There is an overall positive trend when increasing aeration rate and agitation speed, which would be expected as both are positive main effects. When aeration rate is low, the effect of changing agitation speed is small, however when aeration rate is high the effect of changing agitation speed is large and positive, rising from ~0.035 to 0.08s⁻¹ across the experimental range. It is

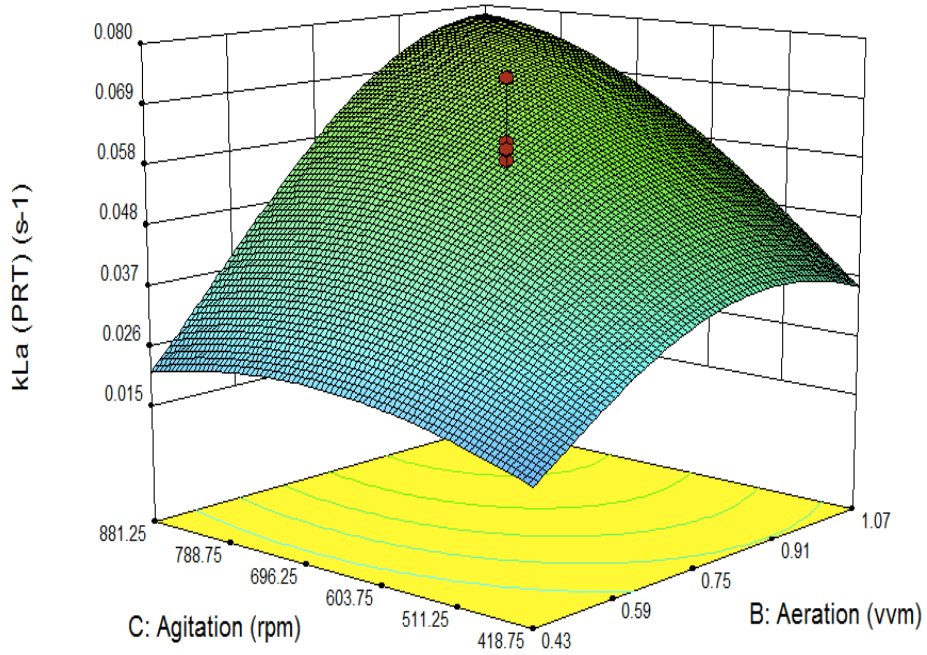


Figure 5.2. Three-dimensional surface plot showing the impact on k_{La} of the interaction between agitation speed and aeration rate. Red dots represent experimental values at the centre point of the experimental design. Experiments and analysis performed as described in Section 2.7.

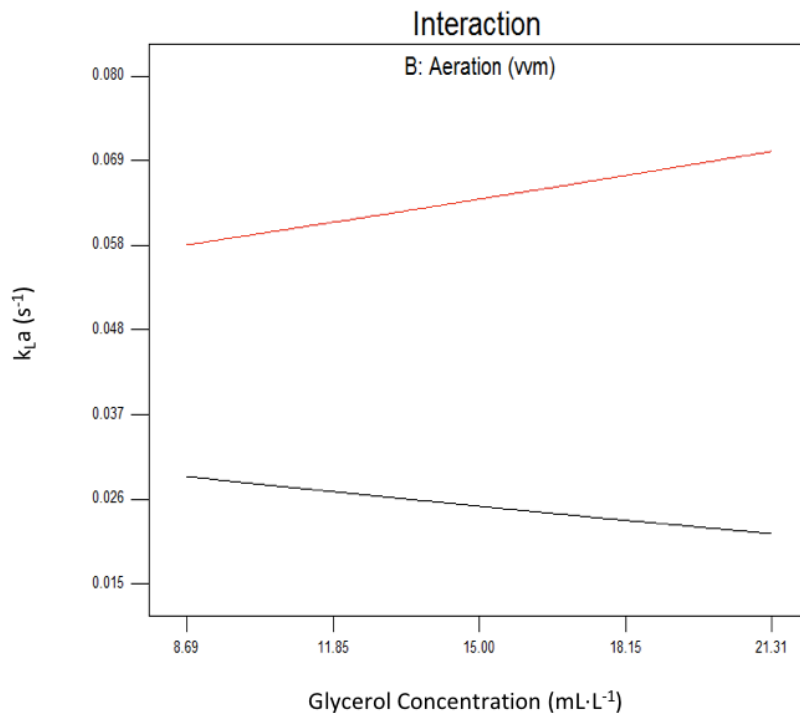


Figure 5.3. Interaction plot to demonstrate the impact on oxygen mass transfer coefficient of the interaction between viscosity and aeration rate, when aeration rate is high (red) and low (black). Experiments and analysis performed as described in Section 2.7.

seen also that when both factors are high the interaction begins to plateau, indicating that a local optimum has either been reached or is close.

This interaction is a result of increased oxygen flow due to greater aeration and the effective breakdown and dispersion of bubbles at high agitation speeds. As such there is an increased interfacial surface area for gas transfer, reduced coalescence of the bubbles and a thinning of the film at the gas-liquid interface (Stanbury et al, 1995). This results in the minimum distance and resistance to diffusion and maximisation of oxygen transfer.

As with high agitation speeds and aeration rates individually, there is a point at which the oxygen mass transfer stops rising. This is likely a result of flooding the impeller region of the reactor meaning that dispersion becomes less effective and gas travels directly from the sparger to the surface of the liquid, minimising residence time and the opportunity for oxygen transfer. Additionally, bubbles of a small diameter (<3mm) resulting from greater agitation speeds become less proficient at mass transfer as they become rigid and surface tension regulates gas exchange (Doran, 1995).

The interaction between aeration rate and viscosity is complex. Figure 5.3. shows that at a low aeration rate, increasing viscosity has a detrimental effect on oxygen transfer, whereas at a high aeration rate the impact of increasing viscosity is positive. It is probable that this is due to a trade-off between residence time and the thickness of the film formed around the bubbles, both of which increase with viscosity (Doran, 1995).

Figure 5.4. shows the interaction between viscosity and temperature, and the impact on $k_L a$. It shows a relationship known as a saddle point which is a complicated interdependence of the two contributing factors, wherein the influence of changing one factor is reversed on the other side of the experimental range. For example, at low temperature the effect of increasing viscosity is positive and linear, rising from 0.035 to 0.065, whereas at high temperature, the effect is reversed with increasing viscosity leading to a linear reduction in $k_L a$ of approximately the same magnitude. Similarly, at low viscosity, the impact of increasing temperature is positive but tapers off above 35°C, while at high viscosity the opposite is observed, an increase in temperature results in a decrease in $k_L a$ of the same magnitude. In this interaction, the most stable area of the design space is in the centre of the two ranges.

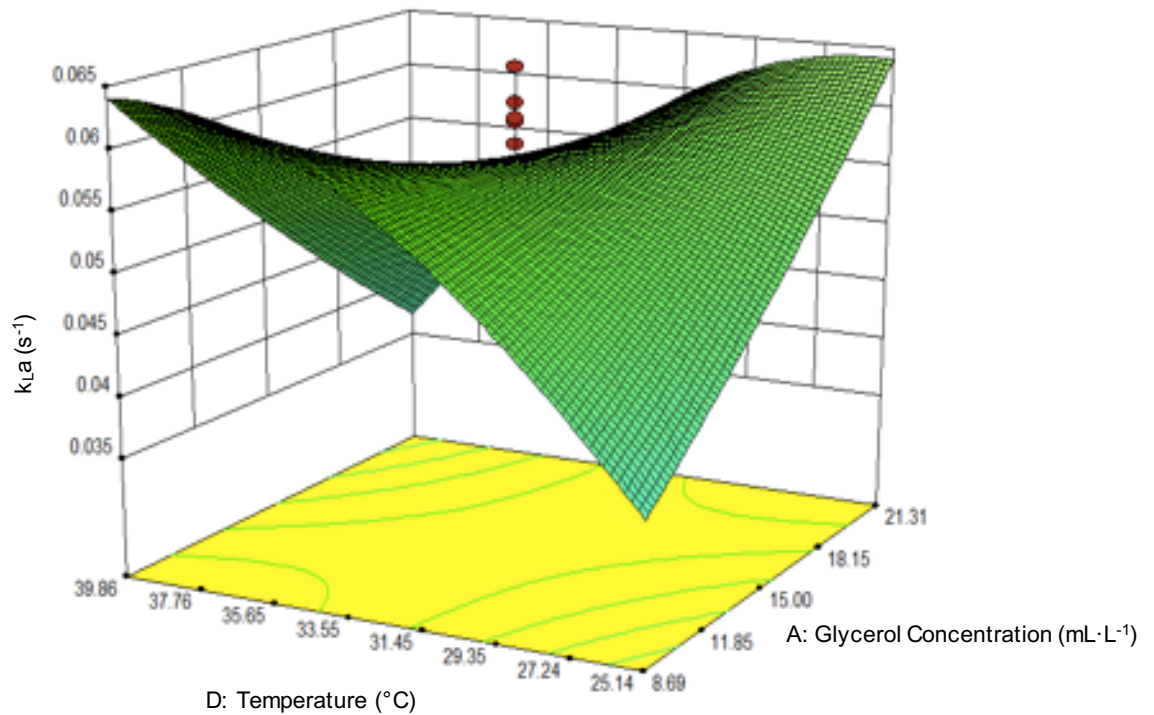


Figure 5.4. Three-dimensional surface plot showing the interaction between viscosity and temperature and the effect on the oxygen mass transfer coefficient. Red dots represent experiments at the centre point of this interaction in two dimensions. Experiments and analysis performed as described in Section 2.7.

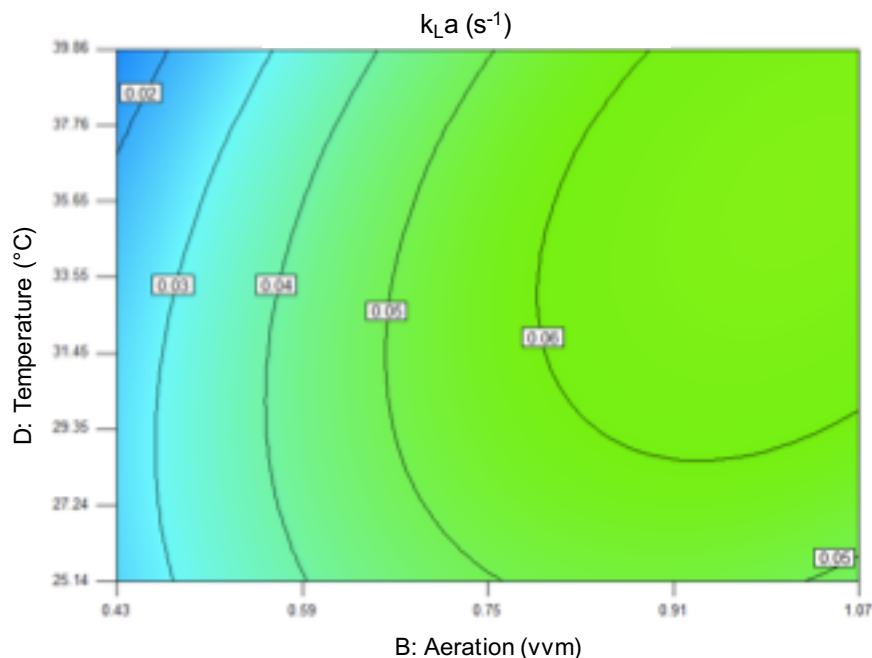


Figure 5.5. Contour plot showing the relationship between temperature and aeration rate, and the effect on oxygen mass transfer. Dark blue represents the lowest observed k_{La} ($\sim 0.02s^{-1}$), ranging to dark green representing the highest k_{La} ($\sim 0.06s^{-1}$). Experiments and analysis performed as described in Section 2.7.

The likely cause of this phenomenon is that, as temperature increases, there is a reduction in surface tension leading to a decrease in the diameter of bubbles formed and therefore an increase in the interfacial area available for mass transfer (Doran, 1995). In addition, greater temperatures result in improved diffusivity, particularly at low viscosity, and together these result in an increased capacity for oxygen mass transfer. However, at high temperatures, although diffusivity increases, solubility of oxygen decreases. This effect is then compounded at higher viscosities, as the thickness of the liquid film increases, adding resistance to gas-liquid mass transfer.

Figure 5.5. shows a contour plot for the interaction between aeration rate and temperature. In comparison to those relationships seen previously it is relatively simple. With increased aeration and temperature, there is an increase in oxygen mass transfer across the range from 0.02 to 0.06s⁻¹. As discussed in Section 1.2.6., temperature has an effect over the solubility and diffusivity of oxygen in the media, while aeration rate affects the available oxygen for mass transfer in the fluid and the form that the bubbles take in terms of their interfacial surface area and residence time. Operational ranges in which the oxygen mass transfer exceeds 0.06s⁻¹ are seen at 30°C and 0.8vvm and above.

Antifoam concentration interacts with two other factors; agitation speed and temperature. When interacting with agitation speed, there is a more significant increase in the volumetric oxygen mass transfer coefficient when the antifoam concentration is greater (Figure 5.6), rising from 0.035 to 0.08s⁻¹. A similar effect is seen when antifoam concentration interacts with temperature with higher concentrations seeing a rise between 0.05 and 0.065s⁻¹, while the lower concentration shows a negative trend overall (Figure 5.7).

In the case of the interaction with agitation speed, this is likely to be due to a relationship caused by the surfactant between the surface tension of the bubbles and the mobility of the gas-liquid interface. Although it is expected that the result will be an overall decrease in $k_L a$ due to the decrease in k_L outweighing the increase in interfacial surface area (a), there are conflicting reports which suggest that size of the increase in the interfacial surface area may exceed the decrease in the k_L and therefore the overall $k_L a$ would increase (Kawase & Moo-Young 1990).

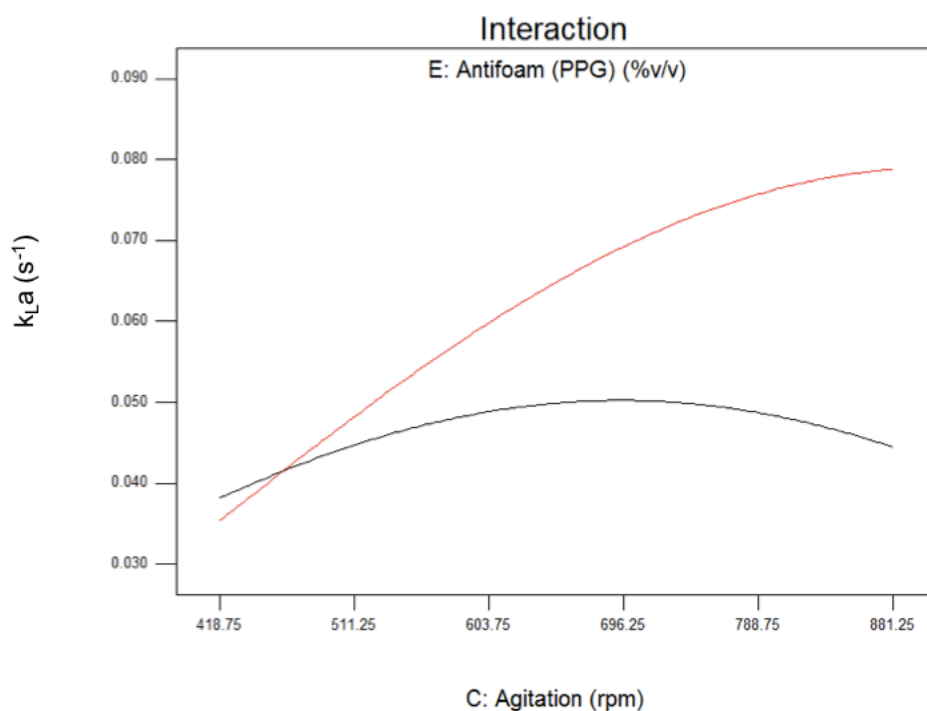


Figure 5.6. Two factor interaction between antifoam concentration and agitation speed. The red line indicated high antifoam concentration (0.07% v/v), while the black line is low antifoam concentration (0.04% v/v). Experiments and analysis performed as described in Section 2.7.

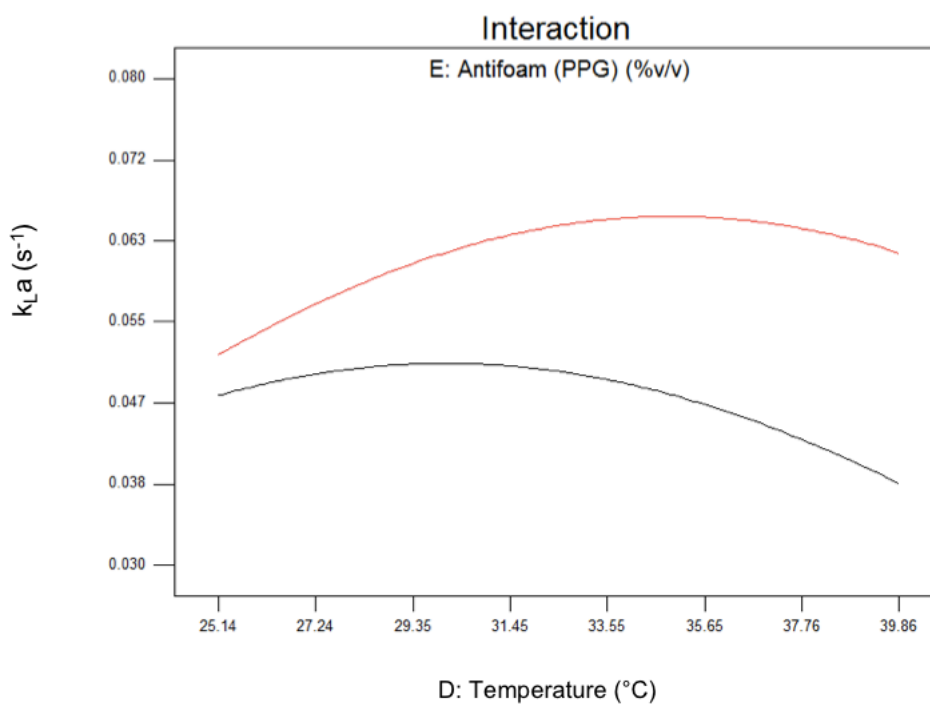


Figure 5.7. Two factor interaction between antifoam concentration and temperature. The red line represents high antifoam concentration (0.07% v/v), while the black line is low antifoam concentration (0.04% v/v). Experiments and analysis performed as described in Section 2.7.

This appears to be the effect seen here. It is likely that the interaction between antifoam concentration and temperature is due to increasing diffusivity of the gas in combination with the reduced effectiveness of the antifoam as more runs are executed at higher temperatures.

5.2.4.3. Analysis of Variance (ANOVA) and Model Diagnostics

Analysis of variance was used to evaluate both the model as a whole (Table 5.2.) and the individual terms within it (Table 5.3.). Four main statistics were used; model F-value and its associated probability as a measure of the model significance, the adequacy of precision which is a measure of signal to noise and should be as great as possible, and the adjusted and predicted R-squared values which are a measure of how closely the model correlates with the experimentally determined data. These values are summarised in Table 5.2.

Table 5.2. Summary of the ANOVA statistics for the model of oxygen mass transfer in a BioFlo 310 stirred tank bioreactor.

R-squared	0.853
Adjusted R-squared	0.805
Predicted R-squared	0.703
Adequacy of precision	18.4
F-value	17.8
Model P-value	<0.0001

The ANOVA indicates a good fit and a strong degree of statistical confidence in the model for $k_L a$ in the BioFlo310. The R-squared value is greater than 0.85 and the difference between the adjusted and predicted values is low (~0.1). Additionally, the adequacy of precision is in excess of 18, indicating that values obtained are unlikely to be as a result of systematic noise.

The majority of the individual terms are also significant, with p-values less than 0.0001. There are some terms however, including the interactions between viscosity and aeration rate, and temperature and antifoam concentration, which make a much less significant contribution to the model, however these terms are included in order to make the model hierarchical (Raudenbush & Bryk 2002).

Additional diagnostics were carried out on the model and are shown in Figure 5.8. The predicted versus actual plot (Figure 5.8A) shows that there is a generally good fit, with most points lying on, or close to the line of regression ($y=x$). The normal probability plot (Figure 5.8B) shows that the values and terms in the final model are included with a high degree of confidence. Figure 5.8C indicates that there is a random scatter to the data and so there appears to be no bias on k_{La} .

Using the ANOVA evidence, it can be said that a high degree of confidence can be placed in this model and that interrogating it across the multidimensional experimental landscape is valid, and that observations made are genuine.

It is worth noting also that the k_{La} values seen during this investigation were typical for an STR (Van't Riet, 1979).

Table 5.3. ANOVA for the terms contained within the quadratic model for oxygen mass transfer coefficient (k_{La}) in a BioFlo 310 stirred tank bioreactor.

Term	F value	P-value, Prob. > F
Model	17.84	< 0.0001
Aeration rate	74.55	< 0.0001
Agitation speed	24.96	< 0.0001
Antifoam conc.	8.93	0.0050
Viscosity-Aeration rate	3.51	0.0688
Viscosity-Temperature	23.60	< 0.0001
Aeration rate-Agitation	9.18	0.0044
Aeration-Temperature	8.24	0.0067
Agitation-Antifoam	9.40	0.0040
Temperature-Antifoam	3.05	0.0892
Aeration rate²	38.77	< 0.0001
Agitation speed²	18.81	0.0001
Temperature²	12.44	0.0011

5.3. Xcellerex Disposable Reactor-10 (XDR-10)

The XDR-10 single use bioreactor is an example of a disposable bioreactor bag installed into a solid frame (Sections 1.2.7.4, 2.7.3. and Table 2.1). Though quite advanced there are limitations to the XDR-10. For example, temperature control requires heating an element in the frame, which heats the SUB bag before transferring energy to the culture itself, making it slow. Limitations on pressure due to the bag

construction, mean that the maximum volumetric airflow rate which can be applied to the system is restricted to 1.25 vvm.

Similar to the BioFlo310, DOT probe calibration must be carried out prior to installation into the bag through a single use sheath. Also, software used in conjunction with this bioreactor was not capable of consistent logging of the online parameters, and so during each run, DOT had to be measured and recorded manually every 10 seconds. This prevented software impacting on the frequency of the readings, but introduced a reliance on the operator and a significantly greater chance of human error. It is worth noting here that due to the design of the bag based SUBs, particular care must be taken with their installation and filling so as not to introduce creases or tears into the bag as this could in turn impact on hydrodynamics and mass transfer.

5.3.1. Building the Experimental Design

Factors selected were based on a refined list of those examined in the BioFlo 310. As there was little influence of the antifoam concentration and viscosity (Section 5.2.4.), and with there being significant geometric and control differences between the two designs, it was decided that focusing on the engineering parameters of aeration rate, agitation speed and temperature would yield a more instructive data set and therefore descriptive and insightful model. Again, ranges were set in accordance with prior knowledge, literature information and the constraints of the system, as well as, in this case the previous experiments in the BioFlo 310. A summary of the factors and set points investigated can be seen in Table 5.4.

Table 5.4. Factors and ranges for the investigation into oxygen mass transfer in a tank liner style SUB.

Factor	Unit	Set points				
		Minimum	Low	Centre	High	Maximum
Aeration Rate	vvm	0.25	0.58	0.75	0.92	1.25
Agitation Speed	rpm	120	200	240	280	360
Temperature	°C	15.0	26.7	32.5	38.3	50.0

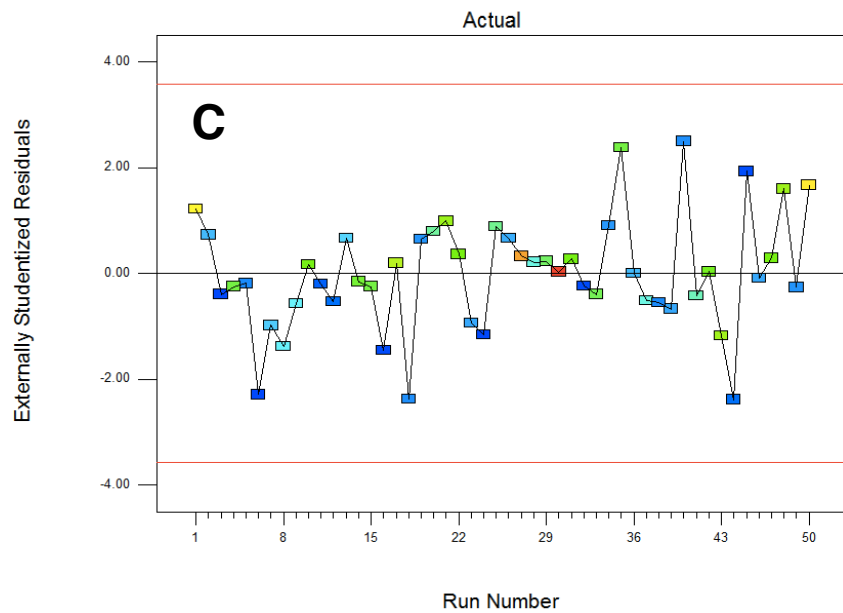
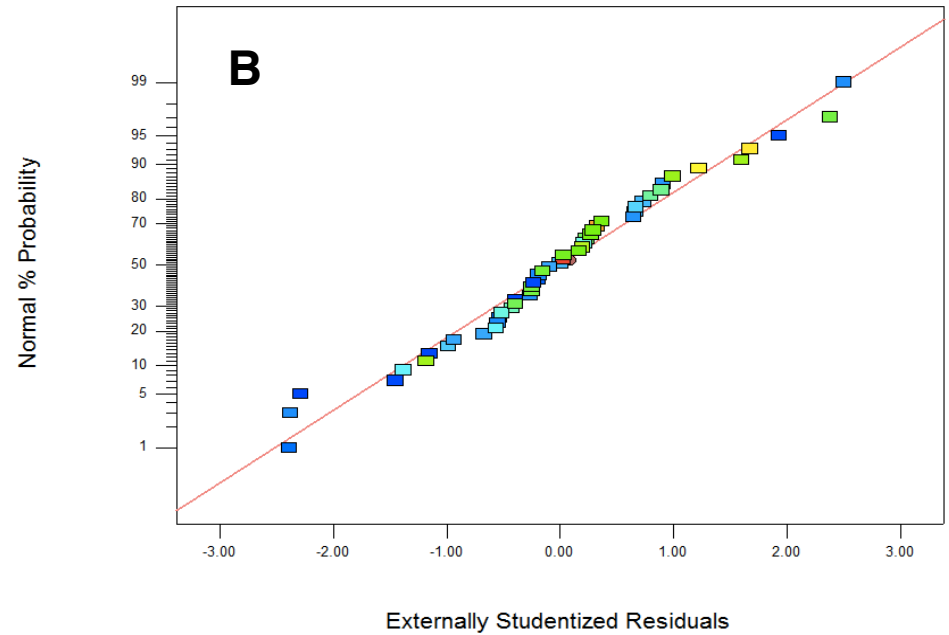
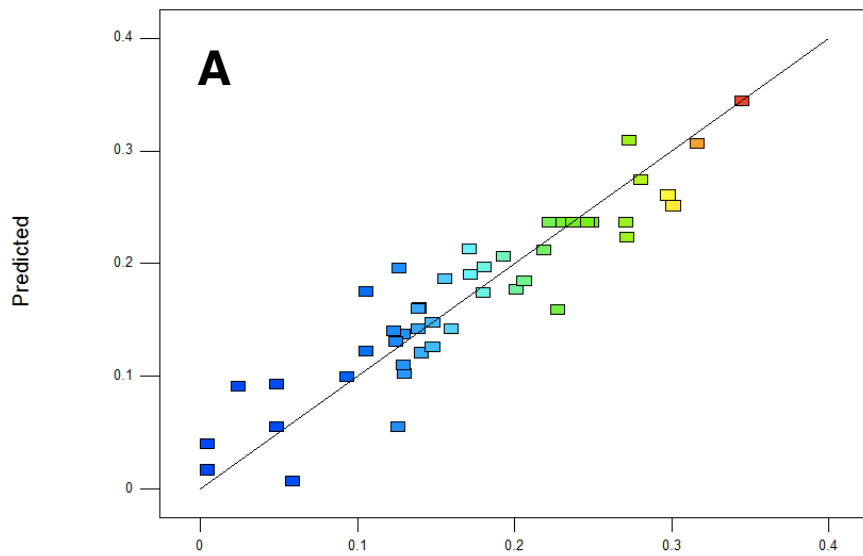


Figure 5.8. Diagnostic plots for the model for oxygen mass transfer coefficient (k_{La}) in a bench top BioFlo 310 stirred tank bioreactor. Predicted vs actual plot (A), the normal distribution plot (B) and externally studentised residuals against run number are used to determine that the model is a good fit for the experimental data, that there is nothing biasing the model, and that it can be used with a high degree of statistical confidence. Analysis as described in Section 2.7.

Aeration rate is limited by the XDR-10 to 7.5 Lmin^{-1} (1.25 vvm), while the minimum value used (based on preliminary experiments) was set to 0.25 vvm (1.5 Lmin^{-1}), allowing for even distribution of set points across the experimental range. The maximum agitation speed that the system is capable of is 360 rpm, significantly lower than either the STR or the Ambr[®]250, suggesting possible limitations in oxygen mass transfer capacity; particularly when considering the pitch blade design of the impeller (Karimi et al. 2013). The minimum value chosen was 120 rpm. The temperature range used was as close as feasible to that applied to the STR (maximum of 50°C), however the minimum value which could be used was 23.5°C as the element on the XDR-10 is not cooled and as such environmental temperature is the lowest value available. This was retrospectively incorporated into the DoE design.

5.3.2. Fixed Factors

In addition to the factors fixed during experiments with the BioFlo 310 (Section 5.2.2.), both the viscosity of the media and the concentration of antifoam were fixed for experiments in the XDR-10. This was in part due to their relatively small effects on the oxygen mass transfer model in the STR (Section 5.2.4.) and the potential for convolution of the effect between viscosity and temperature. As with the BioFlo 310, the order and groups in which runs took place was an important consideration. The reasoning behind the run ordering is described in Section 5.2.3.

The determination and analysis of $k_{\text{L}}a$ across the experimental landscape is as described in Section 2.7.1.2. This includes plotting and adjustment for probe response time. The only difference was in the recording of the data, which, as previously noted (Section 2.7.3.) was carried out manually due to a lack of online recording system. Good agreement is seen between the unadjusted data and those corrected for the probe response time. Several example data points from across the experimental range are shown in Table 5.5. A table of calculated $k_{\text{L}}a$ values for this investigation can be found in Appendix 4.3.

Table 5.5. Example k_{La} and PRT corrected k_{La} data from across the experimental design in an XDR-10 single use bioreactor bag.

Aeration rate (vvm)	Agitation speed (rpm)	k_{La} (s^{-1}) ($\times 10^{-3}$)	k_{La} corrected for PRT (s^{-1}) ($\times 10^{-3}$)
0.58	200	7.90	8.26
0.92	200	8.90	9.30
0.58	280	12.2	13.5
0.92	280	12.8	14.0

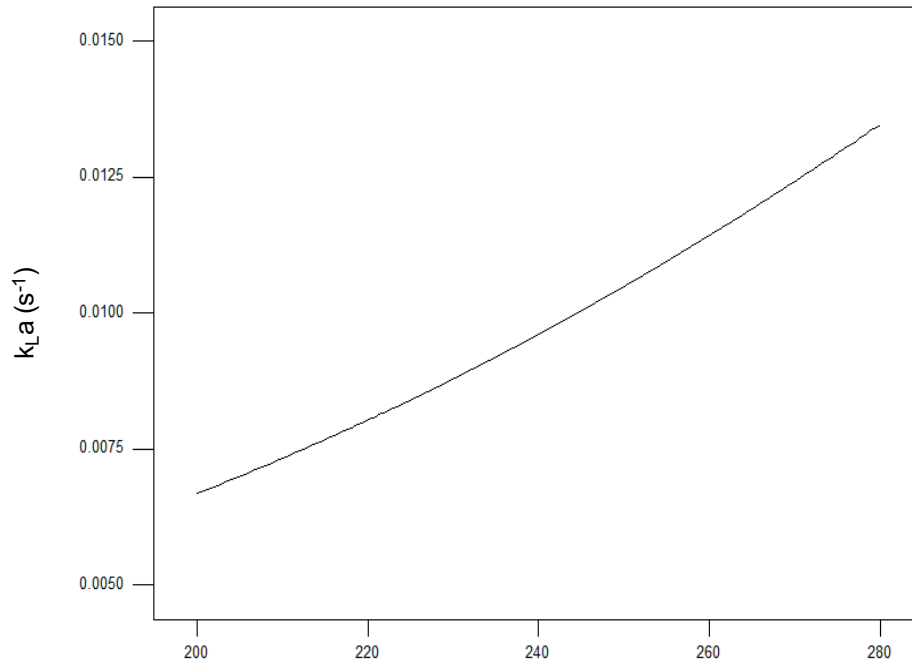
5.3.3. Modelling Oxygen Mass Transfer Coefficient in a Single Use Bioreactor Bag (XDR-10)

As with the BioFlo investigation (Section 5.2), a quadratic model was built. Although fewer factors and fewer experiments were performed, an RSM was used in order to ensure that the model could be interrogated for curvature. Additionally, the statistics supporting the use of a quadratic model when compared with the alternatives made it the preferred option. A p-value of 0.0078, an R-squared of 0.955 and the lowest standard deviation were all significantly better than the equivalent values for the cubic and linear model alternatives. A backward elimination was used, removing factors and interactions with the smallest effects first and continuing until only significant terms remain as part of the model.

Once the model was built, it was essential to determine the validity using statistical diagnostics (Section 5.3.3.3). The model equation can be found in Appendix 4.6.

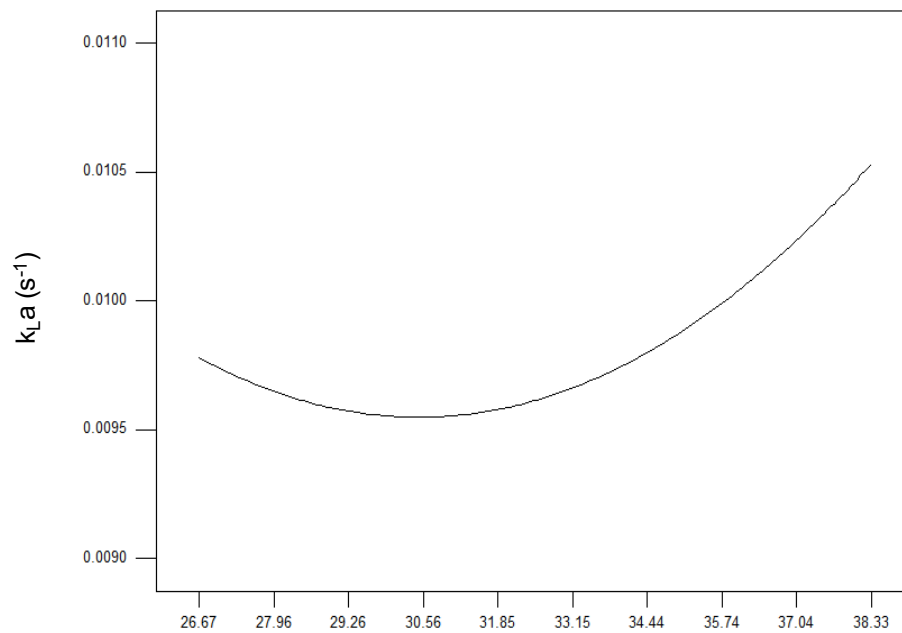
5.3.3.1. Main Effects

Two main effects were observed across the experimental landscape for the XDR-10. These were agitation speed and temperature. Surprisingly, aeration rate was not seen to be a main effect, however this is most likely because the range over which aeration was varied on the XDR system was limited. In addition, the sparger is a frit type, and so bubbles delivered into the liquid are already very small regardless of aeration rate so the interfacial surface area is unlikely to change significantly as a result of this factor.



B: Agitation (rpm)

Figure 5.9. Main effect plot for the observed impact on agitation speed on the model of oxygen mass transfer coefficient in the XDR-10 single use bioreactor. Experiments and analysis performed as described in Section 2.7.



C: Temperature ($^{\circ}C$)

Figure 5.10. Main effect plot for the quadratic relationship observed as a result of temperature on the model of oxygen mass transfer coefficient in the XDR-10 single use bioreactor. Experiments and analysis performed as described in Section 2.7.

There is an almost linear positive correlation between agitation speed and oxygen mass transfer coefficient, with k_{La} doubling from $0.007s^{-1}$ to $0.014s^{-1}$ across the experimental range (Figure 5.9). This is a significantly smaller increase in k_{La} than seen when investigating the STR, where the maximum k_{La} measured in the XDR-10 was $0.024s^{-1}$. Increased agitation speed commonly results in bubble breakdown. However, the design of the impeller (40° pitched blade) is likely to be responsible for generating a combination of axial and radial flow, resulting in greater mixing around the reactor (Mirro & Voll, 2009), greater bubble dispersion and therefore enhanced k_{La} .

Figure 5.10 indicates a parabolic relationship between temperature and k_{La} . Fluctuations in solubility and diffusivity of oxygen as a result of changing temperature are as described in Section 1.2.6.4. Up to approximately $30^\circ C$ the k_{La} decreases until the two effects reach equilibrium, after which diffusivity has the dominant effect on mass transfer. Again, the effect in the XDR is relatively small, with the influence on the model due to temperature changing k_{La} values by just $0.01s^{-1}$. Though a small increase, this is still significant in terms of the model.

5.3.3.2. Two Factor Interaction

A single two factor interaction was seen between the two main effects, temperature and agitation speed. The three-dimensional surface plot seen in Figure 5.11A. shows the interaction and the influence on k_{La} . At high or low temperature, increasing the agitation has a positive, linear effect on k_{La} although the effect is much greater at high temperature with k_{La} increasing from 0.007 to $0.015s^{-1}$. This can also be seen in the contour plot (Figure 5.11B.) with smaller gaps between contour lines along the high temperature edge of the plot.

However, the effect of temperature at high or low agitation speeds is reversed. At low agitation speed, the effect of increasing temperature is small and negative (0.008 to $0.007s^{-1}$), whereas at a high agitation speed, the effect of increasing temperature is larger and positive (0.012 to $0.015s^{-1}$). This is shown in Figure 5.11. This relationship is a result of the two main effects discussed in Section 5.3.3.1, with increasing agitation leading to greater breakdown and dispersion of bubbles, and the complex dynamic between solubility and diffusivity that results from changing temperature. At higher temperatures, the increased diffusivity combined with the better dispersion of bubbles results in higher k_{La} , with the effect driven by agitation (hence it remains linear). At low agitation speeds the detrimental effect of increasing temperature (a decrease in

oxygen solubility) appears to be dominant, while at greater agitation speeds the positive influence of increasing temperature (an increase in oxygen diffusivity) combined with the increased dispersion causes the inversion of this relationship.

5.3.3.3. Analysis of Variance (ANOVA) and Model Diagnostics

As with the BioFlo 310 model (Section 5.2.4.), four main diagnostic tests were used in order to evaluate the XDR-10 model (Table 5.6.) and the significant terms (Table 5.7.). The reasoning for these four diagnostics are discussed in Section 5.2.4.3. The ANOVA indicates a good fit between the model and the experimental data and that a high degree of statistical confidence can be had in the model for k_{La} in the XDR-10. The R-squared value is around 0.94 and the difference between the adjusted and predicted values is relatively low (~0.07). Additionally, the adequacy of precision is approximately 26, indicating values obtained are not an artefact of system noise.

Diagnostic values for the individual terms are shown in Table 5.7. The model itself and the major main effect (agitation speed) are seen to be highly significant, the statistics available for the additional terms, while not as good, are still significant. The (non-quadratic) temperature term is also included in order to make the model hierarchical.

Table 5.6. Summary of the ANOVA statistics for the model of oxygen mass transfer in a XDR-10 disposable bioreactor.

R-squared	0.94
Adjusted R-squared	0.92
Predicted R-squared	0.84
Adequacy of precision	26.0
F-value	39.3
Model P-value	<0.0001

Additional diagnostics were carried out as with the STR (Section 5.2.4.3.) and are shown in Figure 5.12. Again, they highlight good agreement between the model and the experimental data (A), the terms for inclusion in the model (B) and that there is no systematic bias in the data (C). The ANOVA analysis demonstrates that the model is a good fit with the experimental data and that it can be used with a high degree of statistical confidence.

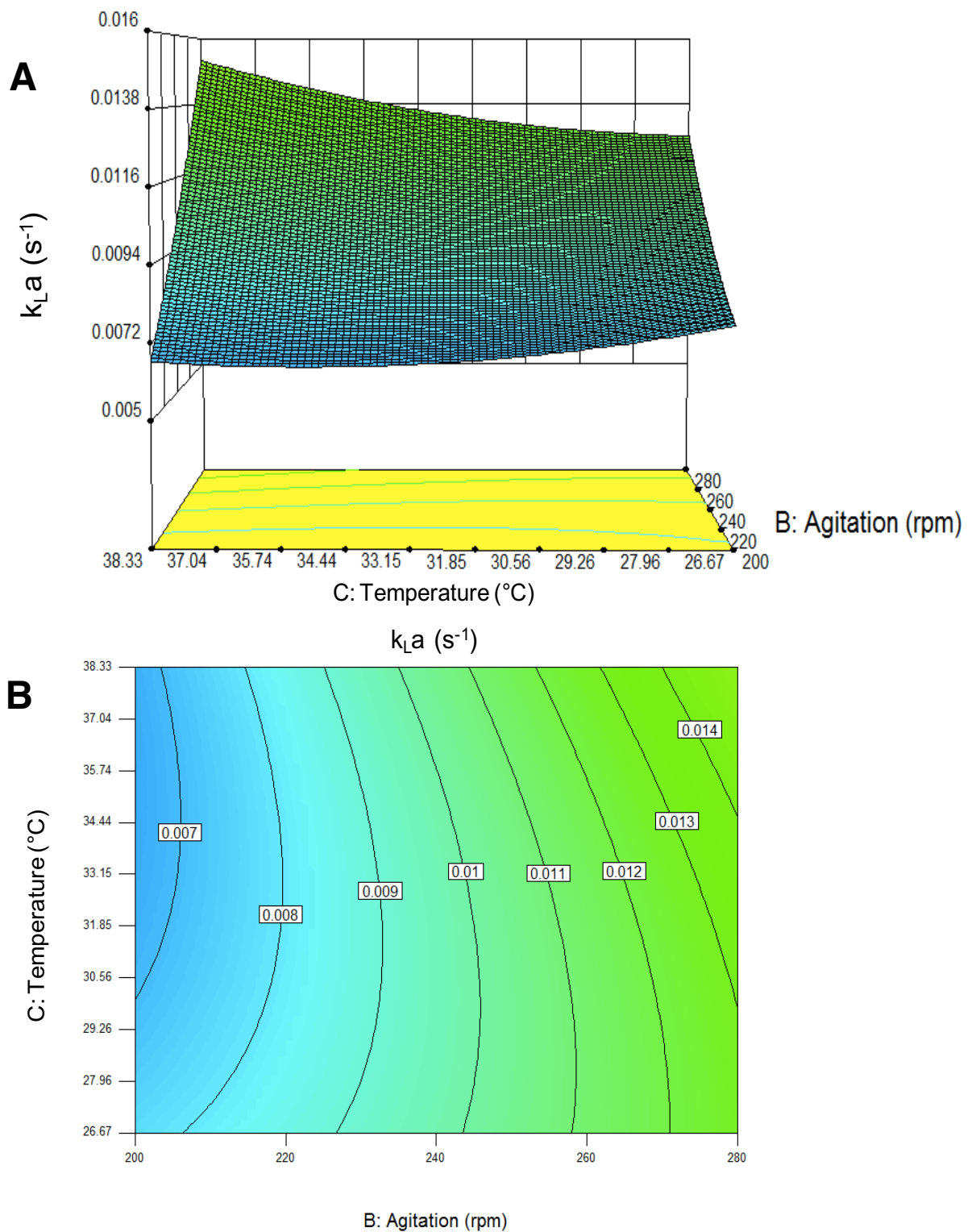


Figure 5.11. Three-dimensional surface plot (A) and contour plot (B) showing the interaction between temperature and agitation speed and its effect on oxygen mass transfer in an XDR-10 single use bioreactor. Increase in k_{La} is represented from dark blue to green. Experiments and analysis performed as described in Section 2.7.

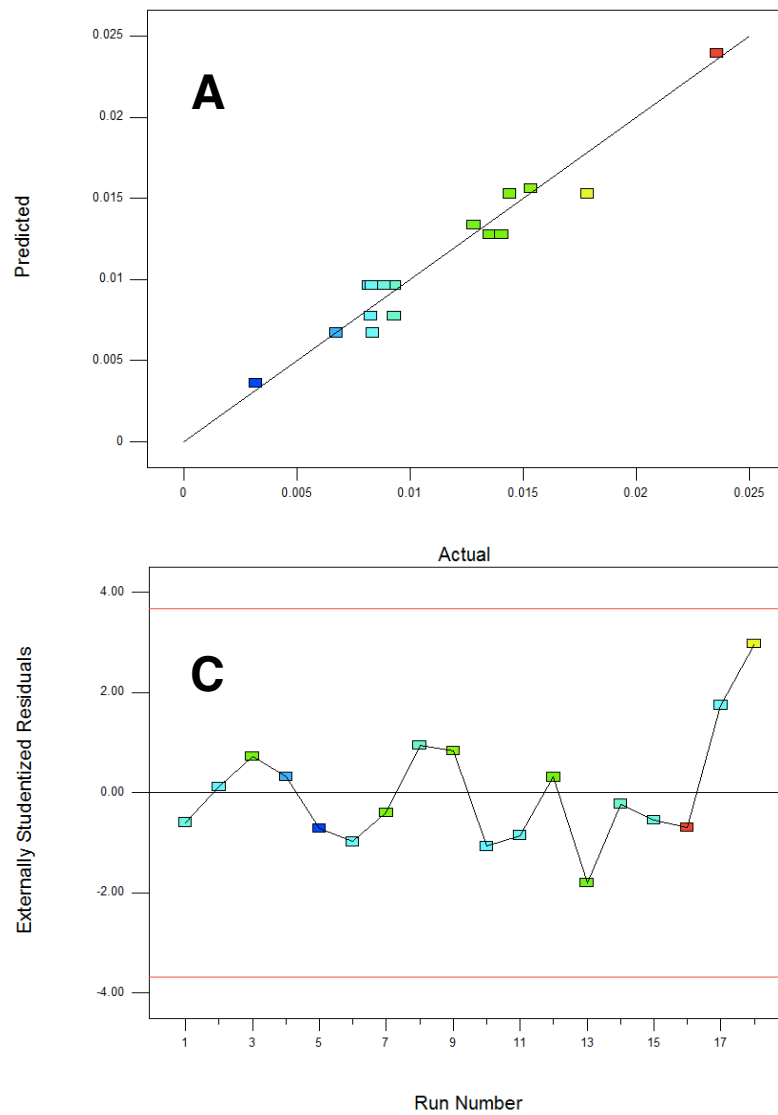


Figure 5.12. Diagnostic plots for the quadratic model built to describe k_{La} in an XDR-10 single use bioreactor bag. The predicted versus actual plot (A), the normal probability plot (B) and the residuals versus run number plot (C), all highlight a good agreement between the model generated and the experimental data. Analysis as described in Section 2.7.

Table 5.7. ANOVA for the terms contained within the quadratic model for oxygen mass transfer coefficient in a XDR-10 single use bioreactor.

Term	F value	P-value, Prob. > F
Model	39.3	< 0.0001
Agitation speed	162.6	< 0.0001
Temperature	1.99	0.183
Agitation speed-Temperature	3.45	0.088
Agitation speed²	14.6	0.002
Temperature²	20.1	0.0008

5.4. Ambr[®]250 Single Use Bioreactor

The Ambr[®]250 parallel automated bioreactor system is geometrically similar to a conventional stainless-steel bioreactor and is constructed from moulded polycarbonate, removing potential issues of bag creasing and introduction of additional dead zones. In addition Ambr[®]250 reactors are fitted with online monitoring and control including for DO, temperature and off gas (Sections 1.2.7.4., 2.3.1. and 2.7.2.).

Conditioning and calibration of the Ambr[®]250 and its probes differs significantly from the XDR10 and BioFlo310, particularly in terms of DOT. This is due to the Ambr[®]250 using an optical sensor as the measurement method for DOT (Rameez et al. 2014). This is provided pre-calibrated, but must undergo quenching and single point (100%) recalibration once the reactor is charged. The parameters of this calibration can be altered by the operator, and for these experiments an overnight calibration period with small variance (within 0.1% saturation for one hour) used in order to ensure the stability of the data stream. In addition, logging of data is through the Ambr's proprietary 'Pegasus' software at consistent 12 second intervals.

Using parallel bioreactors, it is possible to interrogate multifactorial landscapes in a single experiment. As such, a sub-objective of the Ambr[®]250 investigation is to establish an automated protocol for determining $k_{L,a}$ in a high throughput manner such that it could run a large number of experimental determinations in a short time. This would then be used as a generic procedure for rapid determination of $k_{L,a}$ under different conditions in the future. Additional considerations regarding set up and configuration of the Ambr[®]250 are discussed in Section 2.7.2.

5.4.1. Preliminary Determination of k_{La}

A preliminary investigation to determine k_{La} in the Ambr[®]250 using water and a small number of experimental set points was carried out. This was undertaken in order to reproduce values reported in literature as a means of showing minimal system to system variance, and because the protocol developed here was automated and so differed from those used previously (e.g. Bareither et al, 2013). In addition, development of the automated protocol would require a number of iterative stages.

Five independent experiments were executed to have as broad a range of conditions as possible within the limitations of the Ambr[®]250 bioreactor system. Three factors which had been seen previously (in literature and experimentally) to have a significant influence on oxygen mass transfer were selected: agitation speed, aeration rate and temperature. The set points were as shown in Table 5.8.

Using the method of quantification described in Section 2.7.1, a range of k_{La} values were observed (from 0.002 to 0.19s⁻¹) under the conditions outlined above. Agitation speed appears to be the greatest influencer on oxygen mass transfer, with aeration rate also significant and temperature of little effect. Figure 5.13. shows the size of the effects caused by the changing parameters. It should be noted that these are individual points and not evaluated using a multifactorial design, so these responses cannot be modelled or statistical analysis undertaken.

Table 5.8. Set points for the preliminary investigation of k_{La} in Ambr[®]250 bioreactor. Experiments performed as described in Section 2.7.

Condition	Agitation speed (rpm)	Aeration rate (vvm)	Temperature (°C)
1	1500	1.0	25
2	500	0.5	25
3	3000	2.0	25
4	500	2.0	35
5	3000	0.5	45

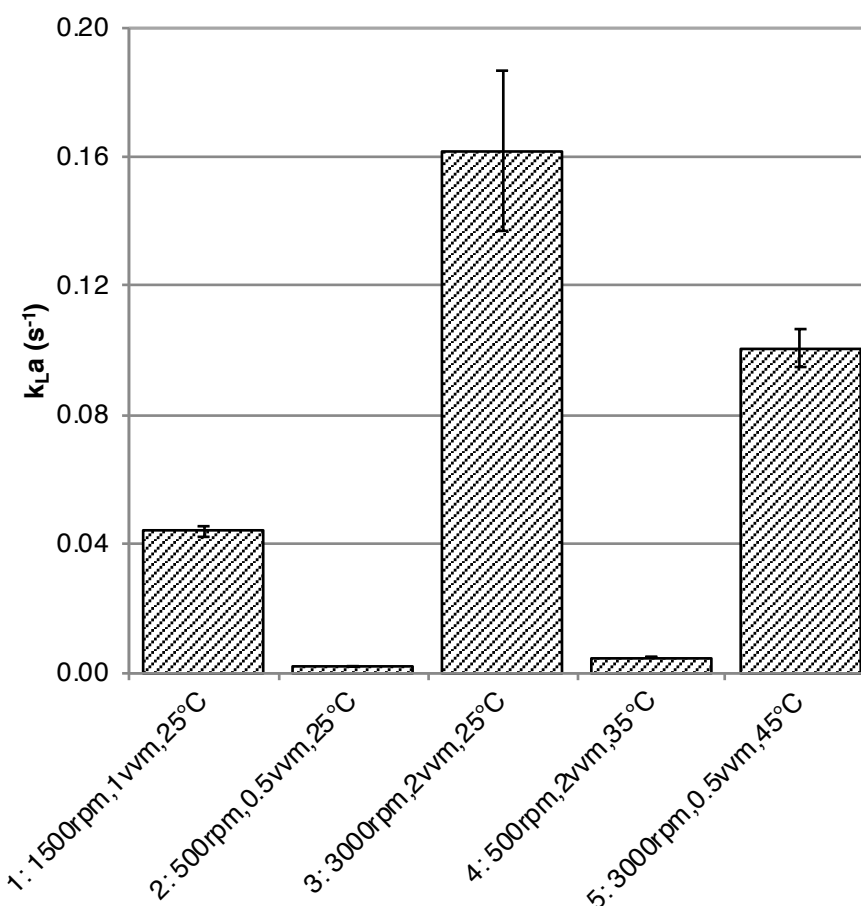


Figure 5.13. Oxygen mass transfer coefficient (k_{La}) as determined in Ambr[®]250 bioreactors under a range of set conditions. Error bars represent one standard deviation about the mean ($n=3$). Experiments and analysis performed as described in Section 2.7.

These values are in keeping with those determined in the literature during Ambr[®]250 prototype evaluation (Bareither et al, 2013), demonstrating minimal system to system variation. Differences seen can be attributed to the reduced manual intervention in this protocol. In addition, the protocol established in the Ambr[®]250 software was successful in executing triplicate runs without mechanical or experimental difficulty and with low variability (Figure 5.13.).

5.4.2. Experimental Design for Modelling Oxygen Mass Transfer Coefficient (k_La) in an Ambr[®]250 SUB

The Ambr[®]250 is a good geometric mimic of a traditional STR, and so it was decided that all five factors from the BioFlo 310 investigation (Section 5.2.) should be included, rather than just those with the greatest influence over the STR model. This would allow a much more inclusive and comprehensive model, which would relate as closely as possible the Ambr[®]250 and the BioFlo 310 STR. It will also highlight whether details in reactor geometry or materials of construction appear to be a strong influence on k_La .

Ranges have been selected in consideration of the literature, prior knowledge, limitations of the system and the previous experiments. A summary of the factors and ranges is shown in Table 5.9. The ranges selected for the physical engineering parameters (agitation speed, aeration rate and temperature) were also influenced by the preliminary work carried out in the Ambr[®]250 (Section 5.4.1.).

The ranges for temperature, viscosity and antifoam concentration were set to match those of the stirred tank bioreactor (Section 5.2.1.). Aeration rate though was set between zero and 2.0 vvm (0.0 and 0.3 Lmin⁻¹), providing the maximum possible range. Agitation speed is limited to a maximum of 3000 rpm (~3 ms⁻¹), while the lower limit was set at 100 rpm as this has been demonstrated on the Ambr system as the minimum set point capable of spanning sufficient dissolved oxygen tensions.

Table 5.9. Factors and ranges for the investigation into oxygen mass transfer in an Ambr[®]250 bioreactor.

Factor	Unit	Set points				
		Minimum	Low	Centre	High	Maximum
Aeration Rate	vvm	0.5	1.0	1.5	2.0	2.5
Agitation Speed	rpm	100	825	1550	2275	3000
Viscosity by [Gly]	mLL ⁻¹	0.0	7.5	15.0	22.5	30.0
Temperature	°C	15.0	23.8	32.5	41.3	50.0
Antifoam	%v/v	0.0	0.025	0.05	0.075	0.10

Six parallel bioreactors were used to undertake an RSM design, executed over a short timeframe (compared with independent manual experiments). Once developed, the k_{La} protocol was capable of running a full RSM in triplicate in approximately a day and a half by a single operator. This included the system set up, filling, calibration of the bioreactors and running all 156 determinations. This is a significant resource saving when compared with the manual experiments in the STR and single use bags. The automated protocol can be seen in Appendix 4.8.

Additionally, parallelisation enabled replication, which was useful for establishing that there was no bias in the bioreactor system as a result of bioreactor position, and no temporal drift in the experimental data. It was also important to the proof of concept. Complex systems will be evaluated using this protocol in future and so replication (even within a DoE landscape), will aid in providing the greatest possible statistical significance when used as part of a generic evaluation platform.

As with the XDR-10 or the BioFlo 310 it was necessary to carefully consider the order in which the runs were executed. Here, the consideration was on the basis of what could be run in a single bioreactor. The restrictions though, are as outlined in Section 5.2.3.

The quantification of k_{La} values across the experimental landscape is as described in Section 2.7.1.2. The subsequent analysis of the data though was done using JMP12 software. The underlying mathematics in the software is very similar and so this will not affect the ability to compare the models generated for the different reactor types. A table of calculated k_{La} values for this investigation, can be found in Appendix 4.4. The model equation can be found in Appendix 4.7.

5.4.3. Establishing a Protocol to Automate an O_2 Mass Transfer Investigation in a SUB

The protocol developed for automated k_{La} investigation on the Ambr[®]250 was based on the method described in Section 2.7. which was used to measure k_{La} in the BioFlo310 stirred tank bioreactor. The major challenge was programming explicitly each step of the experimental method. Instructions, set points, timings, limits and dead bands were all required and needed to be programmed in accordance with the limitations of the Ambr 'Pegasus' software. Each step of the method needed to be

incorporated in a form that the system can interpret and execute before the run commenced.

A number of iterations were required in order to develop this, and to implement the protocol on six bioreactors in parallel. The final protocol, which ran the full method, can be seen in Appendix 4.8. Simple additions could be made to run a larger investigation into oxygen mass transfer in the Ambr[®]250.

5.4.4. Modelling Oxygen Mass Transfer Coefficient in an Ambr[®]250

Although a cubic model was offered by the JMP software, a quadratic model was again the most appropriate. The model coefficients are shown in Table 5.10. and the model equation in Appendix 4.7. As with the STR model there were five factors arranged in an RSM design, this time with runs in triplicate, and so the landscape could be interrogated for curvature. The quadratic model gave an R-squared value of 0.96, a p-value of <0.0001 and although there is no specific adequacy of precision statistic as with previous experiments, there is a root mean square error which can be used as a measure of noise, which is low at 0.021. Additionally, the standard deviation was significantly better than the equivalent values for the cubic and linear models. This is summarised in Table 5.11. Once the model was built, it was important to determine its validity using statistical diagnostics (see section 5.4.4.3).

5.4.4.1. Main Effects

Each of the factors included in this design demonstrated a significant effect on the oxygen mass transfer coefficient. Interestingly this was not the case in the bench-top STR, and so highlights the importance of investigating each bioreactor type thoroughly to understand the oxygen mass transfer capabilities.

Agitation speed is the greatest contributing main effect. Figure 5.14B shows the dramatic rise in k_La from 0.08 to 0.135s⁻¹ as agitation speed increases to approximately 1850rpm. Above 1850rpm, k_La begins to decline. This is due to the impellers reaching the limit of their effectiveness and starting to flood the impeller region. In addition, there is an interaction between agitation speed and aeration rate (discussed in Section 5.4.4.2.), which at high values of both factors results in a greater negative effect. The large impact agitation speed has on oxygen mass transfer (discussed also in Sections 1.2.6.2. and 5.2.4.1.), this is a result of effective bubble breakdown and dispersion by

the two, six blade Rushton turbine impellers, thus the interfacial surface area (and therefore area available for mass transfer) is greater at higher agitation speeds.

Figure 5.14A shows the impact of aeration rate, the next greatest main effect on k_{La} . Coefficients for the aeration terms in the model (Table 5.10) are high, with both the linear and quadratic terms within 0.005 of those for agitation speed. Once the aeration rate exceeds 1.2vvm, there is a reduction in the oxygen mass transfer. As previously noted (Sections 1.2.6.1. and 5.2.4.1.), is most likely due to the greater size of bubbles from the open tube sparger, combined with the reduced residence time of these bubbles and flooding of the impeller region at higher aeration rates.

Viscosity only has a quadratic term in the model. There is no overall change in the k_{La} across the range and the maximum is positioned at the centre point. This is shown in Figure 5.14C. It appears that this is where there is a balance between encouraging stable bubble formation using a viscous component, and the detrimental thickening of the liquid film.

Temperature is seen to have an overall positive effect, responsible for a rise in k_{La} from 0.114 to 0.133s⁻¹. Interestingly, the peak is at approximately 37°C, the set point commonly used for a number of microbial expression systems, notably *E. coli*. After this point, a decline is seen as a result of reducing solubility of oxygen becoming dominant over the increasing diffusivity. The effect can be seen in Figure 5.14D.

The overall effect of increasing antifoam concentration is a negative one, with the k_{La} decreasing from a peak of 0.132s⁻¹ to 0.110s⁻¹. As explained previously (Section 5.2.4.1.), it has been hypothesised that an increase in antifoam concentration could cause an increase in oxygen mass transfer which may explain the small increase before the negative trend takes over and the primary function of the antifoam becomes dominant (Figure 5.14E).

It is interesting to note that there are no linear relationships for any of the main effects. All either have a quadratic element or an interaction with another factor. This is indicative of a highly interdependent and dynamic system and speaks heavily both to the power of using multifactorial DoE for this type of work, and to the necessity for this kind of characterisation to be undertaken. Without it, it would be difficult to understand the oxygen mass transfer in a bioreactor under culture relevant conditions.

5.4.4.2. Two Factor Interactions

There are two, two-factor interactions, one between aeration and agitation speed, and the other between temperature and antifoam concentration. Both of these were seen in the stirred tank bioreactor, where the effect of the latter was minimal, however this does not appear to be the case here.

Figure 5.15. and Table 5.10. show how substantial the effect is of the interaction between agitation and aeration rates, with the minimum k_{La} almost zero and the maximum observed here almost $0.12s^{-1}$ depending on just these two factors. There is also a definitive peak in k_{La} , at around 1500rpm and 1.0vvm, with all conditions around this point quite detrimental. The cause of the decline in oxygen mass transfer has been discussed previously (Sections 1.2.6. and 5.2.4.2.), with flooding of the impeller region the cause of increasing aeration and agitation speeds having a negative effect on k_{La} . Interestingly, in the overall model the additional factors appear to have a stabilising effect on the oxygen mass transfer at higher values, as, although there is a decline in the oxygen mass transfer around the maximum, it is not so pronounced.

The action of antifoams is temperature and time dependent. As such the two-factor interaction between antifoam concentration and temperature is due to temperature influencing the mechanism of the antifoam and diminishing the ability of the surfactant to reduce the surface tension of the gas-liquid interface. The effect is seen to be positive overall (Figure 5.16.), confirming that the increase in temperature is detrimental to the action of the antifoam. This is particularly evident at the high end of the temperature range ($50^{\circ}C$), where the k_{La} is approximately quadruple the minima.

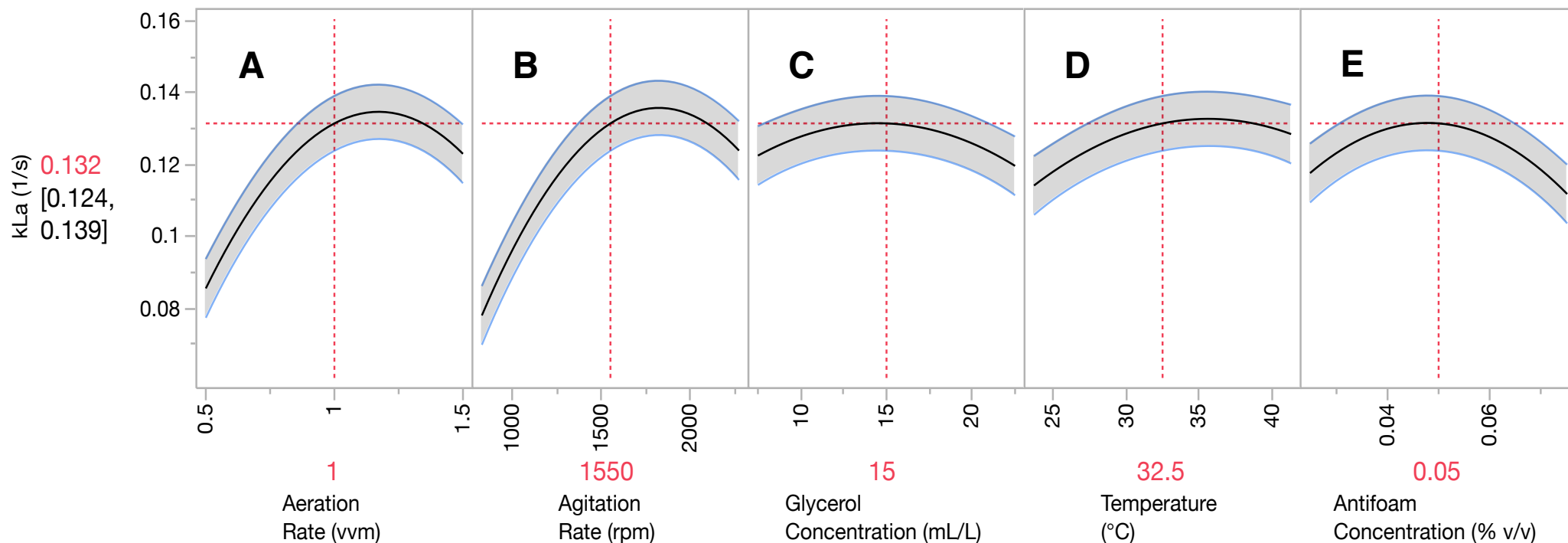


Figure 5.14. Profiles of k_La as a result of each of the factors in the model for oxygen mass transfer coefficient in the Ambr®250. (A) shows the effect of aeration rate, (B) of agitation rate, (C) of glycerol concentration (as a proxy for viscosity), (D) of temperature and (E) of antifoam concentration. Red lines represent the k_La value at the centre point of each of the factor ranges. Blue lines represent the confidence intervals for the model as influenced by each of the main effects. Experiments and analysis performed as described in Section 2.7.

Table 5.10. shows the parameter coefficients for each of the terms in the model, along with the standard error and the p statistic for each. Here, the standard error has been included, which is a measure of the accuracy of an estimated parameter coefficient. It is similar to the standard deviation in that it estimates the variability between the sample values (in this case k_La determined from each experimental run), and therefore the lower the value the more accurate the coefficient.

This reiterates what has been stated previously, that the aeration and agitation speeds, as well as the interaction between the two, are the greatest contributors to influencing the oxygen mass transfer. Graphical representations of the overall model are shown in Figure 5.17. These show an area of maximal, and relatively stable k_La ($>0.14s^{-1}$) at an aeration rate of around 1.1-1.35 vvm and agitation speed of 1750-2250rpm. This is an important observation as it describes an area of suitable operation for the maximisation of oxygen mass transfer.

Table 5.10. Coefficient values and statistical analysis for each of the terms in the model for oxygen mass transfer coefficient in the Ambr[®]250. The model expression can be found in Appendix 4.7.

Term	Parameter coefficient	Standard error	p-Value	T-ratio
Intercept	0.1315	0.0038	<0.0001	27.80
Agitation speed	0.0230	0.0019	<0.0001	22.69
Aeration rate	0.0188	0.0019	<0.0001	8.67
Temperature	0.0072	0.0019	0.0003	3.53
Antifoam concentration	-0.0029	0.0019	0.1312	36.32
Agitation speed ²	-0.0305	0.0021	<0.0001	19.00
Agitation speed-Aeration rate	0.0176	0.0021	<0.0001	31.49
Aeration rate ²	-0.0272	0.0021	<0.0001	12.21
Temperature ²	-0.0101	0.0021	<0.0001	5.81
Temperature-Antifoam concentration	0.0054	0.0021	0.0134	18.84
Antifoam concentration ²	-0.0168	0.0021	<0.0001	11.46
Viscosity ²	-0.0104	0.0021	<0.0001	27.80

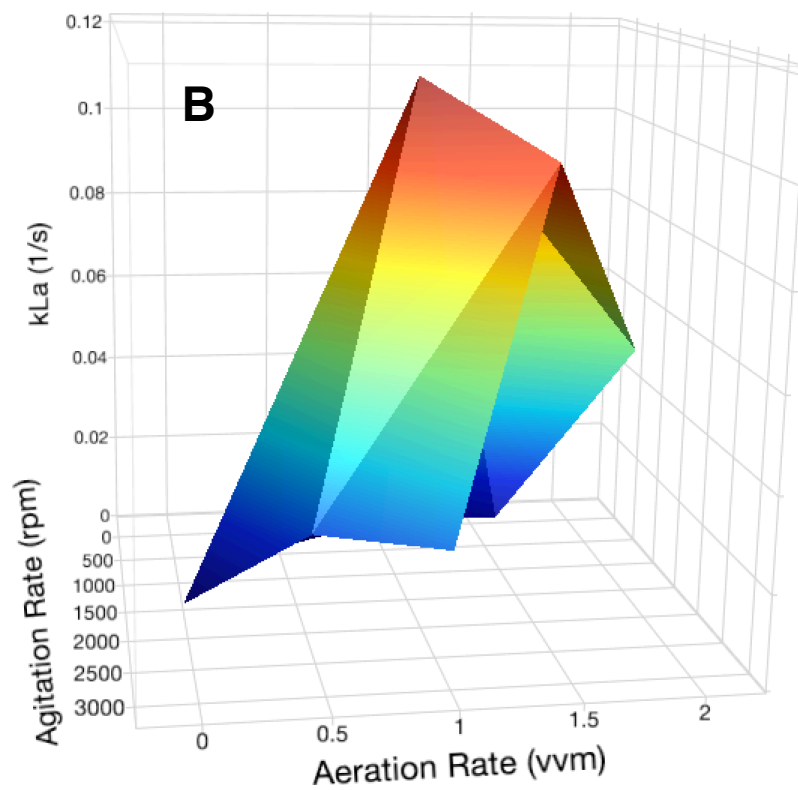
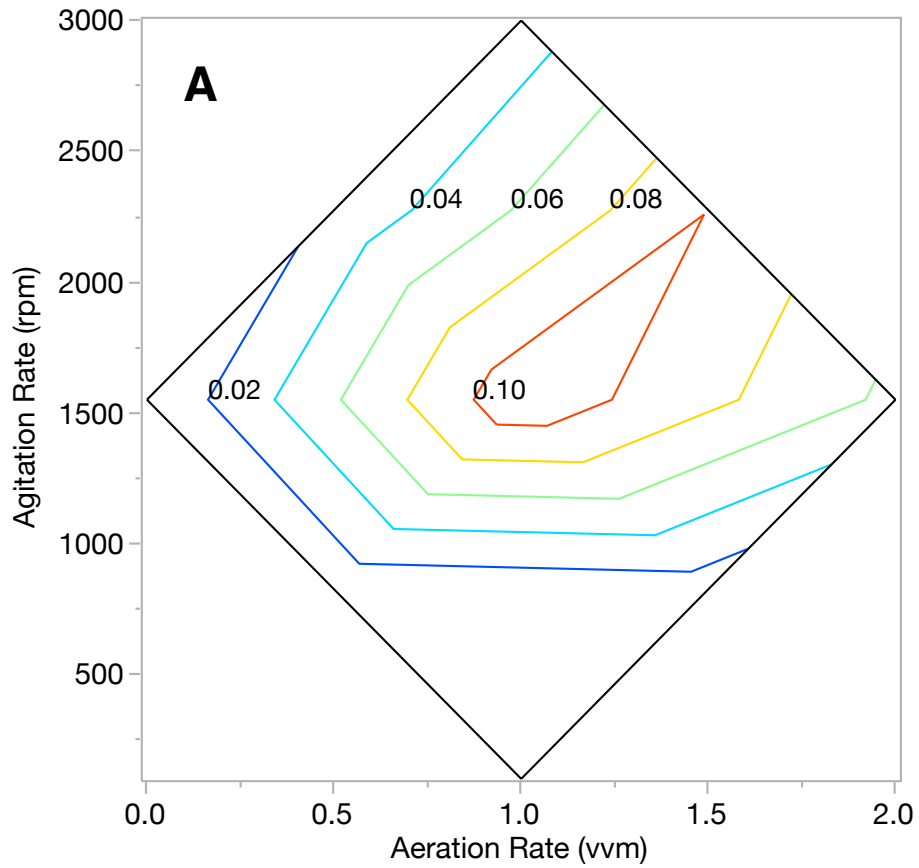


Figure 5.15. Contour (A) and three-dimensional response (B) plots for the two-factor interaction between agitation rate and aeration rate. Shading blue to red indicates an increase in k_{La} in both figures. k_{La} on the contour lines is represented in reciprocal seconds. Experiments and analysis performed as described in Section 2.7.

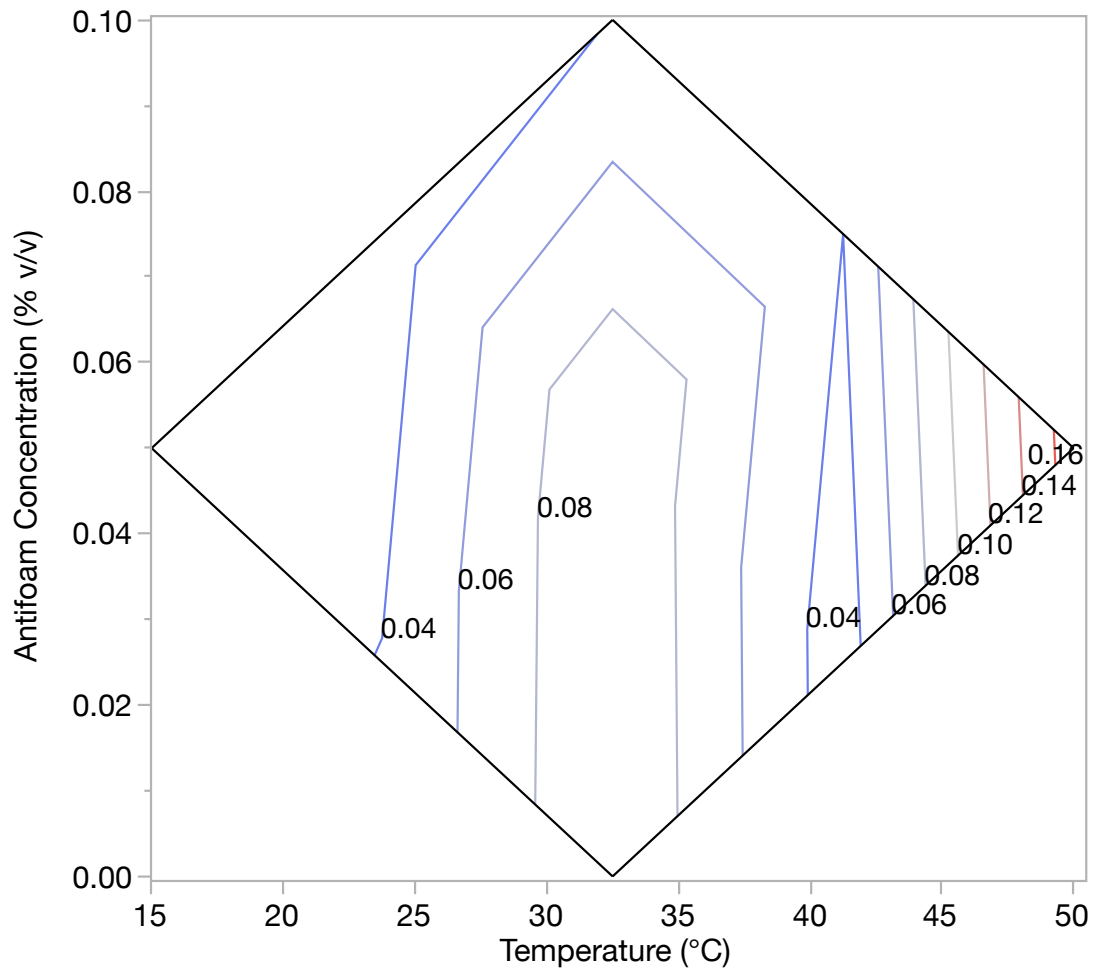


Figure 5.16. A contour plot showing the two-factor interaction between antifoam concentration and temperature and the effect on k_{La} in an Ambr[®]250 bioreactor. Contour lines are coloured blue to red with increasing k_{La} and are labelled with k_{La} in reciprocal seconds. Experiments and analysis as described in Section 2.7.

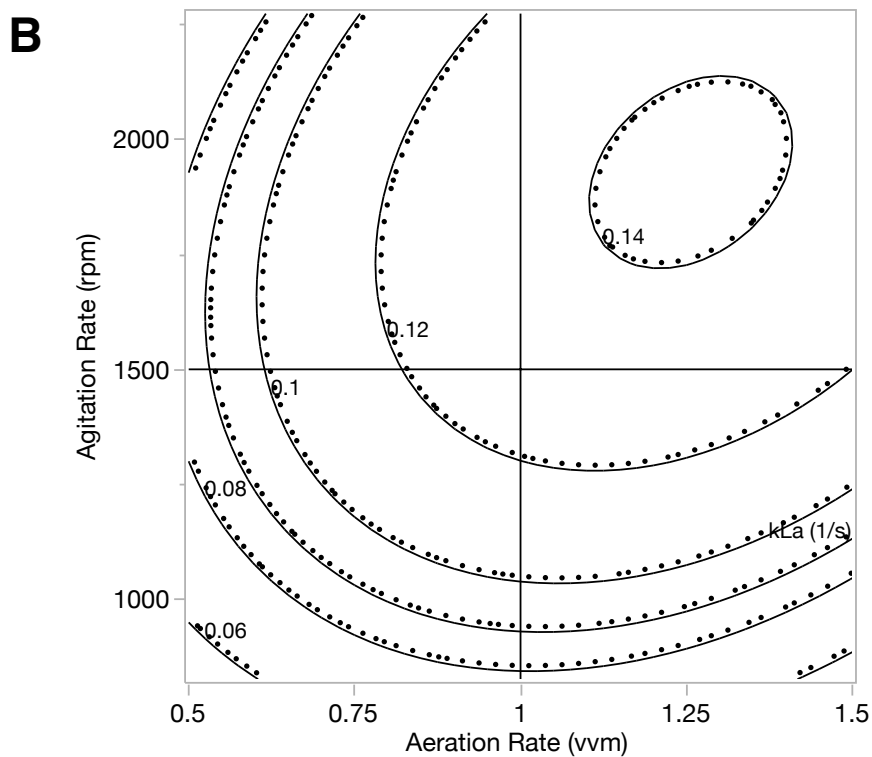
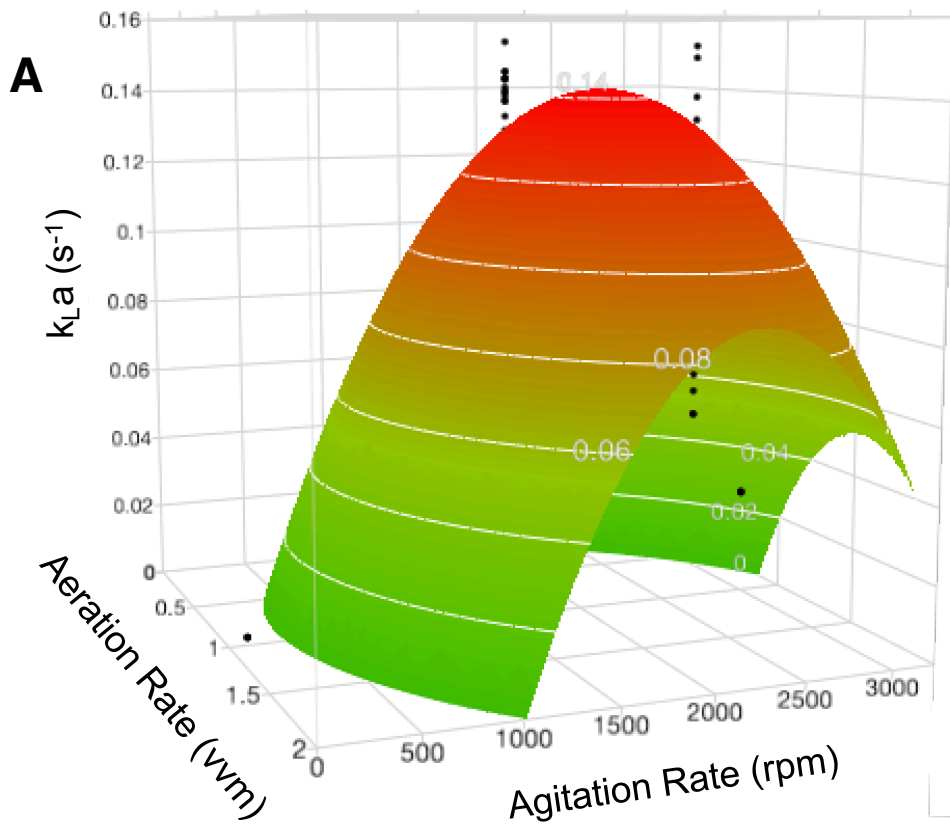


Figure 5.17. Three-dimensional response (A) and contour (B) plots for the overall model of k_{La} in an Ambr[®]250 bioreactor. Shading green to red indicates an increase in k_{La} . k_{La} on the contour lines is shown in reciprocal seconds. Experiments and analysis performed as described in Section 2.7.

5.4.4.3. Analysis of Variance (ANOVA) and Model Diagnostics

As with previous models, analysis of variance was undertaken in order to ensure the validity of the model. Table 5.11. highlights that there is a good agreement between the model and the experimental data. Table 5.10. provides statistical diagnostic values for the individual terms, which also indicate good agreement with the model, with most p-values less than 0.0001, and large t-values in all cases. A t-test is used here as a means of showing if single variables are significant.

As additional diagnostics a parity plot of predicted versus actual data (Figure 5.18A) indicating some outlying data points but a broadly conformational correlation. The half normal plot (Figure 5.18B) is used to highlight the terms of greatest statistical significance, and therefore confirm those that are included in the model. The ANOVA indicates that the model is a good fit and can be used with a high degree of confidence for determining and predicting the oxygen mass transfer coefficient in an Ambr[®]250 bioreactor.

Table 5.11. Summary of the statistical diagnostics for the overall model of k_{La} in an Ambr[®]250 bioreactor system.

R-squared	0.955
Root mean square error (RMSE)	0.021
p-value	<0.0001
Sequential p-value	0.078

5.5. Comparison of Oxygen Mass Transfer in Different Bioreactor Types

In addition to determining the oxygen mass transfer capabilities of each of the reactor types, it is important to compare these capabilities between bioreactors. How the models compare with traditional literature correlations is also necessary. Finally, comparing the oxygen mass transfer values with the reported oxygen demands for different expression systems which it may be desirable to cultivate. As such it is first important to compare the three bioreactors investigated here (BioFlo 310 STR, XDR-10 and Ambr[®]250) with respect to the factors which influence oxygen availability and mass transfer.

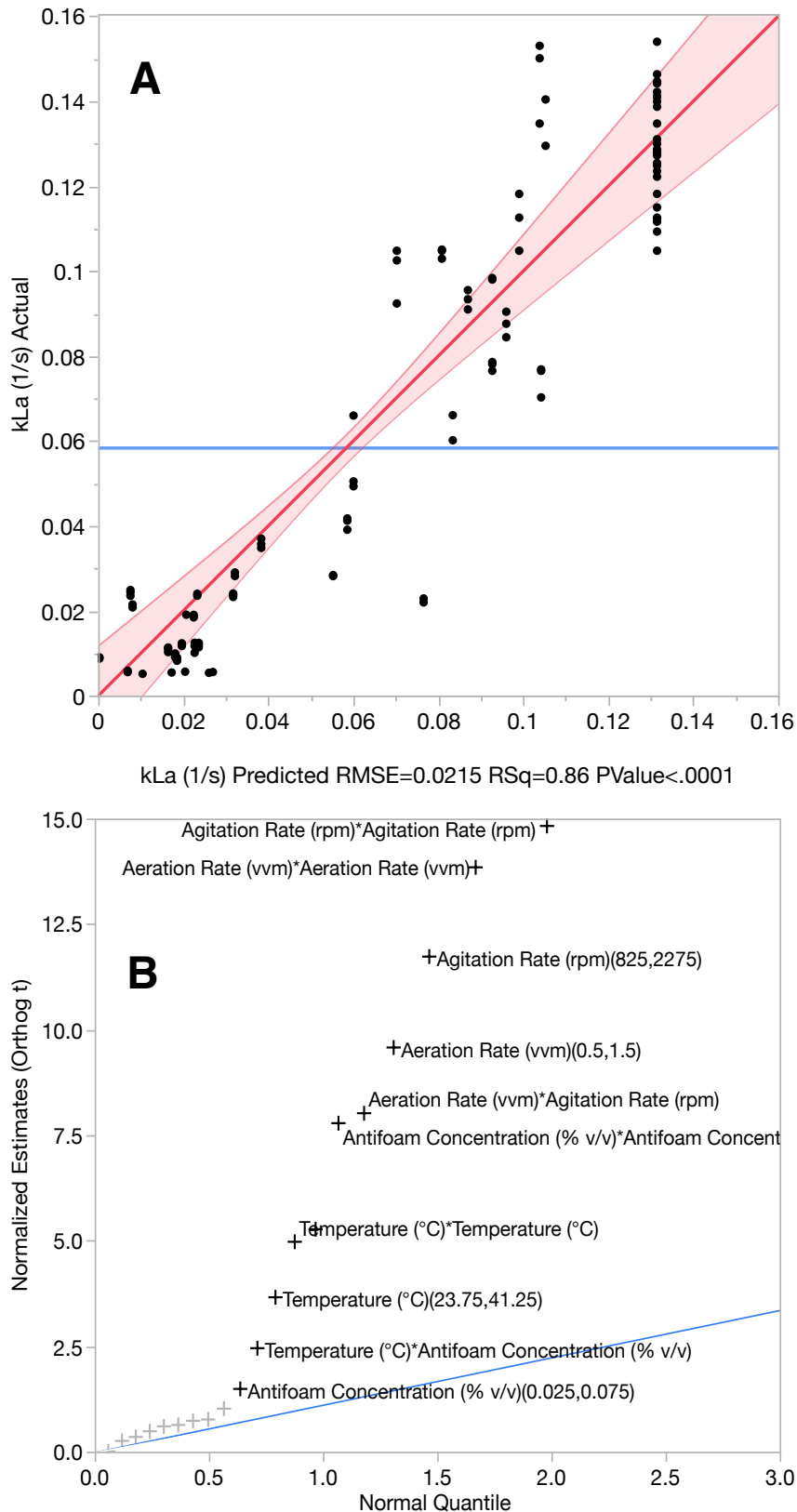


Figure 5.18. Diagnostic plots for the quadratic model built to describe k_{LA} in an Ambr[®]250 single use bioreactor system. The predicted versus actual plot (A) and the normal probability plot (B), all highlight a good agreement between the model generated and the experimental data. Analysis as described in Section 2.7.

5.5.1. Comparison of Models for Three Different Bioreactors

Each of the models generated indicate similar factors are of significant influence on oxygen mass transfer (Table 5.12.), highlighting aeration rate as a main effect, and the Ambr®250 and BioFlo 310 also showing agitation speed to be important. It is useful to note these as common critical factors and that they agree with previously reported correlations.

The Ambr®250 also demonstrates that temperature, antifoam concentration and viscosity are significant main effects, while the XDR-10 and BioFlo 310 have only one additional main effect each (temperature and antifoam concentration respectively). This indicates that each bioreactor configuration and set up has distinct contributors to oxygen mass transfer. Again, highlighting the necessity of this work on different bioreactor types to understand their suitability for specific applications.

Multi factor interactions in the models do not demonstrate a particular trend, indicating that smaller influencers on oxygen mass transfer are highly system dependent. The Ambr®250 and the BioFlo 310 though do share a two-factor interaction between aeration and agitation speeds, further supporting the theory that these are the two most critical factors which influence oxygen mass transfer in stirred tank reactors.

Table 5.12. includes the maximum observed k_{La} values for each of the bioreactor investigations. Values for the XDR-10 are an order of magnitude lower than those seen in the BioFlo 310 and Ambr®250 bioreactors, showing the negative effect of the pitch blade impeller, frit sparger and the operational constraints imposed by the engineering design of the system. The maximum k_{La} observed in the BioFlo 310 is more than 1.5 times that in the Ambr®250. Although the magnitude of the difference is surprising, this maximum is an outlying single point, with the next greatest value ($0.193s^{-1}$), and a high degree of similarity between the rest of the two data sets.

Table 5.12. Maximum k_{La} values and significant main effects observed in models of k_{La} for each bioreactor type investigated

Bioreactor	Max. k_{La} (s^{-1})	Main Effects
BioFlo 310	0.293	Aeration rate, Agitation speed, Antifoam concentration
XDR-10	0.018	Agitation speed, Temperature
Ambr®250	0.171	All (Aeration rate, Agitation speed, Temperature, Antifoam concentration, Viscosity)

5.5.2. Comparison of k_La Models with Literature Correlations

There are a number of correlations available for determining oxygen mass transfer coefficients in a stirred tank bioreactor (Section 1.2.8.). The major difficulty with their use is that these correlations are often empirical and very specific to the experimental set up. As yet there is no generically applicable relationship. As a result, it is often necessary to either compromise and select the correlation that most closely resembles the relevant culture set up, or determine a new empirical relationship. Although this is also the case to some extent for the DoE models produced by this work, a major insight is that the models, and therefore oxygen mass transfer capabilities are system specific. This goes for both the physical and environmental factors, and more information is gained into the effects of smaller factors.

The most commonly applied correlation for calculation of k_La is:

$$k_La = C.(P_g/V)^\alpha.V_s^\beta \quad \textbf{Equation 5.1.}$$

Where P_g is the gassed power consumption in Watts, V is the volume of liquid in the vessel in m^3 , V_s is the superficial gas velocity in ms^{-1} and C , α and β are empirically determined coefficients specific to the system being investigated.

Based on the geometries and set up of the BioFlo 310, the most appropriate relationship which could be found was determined by Linek et al (2004) and is shown in Equation 5.2. however, this was based on the use of air and water rather than culture relevant media.

$$k_La = 0.01(P_g/V)^{0.699}V_s^{0.581} \quad \textbf{Equation 5.2.}$$

Where the gassed power consumption, P_g is calculated using Equation 5.3. Where P is the power rating of the motor (in Watts), N is the impeller rotational speed in ms^{-1} , D_i is the diameter of the impeller in m , Q is the volumetric air flowrate in m^3s^{-1} and K , a and b are empirical coefficients specific to the system.

$$P_g = K.(P^2.N.D_i/Q^a)^b \quad \textbf{Equation 5.3.}$$

Equation 5.4. includes the appropriate coefficients (K , a and b) values for an STR with 2 Rushton turbine impellers (such as the BioFlo310), as determined by Patrick and Kennedy (1995).

$$P_g = 1.26(P^2.N.D_i/Q^{0.56})^{0.45} \quad \textbf{Equation 5.4.}$$

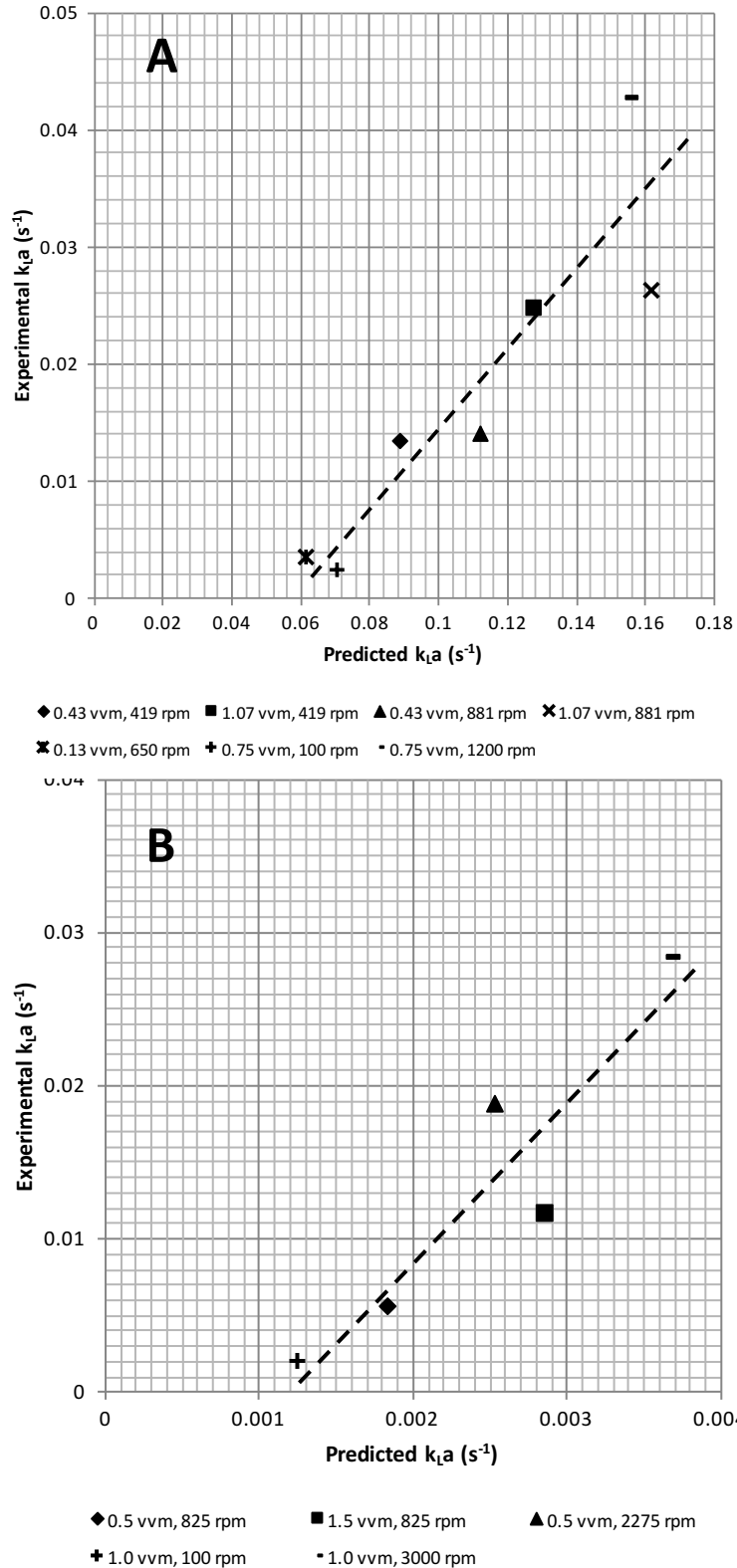


Figure 5.19. Parity plot of empirically determined k_{La} values and those predicted using the Van't Riet equation (Equations 5.1 to 5.4) for a New Brunswick BioFlo 310 STR (A) and an Ambr®250 bioreactor (B). The dashed line highlights the correlation between experimental and predicted values across the majority of the experimental range. In the case of the Ambr®250, values are the mean of $n=3$ runs for each of the set points. Experiments and analysis performed as described in Section 2.7.

The calculated values of k_{La} for the BioFlo 310 using Equations 5.2. and 5.4. are plotted against the experimentally determined values in Figure 5.19A. This highlights a strong proportional correlation across the range. The experimentally determined k_{La} values are significantly lower than those calculated while the trend holds (~20%). This is most likely due to the increased solubility of air in water when compared with culture media, in addition to differences in the systems (e.g. motor power usage). However, the key observation is the correlation between the predicted (calculated) and experimental data.

The same analysis was carried out for the Ambr[®]250. The bioreactor is of a similar geometrical configuration and so the main difference when calculating the predicted k_{La} using Equations 5.2 and 5.4 is to account for the change in gassed power input. This is due to the use of a lower power motor (RE-max, Maxon, Switzerland). The results are shown in Figure 5.19B. Again it can be seen that there is a strong correlation between the values determined experimentally and through predictive calculation.

5.6. Applicability of Single Use Bioreactors to Microbial Fermentation

The overall aim of this chapter is to understand the applicability of single use bioreactor systems for microbial fermentation. Ideally, this would be done with a direct comparison of supply (i.e. k_{La}), and demand (i.e. OUR). However, it is difficult to directly compare the oxygen uptake rates, and therefore the direct demand of a culture system, with the volumetric mass transfer coefficients which have been determined here. Instead it is necessary to convert k_{La} to an oxygen transfer rate which can then be compared with OUR.

5.6.1. Comparison of Oxygen Demands Determined in this Thesis and Oxygen Mass Transfer Capabilities of Three Different Bioreactors

In order to calculate and compare oxygen transfer rates, it is first necessary to determine the solubility of oxygen, which changes based on the temperature and the composition of the medium, both of which are changed continuously throughout the experimental runs performed. As such, a number of assumptions are made in order to achieve the most appropriate comparison.

Firstly, that the maximum solubility of oxygen in microbial liquid culture media is $8.181 \text{ mgO}_2\text{L}^{-1}$ (calculated using Vendruscolo et al. 2012; Gros et al. 1999) for a model solution similar to fermentation media). Air is supplied at atmospheric pressure meaning that the partial

pressure of oxygen is 0.20946 atm. As there are no cells present during this k_La investigation, we can equate OTR and k_La using:

$$OTR = k_La (C^* - C_L) \quad \textbf{Equation 5.5.}$$

Where C_L is zero. The estimated oxygen transfer rate can then be calculated as follows (using the BioFlo 310 as an example):

$$\begin{aligned} OTR &= 17.58 \times 8.181 \\ &= 143.82 \text{ mgO}_2\text{L}^{-1}\text{min}^{-1} \\ &= 8.99 \text{ mmolL}^{-1}\text{min}^{-1} \end{aligned}$$

Comparing this with the OURs determined in Section 3, where values between 5.68 and 25.8 $\text{mmolL}^{-1}\text{min}^{-1}$ were seen (during culture in the same bioreactor investigated here), this would be capable of sustaining a non-induced batch culture with air alone. However, if the culture is fed and induced, which is where the higher peak OURs are seen, it would be necessary to work with oxygen enriched air or to increase the operating pressure. This is in agreement with what was observed during these experiments (Section 3). The system was configured to determine the highest achievable oxygen demand. This means that when required by the DOT control loop, pure oxygen was blended with air, raising the composition of the inlet gas, and therefore the potential achievable OTR to approximately five times what was observed here (around 45 $\text{mmolL}^{-1}\text{min}^{-1}$). This confirms that the BioFlo 310 can meet the oxygen demand of the fed batch microbial fermentation in Chapter 3.

Based on these calculations, the Ambr[®]250 would be able to support batch cultures of *E. coli* at maximum demand. It would not however be able to support the maximum demands of the induced or fed-batch cultures. What this means is not that the culture and the bioconversion would not be able to be run, but rather that this would change the dynamics and potentially productivity of the culture, unless measures were taken to reconcile the shortfall in oxygen mass transfer (e.g. increased operating pressure or oxygen enriched air).

OTRs in the XDR-10 would not be capable of supporting microbial fermentation under any of the three culturing strategies investigated in this thesis based on the maximum OURs observed.

5.6.2. Comparison of Oxygen Demands Determined in Industrial Microbial Fermentations and Oxygen Mass Transfer Capabilities of Three Different Bioreactors

The oxygen mass transfer capabilities of the single use bioreactor systems investigated are also compared with industrial microbial fermentations carried out at Synthace Ltd.

Figure 5.20. shows relevant on- and off-line profiles (OUR and biomass accretion) for a fermentation using an *E. coli* BL21 strain expressing a heterologous reductase, making it similar to the expression system used in Chapter 3 for evaluation of the maximum oxygen demand. The maximum OUR observed in this fermentation was $281 \text{ mmolL}^{-1}\text{h}^{-1}$. Here, maximum oxygen uptake rate occurs during the period of maximum volumetric productivity with respect to biomass accumulation (as was previously seen in Chapter 3). This was representative of the highest OURs seen from 26 Ambr[®]250 runs (300 fermentations) from which relevant data was available, supporting biomass concentrations up to $142 \text{ g}_{\text{WCW}}\text{L}^{-1}$.

Using the calculations from Section 5.6.1. the maximum oxygen transfer rates seen in the Ambr[®]250 and the XDR-10 were 5.25 and $0.55 \text{ mmolL}^{-1}\text{min}^{-1}$ respectively (equating to 315 and $33 \text{ mmolL}^{-1}\text{h}^{-1}$). This demonstrates that the Ambr[®]250 is suitable for industrial microbial fermentation, and that the XDR-10 is inappropriate for this use.

Additional industrial fermentations have been summarised with respect to their peak oxygen uptake rates in Table 5.13. It is interesting to note the range of demands placed on the culture environment by the different expression systems, and the expressions or bioconversions that they are undertaking. Given the differences in growth rates and maximum biomass concentrations and titres this is to be expected.

5.6.3. Comparison of Oxygen Mass Transfer Coefficients in SUBs and Microwell Plates

It is important to compare the oxygen mass transfer capabilities of the two different bioreactor scales characterised in this thesis; microtitre plates and lab scale bioreactors. Table 5.14. summarises the oxygen mass transfer coefficients of a number of commercially available single use bioreactors at a range of scales. With respect to the bioreactors characterised in this thesis, $k_{\text{L}}a$ values in 24 DSW plates are significantly lower than in the BioFlo 310 and Ambr[®]250 bioreactors. Maximum values observed were approximately 5 and 9 times greater in the Ambr[®]250 and BioFlo 310 respectively compared with 24 DSW. These significantly higher $k_{\text{L}}a$ values provide confidence that batch fermentation performance from the microtitre plates can be reproduced or improved on in the BioFlo 310 and Ambr[®]250.

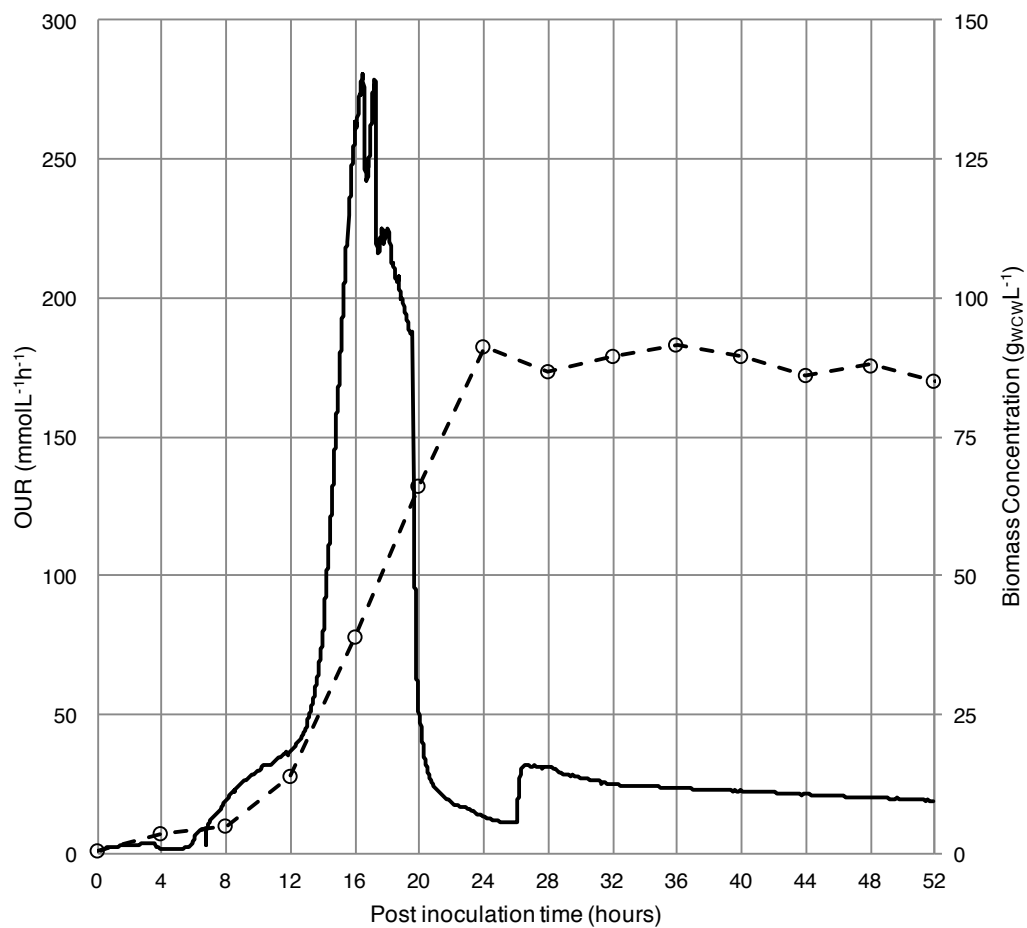


Figure 5.20. Representative example traces of oxygen uptake and biomass concentration profiles from an industrial *E. coli* fermentation expressing a heterologous reductase. Solid line represents OUR, while the dashed line shows the biomass concentration in g_{wcwl}L⁻¹. Experiments performed at Synthace using proprietary bioprocesses.

Although the OTR values determined in microtitre plates in Sections 4.2.3. and 4.3.3. were lower than the highest literature values found, the maximum oxygen transfer rates quantified in the lab scale bioreactors are still significantly higher. As such, significant confidence can be had with respect to reproducing the performance of a microtitre culture.

5.7. Summary

The aim of this chapter was to evaluate the oxygen mass transfer capabilities of a number of commercially available single use bioreactor systems and therefore their ability to undertake microbial fermentation. A method for developing multidimensional models for accurate determination and prediction of oxygen mass transfer rates in SUBs has been established. This was one of the key objectives for this chapter of work as typically, correlations for oxygen mass transfer have been limited to highly empirical characterisations using a limited number of experimental set points.

Table 5.13. Observed oxygen uptake rates and maximum biomass concentrations for a number of industrial microbial fermentations using different expression systems under different modes of operation. Experiments carried out at Synthace Ltd. I-B denotes induced batch culture and I-FB, induced fed batch.

Expression system	Product or activity	Mode of operation	Maximum observed OURs (mmolL ⁻¹ h ⁻¹)	Maximum biomass concentration (g _{WCW} L ⁻¹)
<i>E. coli</i> BL21 expressing heterologous reductase	Heterologous reductase	I-FB	122.2	74.0
			278.2	138.5
			233.1	113.9
			187.3	141.9
			144.3	142.2
			283.8	124.7
			148.8	82.3
<i>E. coli</i> with membrane protein knockout	Recombinant protein	I-B	302.8	30.4
			207.7	59.2
Wild type filamentous fungus	Oxidative bioconversion	I-FB	21.3	15.7
			16.8	26.4
			48.9	17.2
			29	9.3
			36.3	23.1

This method has been applied to the generation of models for a classical, bench top stirred tank bioreactor (BioFlo 310), a tank liner type single use bioreactor (XDR-10) and a moulded polycarbonate single use bioreactor (Ambr®250). As anticipated, k_La was shown to be the greatest in the benchtop bioreactor (Section 5.5.) closely followed by the Ambr®250 which is geometrically and operationally similar to the traditional style reactor (around 0.29 and 0.17s⁻¹ respectively). The k_La in the XDR-10 was an order of magnitude lower (Table 5.12.).

Additionally, a high degree of automation was incorporated into the investigation with the Ambr®250, making the process more robust and reproducible compared with a manual protocol, and meaning that the operation could be repeated if desired, or, with minimal adaptation expanded to include a wider range of potentially significant factors.

When compared with data predicted by literature relationships (Figure 5.19), a proportional correlation is seen across the majority of the experimental space. This is the case for both the BioFlo 310, and the Ambr®250.

Comparisons were also made with the maximum OURs determined for microbial fermentation and bioconversion in Chapter 3, approximately 26 mmolL⁻¹min⁻¹ (Section 5.6.1.). This highlighted that without additional measures to increase the solubility of oxygen in the culture media (e.g. oxygen blending or headspace pressure), it would be difficult to match the peak demands of the cultures, although it should be noted that for many fermentations the Ambr®250 and the BioFlo 310 would be able to meet the requirements without these additional measures. The XDR-10 would not.

This work has highlighted that differences in reactor geometries and configurations influence the factors that impact on oxygen mass transfer and their contribution, further demonstrating the need for this level of characterisation in SUBs. Smaller influences on oxygen mass transfer are highly system dependent, insight that would be very difficult to gain without the use of multifactorial experimental methods. The methodology established in this chapter also represents an improvement in the way that oxygen mass transfer capabilities are characterised, although limitations are still seen when comparing reactor types due to differences in both hardware and software.

In the next chapter, now that the potential for the Ambr®250 SUB system to culture microbial expression systems has been established from a scientific stand point, the suitability from an economic perspective will be investigated. A prototype computational tool capable of

estimating the cost of a run in the Ambr®250 will be developed and tested, and by the conclusion of the chapter, be suitable for internal deployment at Synthace.

Table 5.14. k_La values and estimated equivalent oxygen transfer rates determined for a range of commercially available single use bioreactors, including those investigated as part of this thesis.

Bioreactor	Bioreactor Type	Working Vol. (L)	k_La^* (s ⁻¹)	k_La^* (min ⁻¹)	Estimated equiv. OTR (mmolL ⁻¹ min ⁻¹)
BioFlo 310**	Glass STR	2-6	0.293	17.58	8.99
Ambr®250**	Moulded PC STR	0.1-0.25	0.171	10.26	5.25
XDR-10**	Tankliner	2-7	0.018	1.08	0.55
Wave Bioreactor™	Pillow	1-200	<0.003	<0.17	0.09
Cell-tainer®20	Pillow or Square	0.2-25	>0.111	>6.67	3.41
Cell-tainer®200	Pillow or Square	5-200	>0.111	>6.67	3.41
BIOSTAT Cultibag	Tankliner	50-200	>0.042	>2.50	1.29
HyPerforma SUB	Tankliner	30-300	>0.167	>10	5.12
XDR SUB (up to 2000L reported)	Tankliner	10-2000	<0.006	<0.33	0.18
Mobius® Cell Ready	Tankliner	50-200	<0.019	<1.17	0.58
Ambr®15	Moulded PC STR	0.01-0.015	<0.006	<0.33	0.18
Ambr®250 (reported)	Moulded PC STR	0.1-0.25	≤0.139	≤8.33	4.26
24DSW**	Microwell Plate	0.002-0.006	0.033	2.0	1.01
24DSW (reported)	Microwell Plate	0.002-0.006	0.097	5.83	2.98

Table adapted from Oosterhuis et al. 2013, Bareither et al. 2013, Nienow et al. 2013, Jones 2015 and Kensy et al, 2009. *Values from this thesis or the maximum of those observed. **Bioreactors investigated as part of this work. DSW Deep Square Well Microtitre Plate, SS STR Stainless Steel Stirred Tank Bioreactor, PC STR Polycarbonate Stirred Tank Bioreactor.

6. An Economic Evaluation Tool for Bioprocess Development using the Ambr[®]250 System[†]

6.1. Context & Aim

The cost of experimentation during bioprocess development is a key issue in industry. There is a constant drive to bring down financial and resource requirements in order to reduce the overall development cost, reduce time to market and make a final process as commercially competitive as possible (Paul et al. 2010) This makes the economic evaluation of using single use technologies for fermentation a critical part of assessing their potential application (Shukla & Gottschalk 2013). In order to enable this, there is a need for tools which can accurately predict the economic burden of a bioprocess experiment using single-use equipment (termed a 'run' in this chapter) and a bioprocess development campaign (comprising multiple 'runs').

The Ambr[®]250 system is a multi-bioreactor system for upstream bioprocess development as described in Section 2.3.1. and 2.7.2. Parallel fermentation with generation of large online data sets and automated liquid handling mean diverse bioprocesses can be investigated concurrently and available offline data captured as shown in Section 5.6.2.

Use of parallel, single-use systems, even during the early stages of bioprocess development, needs to be balanced against the cost of doing so. In addition to the logistical challenge associated with planning, preparing, setting up and operating 12 or 24 parallel fermentations, the cost of operating such a system in which many different components are single use, or need replacing on a regular basis, is complex to estimate. The number of different disposable components involved in a single bioreactor run is in double figures and all need to be considered in order to estimate a realistic run cost. As a confounding factor, the number, and in some instances the type of each consumable is influenced by the objective of an experiment (e.g. looking at process kinetics as opposed to final conversion yield) and design of an experiment (e.g. batch versus fed-batch operation) which can change considerably from run to run. A software tool capable of rapidly capturing this flexibility and is able to model cost of an individual run would be useful for application in an industrial context.

[†] This chapter is included as part of the requirement for award of the UCL EngD in Biochemical Engineering and Bioprocess Leadership.

6.1.1. Aims

Chapters 4 and 5 have concluded that a number of single use bioreactor technologies commercially available are incapable of being used for experimental investigation of microbial expression systems. However, it was also shown that the Ambr®250 bioreactors can be used and so are a good model to evaluate here.

The aim of this chapter is to build and develop a prototype computational tool capable of estimating the cost of a given bioprocess development run in the Ambr®250. A range of key inputs will be modelled which capture the complexity of a fermentation run, combined with the single use elements of the Ambr®250 system. As the tool will be used for evaluation of bioprocessing on the Ambr®250, for convenience it will henceforth be referred to as the ARC (Ambr Resourcing and Costing) tool. By the end of this work the goal is that the ARC tool should be suitable for deployment within Synthace Ltd for use on other projects with industrial partners. Specific objectives are therefore:

- Initial development of a costing tool in Microsoft Excel in order to determine the validity of the approach,
- Subsequent development of a more robust, accurate version of the ARC tool in Jupyter Notebooks using the Python programming language (selection of Jupyter and Python will be discussed in Section 6.3.),
- Use of the improved tool for analysis of the major costs and how much they influence the overall cost of a single run.

A diagrammatic representation of the proposed structure for calculating resource demand and cost is shown in Figure 6.1. Resource requirements will be determined taking inputs relating to a particular run such as number of samples, timings and tubing. These inputs can then be taken and passed through a prototype framework for calculating the operating resource demands (mainly consumables and time). The outputs of this first step then need to be used to approximate the total cost of a bioprocess run using unit costs. The calculations are based on experience with the Ambr®250 system, previous bioprocess development projects and prior knowledge on the costing and usage of Ambr®250 disposables.

In calculating resource and cost requirements, the ARC tool will serve a dual purpose. First, it will be used for consumables projection (over a campaign or series

of projects), allowing negotiation of the best price for consumables with the supplier, and resulting in minimal overspend on unused materials. Also, it will be used for cost analysis of bioprocess development runs. This will allow tracking and projection of finances for a given bioprocess development run or project (necessary for accurate budgeting) and, where necessary, adapting a run strategy in order to improve the value of a run i.e. decrease cost to meet a target set of objectives.

It will also be crucial to ensure that however the ARC tool is finally deployed, it should be as user friendly as possible to encourage adoption and use. Simplification of the bioprocess complexity for the end user will be critical.

6.2. Ambr®250 Resourcing and Costing (ARC) Tool - Version 1.0 (Microsoft Excel).

An initial User Requirement Specification (URS) was written, defining the input and output requirements for the ARC tool, as well as the requirements for usability. For example, simple information inputs such as dropdown lists or textboxes, rather than having to enter them using low level methods such as the command line, and refinement of the available inputs based on groupings such as experimental strategy.

Once the user requirements were set out, Version 1.0 of the ARC tool was built in Microsoft Excel 2013. This made it relatively quick and simple to build, and meant that the focus could be on the calculations that would be used to take the input of process information and determine the consumables usage and resultant cost. The primary purpose of Version 1.0 of the ARC tool was to establish the validity of building this tool and whether the outputs yielded sufficient information and knowledge to justify the investment in building something more accurate and robust which could then be deployed within the company.

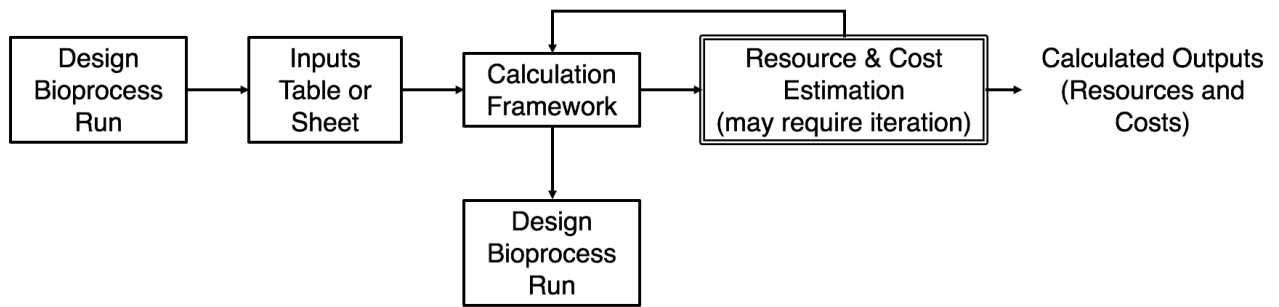


Figure 6.1. Basic structure for estimation of the resource demands for a given bioprocess development run in the Ambir[®]250 bioreactor. Arrows represent the flow of information.

Building of the calculation framework (Figure 6.1) required determination of all of the steps that use consumables during an individual bioprocess run. This is shown diagrammatically in Appendix 5.1. It can be seen that there are a number of dependencies and that in a number of cases, there are multiple consumables options for fulfilling a task. This in turn needed to be considered during calculation and an element of prioritisation and logic embedded to ensure that the most appropriate consumable was selected and included.

A simple example calculation for calculating the total number of samples taken (Equation 6.1) and basic Excel code are shown in Figure 6.2. to demonstrate the structure and information required. In addition, in order to process some of the inputs, fields are required to convert instructions into binary inputs for calculation.

Samples: (to be used for tips and plates)		Code:
Primary Seed Samples		6 =(C4*Inputs!E17)*Inputs!E37
Secondary Seed Samples		6 =(C5*Inputs!E17)*(2^Inputs!E11)*Inputs!E38
Finals:		
Taking Pre and Post Inoc (t0) samples? Yes=2, No=0		2 =IF(Inputs!E26="Yes",2,0)
Taking Pre and Post Ind Samples? Yes=2, No=0		2 =IF(Inputs!E27="Yes",2,0)
	=	4 =SUM(C23:C24)
	=	32 =C25*C10
Sampling frequency (e.g. hourly =1, 4 hourly=4 etc)		=IF(Inputs!E28="Hourly",1,IF(Inputs!E28="2 Hourly",2,IF(Inputs!E28="3 Hourly",3,IF(Inputs!E28="4 Hourly",4,IF(Inputs!E28="6 Hourly",6,IF(Inputs!E28="8 Hourly",8,IF(Inputs!E28="12 Hourly",12,IF(Inputs!E28="24 Hourly",24,0))))))))
Regular samples throughout final stage		24 =Inputs!E23/Calcs.!C28
	=	24 =ROUNDUP(C29,0)
	=	192 =C30*C10
Total number of samples from each finals reactor		28 =C30+C25+C36
Total number of samples during finals stage		224 =C31+C26+C37
Total number of samples:	=	236 =C34+C19+C16

Figure 6.2. Illustration of the inputs and code in Microsoft Excel cells in order to determine the output from Equation 6.1, calculating the total number of samples taken during a bioprocess run.

$$Total\ Samples = Primary\ Samples + Secondary\ Samples + Finals\ Stage\ Samples$$

Equation 6.1.

Several options have been provided for insertion of information depending on what the input to the calculations require. Some information is inserted manually, but constrained by the calculation to be performed, others from a dropdown list of predefined options.

Figures 6.3. and 6.4. provide an example of a completed inputs page and outputs page respectively for this first iteration of the ARC tool. Where the inputs page indicates 'select', there are drop down options, and where the page shows 'enter' as an instruction, input of an integer value is required.

Although outwardly a simple example of what the ARC tool is intended to do, Version 1.0 has demonstrated that the principles under which it operates, and the means by which the resource and cost estimations are achieved are sufficient to justify further development. The real cost was determined by retrospectively calculating the cost incurred by individual bioprocess runs as part of client projects, and comparing these with the cost when the run was replicated in the ARC tool. It indicated that Version 1.0 of the ARC tool was estimating the cost of a run to within 10%.

There are however a number of issues to be addressed. These include improving the accuracy of calculations by incorporating more comprehensive coverage of the potential variables, the ease of usability, access and updating of fixed values (e.g. costs) and protection of the calculation framework level from editing. These will need to be resolved in Version 2.0 of the tool.

6.3. Ambr[®]250 Resourcing and Costing (ARC) Tool - Version 2.0 (Jupyter Notebooks).

Taking into account the conclusions from Version 1.0 of the ARC tool in Microsoft Excel 2013 (Section 6.2), Version 2.0 of the ARC tool was constructed using the Python programming language in Jupyter Notebooks.

Python was selected as it is a high level, open source programming language which is based on English language keywords rather than using more complex abbreviated structures in the syntax (Nagar 2017); this makes it relatively easy to self-teach as a programmer with little previous experience. There is also a large community of Python users, which is constantly improving the code base, and its implementation. Deployment to a public server can be made relatively simple, enabling wider access and uptake. Therefore, successful construction of Version 2.0 of the ARC tool in Python would seem to overcome the majority of limitations seen from Version 1.0.

Inputs			
Select from dropdowns or enter values for each of the following:			
Run Code:		JDR Example	
Run Structure			
DoE	No. DoE Factors	4	Select 0 to 6
	No. Seed Factors (not construct)	0	Select 0 to 2
	No. Genetic Factors	1	Select 0 to 3
	No. Media Factors	1	Select 0 to 3
	No. Runs	8	Select 1 to 12
	Is Induction time a factor?	Yes	Yes or No
Seeds	No. genetic constructs?	2	
	Primary seed vessels?	Ambr250 Bioreactor	
	Secondary seed vessels?	Ambr250 Bioreactor	
Timeline	Length of Primary Seed in Ambr?	16	Enter value in hrs
	Length of Secondary Seed in Ambr?	18	Enter value in hrs
	Length of Production Stage?	72	Enter value in hrs
Sampling			
(Production Stage)	Pre and Post Inoc (t0) Samples?	Yes	Select Yes or No
	Pre and Post Induction Samples?	Yes	Select Yes or No
	Frequency of sampling?	3 Hourly	Select one
	Typical sample volume	1	Enter value in mL
	Typical sample destination	24 DSW	Select one
	Harvest Sample for storage/DSP?	Yes	Select Yes or No
	Harvest Sample volume?	5	Enter value in mL
	Harvest Sample Destination	20mL Universal	Select one
(Seeds)	Samples during primary seed?	3	Enter value
	Samples during secondary seed?	3	Enter value
	Sample volume	1	Enter value in mL
	Sample destination	24 DSW	Select one

A.

(Specials) e.g. if samples required for immediate processing	No. samples which do not fit with typical sample frequency?	1.5	Enter value
	Sample destination?	2mL Tube	Select one
Media	No. Primary Seed Media	1	Select value
	No. Secondary Seed Media	1	Select value
	Starting vol. in Ambr250 bioreactor	150	Enter value in mL
	No. Production Stage Media	3	Select value
	Starting vol. in Ambr250 bioreactor	150	Enter value in mL
Inoculation	Primary seed source	Freezer vial	Select one
	Secondary seed source	Seed Ambr	Select one
	Production Stage source	Seed Ambr	Select one
	Inoculum volume	1.5	Enter value in mL
Induction	Volume of inducer	0.15	Enter value in mL
	Source of inducer	24 DSW	Select one
Titriments and Feeds	Type of antifoam	PPG	Select one
	Control loop	Pumped	Select Bolus or Pumped
	Which acid(s) are to be used?	Hydrochloric Acid (HCl)	Select from list
	Which base(s) are to be used?	Sodium Hydroxide (NaOH)	Select from list
	pH Control loop	Pumped	Select Bolus or Pumped
	No. feeds	2	Select one
	No. fed Ambr250 bioreactors?	8	Select one
	Are feeds bolus or pumped?	Pumped	Select bolus, pumped or batch process
Contingency	Contingency %	5.0%	
Inherent/Overhead	Need to be taken into consideration but do not need own section - can take info from other selections (Tips and 1L bottles for filling - Tubing, 175mL bottles and 300ul tips for bathced a/f)		

B.

Figure 6.3. Example of the Inputs page from the Version 1.0 of the ARC tool in Microsoft Excel 2013, split into the top (A) and bottom (B) halves of the inputs page. Dropdown selection is indicated using a 'Select' instruction, while text inputs are required where 'Enter' is requested.

Consumable outputs for run:		JDR Example	
		Cost (£)	
Bioreactors	Seed	4	
	Production Stage	8	
	Total	12	1750.00
24DSW Plates		12	116.76
300uL Tips (boxes)		1	16.98
10mL Tips (boxes)		11	118.23
1L Reagent Bottles		5	54.69
175mL Reagent Bottles		0	0.00
Drip catcher pads		6	21.88
Tubing Sets	(12-way)	3	240.63
	(4-way)	2	160.42
Air filters		6	63
2mL Tubes		0	0
20mL Universals		2	0.4
		Total Consumables Cost:	2542.97
Approximated Labour:		72.19 hrs	3850.00
Total Cost for Ambr Process:			£ 6392.97

Figure 6.4. Example of the Outputs page from Version 1.0 of the ARC tool in Microsoft Excel 2013. Cost figures for the consumables are for illustrative purposes only.

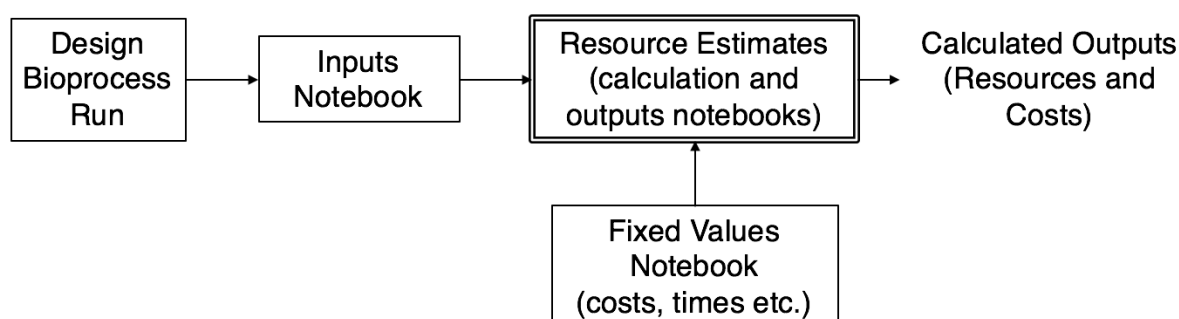


Figure 6.5. Basic structure for estimation of the resource demands for a given bioprocess development run in the Ambr®250 using Version 2.0 of the ARC tool in Python using Jupyter Notebooks. Arrows represent the flow of information.

The Jupyter Notebook is a web-based environment in which Python code can be scripted, saved and shared in a relatively simple format (Ragan-Kelley et al. 2014). There are also a large number of extensions and libraries available for the Jupyter Notebook including widgets (useful for simple, constrained information entry in real time e.g. slide bars and tick boxes), and graphing tools. For these reasons, Jupyter notebooks are commonly employed in end user laboratories for a wide range of applications including data handling, genetic sequencing and collaborative projects in areas such as bioinformatics (Shen 2014).

The use of Python and Jupyter Notebooks also meant that separate parts of the ARC tool could be built in isolation, saved separately and imported to the final notebook to enable protection of the coded calculations and fixed data, and improve the ease with which updates could be implemented. This meant that the structure of the workflow was simplified slightly, with the calculations being built into a single notebook that would enable simultaneous calculation of the resources and costing. This is represented diagrammatically in Figure 6.5.

Improved understanding of the Ambr[®]250 system was incorporated into the building of Version 2.0 of the ARC tool, but the same approach was used for the calculations i.e. using the process design inputs (Appendix 5.1.) to estimate resource demand. The increased knowledge of the system acquired between the building of the Version 1.0 and Version 2.0 meant that the algorithms used for calculation were improved, while the number of input variables was increased to include additional detail and try to ensure that different process-to-process options can be incorporated, thus improving the accuracy of the eventual estimations. An example of a calculation for the number of primary stage bioreactor samples (Equation 6.2.). The corresponding Python code is shown in Figure 6.6 to demonstrate the structure and information required. Unlike with the first iteration, to code the calculation for the total number of samples taken is extensive, and so here, the calculation for the number of primary seed stage samples only has been included to demonstrate the principle.

$$\text{No. Primary Samples} = \text{No. Primary Seed Ambr}^{\text{®}}\text{250s} \times \text{No. Samples from each}$$

Equation 6.2.

```

primQ=(0)
def f(PrimSampQ):
    PrimQ=PrimSampQ
    if PrimSampQ=='Yes':
        primq=1
    else:
        primq=0
    return (primq)
PrimSamplesYesNo=f(savedvalues['PrimSamplesQ'])

primVess=(0)
def f(PrimVessQ):
    PrimVess=PrimVessQ
    if PrimVessQ=='Ambr250 Bioreactor':
        primvess=1
    else:
        primvess=0
    return (primvess)
PrimVesselQ=f(savedvalues['PrimaryVessel'])

print 'Primary:'
NoPrimarySamples=PrimSamplesYesNo*PrimVesselQ*savedvalues['PrimSampleNo']
print NoPrimarySamples,'Primary Samples'

```

Figure 6.6. Illustration of the code in Jupyter Notebooks to determine the output from Equation 6.2, for calculating the number of samples taken during the primary seed stage of a bioprocess run in the Ambr[®]250 system.

Further inputs were added during development of Version 2.0 as it was proposed that the original remit for the ARC tool could be extended beyond resource and cost estimation to include generation of process documentation from templates, media preparation recipes, and eventually, construction of the process run file for the Ambr[®]250 system. This is beyond the scope of this current work and will be discussed further in Section 6.6.

The inputs notebook for Version 2.0 of the ARC tool therefore is thorough, but more extensive than would be necessary for many cases. As such, measures were taken to ensure that details which were not required based on already provided inputs were not included and hidden from the operator where appropriate, making the inputs notebook as comprehensive, but versatile as possible. Figure 6.7. shows a simple example of this for feed line allocation.

One of the major improvements made between Version 1.0 and 2.0 of the ARC tool was greater functionality, making the tool easier to use and more difficult to misconstrue the required input information. Images of the user interface for the Inputs Notebook and Resource Estimates Notebook (representing calculations and outputs

respectively) are shown in Figures 6.8, 6.9 and 6.10. They highlight the aesthetic improvement from the initial version, but also the increased level of detail where relevant options have been selected.

6.3.1. Summary of Developments

Version 2.0 of the ARC tool has built upon the foundations of Version 1.0 by utilising a high-level programming language (Python) to improve functionality and usability as well as making the user interface much clearer. Additional knowledge gained on the Ambr®250 system has been incorporated in the form of added detail and inputs where relevant. These have subsequently been used in calculations to improve the accuracy of resource and costing estimations. Additionally, use of the Python programming language over Microsoft Excel for building this tool has resulted in the long term aim of the ARC tool being expanded to incorporate greater functionality including the generation of process documentation and run files for the Ambr®250 system. To this end, Version 2.0 of the ARC tool has been built with consideration for this increased demand for information in the future, with additional data input options and the choice to include small data tables and predefined template text structures (e.g. introductory paragraphs of text for run documents).

Importantly, Version 2.0 of the ARC tool also provides a much more extensive breakdown of where consumables are used in order to highlight major contributors to cost are and how this might be reduced.

6.4. Case Studies

Once the ARC tool was developed in the Jupyter Notebook (Section 6.3), a series of case studies were undertaken with respect to the cost of a bioprocess run in the Ambr®250. The purpose of this was two-fold. First, to test the robustness and usability of the ARC tool, but also to investigate where the greatest contributions to the cost of an Ambr®250 run are, and therefore where savings could be made.

Titration & Feeds:

× Is feeding Pumped or Bolus? No Feed Pumped Bolus

Is pH control Pumped or Bolus? No pH Control Pumped Bolus

× Line A Function: ▾

Line B Function: ▾

Line C Function: ▾

Line D Function: ▾

Titration & Feeds:

× Is feeding Pumped or Bolus? No Feed Pumped Bolus

Is pH control Pumped or Bolus? No pH Control Pumped Bolus

× Line A Function: ▾

Acid: HCl H2SO4 H3PO4 HNO3

Trigger: ▾

Line B Function: ▾

Base: NaOH NH3OH other

Trigger: ▾

Line C Function: ▾

Feed Components: ▾

[Carbon Source] (uM) 0

[Nitrogen Source] (uM) 0

Trigger: ▾

Line D Function: ▾

Figure 6.7. Example of the dynamic properties of the ARC tool built in the Jupyter notebook. This example is for the use of feed lines for pumping of feeds and pH control titrants. Upon selection of the method of feed or titrant supply, the section expands to allow input of additional details. The expansion is reversed and any inputs contained within ignored should the selection be changed to not require pumping.

Bioprocess Run Inputs.

Header Info.

User: JDR, CJLG, SB, LN, VS, CW, MG, etc.

Project Name: EngD Thesis

Run Number: 1

Run Designation: EngD 1

Strain: E.coli

Strain Designation: E.coli EngD 1

Product: RecomProt A

Stock Vial Location: Freezer 2, Shelf 1, Draw 1, Box 4

Antibiotic Resistance Marker: Chloramphenicol

Antibiotic Concentration (ug/ml): 50

Inducer: IPTG

Inducer Concentration (uM): 500

Header Information:

Strain Designation	E.coli EngD 1
Product	RecomProt A
Stock Vial Location	Freezer 2, Shelf 1, Draw 1, Box 4
Inducer Concentration (uM)	500
Run Designation	EngD 1
Inducer	IPTG
Project	EngD Thesis
Strain	E.coli
User	JDR
Antibiotic Resistance Marker	Chloramphenicol
Antibiotic Concentration (ug/mL)	50
Run No.	1

Bioprocess Train

Vial Recovery

Information pertaining to vial recovery (including location and strain information) can be found above, in the header table.

Or better yet:

E.coli containing IPTG inducible RecomProt A should be recovered from Freezer 2, Shelf 1, Draw 1, Box 4

Primary Seed

Primary Seed Vessel: Ambr250 Bioreactor

Primary Seed Volume (mL): 150

Primary Seed Media: TB

OR

Primary Media C:N Ratio: 0.1

Primary Media C Source: Glycerol

Primary Media C Concentration: 0.1

Primary Media N Source: Complex

Inoculum % v/v: 5

Inoculum Volume (calculated) (mL): 7.5

Culture Conditions:

Primary Seed Culture Temperature (degC): 35.5

Primary Seed Length (hrs): 12

Primary Seed Incubator: Ambr250 Bioreactor

Primary Seed Shaking Speed

Primary Seed Harvest Vessel: Ambr250 Bioreactor

Primary Harvest Conditions: 12 hours post inoc.

Inoculum Volume (mL): 7.5

Secondary Seed

Secondary Seed Vessel: Ambr250 Bioreactor

Secondary Seed Volume (mL): 150

Secondary Seed Media

OR

Secondary Media C:N Ratio: 5

Secondary Media C Source: Glycerol

Secondary Media C Concentration: 9

Secondary Media N Source: Complex

Secondary Inoculum % v/v: 8

Secondary Inoculum Volume (calculated) (mL): 12

Culture Conditions:

Secondary Seed Culture Temperature (degC): 35.5

Secondary Seed Length (hrs): 16

Secondary Seed Incubator: Ambr250 Bioreactor

Secondary Seed Shaking Speed

Secondary Seed Harvest Vessel: Ambr250 Bioreactor

Secondary Harvest Conditions: 16 hours post inoc.

Secondary Inoculum Volume (mL): 12.0

Figure 6.8. Example of the first part of the Inputs Notebook for the ARC tool built in Jupyter Notebooks using the Python programming language. This includes the input of experiment information and details of the bioprocess train.

Finals

Number of Final Stage Bioreactors: 10
 Initial Volume Per Finals Reactor (mL): 175

Media:

Number of Finals Media: 1
 Number of Vessels with Media 1?: 2

Finals Media 1:
 Finals Media 1:
 OR
 Final Media 1 C:N Ratio: 10
 Final Media 1 C Source:
 Final Media 1 C Concentration: 12.5
 Final Media 1 N Source:

Finals Inoculum % v/v: 4.1
 Finals Inoculum Volume (calculated) (mL): 7.17

Culture Conditions:

Finals Length (hrs): 48
 Finals Culture Temperature (degC): 36
 Finals Impeller Speed: 1500
 Final stage reactors to be harvested for further investigation or processing?

Control:

Control Loops:
 Is DOT control loop required?:
 DOT Set point: 30
 DOT Control Strategy:
 Maximum RPM: 3000
 Maximum VVM: 2

Is a pH control loop required?:
 pH Set point: 7.2
 pH Control strategy:
 pH Control Loop:
 pH deadband: 0.2

Is an antifoam control loop required?:

Induction:

How is the product expressed?:

Titants & Feeds:

Is feeding Pumped or Bolus?
 Is pH control Pumped or Bolus?

Line A Function:
 Acid:
 Trigger:

Line B Function:
 Base:
 Trigger:

Line C Function:
 Line D Function:

Sampling

Primary Seed:

Samples to be taken during Primary Seed?:
 No. samples to be taken?(including end point): 1
 Sample volume (mL): 2
 Sample receptacle:

Secondary Seed:

Secondary Seed Sampling Regime:
 Sample Volume(mL): 2
 Sample receptacle:

Final Stage Bioreactors:

Sampling Regime:

- Event Based Sampling:

Will there be event based sampling?
 Pre and Post Inoc (t0) samples?:
 Pre and Post Induction samples?:
 Post Feed Trigger sample?:
 Pre and Post Mini Harvest samples?:
 Sample Volume (mL): 1.5
 Sample receptacle:

- Final Stage Sampling Regime:

Will there be a Final Stage Sampling Regime?:
 Frequency of samples:
 Sample Volume (mL): 1.5
 Sample receptacle:

Atypical/Special Samples:

Are there samples to be taken outside of the regular sampling regime?:

Outputs:

Total Run Time:
 76 hours

Total Ambr250 Bioreactors:
 12 Bioreactors

Hide Script Button:
 The raw code for this IPython notebook is by default hidden for easier reading. To toggle on/off the raw code, click [here](#).

Figure 6.9. Example of the second part of the Inputs Notebook for the ARC tool built in Jupyter Notebooks using the Python programming language. This includes the input of bioprocess train details, control strategy and a brief summary of outputs.

Ambr Resource Calculator

Ambr250 Bioreactors:

Total Ambr250 Bioreactors:
12 Bioreactors

Samples:

Primary:
2 Primary Samples

Secondary:
1.0 Secondary Samples

Finals:
4 Event Based Samples (per bioreactor)
24 Finals Samples in regime (per bioreactor)
0 Atypical Samples (per bioreactor)

Total:
Total Samples - 283.0

Consumables:

24DSWs

14.0 24 DSW Plate(s) for Final Stage Bioreactors
0.0 24 DSW Plate(s) for Primary Seed samples
1.0 24 DSW Plate(s) for Secondary Seed samples
1 24 DSW Plate(s) for harvested culture

Total 24DSWs: 16.0

10mL Tips

Total 10mL Tips Required: 299.0

Boxes of 10mL Tips Required: 13.0

300uL Tips

Total 300uL Tips Required: 22

Boxes of 300uL Tips Required: 1.0

1L Reagent Bottles

0 1L Bottle(s) for Primary Seed Media
0 1L Bottle(s) for Secondary Seed Media
1.0 1L Bottle(s) for Final Media 1
1.0 1L Bottle(s) for Final Media 2
0 1L Bottle(s) for Final Media 3
0 1L Bottle(s) for Final Media 4
0 1L Bottle(s) for Final Media 5

Total 1L Bottle(s) Required: 2.0

175mL Reagent Bottles

0 175mL Bottle(s) for Primary Seed Media
0 175mL Bottle(s) for Secondary Seed Media
0 175mL Bottle(s) for Final Stage Media
0 175mL Bottle(s) for Bolus Antifoam
0 175mL Bottle(s) for Bolus pH control

Total 175mL Bottle(s) Required: 0

Tubing Sets (12 way)

1 12-way line(s) required for antifoam
2 12-way line(s) required for pH control
1 12-way line(s) required for pumped feeds

Total 12-way Lines Required: 4

Tubing Sets (4 way)

0 4-way line(s) required for antifoam
0 4-way line(s) required for pH control
0 4-way line(s) required for pumped feeds

Total 4-way Lines Required: 0

Drip catcher Pads

3 Drip Pads Required

Air filters

6.0 Air Filters Required

2mL Eppendorf Tubes

0 2mL Eppendorfs required for Primary Seed harvest
0 2mL Eppendorfs required for Secondary Seed harvest
0 2mL Eppendorfs required for Final Stage harvest
0 2mL Eppendorfs required for Inducer
2 2mL Eppendorfs required for Primary Seed Samples
1.0 2mL Eppendorfs required for Secondary Seed Samples
0 2mL Eppendorfs required for Final Stage Event based Samples
0 2mL Eppendorfs required for Final Stage Sample Regime
0 2mL Eppendorfs required for Final Stage Atypical Samples

Total 2mL Eppendorfs required: 3.0

20mL Universals

0.0 20mL Universals required for Primary Seed harvest
0.0 20mL Universals required for Secondary Seed harvest
0 20mL Universals required for Final Stage harvest
0 20mL Universals required for Inducer
0 20mL Universals required for Primary Seed Samples
0.0 20mL Universals required for Secondary Seed Samples
0 20mL Universals required for Final Stage Event based Samples
0 20mL Universals required for Final Stage Sample Regime
0 20mL Universals required for Final Stage Atypical Samples

Total 20mL Universals required: 0.0

Labour

Total Working Hours: 48.75

Resources Outputs Summary:

Item:	Units	Cost (£)
Drip Catcher Pads	3	10.95
20mL Universals	0.0	0.0
Bioreactors (Total)	12	1749.96
Air Filters	6.0	63.0
175mL Reagent Bottles	0	0.0
300uL Tip Boxes	1.0	16.98
24DSW Plates	16.0	155.68
2mL Eppendorf Tubes	3.0	0.12
Tubing Sets (4-Way)	0	0.0
10mL Tip Boxes	13.0	139.75
1L Reagent Bottles	2.0	21.88
Tubing Sets (12-Way)	4	320.84

Total Consumables Cost Estimate:
£ 2479.16

Total Labour Cost Estimate:
£ 2599.84

Total Cost Estimate:

£ 5079.0

Figure 6.10. Example of the Resource Estimates Notebook for the ARC tool built in Jupyter Notebooks using the Python programming language. This includes a comprehensive summary of all of the required consumables and a resource and cost estimate for the whole run.

The inputs tested were some of those commonly seen to change between runs and therefore appeared to constitute a good set of test cases. These were; the number of bioreactors used in total (Section 6.4.1.), the bioprocess run structure and duration (Section 6.4.2.), the consumables discount from the supplier (Section 6.4.3.) and the sampling regime throughout the duration of the production stage culture (Section 6.4.4.). Each of these scenarios require assumptions which will be discussed individually throughout this section.

It should be noted that cost figures for the consumables are for illustrative purposes only.

6.4.1. Total Bioreactors

Single use bioreactors are the most expensive individual consumable used during an Ambr[®]250 bioprocess. As such it is one of the key factors to look at in terms of an effect on the cost of the run as a whole. The run has been assumed to be a 48hr final stage process, and that this is the only stage at which the Ambr[®]250 vessels are used. A 16 hour primary and secondary seed stage (in shake flasks) are also assumed, in order to be factored into total run time and labour requirement. This was a simple first test of the output response of the ARC tool.

Figure 6.11. shows that there is a linear trend in total costs and bioreactor cost. This is to be expected as the number of bioreactors used was changed equally each time. Interestingly, under these test conditions, reducing the number of final stage bioreactors, reduces total cost of run by approximately 2.9% per bioreactor, indicating that the contribution to run cost of the single use bioreactors is over a third (approximately 34.8%). It should also be noted that labour remains constant and is the largest contributor to overall cost. Labour is calculated using an approximate full time employee (FTE) salary, and estimating an hourly cost assuming a 37.5 hour per week contract.

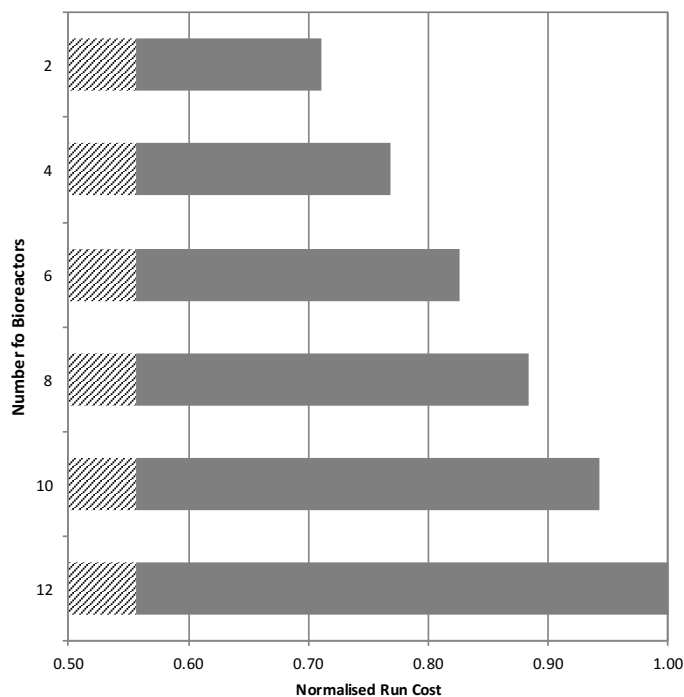


Figure 6.11. Effect of changing the number of production stage bioreactors used on the cost of a bioprocess run in the Ambr[®]250 system. Striped areas are the contribution to cost of labour, while solid grey is the cost due to consumables. Costs have been normalised to the highest total cost.

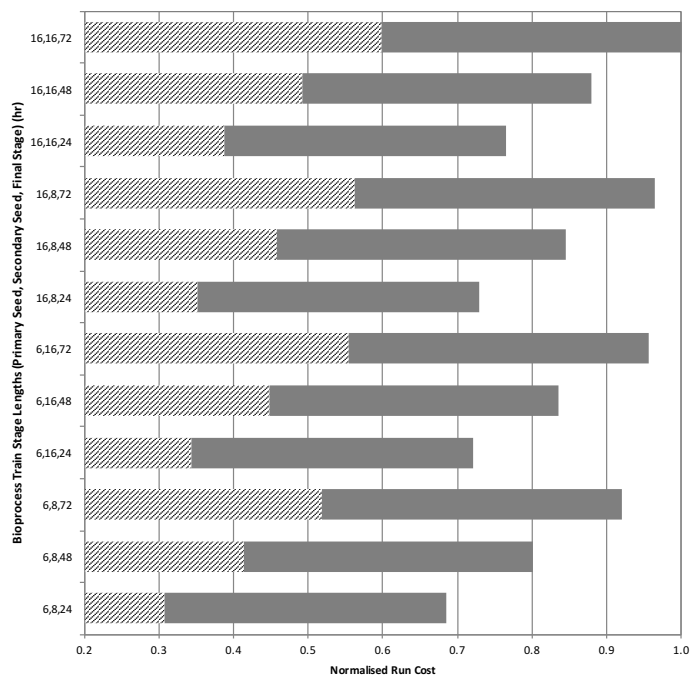


Figure 6.12. Effect of changing the duration of each of the stages of the bioprocess run on the cost of a bioprocess run in the Ambr[®]250 system. Striped areas are the contribution to cost of labour, while solid grey is the cost due to consumables. Costs have been normalised to the highest total cost.

6.4.2. Bioprocess Run Structure and Duration

The structure of the bioprocess train influences not only the number of bioreactors and other consumables used, but also the duration of a run and the required labour. As such, combinations of the structure and duration of the bioprocess train were tested for their influence on the overall cost, as well as the relative contributions to labour and consumables. It has been assumed that there were 10 final stage bioreactors, and a single primary and secondary seed stage (it was deemed unlikely that a bioprocess would run without the inclusion of seed stages). A four hourly sampling regime was also assumed. The combinations of bioprocess train structures and durations are shown in Table 6.1.

The overall process cost changes by almost a third between a 38 hour run, and a 104 hour run (total for all stages). This demonstrates the proportional impact of the overheads for a run. There is understandably a relationship between the overall run cost and its duration, as was seen previously, since labour is a major contributor to the total cost of a bioprocess development run. Figure 6.12. highlights that by shortening the final stage by 24 hours resulted in the run cost reducing by approximately 11%; interestingly the cost of consumables changed very little (~1%) despite the decrease in tip and microtitre plate usage. In many cases the cost of labour exceeded half of the cost of the maximum normalized run. In 8 of the 12 examples, the cost of labour exceeds the cost of consumables.

Table 6.1. Bioprocess train sequences and durations investigated for their effect on cost of a bioprocess run in the Ambr[®]250 system. All values are in hours.

Primary Seed Duration	6						16					
Secondary Seed Duration	8		6		8		16					
Production Stage Duration	24	48	72	24	48	72	24	48	72	24	48	72
Combination	6,8, 24	6,8, 48	6,8, 72	6,16, 24	6,16, 48	6,16, 72	16,8, 24	16,8, 48	16,8, 72	16,16, 24	16,16, 48	16,16, 72
Total	38	62	86	46	70	94	48	72	96	56	80	104

6.4.3. Supplier Discount

Discount provided by a consumables supplier could have a significant influence on the cost of each run, with greater discount often given for larger orders. However, use of a tool such as the ARC tool which would be capable of projecting consumables usage taking into account factors such as number of projects over a given period, their scheduled duration, and accurate prediction of demand could in turn lead to favourable costing. As such, a number of possible supplier discounts have been looked at (0%, 5%, 10%, 30% and 50%). Here, the cost of labour would not be impacted upon hence it is not included in the analysis.

A simple process incorporating 12 bioreactors, including a secondary seed in the Ambr[®]250 and 11 final stage bioreactors, run for a total of 64 hours with a two hourly sampling regime has been used as the baseline experiment. Although there is a proportional decrease in the consumables cost due to an increase in supplier discount, the impact on the overall cost of undertaking a run is not so great, with the maximum difference (due to a 50% discount) resulting in a reduction of just over 20% in the total cost. This is shown in Figure 6.13.

6.4.4. Sample Regime During Production Stage Culture

The ability to use the liquid handling arm of the Ambr[®]250 to carry out time-dependent sampling and storage is a distinct advantage of the system. As such, there is value in attempting to understand what the impact on cost is of using different sampling regimes. Greater frequency sampling means a more complete data set and more information from which to draw conclusions and make process decisions. However, it also means a greater burden on analytics and an increase in consumables usage.

In this analysis, ten production stage bioreactors were assumed to run for 48 hours, in addition to 16 hour primary and secondary seed stages in Ambr[®]250 vessels. Each of the seed stages would be sampled three times, and the sampling regime would be altered not only in terms of sample frequency, but for the inclusion of event-based sampling (e.g. pre-and post-induction). The timings included for this hypothetical run are not altered so again there is no impact on the cost of labour and it will not be discussed here.

Figure 6.14 shows a 15% difference in the consumables cost that can be attributed to the choice of sampling regime in this bioprocess. The majority of this cost coming from the increase in tip and storage plate usage. This is a significant contribution to the cost of a run and so demonstrates the need to consider what the increase in sample frequency offers in

terms of the objective of an experiment. For instance, if a higher density data set is going to enhance understanding of a process e.g. if knowledge of accurate substrate utilization rates are considered likely to aid in the development of a process, then the additional cost may be justified. Furthermore, it is shown that an additional 3.5% is added to the consumables cost by adding event based sampling to the regime. This is relatively minor and could lead to valuable insights, and so would likely be retained within the experimental design.

Sections 6.4.1 – 6.4.4 represent just a few examples of factors which could be investigated for their influence on the cost of the bioprocess. The comprehensive inclusion of potential inputs into the ARC tool means that a large number of combinations of parameters could be tested. This may be done with a view to understanding how to get the most value out of the bioprocess. In addition, it could also be used to understand the economic impact of, for example, a switch from complex to defined media, or changes to media component concentrations. These changes are highly convoluted, and understanding the impact on cost is an important part of decision making, and would be difficult to quantify by other means.

It has also been observed through this demonstration of the ARC tool that for most run configurations the labour is the major contributor to cost. However, it is worth considering that this is likely to be significantly smaller than it would be for a traditional stainless steel fermentation systems, which would not benefit from the advantages of single use technology (e.g. removed need for cleaning), many of which require significant time and labour.

6.5. Summary

The primary objective of this chapter was to develop a prototype tool for cost estimation for upstream bioprocess development runs in the Ambr[®]250 system. This has been achieved. In doing this the potential for expansion of the objective to include a broader range of outputs (e.g. scheduling, process documentation) was realised and so Version 2.0 of the ARC tool is under further development to include these.

In its current form, the ARC is a useful tool, currently implemented within Synthace for project costing and to provide insight into consumable resource demand. Progression from Version 1.0 to Version 2.0 of the ARC tool represents a significant improvement in functionality and usability.

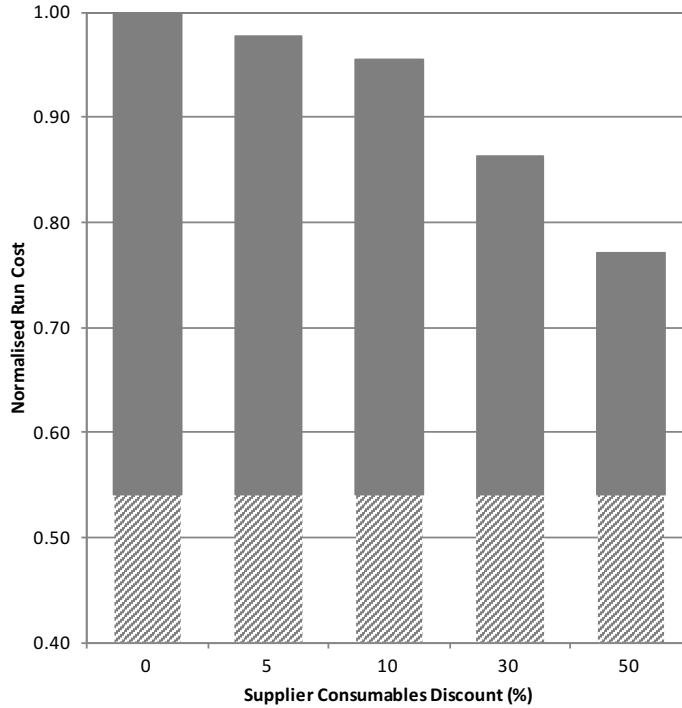


Figure 6.13. Effect of increasing the supplier discount on consumables on the cost of a bioprocess run in the Ambr[®]250 system. Striped areas are the contribution to cost of labour, while solid grey was the cost due to consumables.

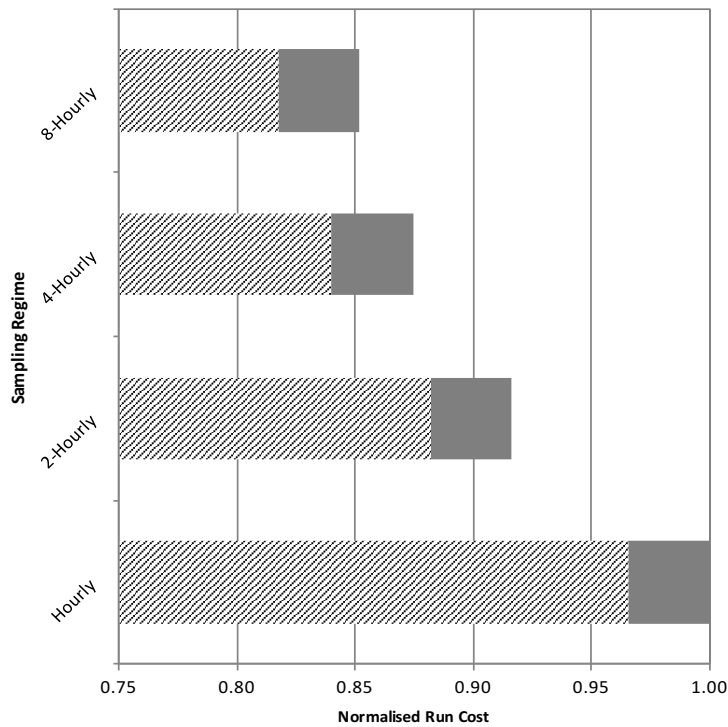


Figure 6.14. Effect of changing sampling regime on the cost of a bioprocess run in the Ambr[®]250 system. Striped areas are the contribution to cost of changing the sampling regime, while solid grey was the cost which can be attributed to the inclusion of event based sampling. Costs have been normalised to the highest total cost.

The ARC tool has been designed to include most important potential factors in an upstream bioprocess. However, due to the complexity these will change from run to run, and some may not be captured. Currently, the majority of factors which contribute to the potential variability are included in the calculations for estimating bioprocess cost, meaning the values are a good approximation of the actual cost. As the ARC tool is expanded and refined, this accuracy will continue to improve. Undertaking each of the case studies described in Section 6.4 has demonstrated the ease of use and functionality of this second iteration of the ARC tool.

Operation of an Ambr®250 upstream process is expensive, and, although generally cheaper than a traditional stainless steel fermentation (especially when considering the high-throughput, parallel processing capabilities), the cost must be justified. The first step in this is being able to accurately determine the cost of a run, and the ARC tool provides a means of achieving this and a method for tracking it.

6.6. Future Developments

In its current form, Version 2.0 of the ARC tool makes it useful as a costing and decision making tool for Ambr®250 bioprocess development runs. There are a number of areas in which the functionality or input variables of the model could be expanded with a view to making it a more inclusive and accurate resource.

The ARC tool represents the early stages of a tool which, with additional development, could be a means of standardising the generation of bioprocess documentation and run files for bioprocess development on the Ambr®250 system. In order to achieve this, there are a number of areas that will need to be worked on.

Improved functionality is necessary for the ARC tool to be most useful. One significant advancement which should be made is the ability to import a DoE design file e.g. from JMP or Design Expert software, to have this populate a number of the input parameters such as number of bioreactors, media compositions etc. This would improve the efficiency and accuracy of completing the inputs notebook. It would also likely provide a route to prioritising the most important factors to be included.

This in turn may lead to a significant extension to functionality, by developing the ARC to

be capable of generating process documentation and run files for the Ambr[®]250 system using template document structures and incorporating some additional key inputs. A considerable amount of the information included in process documentation is repeated from run to run. As such this is something that could be streamlined with the use of templates. There is a simple example of this included in the images from the ARC tool (Figure 6.8, 6.9 and 6.10).

In order to increase the accuracy of resource demand projection, the ARC tool should be integrated with a scheduling tool. This will enable the projection of consumables usage at suitable intervals e.g. one, three, six and 12 months. This would aid risk mitigation ensuring consumable availability does not become a bottleneck, and conversely that excess consumables are not purchased.

An additional improvement may come from developing input notebooks with constraints incorporated within them. For example, input notebooks could be constructed to allow for different organisms, and the process constraints that these impose. Alternatively input notebooks could be constrained by run objective e.g. seed train optimisation or production stage robustness testing.

Another area which could be improved is in expanding the stages of the run which can be cost projected. Currently, the ARC tool is capable of estimating the cost of fermentation, but there is a significant resource burden associated with analytics. Current approximations suggest that these are around the same as the cost of the fermentation run, depending on the analytical methods used and sample numbers. A principal objective when undertaking a bioprocess development run is the generation and interpretation of data which informs the next stage of development until a robust, optimised, validated production process is formalised. To this end, analytics is vital. Additionally, the cost data itself will need to be expanded and updated on a periodic basis in order to ensure accuracy and relevance of the cost estimations.

Finally, in order to integrate the ARC tool properly with Synthace's software platform, in time it will need to be written in the Antha programming language. This will allow it to operate as an element within the wider design and execution of a bioprocess.

7. Conclusions and Future Work

7.1. Conclusions

Microbial fermentation and biocatalysis have long been applied in an industrial context for the generation of commercially valuable biomolecules (Section 1.2.1). Advancements in genetic engineering techniques provide routes to new or improved biomanufacturing processes, but there are limitations to the expansion of their use. The findings that can be translated from high throughput screening at microwell scales are limited due to the restrictions on oxygen mass transfer (Section 1.2.7), and the relative oxygen demands of microbial expression systems (Section 1.2.4). Scaling into single use bioreactors at pilot or production scale, which is the direction in which the industry is moving, comes with additional challenges. These include a lack of detailed engineering characterisation (Section 1.2.7.4), and the fact that many commercially available SUBs have been designed for mammalian expression systems, where the specific oxygen demand is significantly less (Dreher et al. 2013).

The aim of this thesis was to determine the applicability of commercially available single use bioreactor technologies for microbial fermentation; in particular microbial whole cell bioconversions. Specific objectives were: to optimise a whole cell P450 bioconversion in *E.coli* to provide a commercially relevant expression system with high oxygen demand for further investigation (Chapter 3); develop methods to improve the accuracy of oxygen mass transfer quantification in microwell plates (Chapter 4) and commercially relevant single use bioreactors (Chapter 5), use these to build models to characterise k_{La} and OUR in each bioreactor format; and finally, to build a tool to evaluate the economic feasibility and sensitivity of using a SUB system for performing microbial whole cell bioconversions (Chapter 6).

In order to establish a foundation for investigations into the applicability of single use bioreactors for microbial cultivation, the oxygen demand of a whole cell P450 monooxygenase bioconversion in *E.coli* BL21 was characterised in Chapter 3. P450 systems often have low expression levels (Section 1.2.2) and so enhancement of the enzyme activity level was first explored using multifactorial experimental design (Section 1.2.10) in conjunction with microwell scale experiments (Section 2.5). Enzyme activity levels were enhanced by increasing shaking speed (Figure 3.2) and post induction temperature (Figure 3.6). The optimised culture conditions resulted in a 3.3-fold increase in bioconversion product titre (Table 3.4). The optimised conditions were subsequently scaled-up 3000-fold using three different fermentation strategies (Section 3.2): batch, induced batch and induced fed-batch.

This resulted in peak oxygen demands in the range of 5.7 to 25.8 mmolL⁻¹min⁻¹ depending on the fermentation strategy employed (Table 3.6). The inability of microwells to support these peak demands was demonstrated, and the identification of the relationship between the three main contributors to oxygen mass transfer (maintenance, growth and bioconversion) determined. This led to the identification of the mechanisms for oxygen utilisation, with biomass accumulation shown to be the priority over additional cellular activities such as bioconversion. The different demands for oxygen in whole cell oxidative bioconversions have not been thoroughly investigated, and so this finding improves understanding of whole cell oxidative bioconversions and how to improve their development for commercial application.

Due to the main requirement for oxygen being associated with biomass growth (Table 3.7) and the low productivity of the *E.coli* PQR368 strain, subsequent investigations focused on culture of an *E.coli* strain containing a fluorescent reporter (Section 2.6) in order to more readily measure the responses of the expression system in terms of productivity. Given the importance of oxygen mass transfer in microbial fermentation (Section 1.2.4), an improved methodology for determination of oxygen transfer values (including OUR, k_{La} and OTR) based on the dynamic gassing out method was developed in Chapter 4. This involved building a linear model for k_{La} in 24 DSW plates using the dynamic gassing out method (Section 4.2), before comparing online DOT profiles with the linear model in order to determine OUR values during culture.

Using the improved method with multifactorial statistical analysis, models were built to characterise k_{La} and OUR in 24 DSW plates. Experiments showed that k_{La} increased as a function of shaking speed and reduced fill volume (Figure 4.9). The maximum value of k_{La} was 103.5 h⁻¹ (Figure 4.3) while the maximum OUR observed was approximately 600 mgO₂L⁻¹h⁻¹ (Table 4.11). Additional models were constructed for biomass accretion and recombinant protein expression in *E.coli*, enabling the approximation of process parameter set points for matched oxygen mass transfer between 96 and 24 DSW plates.

Since the overall aim of this work was to explore scale-up of microbial fermentation into single-use bioreactors the oxygen transfer capability of two representative single-use bioreactor designs was explored in Chapter 5. A tank liner style SUB, the Xcellerex XDR-10 (Figure 2.2) and an Ambr[®]250 (Figure 2.3) of rigid construction were the single use bioreactors characterised. Using a BioFlo 310 traditional benchtop STR (Figure 2.1) as a reference standard, the bioreactors were characterised using DoE Response Surface Methodology (RSM) designs investigating process relevant parameters and conditions. Models were built

for the quantification of oxygen mass transfer coefficients in the BioFlo310 (Figure 5.1 to 5.7), the XDR-10 (Figure 5.9 to 5.11) and the Ambr[®]250 (Figure 5.14 to 5.17). Smaller influences on oxygen mass transfer were shown to be highly system dependent, a finding which would not have been possible without the use of a multifactorial DoE approach.

The k_{La} in the Ambr[®]250 was shown to be similar to that of the traditional STR across the majority of the experimental landscape (Figure 5.19). Maximum k_{La} values observed were 1054, 616 and 65 h⁻¹ (Table 5.12) for the benchtop STR, the Ambr[®]250 and the XDR-10 respectively. Analysis of the peak oxygen uptake rates determined in Chapter 3, and approximately 300 industrial microbial fermentations (carried out by the author) showed that the Ambr[®]250 is capable meeting the peak oxygen demands of microbial whole cell oxidative bioconversions, and that the XDR-10 is not.

Once the applicability to industrial microbial fermentation of the Ambr[®]250 was shown (Section 5.6.2), the wider industrial utilisation of this type of single-use bioreactor was considered in Chapter 6. It was pertinent to investigate the resource demand of using a system in which many components are single use, and one run may change dramatically from the next. As such an Ambr resourcing and costing (ARC) tool has been developed in the Python programming language in order to rapidly capture the resource demands of a given bioprocess development run in the Ambr[®]250 system and aid in project costing and planning (Section 6.3). The ARC tool was used to carry out sensitivity analyses on an Ambr[®]250 bioprocess run, highlighting that the number of bioreactors used could save up to 35% of the run cost (Figure 6.11) and the length and number of stages of the bioprocess train approximately 32% (Figure 6.12). Additional observations using this tool highlighted labour as the greatest contributor to cost, with replacement single use bioreactors the next most significant. This tool is now implemented within the industrial sponsor company for this research.

Overall, the results presented in this thesis have shown the applicability of commercially available single use bioreactors for microbial whole cell bioconversions. The investigation has also yielded novel insights into the mechanism of oxygen utilisation (Section 3.2.7), the characterisation of oxygen mass transfer coefficients in scale down platforms (Section 4.2) and devised methodologies for the improved quantification of k_{La} s in SUBs (Section 5.2 to 5.4) and OURs in microwell systems (Section 4.3). In the following section options for future work are considered.

7.2. Future Work

Now that the methodology has been established for optimisation and scaling of a microbial fermentations in small scale single-use systems (Section 3), this multifactorial optimisation and analysis should be undertaken with a wider range of microbial expression systems which carry out a diverse range of bioconversions or expression of different recombinant proteins. This should include industrially relevant P450 systems such as the one in this thesis, which are likely to have the highest oxygen demand. It will be critical to understand the oxygen demands of different expression systems in order to develop the most suitable processes and technologies.

Something that has become clear throughout this work is that there is a need to develop new high throughput systems, including microwells, with higher oxygen transfer rates which match larger scale STRs. These systems should also be capable of carrying out different operating strategies such as fed batch and induced fermentations. It is important that there be a clearer definition of the optimum use of microwells in early stage microbial development, understanding what information can be reliably gained from microwell studies.

Regarding the characterisation of microbial fermentations in microwell plates (specifically with respect to oxygen mass transfer), there are several additional pieces of work which should be undertaken in order to further this area and extend its practical application. These include development of a more detailed model to incorporate more factors, expand the ranges used and increase the number of experimental points in them to determine whether these also have an effect on microwell oxygen mass transfer. It would also be useful to investigate whether, even over this relatively small design space, the model is non-linear and a local optimum could be identified. Additionally, expanding the multifactorial design to include greater range of (particularly) agitation speeds and fill volumes may aid with this.

Characterisation of O₂ mass transfer for a greater number of relevant scale down bioreactor geometries is crucial, as many of the potentially influencing factors need to be taken into account. This will require accurate measurement of oxygen concentration in 96DSW to build and validate multifactorial models. Currently, the technology to do this across an entire plate geometry, is not available. As such an advancement in the available apparatus is required, either as a small probe (or set of probes) which could be used in a 96 DSW without influencing the hydrodynamics, or, a non-invasive technology similar to the PreSens SDR®

system which is used in this work with 24 DSW plates (Section 2.6). In turn, this would enable the investigation of overlaps in oxygen mass transfer values, all the way from microwells up to stirred tank bioreactors.

It is important to note the increasing integration of mathematical and computational tools (such as DoE) into bioprocess development. The insight that these can help to provide, when considered in conjunction with the generation of increasingly large data sets generated by high throughput processing tools means that bioprocess development could be streamlined if these tools are harnessed effectively. In the context of this research, it would be beneficial to develop improved correlations and build a predictive tool which, based on literature correlations for k_{La} as well as ongoing research, would estimate oxygen mass transfer in a particular bioreactor geometry with the only experimental requirement being validation of the models. To that end, bioprocess validation runs should be undertaken to support the industrial data in the conclusion that the Ambr[®]250 is suitable for cultivation of microbial expression systems carrying out oxidative bioconversions.

Now that the principle has been demonstrated for showing where single use bioreactors can be applied in the fermentation of an *E.coli* expression system, it is now important to interrogate single use bioreactors in addition to the Ambr[®]250 and the XDR-10 (investigated here). Multifactorial characterisation of larger scale systems such as the Xcellerex XDR MO from GE Healthcare and the Hyperforma SUF from ThermoFisher, designed for cultivation of microbial expression systems, will provide an insight into the current potential for fermentation of microbial whole cell bioconversions at a more manufacturing relevant scale. This will then need to be coupled with characterisation of additional expression systems and bioconversions in order to understand which microbial expression systems, fermentations and bioconversions can be undertaken in which commercially available technologies. Indeed, this will also inform on where the shortfalls lie and what the requirements are for the next generation of single use technologies.

Finally, expansion of the Ambr[®]250 Resourcing and Costing (ARC) tool, will improve its usefulness and uptake within the Synthace organisation. This should include the ability to incorporate DoE design files from programs such as JMP and Design Expert such that this information would populate inputs for resource calculation. In addition, integration of a scheduling tool which would incorporate all planned runs in order to project consumables usage, resourcing and costing in one, three, six and 12 month intervals. This then aids risk mitigation, ensuring consumable availability does not become a resource bottleneck, and

conversely that excessive single use consumables (with defined shelf lives), are not unnecessarily purchased. In turn, this should lead to the most significant improvement in functionality, by having the ARC capable of generating process documentation and run files for the Ambr[®]250 using document templates, and prefabricated design file structures.

In summary, a clear strategic priority for future work, is the expansion of single use bioreactor technologies and microbial expression systems that are comprehensively characterised using the methodologies developed or improved in this thesis. This will ensure a robust engineering understanding of both the demand and supply of oxygen to microbial fermentations and where commercially available SUBs can be applied in this area of bioprocess development.

References

- Adinarayana, K. & Ellaiah, P., 2002. Response surface optimization of the critical medium components for the production of alkaline protease by a newly isolated *Bacillus* sp. *J Pharm Pharmaceut Sci*, 5(3), pp.272–278.
- Alcaíno, J. et al., 2012. Modeling the interfacial interactions between CrtS and CrtR from *Xanthophyllomyces dendrorhous*, a P450 system involved in astaxanthin production. *Journal of agricultural and food chemistry*, 60(35), pp.8640–7.
- Anderlei, T., Zang, W., Papaspyrou, M. & Büchs, J. 2004. Online respiration activity measurement (OTR, CTR, RQ) in shake flasks. *Biochemical Engineering Journal*, 17, p187-194.
- Anderson, M.J. & Whitcomb, P.J., 2007. *DOE Simplified Second.*, CRC Press.
- Andrew, S., 1982. Gas-Liquid Mass Transfer in Microbiological Reactors. *Trans. Inst. Chem. Eng.*, 60, pp.3–13.
- Andrianantoandro, E. et al., 2006. Synthetic biology: new engineering rules for an emerging discipline. *Molecular Systems Biology*, 2(1), p.2006-28.
- Anzai, Y. et al., 2012. Function of cytochrome P450 enzymes MycCl and MycG in *Micromonospora griseorubida*, a producer of the macrolide antibiotic mycinamicin. *Antimicrobial agents and chemotherapy*, 56(7), pp.3648–56.
- Arinc, E., Schenkman, J.B. & Hodgson, E., 1999. *Molecular and Applied Aspects of Oxidative Drug Metabolising Enzymes*, Plenum Publishers.
- Baboo, J., 2012. *Automated High-throughput Approaches for the development and investigation of Novel Oxidative Biocatalytic Processes*. Thesis. University of London.
- Baboo, J.Z. et al., 2012. An automated microscale platform for evaluation and optimization of oxidative bioconversion processes. *Biotechnology progress*, 28(2), pp.392–405.
- Bak, S. et al., 2011. Cytochromes p450. *The Arabidopsis book / American Society of Plant Biologists*, 9, p.0144.
- Baldwin, C.V.F. & Woodley, J.M., 2006. On Oxygen Limitation in a Whole Cell Biocatalytic Baeyer – Villiger Oxidation Process. *Biotechnology and Bioengineering*, 95 (1), pp.3–10.
- Bandyopadhyay, B., Humphrey, A.E. & Taguchi, H., 1967. Dynamic measurement of the volumetric oxygen transfer coefficient in fermentation systems. *Biotechnology and*

Bioengineering, 9(4), pp.533–544.

Bareither, R. et al., 2013. Automated disposable small scale reactor for high throughput bioprocess development: A proof of concept study. *Biotechnology and Bioengineering*, 110(12), pp.3126–3138.

Barker, T.B. & Milivojevich, A., 2016. *Quality by Experimental Design* 4th Editio., CRC Press.

Bartholomew, W., Karow, E. & Sfat, M., 1950. Oxygen transfer and agitation in submerged fermentations. Mass transfer of oxygen in submerged fermentation of *Streptomyces griseus*. *Ind. Eng. Chem.*, 42, pp.1801–1809.

Beilen, J.B. va. & Li, Z., 2002. Enzyme technology: an overview. *Current Opinion in Biotechnology*, 13(4), pp.338–344.

van Beilen, J.B. et al., 2003. Practical issues in the application of oxygenases. *Trends in biotechnology*, 21(4), pp.170–7.

Bell, S.G. et al., 2010. A cytochrome P450 class I electron transfer system from *Novosphingobium aromaticivorans*. *Applied microbiology and biotechnology*, 86(1), pp.163–75.

Benadda, B., Ismaili, S. & Otterbein, M., 1997. Relation of mechanical power to gas holdup and mass transfer in an agitated vessel. *Chemical and Engineering Technology*, 20(3), pp.192–198.

Bernhardt, R., 2006. Cytochromes P450 as versatile biocatalysts. *Journal of biotechnology*, 124(1), pp.128–45.

Betts, J.P.J. et al., 2014. Impact of aeration strategies on fed-batch cell culture kinetics in a single-use 24-well miniature bioreactor. *Biochemical Engineering Journal*, 82, pp.105–116.

Bhat, M.K., 2000. Cellulases and related enzymes in biotechnology. *Biotechnology advances*, 18(5), pp.355–83.

Biesecker, B.O., 1972. Gassing of liquids in stirred tanks. *VDI-Forschungsh.*, (554), p.4.

Bliem, R. & Katinger, H., 1988. Scale-up engineering in animal cell technology: Part II. , 86(1986).

Boesten, W., Moody, H. & Roos, E., 1996. Process for the recovery of ampicillin from enzymatic acylation Of 6-aminopenicillanic acid.

Box, G.E.P., Hunter, J.S. & Hunter, W.G., 2005. *Statistics for Experiments*, Wiley.

- Brecht, R., 2009. Disposable Bioreactors: Maturation into Pharmaceutical Glycoprotein Manufacturing. In *Disposable Bioreactors*. pp. 1–31.
- Brückner, R. & Titgemeyer, F., 2002. Carbon catabolite repression in bacteria: Choice of the carbon source and autoregulatory limitation of sugar utilization. *FEMS Microbiology Letters*, 209(2), pp.141–148.
- Büchs, J., 2001. Introduction to advantages and problems of shaken cultures. *Biochemical Engineering Journal*, 7(2), pp.91–98.
- Buckland, B.C. et al., 1988. Improved performance in viscous mycelial fermentations by agitator retrofitting. *Biotechnology and Bioengineering*, 31(7), pp.737–742.
- Burton, S.G., 2003. Oxidizing enzymes as biocatalysts. *Trends in Biotechnology*, 21(12), pp.543–549.
- Çalik, P. et al., 2004. Oxygen transfer effects on recombinant benzaldehyde lyase production. *Chemical Engineering Science*, 59(22–23), pp.5075–5083.
- Çalik, P., Yilgör, P. & Demir, A.S., 2006. Influence of controlled-pH and uncontrolled-pH operations on recombinant benzaldehyde lyase production by *Escherichia coli*. *Enzyme and Microbial Technology*, 38(5), pp.617–627.
- Cao, L., 2005. Immobilised enzymes: science or art? *Current opinion in chemical biology*, 9(2), pp.217–26.
- Carragher, J.M. et al., 2001. The use of oxygen uptake rate measurements to control the supply of toxic substrate: Toluene hydroxylation by *Pseudomonas putida* UV4. *Enzyme and Microbial Technology*, 28(2–3), pp.183–188.
- de Carvalho, C.C.C.R., 2011. Enzymatic and whole cell catalysis: finding new strategies for old processes. *Biotechnology advances*, 29(1), pp.75–83.
- Casas, J., 1996. *Producción de Soforolípidos con Candida bombicola*. Universidad Complutense, Madrid.
- Castro, G.R. & Knubovets, T., 2003. Homogeneous biocatalysis in organic solvents and water-organic mixtures. *Critical reviews in biotechnology*, 23(3), pp.195–231.
- Chen, A. et al., 2009. Twenty-four well plate miniature bioreactor system as a scale-down model for cell culture process development. *Biotechnology and bioengineering*, 102(1), pp.148–60.
- Cheng, A.A. & Lu, T.K., 2012. Synthetic Biology: An Emerging Engineering Discipline.

- Annual Review of Biomedical Engineering*, 14(1), pp.155–178.
- Chibata, I. & Tosa, T., 1977. Transformations of organic compounds by immobilised microbial cells. *Advances in Applied Microbiology*, 22, pp.1–25.
- Chisti, Y. & Moo-Young, M., 2001. Bioreactor Design. In C. Ratledge & B. Kristiansen, eds. *Basic Biotechnology*. Cambridge University Press, pp. 151–172.
- Choi, J-M., Han, S-S. & Kim, H-S. 2015. Industrial applications of enzyme biocatalysis: Current status and future aspects. *Biotechnology Advances*. 33: 1443-1454.
- Chu, L. & Robinson, D.K., 2001. Industrial choices for protein production by large-scale cell culture. *Current opinion in biotechnology*, 12(2), pp.180–7.
- Clomberg, J.M., Crumbley, A.M. & Gonzalez, R. 2018. Industrial biomanufacturing: the future of chemical production. *Science*. 355, 38.
- Cooper, C., Fernstrom, G. & Miller, S., 1944. Performance of Agitated Gas Liquid Contactors. *Ind. Eng. Chem*, 36(6), pp.504–509.
- Cooper, D.Y. et al., 1965. Photochemical Action Spectrum of the Terminal Oxidase of Mixed Function C) xidase Systems. *Science*, 147(3656), pp.400–402.
- Cooper, G.M., 2000. *The Cell: A Molecular Approach*, Sinauer Associates.
- Corcos, L. et al., 2012. Human Cytochrome P4504F3: Structure, Functions and Prospects. *Drug metabolism and Drug Interactions*, 27(2), pp.63–71.
- Cragg, G.M. & Newman, D.J., 2005. Plants as a source of anti-cancer agents. *Journal of ethnopharmacology*, 100(1–2), pp.72–9.
- Croteau, R. et al., 2006. Taxol biosynthesis and molecular genetics. *Phytochemistry reviews: proceedings of the Phytochemical Society of Europe*, 5(1), pp.75–97.
- Czitrom, V., 1999. One-Factor-at a Tim Versus Designed Experiments. *The American Statistician*, 53(2), pp.126–131.
- Danckwerts, P. V, 1951. Significance of Liquid-Film Coefficients in Gas Absorption. *Ind. Eng. Chem*, 43(6), pp.1460–1467.
- Degtyarenko, K.N. & Archakov, a I., 1993. Molecular evolution of P450 superfamily and P450-containing monooxygenase systems. *FEBS letters*, 332(1–2), pp.1–8.
- Deshpande, R.R. & Heinzle, E., 2004. On-line oxygen uptake rate and culture viability measurement of animal cell culture using microplates with integrated oxygen sensors. *Biotechnology Letters*, 26(9), pp.763–767.

- DiCosimo, R., McAuliffe, J., Poulouse, A.J. & Bohlmann, G. 2013. Industrial use of immobilized enzymes. *Chem. Soc. Rev.* 42, 6347-6474.
- Diehl, B. et al., 2015. A Biopharmaceutical Industry Perspective on Single-Use Sensors for Biological Process Applications. *BioPharm International*, 28(4), pp.28–31.
- Djelal, H. et al., 2012. Continuous culture for the bioproduction of glycerol and ethanol by *Hansenula anomala* growing under salt stress conditions. *Annals of Microbiology*, 62(1), pp.49–54.
- Doig, S.D. et al., 2002. Reactor operation and scale-up of whole cell Baeyer-Villiger catalyzed lactone synthesis. *Biotechnology progress*, 18(5), pp.1039–46.
- Doig, S.D. et al., 2005. Modelling surface aeration rates in shaken microtitre plates using dimensionless groups. *Chemical Engineering Science*, 60(10), pp.2741–2750.
- Doran, P.M.P., 1995. Bioprocess Engineering Principles. *Bioprocess Engineering Principles*, pp.426–439.
- Dragan, C., Blank, L. & Buriak, M., 2006. Increased TCA cycle activity and reduced oxygen consumption during cytochrome P450-dependent biotransformation in fission yeast. *Yeast*, (23), pp.779–794.
- Dreher, T. et al., 2013. Microbial High Cell Density Fermentations in a Stirred Single-Use Bioreactor. *Disposable Bioreactors II*, pp.127–147.
- Duetz, W. et al., 2000. Methods for Intense Aeration, Growth, Storage and Replication of Bacterial Strains in Microtiter Plates. *Applied and environmental microbiology*, (66), pp.2641–2646.
- Duetz, W. a, 2007. Microtiter plates as mini-bioreactors: miniaturization of fermentation methods. *Trends in microbiology*, 15(10), pp.469–75.
- Duetz, W. a & Witholt, B., 2004. Oxygen transfer by orbital shaking of square vessels and deepwell microtiter plates of various dimensions. *Biochemical Engineering Journal*, 17(3), pp.181–185.
- Dussap, C., Decorps, J. & Gros, J., 1985. Transfert d'oxygene en presence de polysaccharides exocellulaires dans un fermenteur agite aeré et dans un fermenteur de type gazosiphon. *Entropie*, 21(123), pp.11–20.
- Eaton, A.D. et al., 2005. *Standard Methods for the Examination of Water and Wastewater* 21st Editi., American Public Health Association.

- Edwards, V.H., 1970. The influence of high substrate concentrations on microbial kinetics. *Biotechnology and bioengineering*, 12(5), pp.679–712.
- Eibl, R. et al., 2010. Disposable bioreactors: the current state-of-the-art and recommended applications in biotechnology. *Applied microbiology and biotechnology*, 86(1), pp.41–9.
- Ellert, A. & Vikstrom, C., 2014. Design of Experiments with Small-Scale Bioreactor Systems: Efficient Bioprocess Development and Optimisation. *Bioprocess International*. 12(8), pp.10-13.
- Endy, D., 2005. Foundations for engineering biology. *Nature*, 438(7067), pp.449–453.
- Erlenmeyer, E., 1860. Zur chemischen und pharmazeutischen Technik. *Zeitschrift für Chemie und Pharmacie*, 3, pp.21–22.
- Estrada, J.M., Dudek, A., Muñoz, R. & Quijano, G. 2014. Fundamental study on gas-liquid mass transfer in a biotrickling filter packed with polyurethane foam. *J Chem Technol Biotechnol*. 89: 1419-1424.
- Falck, J.R. et al., 2001. Practical , enantiospecific syntheses of 14 , 15-EET and leukotoxin B (vernolic acid). , 42, pp.4131–4133.
- Fandrey, J. et al., 1990. Role of Cytochrome P450 in the Control of the Production of Erythropoietin. *Life Sciences*, 47(c), pp.127–134.
- Fang, X., Kobayashi, Y. & Halpert, J.R., 1997. Stoichiometry of 7-ethoxycoumarin metabolism by cytochrome P450 2B1 wild-type and five active-site mutants. *FEBS Letters*, 416(1), pp.77–80.
- Feijen, J., Heijnen, J.J. & Van't Riet, K., 1987. Gas hold up and flooding in large-scale fermenters. In *Symposium on mixing and dispersion processes. Inst Chem Eng. Delft Technical University*.
- Ferreira-Torres, C., 2008. *Microscale Process Characterisation of Oxidative Bioconversions. PhD Thesis*. University of London.
- Fleishaker, R.J. & Sinskey, A.J., 1981. Microbiology and Biotechnology Applied Oxygen Demand and Supply in Cell Culture. , pp.193–197.
- Fotheringham, I. et al., 2006. Biocatalysis : Enzymes , Mechanisms and Bioprocesses Preparative deracemization of unnatural amino acids. , (November 2005), pp.21–22.
- Fuchs, R., Ryu, D.D.Y. & Humphrey, A.E., 1971. Effect of Surface Aeration on Scale-Up Procedures for Fermentation Processes. *Industrial & Engineering Chemistry Process Design*

and Development, 10(2), pp.190–196.

Fukuda, H. et al., 2008. Whole-cell biocatalysts for biodiesel fuel production. *Trends in biotechnology*, 26(12), pp.668–73.

Fukui, Y. et al., 2003. A rationale for the shift in colour towards blue in transgenic carnation flowers expressing the flavonoid 3',5'-hydroxylase gene. *Phytochemistry*, 63(1), pp.15–23.

Fulco, A.J., 1991. P450BM3 and other inducible bacterial P450 Cytochromes: Biochemistry and Regulation. *Annual review of Pharmacology and Toxicology*, 31, pp.177–203.

Funke, M. et al., 2010. Microfluidic biolector-microfluidic bioprocess control in microtiter plates. *Biotechnology and bioengineering*, 107(3), pp.497–505.

Gaden, E.L., 1962. Improved shaken flask performance. *Biotechnology and Bioengineering*, 4(1), pp.99–103.

Gallihier, P., 2008. Achieving High-Efficiency Production with Microbial Technology in a Single-Use Bioreactor Platform. *BioProcess International December*, pp.2–5.

Gallihier, P., 2007. Review of Single Use Technologies in Biomanufacturing. Review of Single Use Manufacturing Technologies. pp.1-52.

García-Ochoa, F., Castro, E.G. & Santos, V.E., 2000. Oxygen transfer and uptake rates during xanthan gum production. *Enzyme and Microbial Technology*, 27(9), pp.680–690.

Garcia-Ochoa, F. & Gomez, E., 2009. Bioreactor scale-up and oxygen transfer rate in microbial processes: an overview. *Biotechnology advances*, 27(2), pp.153–76.

Garcia-Ochoa, F. et al., 2010. Oxygen uptake rate in microbial processes: An overview. *Biochemical Engineering Journal*, 49(3), pp.289–307.

Garcia-Ochoa, F. & Gomez, E., 1998. Mass transfer coefficient in stirred tank reactors from xanthan gum solutions. *Biochemical Engineering Journal*, 1(1), pp.1–10.

Gavrilescu, M. & Chisti, Y., 2005. Biotechnology - A sustainable alternative for chemical industry. *Biotechnology Advances*, 23(7–8), pp.471–499.

Gill, N.K. et al., 2008. Quantification of power consumption and oxygen transfer characteristics of a stirred miniature bioreactor for predictive fermentation scale-up. *Biotechnology and Bioengineering*, 100(6), pp.1144–1155.

Gillam, E.M. et al., 2000. Oxidation of indole by cytochrome P450 enzymes. *Biochemistry*, 39(45), pp.13817–24.

Gillam, E.M. & Guengerich, F.P., 2001. Exploiting the versatility of human cytochrome P450

- enzymes: the promise of blue roses from biotechnology. *IUBMB life*, 52(6), pp.271–7.
- Gillam, E.M.J., 2008. Engineering cytochrome p450 enzymes. *Chemical research in toxicology*, 21(1), pp.220–31.
- Gillera, C., Herson, A. & Murray, P., 2010. Induction of Enzyme Cocktails by Low Cost Carbon Source for Production of Monosaccharide Rish. 5, pp.634–649.
- Girhard, M. et al., 2009. Regioselective biooxidation of (+)-valencene by recombinant *E. coli* expressing CYP109B1 from *Bacillus subtilis* in a two-liquid-phase system. *Microbial cell factories*, 8(4), p.36.
- Glacken, M.W., Fleischaker, R.J. & Sinskey, a. J., 1983. Mammalian cell culture: engineering principles and scale-up. *Trends in Biotechnology*, 1(4), pp.102–108.
- Gomez, E. et al., 2006. Oxygen-uptake and mass-transfer rates on the growth of *Pseudomonas putida* CECT5279: Influence on biodesulfurization (BDS) capability. *Energy and Fuels*, 20(4), pp.1565–1571.
- Gomez, E. et al., 2006. Oxygen transport rate on *Rhodococcus erythropolis* cultures: Effect on growth and BDS capability. *Chemical Engineering Science*, 61(14), pp.4595–4604.
- Goos, P. & Jones, B., 2011. *Optimal Design of Experiments: A Case Study Approach* L. John Wiley & Sons, ed.,
- Grebe, A. et al., 2014. Innovations in Cell Culture SECTION 1: Upstream Technologies. Design of Experiments with Small-Scale Bioreactor Systems for Efficient Bioprocess Development and Optimization Integrated Optical Single-Use Sensors: Moving Toward a True Single-Use Factory for. *BioProcess International*, 12(5).
- Greenberg, W. a et al., 2004. Development of an efficient, scalable, aldolase-catalyzed process for enantioselective synthesis of statin intermediates. *Proceedings of the National Academy of Sciences of the United States of America*, 101(16), pp.5788–93.
- Gros, J.B., Dussap, C.G. & Catte, M., 1999. Estimation of O₂ and CO₂ Solubility in Microbial Culture Media. , pp.923–927.
- Guengerich, F.P., 2008. Cytochrome p450 and chemical toxicology. *Chemical research in toxicology*, 21(1), pp.70–83.
- Guengerich, F.P., 2002. Cytochrome P450 enzymes in the generation of commercial products. *Nature reviews. Drug discovery*, 1(5), pp.359–66.
- Guengerich, F.P., 1995. Cytochrome P450 proteins and potential utilization in

- biodegradation. *Environmental health perspectives*, 103 Suppl, pp.25–8.
- Gupta, A. & Rao, G., 2003. A study of oxygen transfer in shake flasks using a non-invasive oxygen sensor. *Biotechnology and Bioengineering*, 84(3), pp.351–358.
- Gupta, A.K. & Gover, M.D., 2007. Azelaic acid (15% gel) in the treatment of acne rosacea. *International journal of dermatology*, 46(5), pp.533–8.
- Gupta, M.N. et al., 2011. Nanomaterials as matrices for enzyme immobilization. *Artificial cells, blood substitutes, and immobilization biotechnology*, 39(2), pp.98–109.
- Hall, M., 1973. Foams and Foam Control in Fermentation Processes. *Pro. Ind. Microbiol.*, 12, pp.170–234.
- Hart, C., 2013. Product Focus: Analytical and Preparative Instrumentation. *Journal of Biomolecular Screening*, 18(6), pp.756–758.
- Hasler, J. a et al., 1999. Human cytochromes P450. *Molecular Aspects of Medicine*, 20(1–2), pp.1–137.
- Hatti-Kaul, R. et al., 2007. Industrial biotechnology for the production of bio-based chemicals - a cradle-to-grave perspective. *Trends in Biotechnology*, 25(3), pp.119–124.
- Hebrard, G., Zeng, J. & Loubiere, K., 2009. Effect of surfactants on liquid side mass transfer coefficients: A new insight. *Chemical Engineering Journal*, 148(1), pp.132–138.
- Heijnen, J.J. & Roels, J.A., 1981. A macroscopic model describing yield and maintenance relationships in aerobic fermentation processes. *Biotechnology and Bioengineering*, 23(4), pp.739–763.
- Henzler, H. & Schedel, M., 1991. Bioprocess Engineering Suitability of the shaking flask for oxygen supply to microbiological cultures. , 7, pp.123–131.
- Hermann, R., Lehmann, M. & Büchs, J., 2003. Characterization of gas-liquid mass transfer phenomena in microtiter plates. *Biotechnology and bioengineering*, 81(2), pp.178–86.
- Hermann, R. et al., 2001. Optical method for the determination of the oxygen-transfer capacity of small bioreactors based on sulfite oxidation. *Biotechnology and Bioengineering*, 74(5), pp.355–363.
- Hieber, G. & Ditrich, K., 2001. Introducing ChiPros: Biocatalytic production of chiral intermediates on a commercial scale. *Chimica oggi*, 19(6), pp.16–20.
- Hussain, H.A. & Ward, J.M., 2003a. Enhanced Heterologous Expression of Two *Streptomyces griseolus* Cytochrome P450s and *Streptomyces coelicolor* Ferredoxin

- Reductase as Potentially Efficient Hydroxylation Catalysts. *Applied and environmental microbiology*, 69(1), pp.373–382.
- Hussain, H.A. & Ward, J.M., 2003b. Ferredoxin reductase enhances heterologously expressed cytochrome CYP105D1 in *Escherichia coli* and *Streptomyces lividans*. *Enzyme and Microbial Technology*, 32(7), pp.790–800.
- Hutchison, C.A. et al., 2016. Design and synthesis of a minimal bacterial genome. *Science*, 351(6280).
- Hutzler, J.M. et al., 2003. Activation of cytochrome P450 2C9-mediated metabolism: mechanistic evidence in support of kinetic observations. *Archives of biochemistry and biophysics*, 410(1), pp.16–24.
- Isett, K. et al., 2007. Twenty-four-well plate miniature bioreactor high-throughput system: Assessment for microbial cultivations. *Biotechnology and Bioengineering*, 98(5), pp.1017–1028.
- Ishige, T., Honda, K. & Shimizu, S., 2005. Whole organism biocatalysis. *Current opinion in chemical biology*, 9(2), pp.174–80.
- Islam, R.S. et al., 2008. Scale-up of *Escherichia coli* growth and recombinant protein expression conditions from microwell to laboratory and pilot scale based on matched kLa. *Biotechnology and Bioengineering*, 99(5), pp.1128–1139.
- Islam, R.S. et al., 2007. Framework for the Rapid Optimization of Soluble Protein Expression in *Escherichia coli* Combining Microscale Experiments and Statistical Experimental Design. *Biotechnology progress*, 23, pp.785–793.
- Jansen, R.C., 2003. Studying complex biological systems using multifactorial perturbation. *Nature reviews. Genetics*, 4(February), pp.145–151.
- Jennewein, S. & Croteau, R., 2001. Taxol: biosynthesis, molecular genetics, and biotechnological applications. *Applied Microbiology and Biotechnology*, 57(1–2), pp.13–19.
- Jensen, V. & Rugh, S., 1987. Industrial Scale production and application of immobilised glucose isomerase. *Enzyme Engineering*, 136(1980), pp.356–370.
- John, G.T. et al., 2003. Integrated optical sensing of dissolved oxygen in microtiter plates: A novel tool for microbial cultivation. *Biotechnology and Bioengineering*, 81(7), pp.829–836.
- Junker, B.H., 2004. Scale-up methodologies for *Escherichia coli* and yeast fermentation processes. *J Biosci Bioeng*, 97(6), pp.347–364.

- Kaluzna, A.D.V. & Mink, D. 2015. A sustainable P450 oxygenation technology for the selective synthesis of oxygenated intermediates and APIs. *Chimica Oggi-Chemistry Today*, 33 (2). 54-57.
- Karimi, A. et al., 2013. Oxygen mass transfer in a stirred tank bioreactor using different impeller configurations for environmental purposes. Iranian Journal of Environmental Health Science &. *Iranian Journal of Environmental Health Science & Engineering*, 10(1), p.6.
- Kaster, J.A., Michelsen, D.L. & Velander, W.H., 1990. Increased oxygen transfer in a yeast fermentation using a microbubble dispersion. *Applied Biochemistry and Biotechnology*, 24–25(1), pp.469–484.
- Katsumoto, Y. et al., 2007. Engineering of the rose flavonoid biosynthetic pathway successfully generated blue-hued flowers accumulating delphinidin. *Plant & cell physiology*, 48(11), pp.1589–600.
- Kawase, Y. & Moo-Young, M., 1990. The effect of antifoam agents on mass transfer in bioreactors. *Bioprocess Engineering*, 5(4), pp.169–173.
- Kensy, F. et al., 2005. Characterisation of operation conditions and online monitoring of physiological culture parameters in shaken 24-well microtiter plates. *Bioprocess and Biosystems Engineering*, 28(2), pp.75–81.
- Kensy, F. et al., 2005. Oxygen transfer phenomena in 48-well microtiter plates: Determination by optical monitoring of sulfite oxidation and verification by real-time measurement during microbial growth. *Biotechnology and Bioengineering*, 89(6), pp.698–708.
- Kensy, F., Engelbrecht, C. & Büchs, J., 2009. Scale-up from microtiter plate to laboratory fermenter: Evaluation by online monitoring techniques of growth and protein expression in *Escherichia coli* and *Hansenula polymorpha* fermentations. *Microbial Cell Factories*, 8, pp.1–15.
- Khalil, A.S. & Collins, J.J., 2010. Synthetic Biology: Applications come of age. *Nature reviews. Genetics*, 11, pp.367–379.
- King, S., 2013. The Best Selling Drugs Since 1996 - Why AbbVie's Humira Is Set To Eclipse Pfizer's Lipitor. Available at: <https://www.forbes.com/>
- Kirby, J. & Keasling, J.D., 2009. Biosynthesis of plant isoprenoids: perspectives for microbial engineering. *Annual review of plant biology*, 60, pp.335–55.
- Kirk, O., Borchert, T.V. & Fuglsang, C.C., 2002. Industrial enzyme applications. *Current*

- Opinion in Biotechnology*, 13(4), pp.345–351.
- Klößner, W. & Büchs, J., 2012. Advances in shaking technologies. *Trends in Biotechnology*, 30(6), pp.307–314.
- Kocabaş, P., Çalik, P. & Özdamar, T.H., 2006. Fermentation characteristics of L-tryptophan production by thermoacidophilic *Bacillus acidocaldarius* in a defined medium. *Enzyme and Microbial Technology*, 39(5), pp.1077–1088.
- Kotz, J. et al., 2014. Factors Effecting Solubility: Pressure and Temperature. *Chemistry & Chemical Reactivity.*, 9(13), p.481.
- Kumar, S., 2010. Engineering Cytochrome P450 Biocatalysts for Biotechnology, Medicine and Bioremediation. *Expert opinion on drug discovery*, 6(2), pp.115–131.
- Kumar, S., Wittmann, C. & Heinzle, E., 2004. Sathish Kumar, Christoph Wittmann & Elmar Heinzle. pp.1–10.
- Lagemaat, J. Van De & Pyle, D.L., 2001. Solid-state fermentation and bioremediation : development of a continuous process for the production of fungal tannase. , 84, pp.115–123.
- Lendrem, D.W. et al., 2015. Lost in Space: design of experiments and scientific exploration in a Hogerth Universe. *Drug Discovery Today*, 20(11), pp.1365–1371.
- Leon, R. et al., 1998. Whole-cell biocatalysis in organic media. , 229(98), pp.483–500.
- Li, Y. & Beisson, F., 2009. The biosynthesis of cutin and suberin as an alternative source of enzymes for the production of bio-based chemicals and materials. *Biochimie*, 91(6), pp.685–91.
- Li, Z. et al., 2002. Oxidative biotransformations using oxygenases. *Current opinion in chemical biology*, 6(2), pp.136–44.
- Liese, A., Seelbach, K. & Wandrey, C., 2000. *Industrial Biotransformations*, Weinhein, Germany: VCH Wiley.
- Liese, a & Filho, M. V, 1999. Production of fine chemicals using biocatalysis. *Current opinion in biotechnology*, 10(6), pp.595–603.
- Lima_Ramos, J. Neto, W. Woodley, J.M. 2014. Engineering of Biocatalysts and Biocatalytic Processes. *Topics in Catalysis*. Vol.57(5), pp.301-320
- Linek, V. et al., 2004. Gas-liquid mass transfer coefficient in stirred tanks interpreted through models of idealized eddy structure of turbulence in the bubble vicinity. *Chemical Engineering and Processing: Process Intensification*, 43(12), pp.1511–1517.

- Linek, V. & Vacek, V., 1981. Chemical Engineering Use of Catalyzed Sulfite Oxidation Kinetics for the Determination of Mass Transfer Characteristics of Gas-Liquid Contactors. *Chemical Engineering Science*, (4), pp.1747–1768.
- Liu, Y.S., Wu, J.Y. & Ho, K.P., 2006. Characterization of oxygen transfer conditions and their effects on *Phaffia rhodozyma* growth and carotenoid production in shake-flask cultures. *Biochemical Engineering Journal*, 27(3), pp.331–335.
- Loew, G.H. et al., 1981. Structure, spectra, and function of model cytochrome P450. *Annals of the New York Academy of Sciences*, 367, pp.192–218.
- Luedeking, R. & Piret, E.L., 1959. A Kinetic Study of the Lactic Acid Fermentation . Batch Process at Controlled pH ". *Journal of Biochemical and Microbiological Technology and Engineering*, 1(4), pp.393–412.
- Lye, G.J. et al., 2003. Accelerated design of bioconversion processes using automated microscale processing techniques. *Trends in biotechnology*, 21(1), pp.29–37.
- Lye, G.J. & Woodley, J.M., 1999. Application of in situ product-removal. , 7799(1971), pp.643–646.
- Mahmoudian, M. et al., 1993. Enzymatic production of optically pure Lamivudine): A potent anti-HIV agent. , 15, pp.749–755.
- Maier, B., Dietrich, C. & Büchs, J., 2001. Correct application of the sulphite oxidation methodology of measuring the volumetric mass transfer coefficient k_La under non-pressurized and pressurized conditions. *Food and Bioproducts Processing: Transactions of the Institution of Chemical Engineers, Part C*, 79(2), pp.107–113.
- Maier, U. & Büchs, J., 2001. Characterisation of the gas-liquid mass transfer in shaking bioreactors. *Biochemical engineering journal*, 7(2), pp.99–106.
- Marques, M.P.C., Cabral, J.M.S. & Fernandes, P., 2010. Bioprocess scale-up: Quest for the parameters to be used as criterion to move from microreactors to lab-scale. *Journal of Chemical Technology and Biotechnology*, 85(9), pp.1184–1198.
- Marques, M.P.C. et al., 2009. Characterization of 24-well microtiter plate reactors for a complex multistep bioconversion: From sitosterol to androstenedione. *Journal of Biotechnology*, 141(3–4), pp.174–180.
- Marques, M.P.C. et al, 2010. Bioprocess scale-up: quest for the parameters to be used as criterion to move from microreactors to lab-scale. *J. Chem Technol Biotechnol.* 85: 1184-1198.

- Masutani, G. & Stenstrom, M., 1991. Dynamic Surface Tension Effects on Oxygen Transfer. *Journal of Environmental Engineering*, 117(1), pp.126–142.
- Mayuzumi, H. et al., 1993. Effect of mutations of ionic amino acids of cytochrome P450 1A2 on catalytic activities toward 7-ethoxycoumarin and methanol. *Biochemistry*, 32(21), pp.5622–8.
- Mcdaniel, L.E., Bailey, E.G. & Zimmerli, a, 1965. Effect of Oxygen Supply Rates on Growth of Escherichia Coli. *Applied microbiology*, 13(1), pp.109–14.
- McGinnis, D.F. & Little, J. C. 2002. Predicting diffused-bubble oxygen transfer rate using the discrete-bubble model. *Water Research*. 36: 4627-4635.
- Micheletti, M. & Lye, G.J., 2006. Microscale bioprocess optimisation. *Current opinion in biotechnology*, 17(6), pp.611–8.
- Minow, B. et al., 2014. Harmonization and characterization of different single-use bioreactors adopting a new sparger design. *Engineering in Life Sciences*, 14(3), pp.272–282.
- Montes, F.J. et al., 1997. Oxygen Kinetic and Metabolic Parameters for the Yeast *Trigonopsis variabilis*. *Journal of Chemical Technology & Biotechnology*, 68(2), pp.243–246.
- Montgomery, D.C., 2017. *Design and Analysis of Experiments* 9th Editio., John Wiley & Sons.
- Munro, A.W., Girvan, H.M. & McLean, K.J., 2007. Cytochrome P450--redox partner fusion enzymes. *Biochimica et biophysica acta*, 1770(3), pp.345–59.
- Murakami, A.H., Yabusaki, Y. & Sakaki, T., 1987. P450 Monooxygenase : Construction of the Functional Fused Enzyme between. , 6(3), pp.189–197.
- Nagar, S., 2017. *Introduction to Python for Engineers and Scientists*, Apress.
- Najafpour, G., 2015. *Biochemical Engineering and Biotechnology* 2nd Editio., Elsevier.
- Nettleton, O. & Einolf, H., 2011. Assessment of Cytochrome P450 Enzyme Inhibition and Inactivation in Drug Discovery and Development. *Current Topics in Medicinal Chemistry*, 11(4), pp.382–403.
- Ni, X. et al., 1995. A comparative study of mass transfer in yeast for a batch pulsed baffled bioreactor and a stirred tank fermenter. *Chemical Engineering Science*, 50(13), pp.2127–2136.
- Ni, Y. & Chen, R.R., 2004. Accelerating whole-cell biocatalysis by reducing outer membrane permeability barrier. *Biotechnology and bioengineering*, 87(6), pp.804–11.

- Nienow, A.W. et al., 2013. The physical characterisation of a microscale parallel bioreactor platform with an industrial CHO cell line expressing an IgG4. *Biochemical Engineering Journal*, 76, pp.25–36.
- Nikolova, P. & Ward, O.P., 1993. Whole cell biocatalysis in nonconventional media. *Journal of industrial microbiology*, 12(2), pp.76–86.
- Nodate, M., Kubota, M. & Misawa, N., 2006. Functional expression system for cytochrome P450 genes using the reductase domain of self-sufficient P450RhF from *Rhodococcus* sp. NCIMB 9784. *Applied microbiology and biotechnology*, 71(4), pp.455–62.
- Ogut, A. & Hatch, R., 1988. Oxygen transfer into newtonian and non-newtonian fluids in mechanically agitated vessels. *The Canadian Journal of Chemical Engineering*, 66(1), pp.79–85.
- Oosterhuis, N.M., Neubauer, P. & Junne, S., 2013. Single-use bioreactors for microbial cultivation. *Pharmaceutical Bioprocessing*, 1(2), pp.167–177.
- de Ory, I., Romero, L.E. & Cantero, D., 1999. Laboratory scale equipment for the determination of $k_L a$ in bio-reactors. *Bioprocess Engineering*, 20(1), pp.73–75.
- Osbon, Y. & Kumar, M. 2019. Biocatalysis and Strategies for Enzyme Improvement. IntechOpen. DOI: 10.5772/intechopen.85018.
- Özbek, B. & Gayik, S., 2001. The studies on the oxygen mass transfer coefficient in a bioreactor. *Process Biochemistry*, 36(8–9), pp.729–741.
- Parente, E. et al., 2004. Overall volumetric oxygen transfer coefficient in an aerated bench-top stirred fermenter in aqueous dispersions of sodium alginate. *Biotechnology and Applied Biochemistry*, 40(2), p.133.
- Park, C. & Geng, Q., 1992. Simultaneous fermentation and separation in the ethanol and ABE fermentation. *Separation and Purification Reviews*, 21(2).
- Patel, R.N., 2008. Biocatalysis: synthesis of chiral intermediates for drugs. In *Biocatalysis and Bioenergy*. John Wiley & Sons, p. 319.
- Patel, R.N., 2001. Enzymatic synthesis of chiral intermediates for Omapatrilat, an antihypertensive drug. *Biomolecular engineering*, 17(6), pp.167–82.
- Patrick, A.J. & Kennedy, M.J., 1995. Power consumption of agitated gas-liquid-solid systems with particular relevance to solid substrate submerged culture fermentations. *Biotechnology Letters*, 17(5), pp.487–492.

- Paul, S.M. et al., 2010. How to improve RD productivity: The pharmaceutical industry's grand challenge. *Nature Reviews Drug Discovery*, 9(3), pp.203–214.
- Pessoa, A., Vitolo, M. & Hustedt, H., 1996. Use of kLa as a Criterion for Scaling Up the Inulinase Fermentation Process. *ABAB Symposium*, 57/58, pp.699–709.
- Peter, C.P., Suzuki, Y., Rachinskiy, K., Lotter, S. & Buchs, J. 2006. Volumetric power consumption in baffled shake flasks. *Chemical Engineering Science*. 61. 3771-3779.
- Peterson, D.H. et al., 1952. No Title. *Journal of the American Chemical Society*, p.5933.
- Pokora & Cyrus, 1987. Phenolic developer resins.
- Pollard, D.J. & Woodley, J.M., 2007. Biocatalysis for pharmaceutical intermediates: the future is now. *Trends in biotechnology*, 25(2), pp.66–73.
- Puthli, M.S., Rathod, V.K. & Pandit, A.B., 2005. Gas-liquid mass transfer studies with triple impeller system on a laboratory scale bioreactor. *Biochemical Engineering Journal*, 23(1), pp.25–30.
- Qiagen, 2015. QIAprep ® Miniprep Handbook For purification of molecular biology grade DNA Sample & Assay Technologies. *QIAGEN Sample and Assay Technologies*, (June), pp.20–22.
- Ragan-Kelley, M. et al., 2014. The Jupyter/IPython architecture: a unified view of computational research, from interactive exploration to communication and publication. *AGU Fall Meeting Abstracts*.
- Rameez, S. et al., 2014. High-throughput miniaturized bioreactors for cell culture process development: Reproducibility, scalability, and control. *Biotechnology Progress*, 30(3), pp.718–727.
- Raudenbush, S.W. & Bryk, A.S., 2002. *Hierarchical Linear Models: Applications and Data Analysis Methods*,
- Rice, W.R., 1989. Analyzing Tables of Statistical Tests. *American Sociological Review*, 78(1), pp.1–3.
- Rice, E.W. et al., 2012. *Standard Methods for the Evaluation of Water and Wastewater*, American Public Health Association.
- Roberts, G.A. et al., 2002. Identification of a New Class of Cytochrome P450 from a Rhodococcus sp . Identification of a New Class of Cytochrome P450 from a Rhodococcus sp. 184(14).

- Roberts, S.C., 2007. Production and engineering of terpenoids in plant cell culture. *Nature chemical biology*, 3(7), pp.387–95.
- Roberts, S.M. et al., 1995. *Introduction to biocatalysis using enzymes and microorganisms* 1st ed., Cambridge: Cambridge University Press.
- Rols, J. et al., 1990. Mechanism of enhanced oxygen transfer in fermentation using emulsified oxygen-vectors. *Biotechnology and bioengineering*, 35(4), pp.427–435.
- Rowe, G.E., Margaritis, A. & Wei, N., 2003. Specific Oxygen Uptake Rate Variations during Batch Fermentation of *Bacillus thuringiensis* Subspecies *kurstaki* HD-1. *Biotechnology Progress*, 19(5), pp.1439–1443.
- Rowland, P. et al., 2006. Crystal structure of human cytochrome P450 2D6. *The Journal of biological chemistry*, 281(11), pp.7614–22.
- RSC, 2011. RSC Chemical Industry Profile.
- Rudakov, Y.O. et al., 2008. Stoichiometry of electrocatalytic cycle of cytochrome P450 2B4. *Journal of inorganic biochemistry*, 102(11), pp.2020–5.
- Saibi, W. et al., 2012. Biocatalysts: beautiful creatures. *Biochemical and biophysical research communications*, 426(3), pp.289–93.
- Sakaki, T., 2012. The 50th Anniversary and New Horizons of Cytochrome P450 Research : Expanding Knowledge on the Multiplicity and Versatility of P450 and Its Industrial Applications Practical Application of Cytochrome P450. , 35(6), pp.844–849.
- Sakaki, T. & Inouye, K., 2000. Practical application of mammalian cytochrome P450. *Journal of bioscience and bioengineering*, 90(6), pp.583–90.
- Sakakis, T. et al., 1992. Organella-targeted Expression of Rat Liver Cytochrome P450c27 in Yeast. *The Journal of biological chemistry*, 267(23), pp.16497–16502.
- Sakurai, K. & Cederbaum, a I., 1998. Oxidative stress and cytotoxicity induced by ferric-nitrosyltriacetate in HepG2 cells that express cytochrome P450 2E1. *Molecular pharmacology*, 54(6), pp.1024–35.
- Sanchez, S. & Demain, A.L., 2016. *Useful Microbial Enzymes-An Introduction*, Elsevier Inc.
- Van De Sandt, E.J.A.X. & De Vroom, E., 2000. Innovations in cephalosporin and penicillin production : Painting the antibiotics industry green. *Chimica oggi*, 18(5), pp.72–75.
- Santos, V.E. et al., 2006. Oxygen uptake rate measurements both by the dynamic method and during the process growth of *Rhodococcus erythropolis* IGTS8: Modelling and difference

- in results. *Biochemical Engineering Journal*, 32(3), pp.198–204.
- Schäpper, D. et al., 2009. Application of microbioreactors in fermentation process development: a review. *Analytical and bioanalytical chemistry*, 395(3), pp.679–95.
- Schmidt, F.R., 2005. Optimization and scale up of industrial fermentation processes. *Applied microbiology and biotechnology*, 68(4), pp.425–35.
- Schuler, M. & Kargi, F., 2002. *Bioprocess Engineering* Second., Prentice Hall.
- Segur, J. & Oberstar, H., 1951. Viscosity of Glycerol and Its Aqueous Solutions. *Ind. Eng. Chem.*, 43(9), pp.2117–2120.
- Shafiee, a & Hutchinson, C.R., 1988. Purification and reconstitution of the electron transport components for 6-deoxyerythronolide B hydroxylase, a cytochrome P-450 enzyme of macrolide antibiotic (erythromycin) biosynthesis. *Journal of bacteriology*, 170(4), pp.1548–53.
- Shakunthala, N., 2010. New cytochrome P450 mechanisms: implications for understanding molecular basis for drug toxicity at the level of the cytochrome. *Expert opinion on drug metabolism & toxicology*, 6(1), pp.1–15.
- Sheely, M., 1932. Glycerol Viscosity Tables. *Ind. Eng. Chem.*, 24(9), pp.1060–1064.
- Shen, H., 2014. Interactive Notebooks. *Nature*, 515, pp.151–152.
- Shen, B. & Hutchinson, C.R., 1994. Triple Hydroxylation of Tetracenomycin A2 to tetraenomycin C in *Streptomyces glaucescens*. *The Journal of biological chemistry*, 269(48), pp.30726–30733.
- Shet, M.S., Fisher, C.W. & Estabrook, R.W., 1997. The Function of Recombinant Cytochrome P450s in Intact *Escherichia coli* Cells : The 17 α -Hydroxylation of Progesterone and Pregnenolone by P450c17 1. , 339(1), pp.218–225.
- Shivhare, M. & McCreath, G., 2010. Practical Considerations for DoE Implementation in Quality By Design. *Bioprocess International*, pp.22–30.
- Shukla, A.A. & Gottschalk, U., 2013. Single-use disposable technologies for biopharmaceutical manufacturing. *Trends in Biotechnology*, 31(3), pp.147–154.
- Sigma-Aldrich, 2015. Practical Fermentation for Recombinant Protein.
- Singh, V., 1999. Disposable bioreactor for cell culture using wave-induced agitation. *Cytotechnology*, 30(1–3), pp.149–158.
- Smith, B.D. et al., 2007. Structure of the human lung cytochrome P450 2A13. *The Journal of*

- biological chemistry*, 282(23), pp.17306–13.
- Smith, C.G. & Johnson, M.J., 1954. Aeration requirements for the growth of aerobic microorganisms. *Journal of bacteriology*, 68(3), pp.346–350.
- Smith, J., 1977. Scale-Up of Agitated Gas-Liquid Reactors for Mass Transfer. In *Proc. of the 2nd European Conf. on Mixing, Cambridge, U.K.*
- Sono, M. et al., 1996. Heme-Containing Oxygenases. *Chemical reviews*, 96(7), pp.2841–2888.
- Sridhar, J. et al., 2012. Insights on cytochrome p450 enzymes and inhibitors obtained through QSAR studies. *Molecules (Basel, Switzerland)*, 17(8), pp.9283–305.
- Stanbury, P., Whitaker, A. & Hall SJ, 1995. *Principles of Fermentation Technology* 2nd Editio., New York: Pergamon.
- Stansfield, I., Cliffe, K.R. & Kelly, S.L., 1991. Chemostat studies of microsomal enzyme induction in *Saccharomyces cerevisiae*. *Yeast*, 7(2), pp.147–56.
- Stedim, S., 2016. ambr® 15 fermentation New Microbial Single-Use Advanced Micro Bioreactor System. , pp.1–8.
- Steel, R. & Maxon, W.D., 1966. Studies With a multiple rod mixing impeller. *Biotechnology and Bioengineering*, VIII(1), pp.109–115.
- Straathof, A.J.J., Panke, S. & Schmid, A., 2002. The production of fine chemicals by biotransformations. *Current opinion in biotechnology*, 13(6), pp.548–56.
- Suijdam, J., Kossen, N. & Joha, A., 1978. Model for Oxygen Transfer in a Shake Flask. *Biotechnol Bioeng.*, 20, pp.1695–1709.
- Suzuki, K. et al., 1993. Purification and properties of cytochrome P-450 (P-450_{1un}) catalyzing steroid 11 beta-hydroxylation in *Curvularia lunata*. *Biochimica et biophysica acta*, 1203(2), pp.215–23.
- Szybalski, W. & Shkalka, A., 1978. Nobel Prizes and Restriction Enzymes. *Gene*, 4, pp.181–182.
- Tabora, J.E. & Domagalski, N., 2017. Multivariate Analysis and Statistics in Pharmaceutical Process Research and Development. *Annual Review of Chemical and Biomolecular Engineering*, 8(1), pp.403–426.
- Tao, J. & Xu, J.-H., 2009. Biocatalysis in development of green pharmaceutical processes. *Current opinion in chemical biology*, 13(1), pp.43–50.

- Thibault, J., Leduy, A. & Denis, A., 1990. Chemical enhancement in the determination of K_La by the sulfite oxidation method. *The Canadian Journal of Chemical Engineering*, 68(2), pp.324–326.
- Tholudur, A. et al., 2005. Using Design of Experiments to Assess Escherichia Coli Fermentation Robustness. *BioProcess International*, pp.2–4.
- Thomas, S.M., DiCosimo, R. & Nagarajan, V., 2002. Biocatalysis: applications and potentials for the chemical industry. *Trends in biotechnology*, 20(6), pp.238–42.
- Tian, Z. et al., 2013. Cytochrome P450 107U1 is required for sporulation and antibiotic production in *Streptomyces coelicolor*. *Archives of biochemistry and biophysics*, 530(2), pp.101–7.
- Trejo González, J.A., Longinotti, M.P. & Corti, H.R., 2011. The viscosity of glycerol-water mixtures including the supercooled region. *Journal of Chemical and Engineering Data*, 56(4), pp.1397–1406.
- Tribe, L.A., Briens, C.L. & Margaritis, A., 1995. Communication to the Editor Determination of the Volumetric Mass Transfer Coefficient (k_La) Using the Dynamic “Gas Out-Gas In” Method: Analysis of Errors Caused by Dissolved Oxygen Probes. *Biotechnology and Bioengineering*, 46(4), pp.388–392.
- Tsujita, Y. et al., 1997. Pravastatin Sodium: New Clinical Aspects and Recent progress. *Annu Rep Sankyo Res Lab*, 49, pp.1–61.
- Urlacher, V.B. & Eiben, S., 2006. Cytochrome P450 monooxygenases: perspectives for synthetic application. *Trends in biotechnology*, 24(7), pp.324–30.
- Vail, R.B. et al., 2005. Preparative synthesis of drug metabolites using human cytochrome P450s 3A4, 2C9 and 1A2 with NADPH-P450 reductase expressed in *Escherichia coli*. *Journal of industrial microbiology & biotechnology*, 32(2), pp.67–74
- Van't Riet, K., 1983. Mass Transfer in Fermentation. *Trends in biotechnology*, 1(4), pp.113–119.
- Van't Riet, K., 1979. Review of Measuring Methods and Results in Nonviscous Gas-Liquid Mass Transfer in Stirred Vessels. *Industrial & Engineering Chemistry Process Design and Development*, 18(3), pp.357–364.
- Van't Riet, K. & Van Sonsbeek, H., 1992. Foaming, mass transfer, and mixing: interrelations in large scale fermentors. In *9th Int. Biotechnology Symp. & Exposition*. pp. 189–192.

- Van't Riet, K. & Tramper, J., 1991. *Basic Bioreactor Design*, Marcel Dekker.
- Veljkovic, V.B. et al., 1995. Oxygen transfer in flasks shaken on orbital shakers. *Hemijaska Industrija*, 49, p.265.
- Vendruscolo, F. et al., 2012. Determination of Oxygen Solubility in Liquid Media. *ISRN Chemical Engineering*, 2012, pp.1–5.
- Vera Candioti, L. et al., 2014. Experimental design and multiple response optimization. Using the desirability function in analytical methods development. *Talanta*, 124, pp.123–138.
- de Vetten, N. et al., 1999. A cytochrome b5 is required for full activity of flavonoid 3', 5'-hydroxylase, a cytochrome P450 involved in the formation of blue flower colors. *Proceedings of the National Academy of Sciences of the United States of America*, 96(2), pp.778–83.
- Vilaça, P.R. et al., 2000. Determination of power consumption and volumetric oxygen transfer coefficient in bioreactors. *Bioprocess Engineering*, 22(3), pp.0261–0265.
- Vogelaar, J.C.T. et al., 2000. Research Note Temperature Effects on the Oxygen Transfer Rate Between 20 and 50C, 34(3).
- Wachtmeister, J. & Rother, J. 2016. Recent Advances in Whole Cell Biocatalysis Techniques Bridging from Investigative to Industrial Scale. *Current Opinion in Biotechnology* 2016, 42:169–177
- Wandrey, C., Liese, A. & Kihumbu, D., 2000. ReViews Industrial Biocatalysis : Past , Present , and Future Abstract : , (2), pp.286–290.
- Wang, D. et al., 1979. Aeration and Agitation. In J. W. & Sons, ed. *Fermentation and enzyme technology*. pp. 157–193.
- Wang, D.I.C. & Fewkes, R.C.J., 1977. Effect of operating and geometric parameters on the behavior of non-Newtonian, mycelial, antibiotic fermentations. *Dev. Ind. Microbiol*, 18, p.39.56.
- Watanabe, I., Nara, F. & Serizawa, N., 1995. Cloning, characterization and expression of the gene encoding cytochrome P-450sca-2 from *Streptomyces carbophilus* involved in production of pravastatin, a specific HMG-CoA reductase inhibitor. *Gene*, 163(1), pp.81–5.
- Weber, E. et al., 2011. A modular cloning system for standardized assembly of multigene constructs. *PLoS ONE*, 6(2), pp.1–9.
- Weisenberger, S. et al., 1996. Estimation of Gas Solubilities in Salt Solutions at Temperatures from 273 K to 363 K. , 42(1), pp.298–300.

- Weiss, S. et al., 2002. Modeling of mixing in 96-well microplates observed with fluorescence indicators. *Biotechnology progress*, 18(4), pp.821–30.
- Werck-reichhart, D. & Feyereisen, R., 2000. Protein family review Cytochromes P450: a success story. , pp.1–9.
- Werner, S. et al., 2010. Innovative, Non-stirred Bioreactors in Scales from Milliliters up to 1000 Liters for Suspension Cultures of Cells using Disposable Bags and Containers – A Swiss Contribution. *CHIMIA International Journal for Chemistry*, 64(11), pp.819–823.
- Wester, M.R. et al., 2004. The structure of human cytochrome P450 2C9 complexed with flurbiprofen at 2.0-Å resolution. *The Journal of biological chemistry*, 279(34), pp.35630–7.
- Westerterp, K., Van Dierendonck, L. & De Kraa, J., 1963. Interfacial areas in agitated gas-liquid contactors. , 18(July 1962), pp.157–176.
- Whitcomb, P.J. & Anderson, M.J., 2004. *RSM Simplified*, CRC Press.
- Whitford, W.G., 2010. Single-use systems as principal components in bioproduction. *BioProcess International*, 8(11), pp.34–42.
- Whitman, W.G., 1924. The Two-Film Theory of Gas Absorption. *Chemical and Metallurgical Engineering*, 29(4), pp.146–148.
- Wimmer, E. et al., 2009. Synthetic viruses: A new opportunity to understand and prevent viral disease. *Nature Biotechnology*, 27(12), pp.1163–1172.
- Wise, W.S., 1951. The measurement of the aeration of culture media. *Journal of general microbiology*, 5(1), pp.167–77.
- Wiseman, A. et al., 2000. Comment Cytochromes P450 enzymes for clean food-processing: limitations of imitations! , 5(May 1999), pp.1999–2001.
- Wiseman, A., 2003. Replacement of immobilised cell bioreactors by smaller immobilised enzyme bioreactors: unique-outcome predictability for cytochromes P450 isoforms? *Biotechnology letters*, 25(19), pp.1581–90.
- Wohlgemuth, R., 2010. Biocatalysis--key to sustainable industrial chemistry. *Current opinion in biotechnology*, 21(6), pp.713–24.
- Woodley, J.M., 2008. New opportunities for biocatalysis: making pharmaceutical processes greener. *Trends in biotechnology*, 26(6), pp.321–7.
- Wüst, M. & Croteau, R.B., 2002. Hydroxylation of specifically deuterated limonene enantiomers by cytochrome p450 limonene-6-hydroxylase reveals the mechanism of

- multiple product formation. *Biochemistry*, 41(6), pp.1820–7.
- Xie, X. & Tang, Y., 2007. Efficient synthesis of simvastatin by use of whole-cell biocatalysis. *Applied and environmental microbiology*, 73(7), pp.2054–60.
- Yagi, H. & Yoshida, F., 1975. Enhancement factor for oxygen absorption into fermentation broth. *Biotechnology and Bioengineering*, 17(7), pp.1083–1098.
- Yang, J.D. & Wang, N.S., 1992. Oxygen Mass-Transfer Enhancement Via Fermenter Headspace Pressurization. *Biotechnology Progress*, 8(3), pp.244–251.
- Yano, J.K. et al., 2004. The structure of human microsomal cytochrome P450 3A4 determined by X-ray crystallography to 2.05-Å resolution. *The Journal of biological chemistry*, 279(37), pp.38091–4.
- Zanger, U.M. & Schwab, M. 2013. Cytochrome P450 enzymes in drug metabolism: Regulation of gene expression, enzyme activities, and impact of genetic variation. *Pharmacology & Therapeutics*. 138. 103-141.
- Zhang, X. et al., 2006. Optimization of 1, 3-propanediol production by novel recombinant *Escherichia coli* using response surface methodology. 1078(December 2005), pp.1075–1078.
- Zhang, L. et al., 2009. Predicting drug-drug interactions: an FDA perspective. *The AAPS journal*, 11(2), pp.300–6.
- Zhu, Y., Bandopadhyay, P. & Jie, W., 2001. Measurement of Gas-Liquid Mass Transfer in an Agitated Vessel—A Comparison between Different Impellers. *Journal of Chemical Engineering of Japan*, 34(5), pp.579–584.
- Zieminski, S.A. & Whittemore, R.C., 1970. Behavior of gas bubbles in aqueous electrolyte solutions. *Chemical Engineering Science*, 26, pp.509–520.

Appendices

Appendix 1.1. 9 factor, 64 run DoE design for screening bioconversion of 7-ethoxycoumarin to 7-hydroxycoumarin.

Factor		A	B	C	D	E	F	G	H	J
		Post Ind. Time	[Subs]	Post Ind. Vol.	Pre Ind. Time	Temp. (Post Ind.)	Subs additio n time	[Yeast Extract]	Buffer	Shaker Speed
Plate/Wel I	Std Order	(hrs)	(mM)	(mL)	(hrs)	(°C)	(hrs)	(g/L)		(rpm)
1/D3	1	8	0.1	0.5	2	25	0.167	10	Yes	300
1/D4	2	65	0.1	0.5	2	25	1	30	Yes	300
1/D5	3	8	1.0	0.5	2	25	1	30	No	300
1/D6	4	65	1.0	0.5	2	25	0.167	10	No	300
1/D7	5	8	0.1	1.0	2	25	1	10	No	300
1/D8	6	65	0.1	1.0	2	25	0.167	30	No	300
1/D9	7	8	1.0	1.0	2	25	0.167	30	Yes	300
1/D10	8	65	1.0	1.0	2	25	1	10	Yes	300
1/E3	9	8	0.1	0.5	5	25	0.167	30	No	300
1/E4	10	65	0.1	0.5	5	25	1	10	No	300
1/E5	11	8	1.0	0.5	5	25	1	10	Yes	300
1/E6	12	65	1.0	0.5	5	25	0.167	30	Yes	300
1/E7	13	8	0.1	1.0	5	25	1	30	Yes	300
1/E8	14	65	0.1	1.0	5	25	0.167	10	Yes	300
1/E9	15	8	1.0	1.0	5	25	0.167	10	No	300
1/E10	16	65	1.0	1.0	5	25	1	30	No	300
2/D3	17	8	0.1	0.5	2	37	0.167	10	Yes	300
2/D4	18	65	0.1	0.5	2	37	1	30	Yes	300
2/D5	19	8	1.0	0.5	2	37	1	30	No	300
2/D6	20	65	1.0	0.5	2	37	0.167	10	No	300
2/D7	21	8	0.1	1.0	2	37	1	10	No	300
2/D8	22	65	0.1	1.0	2	37	0.167	30	No	300
2/D9	23	8	1.0	1.0	2	37	0.167	30	Yes	300
2/D10	24	65	1.0	1.0	2	37	1	10	Yes	300
2/E3	25	8	0.1	0.5	5	37	0.167	30	No	300
2/E4	26	65	0.1	0.5	5	37	1	10	No	300
2/E5	27	8	1.0	0.5	5	37	1	10	Yes	300
2/E6	28	65	1.0	0.5	5	37	0.167	30	Yes	300
2/E7	29	8	0.1	1.0	5	37	1	30	Yes	300
2/E8	30	65	0.1	1.0	5	37	0.167	10	Yes	300

2/E9	31	8	1.0	1.0	5	37	0.167	10	No	300
2/E10	32	65	1.0	1.0	5	37	1	30	No	300
3/D3	33	8	0.1	0.5	2	25	0.167	10	Yes	1100
3/D4	34	65	0.1	0.5	2	25	1	30	Yes	1100
3/D5	35	8	1.0	0.5	2	25	1	30	No	1100
3/D6	36	65	1.0	0.5	2	25	0.167	10	No	1100
3/D7	37	8	0.1	1.0	2	25	1	10	No	1100
3/D8	38	65	0.1	1.0	2	25	0.167	30	No	1100
3/D9	39	8	1.0	1.0	2	25	0.167	30	Yes	1100
3/D10	40	65	1.0	1.0	2	25	1	10	Yes	1100
3/E3	41	8	0.1	0.5	5	25	0.167	30	No	1100
3/E4	42	65	0.1	0.5	5	25	1	10	No	1100
3/E5	43	8	1.0	0.5	5	25	1	10	Yes	1100
3/E6	44	65	1.0	0.5	5	25	0.167	30	Yes	1100
3/E7	45	8	0.1	1.0	5	25	1	30	Yes	1100
3/E8	46	65	0.1	1.0	5	25	0.167	10	Yes	1100
3/E9	47	8	1.0	1.0	5	25	0.167	10	No	1100
3/E10	48	65	1.0	1.0	5	25	1	30	No	1100
4/D3	49	8	0.1	0.5	2	37	0.167	10	Yes	1100
4/D4	50	65	0.1	0.5	2	37	1	30	Yes	1100
4/D5	51	8	1.0	0.5	2	37	1	30	No	1100
4/D6	52	65	1.0	0.5	2	37	0.167	10	No	1100
4/D7	53	8	0.1	1.0	2	37	1	10	No	1100
4/D8	54	65	0.1	1.0	2	37	0.167	30	No	1100
4/D9	55	8	1.0	1.0	2	37	0.167	30	Yes	1100
4/D10	56	65	1.0	1.0	2	37	1	10	Yes	1100
4/E3	57	8	0.1	0.5	5	37	0.167	30	No	1100
4/E4	58	65	0.1	0.5	5	37	1	10	No	1100
4/E5	59	8	1.0	0.5	5	37	1	10	Yes	1100
4/E6	60	65	1.0	0.5	5	37	0.167	30	Yes	1100
4/E7	61	8	0.1	1.0	5	37	1	30	Yes	1100
4/E8	62	65	0.1	1.0	5	37	0.167	10	Yes	1100
4/E9	63	8	1.0	1.0	5	37	0.167	10	No	1100
4/E10	64	65	1.0	1.0	5	37	1	30	No	1100

Appendix 1.2. Layout of factors and set points for execution of 9 factor, 64 run DoE design for screening bioconversion of 7-ethoxycoumarin to 7-hydroxycoumarin.

Plate 1 (Post Induction Temperature 25°C, 300rpm)												
	1	2	3	4	5	6	7	8	9	10	11	12
A												
B												
C												
D			A (0.1)	C (0.1)	D (1.0)	B (1.0)	B (0.1) ↑	D (0.1) ↑	C (1.0) ↑	A (1.0) ↑		
E			D (0.1)	B (0.1)	A (1.0)	C (1.0)	C (0.1) ↑	A (0.1) ↑	B (1.0) ↑	D (1.0) ↑		
F							B	D	C	A		
G							C	A	B	D		
H												
Plate 2 (Post Induction Temperature 37°C, 300rpm)												
	1	2	3	4	5	6	7	8	9	10	11	12
A												
B												
C												
D			B (0.1)	D (0.1)	C (1.0)	A (1.0)	A (0.1) ↑	C (0.1) ↑	D (1.0) ↑	B (1.0) ↑		
E			C (0.1)	A (0.1)	B (1.0)	D (1.0)	D (0.1) ↑	B (0.1) ↑	A (1.0) ↑	C (1.0) ↑		
F							A	C	D	B		
G							D	B	A	C		
H												
Grey wells contain sterilised water.												

Included is the assignment of four different medias to wells (capital letters), the substrate addition concentration (concentration in mM in brackets) and the wells to 1mL working volume (arrows). Each plate is also labelled with post induction temperature and shaker frequency. NB. Grey wells contain sterilised water.

Plate 3 (Post Induction Temperature 37°C, 1100rpm)												
	1	2	3	4	5	6	7	8	9	10	11	12
A												
B												
C												
D			D (1.0)	B (1.0)	A (0.1)	C (0.1)	C (1.0)	A (1.0)	B (0.1)	D (0.1)		
E			A (1.0)	C (1.0)	D (0.1)	B (0.1)	B (1.0)	D (1.0)	C (0.1)	A (0.1)		
F			D	B	A	C						
G			A	C	D	B						
H												
Plate 4 (Post Induction Temperature 25°C, 1100rpm)												
	1	2	3	4	5	6	7	8	9	10	11	12
A												
B												
C												
D			C (1.0)	A (1.0)	B (0.1)	D (0.1)	D (1.0)	B (1.0)	A (0.1)	C (0.1)		
E			B (1.0)	D (1.0)	C (0.1)	A (0.1)	A (1.0)	C (1.0)	D (0.1)	B (0.1)		
F			C	A	B	D						
G			B	D	C	A						
H												

Included is the assignment of four different medias to wells (capital letters), the substrate addition concentration (concentration in mM in brackets) and the wells to 1mL working volume (arrows). Each plate is also labelled with post induction temperature and shaker frequency. NB. Grey wells contain sterilised water.

Appendix 1.3. 7 factor, 64 run DoE design for refinement stage of optimising bioconversion of 7-ethoxycoumarin to 7-hydroxycoumarin.

Factor		A	B	C	D	E	F	G
		Post Induction Time	[Subs]	Post Induction Vol.	Pre Induction Time	[Yeast Extract]	Temp. (during bioconversion)	Buffer
Plate/Well	Std Order	(hrs)	(mM)	(mL)	(hrs)	(g/L)	(°C)	
1/C3	1	50	0.75	0.5	2	10	22	Yes
1/C4	2	75	0.75	0.5	2	30	22	No
1/C5	3	50	1.25	0.5	2	30	22	No
1/C6	4	75	1.25	0.5	2	10	22	Yes
1/C7	5	50	0.75	1.0	2	10	22	No
1/C8	6	75	0.75	1.0	2	30	22	Yes
1/C9	7	50	1.25	1.0	2	30	22	Yes
1/C10	8	75	1.25	1.0	2	10	22	No
1/D3	9	50	0.75	0.5	5	30	22	No
1/D4	10	75	0.75	0.5	5	10	22	Yes
1/D5	11	50	1.25	0.5	5	10	22	Yes
1/D6	12	75	1.25	0.5	5	30	22	No
1/D7	13	50	0.75	1.0	5	30	22	Yes
1/D8	14	75	0.75	1.0	5	10	22	No
1/D9	15	50	1.25	1.0	5	10	22	No
1/D10	16	75	1.25	1.0	5	30	22	Yes
1/E3	17	50	0.75	0.5	2	10	22	Yes
1/E4	18	75	0.75	0.5	2	30	22	No
1/E5	19	50	1.25	0.5	2	30	22	No
1/E6	20	75	1.25	0.5	2	10	22	Yes
1/E7	21	50	0.75	1.0	2	10	22	No
1/E8	22	75	0.75	1.0	2	30	22	Yes
1/E9	23	50	1.25	1.0	2	30	22	Yes
1/E10	24	75	1.25	1.0	2	10	22	No
1/F3	25	50	0.75	0.5	5	30	22	No
1/F4	26	75	0.75	0.5	5	10	22	Yes
1/F5	27	50	1.25	0.5	5	10	22	Yes
1/F6	28	75	1.25	0.5	5	30	22	No
1/F7	29	50	0.75	1.0	5	30	22	Yes
1/F8	30	75	0.75	1.0	5	10	22	No
1/F9	31	50	1.25	1.0	5	10	22	No
1/F10	32	75	1.25	1.0	5	30	22	Yes
2/C3	33	50	0.75	0.5	2	10	30	Yes

2/C4	34	75	0.75	0.5	2	30	30	No
2/C5	35	50	1.25	0.5	2	30	30	No
2/C6	36	75	1.25	0.5	2	10	30	Yes
2/C7	37	50	0.75	1.0	2	10	30	No
2/C8	38	75	0.75	1.0	2	30	30	Yes
2/C9	39	50	1.25	1.0	2	30	30	Yes
2/C10	40	75	1.25	1.0	2	10	30	No
2/D3	41	50	0.75	0.5	5	30	30	No
2/D4	42	75	0.75	0.5	5	10	30	Yes
2/D5	43	50	1.25	0.5	5	10	30	Yes
2/D6	44	75	1.25	0.5	5	30	30	No
2/D7	45	50	0.75	1.0	5	30	30	Yes
2/D8	46	75	0.75	1.0	5	10	30	No
2/D9	47	50	1.25	1.0	5	10	30	No
2/D10	48	75	1.25	1.0	5	30	30	Yes
2/E3	49	50	0.75	0.5	2	10	30	Yes
2/E4	50	75	0.75	0.5	2	30	30	No
2/E5	51	50	1.25	0.5	2	30	30	No
2/E6	52	75	1.25	0.5	2	10	30	Yes
2/E7	53	50	0.75	1.0	2	10	30	No
2/E8	54	75	0.75	1.0	2	30	30	Yes
2/E9	55	50	1.25	1.0	2	30	30	Yes
2/E10	56	75	1.25	1.0	2	10	30	No
2/F3	57	50	0.75	0.5	5	30	30	No
2/F4	58	75	0.75	0.5	5	10	30	Yes
2/F5	59	50	1.25	0.5	5	10	30	Yes
2/F6	60	75	1.25	0.5	5	30	30	No
2/F7	61	50	0.75	1.0	5	30	30	Yes
2/F8	62	75	0.75	1.0	5	10	30	No
2/F9	63	50	1.25	1.0	5	10	30	No
2/F10	64	75	1.25	1.0	5	30	30	Yes

Appendix 1.4. 2 factor, 8 run Central Composite DoE design containing 4 centre points for an optimisation timecourse on the bioconversion of 7-ethoxycoumarin to 7-hydroxycoumarin. Each of the eight ‘Std Order’ runs is cultured as a timecourse using the sacrificial well method (Section 2.5.3.)

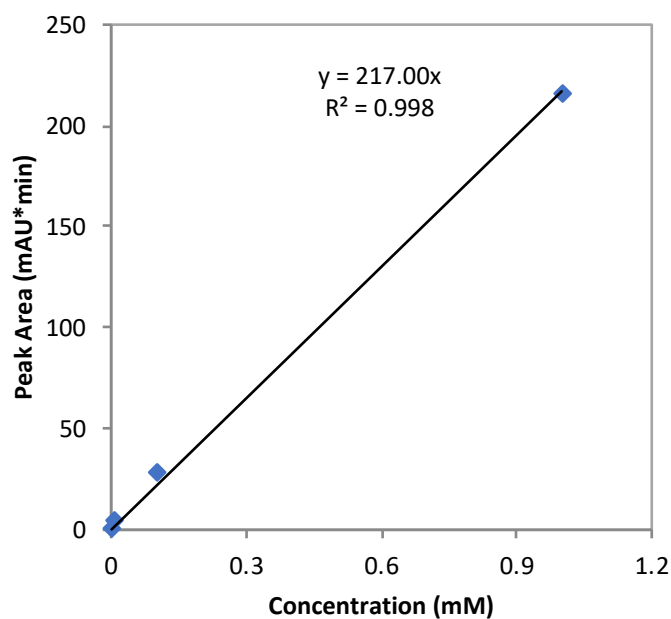
Factor		A	B
		[Subs]	[Yeast Extract]
Row	Std Order	(mM)	(g/L)
A	1	0.75	40
B	2	1.00	40
C	3	0.75	50
D	4	1.00	50
E	5	0.88	45
F	6	0.88	45
G	7	0.88	45
H	8	0.88	45

Appendix 1.5. Arrangement of factors for DoE optimisation timecourse experiment as described in Section 2.5.3.

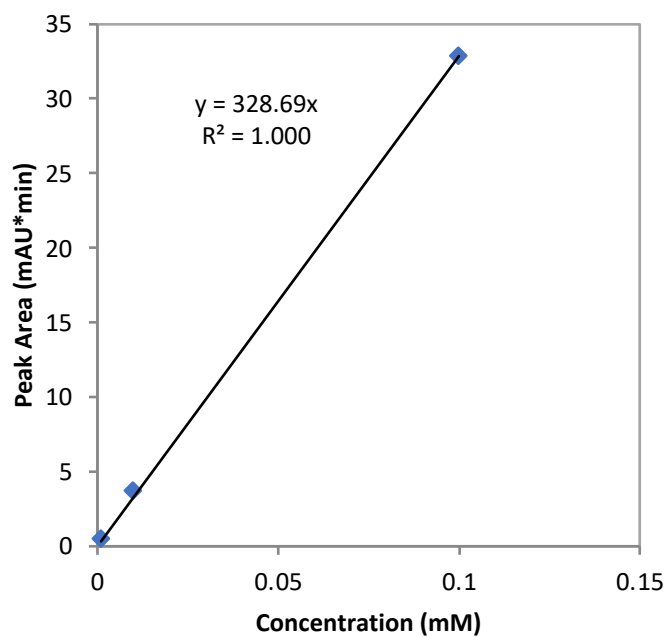
				Post Induction Time of Harvest (hr)											
	Run #	[Subs] mM	[YE] g/L	5	10	20	25	30	35	45	50	55	60	70	75
A	1	0.75	40												
B	2	1.00	40												
C	3	0.75	50												
D	4	1.00	50												
E	5	0.88	45												
F	6	0.88	45												
G	7	0.88	45												
H	8	0.88	45												
				1	2	3	4	5	6	7	8	9	10	11	12

Appendix 1.6.

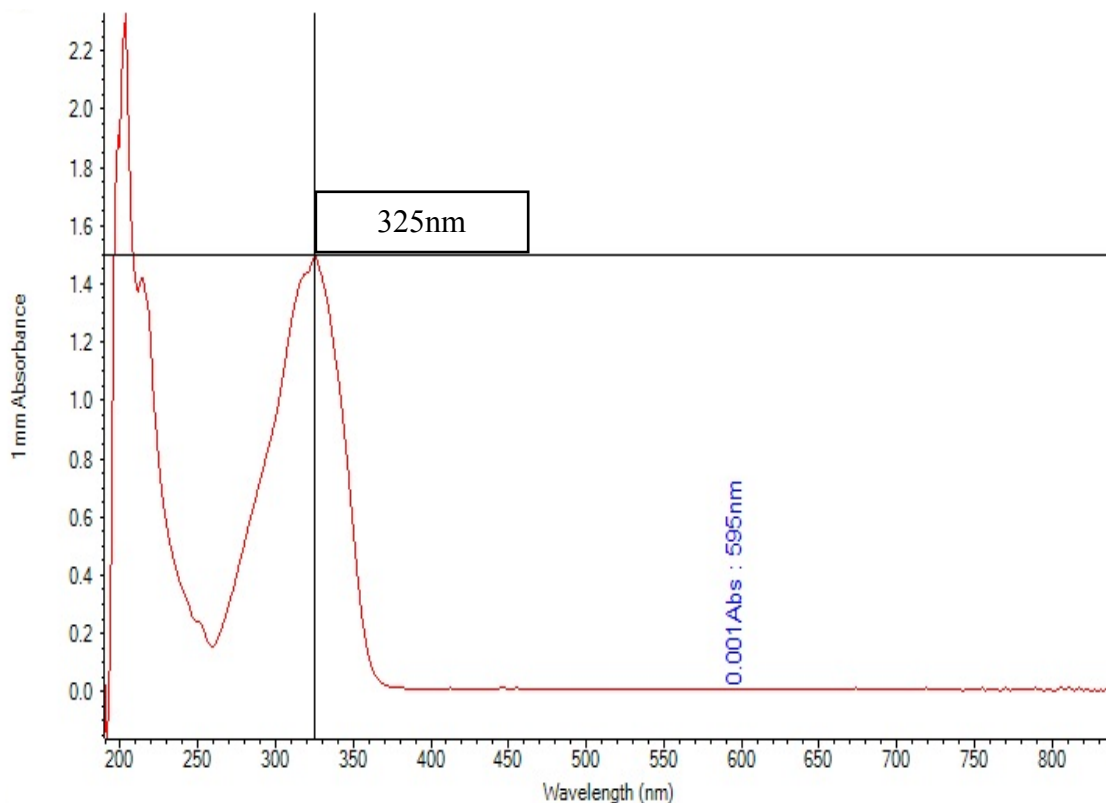
Appendix 1.6a. Sample calibration curve for 7-Ethoxycoumarin (bioconversion substrate) concentration. Experiments carried out as described in Section 2.2.9.2.



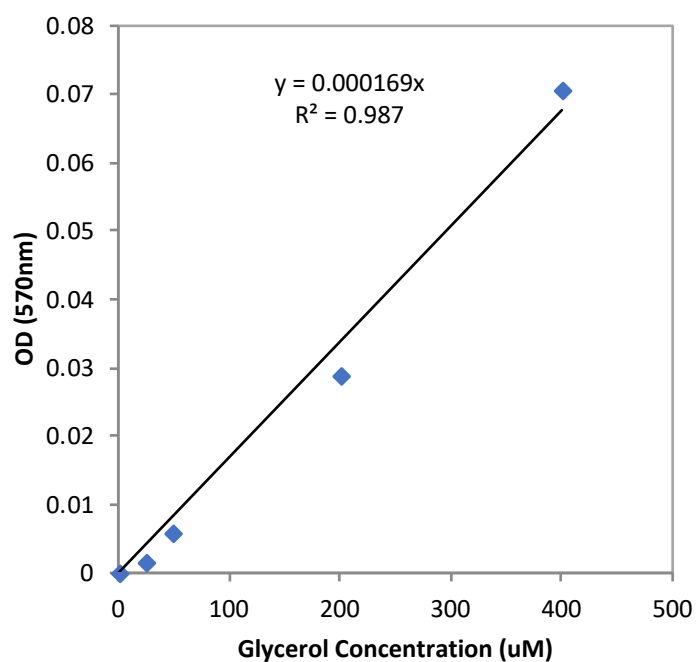
Appendix 1.6b. Sample calibration curve for 7-Hydroxycoumarin (bioconversion product) concentration. Experiments carried out as described in Section 2.8.3.



Appendix 1.7. Determination of optimal absorbance of 7-Ethoxycoumarin by nanodrop measurement.



Appendix 1.8. Sample calibration curve for quantification of free glycerol concentration. Experiments carried out as described in Section 2.8.



Appendix 2.1. Design and raw data for 9 factor, 64 run DoE design for screening bioconversion of 7-ethoxycoumarin to 7-hydroxycoumarin.

Factor		A	B	C	D	E	F	G	H	J	Response
		Post Ind. Time	[Subs]	Post Ind. Vol.	Pre Ind. Time	Temp. (Post Ind.)	Subs addition time	[Yeast Extract]	Buffer	Shaker Speed	[7-hydroxycoumarin]
Std Order		(hrs)	(mM)	(mL)	(hrs)	(°C)	(hrs)	(g/L)		(rpm)	
1	Block 1	8	0.1	500	2	25	0.17	10	Yes	300	0.056
2	Block 1	65	0.1	500	2	25	1	30	Yes	300	0.052
3	Block 1	8	1	500	2	25	1	30	No	300	0.000
4	Block 1	65	1	500	2	25	0.17	10	No	300	0.983
5	Block 1	8	0.1	1000	2	25	1	10	No	300	0.123
6	Block 1	65	0.1	1000	2	25	0.17	30	No	300	0.000
7	Block 1	8	1	1000	2	25	0.17	30	Yes	300	0.000
8	Block 1	65	1	1000	2	25	1	10	Yes	300	0.789
9	Block 1	8	0.1	500	5	25	0.17	30	No	300	0.000
10	Block 1	65	0.1	500	5	25	1	10	No	300	0.272
11	Block 1	8	1	500	5	25	1	10	Yes	300	0.000
12	Block 1	65	1	500	5	25	0.17	30	Yes	300	0.326
13	Block 1	8	0.1	1000	5	25	1	30	Yes	300	0.000
14	Block 1	65	0.1	1000	5	25	0.17	10	Yes	300	0.168
15	Block 1	8	1	1000	5	25	0.17	10	No	300	0.000
16	Block 1	65	1	1000	5	25	1	30	No	300	0.000
17	Block 1	8	0.1	500	2	37	0.17	10	No	300	0.091
18	Block 1	65	0.1	500	2	37	1	30	No	300	0.000
19	Block 1	8	1	500	2	37	1	30	Yes	300	0.000
20	Block 1	65	1	500	2	37	0.17	10	Yes	300	1.289
21	Block 1	8	0.1	1000	2	37	1	10	Yes	300	0.000
22	Block 1	65	0.1	1000	2	37	0.17	30	Yes	300	0.030
23	Block 1	8	1	1000	2	37	0.17	30	No	300	0.000
24	Block 1	65	1	1000	2	37	1	10	No	300	0.928
25	Block 1	8	0.1	500	5	37	0.17	30	Yes	300	0.000
26	Block 1	65	0.1	500	5	37	1	10	Yes	300	0.022
27	Block 1	8	1	500	5	37	1	10	No	300	0.110
28	Block 1	65	1	500	5	37	0.17	30	No	300	0.297
29	Block 1	8	0.1	1000	5	37	1	30	No	300	0.000
30	Block 1	65	0.1	1000	5	37	0.17	10	No	300	0.173
31	Block 1	8	1	1000	5	37	0.17	10	Yes	300	0.047
32	Block 1	65	1	1000	5	37	1	30	Yes	300	0.439
33	Block 2	65	1	1000	5	37	1	30	No	1100	2.613
34	Block 2	8	1	1000	5	37	0.17	10	No	1100	4.944
35	Block 2	65	0.1	1000	5	37	0.17	10	Yes	1100	1.840

36	Block 2	8	0.1	1000	5	37	1	30	Yes	1100	1.197
37	Block 2	65	1	500	5	37	0.17	30	Yes	1100	1.783
38	Block 2	8	1	500	5	37	1	10	Yes	1100	1.829
39	Block 2	65	0.1	500	5	37	1	10	No	1100	5.047
40	Block 2	8	0.1	500	5	37	0.17	30	No	1100	1.954
41	Block 2	65	1	1000	2	37	1	10	Yes	1100	2.458
42	Block 2	8	1	1000	2	37	0.17	30	Yes	1100	1.409
43	Block 2	65	0.1	1000	2	37	0.17	30	No	1100	2.160
44	Block 2	8	0.1	1000	2	37	1	10	No	1100	3.964
45	Block 2	65	1	500	2	37	0.17	10	No	1100	5.189
46	Block 2	8	1	500	2	37	1	30	No	1100	2.012
47	Block 2	65	0.1	500	2	37	1	30	Yes	1100	0.927
48	Block 2	8	0.1	500	2	37	0.17	10	Yes	1100	1.677
49	Block 2	65	1	1000	5	25	1	30	Yes	1100	4.473
50	Block 2	8	1	1000	5	25	0.17	10	Yes	1100	2.507
51	Block 2	65	0.1	1000	5	25	0.17	10	No	1100	3.989
52	Block 2	8	0.1	1000	5	25	1	30	No	1100	2.223
53	Block 2	65	1	500	5	25	0.17	30	No	1100	2.862
54	Block 2	8	1	500	5	25	1	10	No	1100	4.777
55	Block 2	65	0.1	500	5	25	1	10	Yes	1100	1.728
56	Block 2	8	0.1	500	5	25	0.17	30	Yes	1100	1.252
57	Block 2	65	1	1000	2	25	1	10	No	1100	4.267
58	Block 2	8	1	1000	2	25	0.17	30	No	1100	2.073
59	Block 2	65	0.1	1000	2	25	0.17	30	Yes	1100	1.005
60	Block 2	8	0.1	1000	2	25	1	10	Yes	1100	1.580
61	Block 2	65	1	500	2	25	0.17	10	Yes	1100	1.929
62	Block 2	8	1	500	2	25	1	30	Yes	1100	1.420
63	Block 2	65	0.1	500	2	25	1	30	No	1100	2.727
64	Block 2	8	0.1	500	2	25	0.17	10	No	1100	3.916

Appendix 2.2. Example calculation for determining oxygen demand as a result of each of the major contributors during culture and whole cell bioconversion by simultaneous equations.

Using the experimental data generated in Section 3, the following equations can be derived:

$$\text{Peak } OUR_{NI-B} = \alpha [\text{Peak Biomass}] + \beta [\text{Peak Volumetric Productivity}]$$

Equation A1

$$\text{Peak } OUR_{I-B} = \alpha [\text{Peak Biomass}] + \beta [\text{Peak Volumetric Productivity}] + \gamma [\text{Peak Product}]$$

Equation A2

$$\text{Peak } OUR_{I-FB} = \alpha [\text{Peak Biomass}] + \beta [\text{Peak Volumetric Productivity}] + \gamma [\text{Peak Product}]$$

Equation A3

Where, α is the oxygen demand for sustaining peak biomass concentration per unit biomass, β is the oxygen demand for growth per unit volumetric productivity with respect to biomass accumulation and γ is the oxygen demand for bioconversion of 7-ethoxycoumarin to 7-hydroxycoumarin per unit bioconversion product.

Therefore,

$$\text{Peak } OUR_{NI-B} = 14.4\alpha + 2.31\beta$$

Equation A4

$$\text{Peak } OUR_{I-B} = 4.1\alpha + 0.31\beta + 1.36\gamma$$

Equation A5

$$\text{Peak } OUR_{I-FB} = 26.2\alpha + 1.56\beta + 0.66\gamma$$

Equation A6

Resulting in three simultaneous equations:

$$19.9 = 14.4\alpha + 2.31\beta$$

Equation A7

$$5.68 = 4.1\alpha + 0.31\beta + 1.36\gamma$$

Equation A8

$$25.8 = 26.2\alpha + 1.56\beta + 0.66\gamma$$

Equation A9

Which can be solved to give:

$$\alpha = 0.71$$

$$\beta = 4.23$$

$$\gamma = 1.69$$

Appendix 3.1. DoE design and raw data for the linear screening experiment to model oxygen mass transfer values in 24DSW plates.

Temperature (°C)	Shaker Speed (RPM)	Fill Volume (mL)	Biomass Concentration (gDCW/L)	kLa (1/h)	OUR (mgO ₂ /L/hr)
30	250	1600	0.35	121.47	58.34
			0.35	80.03	43.30
		3200	0.35	58.28	68.66
			0.35	52.97	73.46
		1600	1.75	105.45	172.79
			1.75	85.49	163.67
30	200	1600	0.35	65.94	43.88
			0.35	65.07	58.42
		3200	0.35	32.52	77.62
			0.35	30.12	82.89
37	250	1600	0.35	107.82	42.54
			0.35	100.28	32.47
		3200	0.35	39.68	53.55
			0.35	52.54	57.07
		1600	1.75	122.25	156.57
			1.75	120.87	140.64
37	200	1600	0.35	103.05	87.64
			0.35	80.83	57.12
		3200	0.35	31.89	78.04
			0.35	57.07	82.95

Appendix 3.2a. DoE design and raw data for modelling oxygen mass transfer values in 24DSW plates using the new dynamic gassing method in Section 4.

Fill Volume	Shaking Speed	Post Induction Temp.	% Inoculum	Log Hour Time	Max Biomass Conc.	GFP Fluorescence	Max Specific Growth Rate	kLa	OUR
(μ L)	(RPM)	($^{\circ}$ C)		(hr)	(gDCW/L)	($\times 10^6$ RFUs)		(hr $^{-1}$)	(mgO $_2$ /L/h)
1600	200	30	1	0	5.36	1.488	10.22	82.66	518.0
1600	200	30	1	8	5.36	1.441	10.22	82.66	518.0
1600	200	30	5	0	4.79	1.376	0.63	82.66	545.3
1600	200	30	5	8	4.79	1.380	0.63	82.66	545.3
1600	200	37	1	0	4.90	1.659	16.16	82.66	508.2
1600	200	37	1	8	4.90	1.407	16.16	82.66	508.2
1600	200	37	5	0	3.40	1.511	18.89	82.66	507.9
1600	200	37	5	8	3.40	1.842	18.89	82.66	507.9
1600	250	30	1	8	4.33	1.260	0.83	103.5	739.5
1600	250	30	5	8	3.91	1.385	0.77	103.5	684.5
1600	250	37	1	0	8.15	1.348	0.81	103.5	741.2
1600	250	37	1	8	8.15	1.244	0.81	103.5	741.2

1600	250	37	5	0	7.70	1.632	0.72	103.5	736.6
1600	250	37	5	8	7.70	1.381	0.72	103.5	736.6
3200	200	30	1	0	4.31	1.375	5.06	33.97	304.5
3200	200	30	1	8	4.31	1.510	5.06	33.97	304.5
3200	200	30	5	0	3.93	1.332	0.91	33.97	227.7
3200	200	30	5	8	3.93	1.447	0.91	33.97	227.7
3200	200	37	1	0	3.29	1.609	20.45	33.97	197.0
3200	200	37	1	8	3.29	2.146	20.45	33.97	197.0
3200	200	37	5	0	2.32	1.522	7.45	33.97	210.4
3200	200	37	5	8	2.32	1.769	7.45	33.97	210.4
3200	250	30	1	8	3.94	1.265	0.80	54.8	361.7
3200	250	30	5	8	3.81	1.413	1.04	54.8	350.7
3200	250	37	1	0	7.10	1.291	2.62	54.8	415.4
3200	250	37	1	8	7.10	1.213	2.62	54.8	415.4
3200	250	37	5	8	7.02	1.170	2.73	54.8	346.4

Appendix 3.2b. DoE design and raw data for modelling oxygen mass transfer values in 96DSW plates using the new dynamic gassing method in Section 4.

Fill Volume	Shaking Speed	Post Induction Temp.	% Inoculum	Log Hour Time	Max Biomass Conc.	GFP Fluorescence	Max Specific Growth Rate
(μ L)	(RPM)	($^{\circ}$ C)		(hr)	(gDCW/L)	($\times 10^6$ RFUs)	
400	600	30	1	8	2.69	1.67	8.18
400	600	30	1	24	6.14	2.77	8.18
400	600	30	1	32	6.02	2.92	8.18
400	600	30	1	48	6.92	3.10	8.18
400	600	30	1	56	6.04	3.26	8.18
400	600	30	5	8	3.85	1.56	1.64
400	600	30	5	24	5.88	2.81	1.64
400	600	30	5	32	5.87	3.07	1.64
400	600	30	5	48	5.97	3.26	1.64
400	600	30	5	56	5.88	3.35	1.64
400	600	37	1	8	3.21	1.89	14.61
400	600	37	1	24	3.74	4.65	14.61
400	600	37	1	32	4.45	6.55	14.61
400	600	37	1	48	3.41	8.69	14.61
400	600	37	1	56	2.62	4.43	14.61
400	600	37	5	8	2.89	1.95	8.22
400	600	37	5	24	3.90	5.54	8.22
400	600	37	5	32	3.29	4.86	8.22
400	600	37	5	48	1.48	3.22	8.22
400	600	37	5	56	4.63	6.98	8.22
400	1100	30	1	8	0.07	1.28	35.93
400	1100	30	1	24	4.71	2.46	35.93
400	1100	30	1	32	3.73	2.50	35.93
400	1100	30	1	48	1.54	3.29	35.93
400	1100	30	1	56	14.44	1.14	35.93
400	1100	30	5	8	0.28	1.24	8.11
400	1100	30	5	24	4.40	2.64	8.11
400	1100	30	5	32	4.02	2.92	8.11
400	1100	30	5	48	2.65	3.13	8.11
400	1100	30	5	56	8.35	1.72	8.11
400	1100	37	1	8	5.42	1.65	0.86
400	1100	37	1	24	5.94	3.52	0.86
400	1100	37	1	32	7.48	3.41	0.86
400	1100	37	1	48	7.31	4.05	0.86
400	1100	37	1	56	6.24	7.35	0.86
400	1100	37	5	8	6.07	1.91	1.01
400	1100	37	5	24	6.01	2.99	1.01

400	1100	37	5	32	7.62	3.41	1.01
400	1100	37	5	48	7.35	4.19	1.01
400	1100	37	5	56	5.31	8.38	1.01
800	600	30	1	8	2.51	1.57	0.86
800	600	30	1	24	5.17	2.12	0.86
800	600	30	1	32	5.02	2.51	0.86
800	600	30	1	48	5.59	3.18	0.86
800	600	30	1	56	3.99	3.39	0.86
800	600	30	5	8	2.95	1.56	4.08
800	600	30	5	24	4.79	2.19	4.08
800	600	30	5	32	5.30	2.60	4.08
800	600	30	5	48	5.31	3.15	4.08
800	600	37	1	8	0.32	0.11	0.56
800	600	37	1	24	8.36	2.84	0.56
800	600	37	1	32	8.00	2.72	0.56
800	600	37	1	48	5.87	2.00	0.56
800	600	37	1	56	10.71	3.64	0.56
800	600	37	5	8	5.56	1.89	2.91
800	600	37	5	24	7.99	2.72	2.91
800	600	37	5	32	9.43	3.21	2.91
800	600	37	5	48	10.02	3.41	2.91
800	600	37	5	56	10.56	3.59	2.91
800	1100	30	1	8	-0.06	-0.02	6.22
800	1100	30	1	24	1.90	0.65	6.22
800	1100	30	1	32	12.95	4.40	6.22
800	1100	30	1	48	39.29	13.36	6.22
800	1100	30	1	56	11.31	3.85	6.22
800	1100	30	5	8	0.67	0.23	4.45
800	1100	30	5	24	1.47	0.50	4.45
800	1100	30	5	32	9.44	3.21	4.45
800	1100	30	5	48	9.23	3.14	4.45
800	1100	30	5	56	8.73	2.97	4.45
800	1100	37	1	8	12.37	4.21	4.04
800	1100	37	1	24	17.41	5.92	4.04
800	1100	37	1	32	18.01	6.12	4.04
800	1100	37	1	48	18.70	6.36	4.04
800	1100	37	1	56	17.87	6.08	4.04
800	1100	37	5	8	12.28	4.18	4.61
800	1100	37	5	24	17.43	5.93	4.61
800	1100	37	5	32	17.01	5.78	4.61
800	1100	37	5	48	18.47	6.28	4.61
800	1100	37	5	56	12.91	4.39	4.61

Appendix 4.1. Experimental designs for oxygen mass transfer characterisation of single use bioreactors.

Bioreactor Study	Factor	Unit	Range set points					
			Minimum	Low	Centre	High	Maximum	
BioFlo 310 (STR)	A	Viscosity by [Gly]	mL/L	0	8.69	15	21.31	30
	B	Aeration Rate	vvm	0.125	0.43	0.75	1.07	1.5
	C	Agitation Rate	rpm	100	418.8	650	881.2	1200
	D	Temperature	°C	15	25.14	32.5	39.86	50
	E	Antifoam	%v/v	0.0	0.036	0.055	0.074	0.10
XDR-10 (Tank liner)	A	Aeration Rate	vvm	0.25	0.58	0.75	0.92	1.25
	B	Agitation Rate	rpm	120	200	240	280	360
	C	Temperature	°C	15.0	26.7	32.5	38.3	50.0
Ambr®250	A	Aeration Rate	vvm	0.5	1.0	1.5	2.0	2.5
	B	Agitation Rate	rpm	100	825	1550	2275	3000
	C	Viscosity by [Gly]	mL/L	0.0	7.5	15.0	22.5	30.0
	D	Temperature	°C	15.0	23.8	32.5	41.3	50.0
	E	Antifoam	%v/v	0.0	0.025	0.05	0.075	0.10

Appendix 4.2. Pilot Scale STR DoE design and raw data table.

Std	Run	Factor 1 A:Viscosity by [Gly] (ml/L)	Factor 2 B:Aeration (vvm)	Factor 3 C:Agitation (rpm)	Factor 4 D:Temperature (°C)	Factor 5 E:Antifoam (%v/v PPG)	Response kLa (PRT) (s-1)
1	12	8.69	0.43	418.8	25.14	0.0361	0.0112
2	39	21.31	0.43	418.8	25.14	0.0361	0.0195
3	26	8.69	1.07	418.8	25.14	0.0361	0.0199
4	41	21.31	1.07	418.8	25.14	0.0361	0.0373
5	11	8.69	0.43	881.2	25.14	0.0361	0.0087
6	49	21.31	0.43	881.2	25.14	0.0361	0.0167
7	44	8.69	1.07	881.2	25.14	0.0361	0.0112
8	1	21.31	1.07	881.2	25.14	0.0361	0.0887
9	2	8.69	0.43	418.8	39.86	0.0361	0.0219
10	24	21.31	0.43	418.8	39.86	0.0361	0.0000201
11	37	8.69	1.07	418.8	39.86	0.0361	0.0327
12	35	21.31	1.07	418.8	39.86	0.0361	0.0518
13	34	8.69	0.43	881.2	39.86	0.0361	0.017
14	3	21.31	0.43	881.2	39.86	0.0361	0.0000228
15	50	8.69	1.07	881.2	39.86	0.0361	0.0907
16	8	21.31	1.07	881.2	39.86	0.0361	0.293
17	16	8.69	0.43	418.8	25.14	0.0739	0.0024
18	5	21.31	0.43	418.8	25.14	0.0739	0.0156
19	6	8.69	1.07	418.8	25.14	0.0739	0.0006
20	20	21.31	1.07	418.8	25.14	0.0739	0.0405
21	36	8.69	0.43	881.2	25.14	0.0739	0.0219
22	7	21.31	0.43	881.2	25.14	0.0739	0.0243
23	48	8.69	1.07	881.2	25.14	0.0739	0.0737
24	43	21.31	1.07	881.2	25.14	0.0739	0.0746
25	38	8.69	0.43	418.8	39.86	0.0739	0.0152
26	40	21.31	0.43	418.8	39.86	0.0739	0.0159
27	29	8.69	1.07	418.8	39.86	0.0739	0.0479
28	28	21.31	1.07	418.8	39.86	0.0739	0.0325
29	18	8.69	0.43	881.2	39.86	0.0739	0.0161
30	19	21.31	0.43	881.2	39.86	0.0739	0.0168
31	30	8.69	1.07	881.2	39.86	0.0739	0.119
32	27	21.31	1.07	881.2	39.86	0.0739	0.1
33	15	0	0.75	650	32.5	0.055	0.0518
34	4	30	0.75	650	32.5	0.055	0.0518
35	45	15	0.125	650	32.5	0.055	0.0035
36	23	15	1.5	650	32.5	0.055	0.193
37	32	15	0.75	100	32.5	0.055	0.0024
38	25	15	0.75	1200	32.5	0.055	0.0426

39	13	15	0.75	650	15	0.055	0.0256
40	46	15	0.75	650	50	0.055	0.193
41	9	15	0.75	650	32.5	0	0.0297
42	17	15	0.75	650	32.5	0.1	0.0787
43	10	15	0.75	650	32.5	0.055	0.0587
44	22	15	0.75	650	32.5	0.055	0.0621
45	21	15	0.75	650	32.5	0.055	0.0734
46	14	15	0.75	650	32.5	0.055	0.0533
47	33	15	0.75	650	32.5	0.055	0.0495
48	31	15	0.75	650	32.5	0.055	0.0605
49	47	15	0.75	650	32.5	0.055	0.0608
50	42	15	0.75	650	32.5	0.055	0.0564

Appendix 4.3. XDR-10 SUB DoE design and raw data table.

Std	Run	Factor 1	Factor 2	Factor 3	Response
		A:Aeration vvm	B:Agitation rpm	C:Temp DegC	kLa (PRT) s-1
1	2	0.58	200	26.67	0.0083
2	8	0.92	200	26.67	0.0093
3	12	0.58	280	26.67	0.0135
4	3	0.92	280	26.67	0.0140
5	4	0.58	200	38.33	0.0067
6	17	0.92	200	38.33	0.0083
7	7	0.58	280	38.33	0.0144
8	18	0.92	280	38.33	0.0178
9	11	0.25	240	32.50	0.0085
10	1	1.25	240	32.50	0.0088
11	5	0.75	120	32.50	0.0032
12	16	0.75	360	32.50	0.0235
13	13	0.75	240	15.00	0.0128
14	9	0.75	240	50.00	0.0153
15	14	0.75	240	32.50	0.0093
16	10	0.75	240	32.50	0.0082
17	6	0.75	240	32.50	0.0083
18	15	0.75	240	32.50	0.0089

Appendix 4.4. Ambr®250 SUB DoE design and raw data table.

Run	BR Position	Factor	Factor	Factor	Factor	Factor	kLa (s-1)			Mean
		1	2	3	4	5	Repeat 1	Repeat 2	Repeat 3	
1	2	0.5	825	7.5	23.8	0.025	0.0059	0.0055	0.0056	0.0057
2	6	0.5	825	7.5	23.8	0.075	0.0050	0.0049	0.0050	0.0050
3	2	0.5	825	7.5	41.3	0.025	0.0056	0.0056	0.0057	0.0056
4	6	0.5	825	7.5	41.3	0.075	0.0055	0.0056	0.0056	0.0056
5	4	0.5	825	22.5	23.8	0.025	0.0051	0.0051	0.0052	0.0051
6	8	0.5	825	22.5	23.8	0.075	0.0048	0.0048	0.0048	0.0048
7	4	0.5	825	22.5	41.3	0.025	0.0054	0.0055	0.0055	0.0055
8	8	0.5	825	22.5	41.3	0.075	0.0053	0.0053	0.0054	0.0054
9	2	0.5	2275	7.5	23.8	0.025	0.0185	0.0191	0.0189	0.0188
10	6	0.5	2275	7.5	23.8	0.075	0.0249	0.0244	0.0236	0.0243
11	2	0.5	2275	7.5	41.3	0.025	0.0238	0.0241	0.0233	0.0237
12	6	0.5	2275	7.5	41.3	0.075	0.0357	0.0370	0.0348	0.0359
13	4	0.5	2275	22.5	23.8	0.025	0.0191	0.0190	0.0190	0.0190
14	8	0.5	2275	22.5	23.8	0.075	0.0215	0.0208	0.0206	0.0210
15	4	0.5	2275	22.5	41.3	0.025	0.0236	0.0241	0.0236	0.0237
16	8	0.5	2275	22.5	41.3	0.075	0.0290	0.0282	0.0282	0.0285
17	2	1.5	825	7.5	23.8	0.025	0.0091	0.0096	0.0100	0.0096
18	6	1.5	825	7.5	23.8	0.075	0.0091	0.0095	0.0096	0.0094
19	2	1.5	825	7.5	41.3	0.025	0.0101	0.0117	0.0125	0.0115
20	6	1.5	825	7.5	41.3	0.075	0.0114	0.0120	0.0125	0.0120
21	4	1.5	825	22.5	23.8	0.025	0.0083	0.0088	0.0090	0.0087
22	8	1.5	825	22.5	23.8	0.075	0.0088	0.0090	0.0091	0.0089
23	4	1.5	825	22.5	41.3	0.025	0.0103	0.0111	0.0114	0.0109
24	8	1.5	825	22.5	41.3	0.075	0.0118	0.0123	0.0124	0.0121
25	2	1.5	2275	7.5	23.8	0.025	0.1502	0.1348	0.1531	0.1460
26	6	1.5	2275	7.5	23.8	0.075	0.0601	0.0661	0.0602	0.0621
27	2	1.5	2275	7.5	41.3	0.025	0.0765	0.0769	0.0703	0.0746
28	6	1.5	2275	7.5	41.3	0.075	0.1295	0.1404	0.1295	0.1332
29	4	1.5	2275	22.5	23.8	0.025	0.1126	0.1182	0.1048	0.1119
30	8	1.5	2275	22.5	23.8	0.075	0.1029	0.1048	0.1051	0.1043
31	4	1.5	2275	22.5	41.3	0.025	0.0786	0.0781	0.0765	0.0778
32	8	1.5	2275	22.5	41.3	0.075	0.0844	0.0876	0.0905	0.0875
33	3	0.0	1550	15.0	32.5	0.050	0.0016	0.0016	0.0016	0.0016
34	3	2.0	1550	15.0	32.5	0.050	0.0505	0.0493	0.0660	0.0553
35	3	1.0	100	15.0	32.5	0.050	0.0021	0.0021	0.0021	0.0021
36	3	1.0	3000	15.0	32.5	0.050	0.0282	0.0283	0.0284	0.0283
37	1	1.0	1550	0.0	32.5	0.050	0.0980	0.0984	0.0980	0.0982
38	5	1.0	1550	30.0	32.5	0.050	0.0955	0.0910	0.0934	0.0933

39	3	1.0	1550	15.0	15.0	0.050	0.0229	0.0220	0.0220	0.0223
40	3	1.0	1550	15.0	50.0	0.050	0.1737	0.1772	0.1629	0.1713
41	3	1.0	1550	15.0	32.5	0.000	0.1048	0.1026	0.0924	0.0999
42	3	1.0	1550	15.0	32.5	0.100	0.0418	0.0391	0.0413	0.0407
43	7	1.0	1550	15.0	32.5	0.050	0.1279	0.1442	0.1222	0.1314
44	7	1.0	1550	15.0	32.5	0.050	0.1387	0.1126	0.1348	0.1287
45	7	1.0	1550	15.0	32.5	0.050	0.1281	0.1422	0.1463	0.1389
46	7	1.0	1550	15.0	32.5	0.050	0.1387	0.1412	0.1540	0.1447
47	7	1.0	1550	15.0	32.5	0.050	0.1447	0.1464	0.1446	0.1452
48	7	1.0	1550	15.0	32.5	0.050	0.1182	0.1287	0.1093	0.1187
49	7	1.0	1550	15.0	32.5	0.050	0.1236	0.1123	0.1248	0.1202
50	7	1.0	1550	15.0	32.5	0.050	0.1117	0.1255	0.1300	0.1224
51	7	1.0	1550	15.0	32.5	0.050	0.1048	0.1410	0.1273	0.1244
52	7	1.0	1550	15.0	32.5	0.050	0.1311	0.1400	0.1150	0.1287

Appendix 4.5. Model expression for oxygen mass transfer in the New Brunswick BioFlo 310

$$\begin{aligned} & -0.073986893 \\ & + 0.0980723359 \cdot \text{Aeration Rate (vvm)} \\ & + 0.0000708865 \cdot \text{Agitation Rate (rpm)} \\ & + \left(\text{Glycerol Concentration (mL/L)} - 15 \right) \cdot \left(\left(\text{Aeration Rate (vvm)} - 0.7525 \right) \cdot 0.0050414848 \right) \\ & + 0.025815381 \cdot \text{Antifoam Concentration (\%v/v)} \\ & + \left(\text{Glycerol Concentration (mL/L)} - 15 \right) \cdot \left(\left(\text{Temperature (}^\circ\text{C)} - 32.5 \right) \cdot -1.215041\text{e-}5 \right) \\ & + \left(\text{Aeration Rate (vvm)} - 0.7525 \right) \cdot \left(\left(\text{Agitation Rate (rpm)} - 650 \right) \cdot 0.0002398734 \right) \\ & + \left(\text{Aeration Rate (vvm)} - 0.7525 \right) \cdot \left(\left(\text{Temperature (}^\circ\text{C)} - 32.5 \right) \cdot 0.0057338271 \right) \\ & + \left(\text{Agitation Rate (rpm)} - 650 \right) \cdot \left(\left(\text{Antifoam Concentration (\%v/v)} - 0.0548 \right) \cdot -0.000399791 \right) \\ & + \left(\text{Temperature (}^\circ\text{C)} - 32.5 \right) \cdot \left(\left(\text{Antifoam Concentration (\%v/v)} - 0.0548 \right) \cdot -0.039445211 \right) \\ & + \left(\text{Aeration Rate (vvm)} - 0.7525 \right) \cdot \left(\left(\text{Aeration Rate (vvm)} - 0.7525 \right) \cdot 0.0441625747 \right) \\ & + \left(\text{Agitation Rate (rpm)} - 650 \right) \cdot \left(\left(\text{Agitation Rate (rpm)} - 650 \right) \cdot -1.581246\text{e-}7 \right) \\ & + \left(\text{Temperature (}^\circ\text{C)} - 32.5 \right) \cdot \left(\left(\text{Temperature (}^\circ\text{C)} - 32.5 \right) \cdot 0.0001271651 \right) \end{aligned}$$

Appendix 4.6. Model expression for oxygen mass transfer in the Xcellerex XDR-10

$$\begin{aligned} & -0.012667803 \\ & + 0.0000846154 \cdot \text{Agitation Speed (rpm)} \\ & + 0.000063311 \cdot \text{Temperature (}^\circ\text{C)} \\ & + \left(\text{Agitation Speed (rpm)} - 240 \right) \cdot \left(\left(\text{Temperature (}^\circ\text{C)} - 32.5 \right) \cdot 3.9129503\text{e-}6 \right) \\ & + \left(\text{Agitation Speed (rpm)} - 240 \right) \cdot \left(\left(\text{Agitation Speed (rpm)} - 240 \right) \cdot 2.8036527\text{e-}7 \right) \\ & + \left(\text{Temperature (}^\circ\text{C)} - 32.5 \right) \cdot \left(\left(\text{Temperature (}^\circ\text{C)} - 32.5 \right) \cdot 0.0000154672 \right) \end{aligned}$$

Appendix 4.7. Model expression for oxygen mass transfer in the Ambr[®]250



$$\begin{aligned}
 &0.13150783303465 \\
 &+ 0.02297259259259 * \left[\frac{[\text{Agitation rate (rpm)} - 1550]}{725} \right] \\
 &+ 0.01875518518519 * \left[\frac{[\text{Aeration Rate (vvm)} - 1]}{0.5} \right] \\
 &+ 0.00716708333333 * \left[\frac{[\text{Temp (C)} - 32.5]}{8.75} \right] \\
 &+ -0.0029143981481 * \left[\frac{[[A/F] (\% \text{ v/v}) - 0.05]}{0.025} \right] \\
 &+ \left[\frac{[\text{Agitation rate (rpm)} - 1550]}{725} \right] * \left[\left[\frac{[\text{Agitation rate (rpm)} - 1550]}{725} \right] * -0.0305438097372 \right] \\
 &+ \left[\frac{[\text{Agitation rate (rpm)} - 1550]}{725} \right] * \left[\left[\frac{[\text{Aeration Rate (vvm)} - 1]}{0.5} \right] * 0.01755966435185 \right] \\
 &+ \left[\frac{[\text{Aeration Rate (vvm)} - 1]}{0.5} \right] * \left[\left[\frac{[\text{Aeration Rate (vvm)} - 1]}{0.5} \right] * -0.0272352449223 \right] \\
 &+ \left[\frac{[\text{Temp (C)} - 32.5]}{8.75} \right] * \left[\left[\frac{[\text{Temp (C)} - 32.5]}{8.75} \right] * -0.010148786589 \right] \\
 &+ \left[\frac{[\text{Temp (C)} - 32.5]}{8.75} \right] * \left[\left[\frac{[[A/F] (\% \text{ v/v}) - 0.05]}{0.025} \right] * 0.00537112268519 \right] \\
 &+ \left[\frac{[[A/F] (\% \text{ v/v}) - 0.05]}{0.025} \right] * \left[\left[\frac{[[A/F] (\% \text{ v/v}) - 0.05]}{0.025} \right] * -0.0167659162186 \right] \\
 &+ \left[\frac{[\text{Viscosity (by [Gly])} - 15]}{7.5} \right] * \left[\left[\frac{[\text{Viscosity (by [Gly])} - 15]}{7.5} \right] * -0.0104123282557 \right]
 \end{aligned}$$



Appendix 4.8. Examples sections of Ambr[®]250 automated DoE Protocol







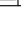
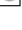


1 2 3 4 5 6 7 8 9 10 11 12
Bioreactor selection

























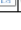

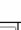













Navigation < Experiment\Protocols\BR7- Media 3 ([Gly]=15) [Bioreactor 7]















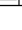
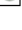








Edit the steps that define what is to be done for the protocol.

Wait loaded				
1.1		Fri 08 Jul 2016 11:14	Fri 08 Jul 2016 11:14	Wait loaded  

Start experiment				
2.1		Fri 08 Jul 2016 11:14	Fri 08 Jul 2016 11:14	Marker for when the experiment :  

Add media				
3.1		Fri 08 Jul 2016 11:14	Fri 08 Jul 2016 11:14	Wait ALL loaded  
3.2		Fri 08 Jul 2016 11:21	Fri 08 Jul 2016 11:21	Wait til Fri 08 Jul 2016 11:15  
3.3		Fri 08 Jul 2016 11:21	Fri 08 Jul 2016 12:05	Fill Media  
3.4		Fri 08 Jul 2016 12:06	Fri 08 Jul 2016 13:46	Bolus A/F (0.05%)  
3.5		Fri 08 Jul 2016 13:46	Fri 08 Jul 2016 13:48	Wait for 2min  

Conditioning and calibration				
4.1		Fri 08 Jul 2016 13:48	Fri 08 Jul 2016 13:48	Wait loaded  
4.2		Fri 08 Jul 2016 13:48	Fri 08 Jul 2016 13:48	Temperature on  
4.3		Fri 08 Jul 2016 13:48	Fri 08 Jul 2016 13:48	Stir speed on  
4.4		Fri 08 Jul 2016 14:03	Fri 08 Jul 2016 14:03	Wait pumps and loops enabled  
4.5		Fri 08 Jul 2016 14:03	Fri 08 Jul 2016 14:03	Turn spot reading on  
4.6		Fri 08 Jul 2016 14:03	Fri 08 Jul 2016 14:03	Turn foam sensor on  
4.7		Fri 08 Jul 2016 14:03	Fri 08 Jul 2016 14:18	Wait until at temperature  
4.8		Fri 08 Jul 2016 14:18	Fri 08 Jul 2016 14:18	Set from loop properties for DO  
4.9		Fri 08 Jul 2016 14:18	Fri 08 Jul 2016 14:18	Set air flow rate if not set by conti  
4.10		Fri 08 Jul 2016 14:18	Fri 08 Jul 2016 18:18	Wait for 4h interval  
4.11		Fri 08 Jul 2016 18:18	Fri 08 Jul 2016 19:18	Calibrate DO spot and offgas sen:  
4.12		Fri 08 Jul 2016 19:18	Fri 08 Jul 2016 19:23	Wait so that got some readings w  
4.13		Fri 08 Jul 2016 19:23	Fri 08 Jul 2016 19:23	Check DO  
4.14		Fri 08 Jul 2016 19:23	Fri 08 Jul 2016 19:23	Check Off-gas O ₂ reading  
4.15		Fri 08 Jul 2016 19:23	Fri 08 Jul 2016 19:23	Set outputs of DO control loop of  
4.16		Fri 08 Jul 2016 19:23	Fri 08 Jul 2016 19:23	Gas flow (Air/mix) on  
4.17		Fri 08 Jul 2016 19:23	Fri 08 Jul 2016 19:23	Stir speed on  
4.18		Sat 09 Jul 2016 11:28	Sat 09 Jul 2016 11:28	Wait til Sat 09 Jul 2016 09:00  
4.19		Sat 09 Jul 2016 11:28	Sat 09 Jul 2016 11:28	pH off  
4.20		Sat 09 Jul 2016 11:28	Sat 09 Jul 2016 11:28	Wait til Sat 09 Jul 2016 09:15  

Run #44				
5.1		Sat 09 Jul 2016 11:28	Sat 09 Jul 2016 11:28	Gas flow (Air/mix) off  
5.2		Sat 09 Jul 2016 11:28	Sat 09 Jul 2016 11:28	N2 on (drop to 0% DOT)  
5.3		Sat 09 Jul 2016 11:28	Sat 09 Jul 2016 11:33	Wait to reach DOT min  
5.4		Sat 09 Jul 2016 11:33	Sat 09 Jul 2016 11:33	Run #44 i  
5.5		Sat 09 Jul 2016 11:33	Sat 09 Jul 2016 11:33	N2 off  
5.6		Sat 09 Jul 2016 11:33	Sat 09 Jul 2016 11:33	Gas flow (Air/mix) on  
5.7		Sat 09 Jul 2016 11:33	Sat 09 Jul 2016 11:39	Wait to reach DOT max  
5.8		Sat 09 Jul 2016 11:39	Sat 09 Jul 2016 11:39	Gas flow (Air/mix) off  
5.9		Sat 09 Jul 2016 11:39	Sat 09 Jul 2016 11:39	N2 on (drop to 0% DOT)  
5.10		Sat 09 Jul 2016 11:39	Sat 09 Jul 2016 11:43	Wait to reach DOT min  
5.11		Sat 09 Jul 2016 11:43	Sat 09 Jul 2016 11:43	Run#44 ii  
5.12		Sat 09 Jul 2016 11:43	Sat 09 Jul 2016 11:43	N2 off  
5.13		Sat 09 Jul 2016 11:43	Sat 09 Jul 2016 11:43	Gas flow (Air/mix) on
5.14		Sat 09 Jul 2016 11:43	Sat 09 Jul 2016 11:48	Wait to reach DOT max
5.15		Sat 09 Jul 2016 11:48	Sat 09 Jul 2016 11:48	Gas flow (Air/mix) off
5.16		Sat 09 Jul 2016 11:48	Sat 09 Jul 2016 11:48	N2 on (drop to 0% DOT)
5.17		Sat 09 Jul 2016 11:48	Sat 09 Jul 2016 11:52	Wait to reach DOT min
5.18		Sat 09 Jul 2016 11:52	Sat 09 Jul 2016 11:52	Run #44 iii
5.19		Sat 09 Jul 2016 11:52	Sat 09 Jul 2016 11:52	N2 off
5.20		Sat 09 Jul 2016 11:52	Sat 09 Jul 2016 11:52	Gas flow (Air/mix) on
5.21		Sat 09 Jul 2016 11:52	Sat 09 Jul 2016 11:58	Wait to reach DOT max
5.22		Sat 09 Jul 2016 11:58	Sat 09 Jul 2016 11:58	End of Run #44

Experiment
System options
Pumped liquid classes
Pipetted liquid classes
Liquid handling scripts

Protocols

- BR1- Media 1 ([Gly]=0)
 - Volumes
 - Pumps
- BR2- Media 2 ([Gly]=7.5)
 - Volumes
 - Pumps
- BR3- Media 3 ([Gly]=15)
 - Volumes
 - Pumps
- BR4- Media 4 ([Gly]=22.5)
 - Volumes
 - Pumps
- BR5- Media 5 ([Gly]=30)
 - Volumes
 - Pumps
- BR6- Media 2 ([Gly]=7.5)
 - Volumes
 - Pumps
- BR7- Media 3 ([Gly]=15)**
 - Volumes
 - Pumps
- BR8- Media 4 ([Gly]=22.5)
 - Volumes
 - Pumps

Control loops
Plates/Bottles/Tube racks
Tubing
Custom variables
Alarms

Results
Tables
Audit

Bioreactor selection

Navigation < Experiment\Protocols\BR7- Media 3 ([Gly]=15) [Bioreactor 7]

Edit the steps that define what is to be done for the protocol.

- Experiment
 - System options
 - Pumped liquid classes
 - Pipetted liquid classes
 - Liquid handling scripts
- Protocols
 - BR1- Media 1 ([Gly]=0)
 - Volumes
 - Pumps
 - BR2- Media 2 ([Gly]=7.5)
 - Volumes
 - Pumps
 - BR3- Media 3 ([Gly]=15)
 - Volumes
 - Pumps
 - BR4- Media 4 ([Gly]=22.5)
 - Volumes
 - Pumps
 - BR5- Media 5 ([Gly]=30)
 - Volumes
 - Pumps
 - BR6- Media 2 ([Gly]=7.5)
 - Volumes
 - Pumps
 - BR7- Media 3 ([Gly]=15)**
 - Volumes
 - Pumps
 - BR8- Media 4 ([Gly]=22.5)
 - Volumes
 - Pumps
- Control loops
- Plates/Bottles/Tube racks
- Tubing
- Custom variables
- Alarms
- Results
 - Tables
 - Audit

12.6		Sat 09 Jul 2016 14:59	Sat 09 Jul 2016 14:59	Gas flow (Air/mix) on		
12.7		Sat 09 Jul 2016 14:59	Sat 09 Jul 2016 15:04	Wait to reach DOT max		
12.8		Sat 09 Jul 2016 15:04	Sat 09 Jul 2016 15:04	Gas flow (Air/mix) off		
12.9		Sat 09 Jul 2016 15:04	Sat 09 Jul 2016 15:04	N2 on (drop to 0% DOT)		
12.10		Sat 09 Jul 2016 15:04	Sat 09 Jul 2016 15:09	Wait to reach DOT min		
12.11		Sat 09 Jul 2016 15:09	Sat 09 Jul 2016 15:09	Run #51 ii		
12.12		Sat 09 Jul 2016 15:09	Sat 09 Jul 2016 15:09	N2 off		
12.13		Sat 09 Jul 2016 15:09	Sat 09 Jul 2016 15:09	Gas flow (Air/mix) on		
12.14		Sat 09 Jul 2016 15:09	Sat 09 Jul 2016 15:14	Wait to reach DOT max		
12.15		Sat 09 Jul 2016 15:14	Sat 09 Jul 2016 15:14	Gas flow (Air/mix) off		
12.16		Sat 09 Jul 2016 15:14	Sat 09 Jul 2016 15:14	N2 on (drop to 0% DOT)		
12.17		Sat 09 Jul 2016 15:14	Sat 09 Jul 2016 15:18	Wait to reach DOT min		
12.18		Sat 09 Jul 2016 15:18	Sat 09 Jul 2016 15:18	Run #51 iii		
12.19		Sat 09 Jul 2016 15:18	Sat 09 Jul 2016 15:18	N2 off		
12.20		Sat 09 Jul 2016 15:18	Sat 09 Jul 2016 15:18	Gas flow (Air/mix) on		
12.21		Sat 09 Jul 2016 15:18	Sat 09 Jul 2016 15:24	Wait to reach DOT max		
12.22		Sat 09 Jul 2016 15:24	Sat 09 Jul 2016 15:24	End of Run #51		

Run #50

13.1		Sat 09 Jul 2016 15:24	Sat 09 Jul 2016 15:24	Gas flow (Air/mix) off		
13.2		Sat 09 Jul 2016 15:24	Sat 09 Jul 2016 15:24	N2 on (drop to 0% DOT)		
13.3		Sat 09 Jul 2016 15:24	Sat 09 Jul 2016 15:28	Wait to reach DOT min		
13.4		Sat 09 Jul 2016 15:28	Sat 09 Jul 2016 15:28	Run #50 i		
13.5		Sat 09 Jul 2016 15:28	Sat 09 Jul 2016 15:28	N2 off		
13.6		Sat 09 Jul 2016 15:28	Sat 09 Jul 2016 15:28	Gas flow (Air/mix) on		
13.7		Sat 09 Jul 2016 15:28	Sat 09 Jul 2016 15:34	Wait to reach DOT max		
13.8		Sat 09 Jul 2016 15:34	Sat 09 Jul 2016 15:34	Gas flow (Air/mix) off		
13.9		Sat 09 Jul 2016 15:34	Sat 09 Jul 2016 15:34	N2 on (drop to 0% DOT)		
13.10		Sat 09 Jul 2016 15:34	Sat 09 Jul 2016 15:39	Wait to reach DOT min		
13.11		Sat 09 Jul 2016 15:39	Sat 09 Jul 2016 15:39	Run#50 ii		
13.12		Sat 09 Jul 2016 15:39	Sat 09 Jul 2016 15:39	N2 off		
13.13		Sat 09 Jul 2016 15:39	Sat 09 Jul 2016 15:39	Gas flow (Air/mix) on		
13.14		Sat 09 Jul 2016 15:39	Sat 09 Jul 2016 15:44	Wait to reach DOT max		
13.15		Sat 09 Jul 2016 15:44	Sat 09 Jul 2016 15:44	Gas flow (Air/mix) off		
13.16		Sat 09 Jul 2016 15:44	Sat 09 Jul 2016 15:44	N2 on (drop to 0% DOT)		
13.17		Sat 09 Jul 2016 15:44	Sat 09 Jul 2016 15:48	Wait to reach DOT min		
13.18		Sat 09 Jul 2016 15:48	Sat 09 Jul 2016 15:48	Run #50 iii		
13.19		Sat 09 Jul 2016 15:48	Sat 09 Jul 2016 15:48	N2 off		
13.20		Sat 09 Jul 2016 15:48	Sat 09 Jul 2016 15:48	Gas flow (Air/mix) on		
13.21		Sat 09 Jul 2016 15:48	Sat 09 Jul 2016 15:54	Wait to reach DOT max		
13.22		Sat 09 Jul 2016 15:54	Sat 09 Jul 2016 15:54	End of Run #50		

Run #46

14.1		Sat 09 Jul 2016 15:54	Sat 09 Jul 2016 15:54	Gas flow (Air/mix) off		
14.2		Sat 09 Jul 2016 15:54	Sat 09 Jul 2016 15:54	N2 on (drop to 0% DOT)		
14.3		Sat 09 Jul 2016 15:54	Sat 09 Jul 2016 15:58	Wait to reach DOT min		
14.4		Sat 09 Jul 2016 15:58	Sat 09 Jul 2016 15:58	Run #46 i		
14.5		Sat 09 Jul 2016 15:58	Sat 09 Jul 2016 15:58	N2 off		
14.6		Sat 09 Jul 2016 15:58	Sat 09 Jul 2016 15:58	Gas flow (Air/mix) on		
14.7		Sat 09 Jul 2016 15:58	Sat 09 Jul 2016 16:03	Wait to reach DOT max		
14.8		Sat 09 Jul 2016 16:03	Sat 09 Jul 2016 16:03	Gas flow (Air/mix) off		
14.9		Sat 09 Jul 2016 16:03	Sat 09 Jul 2016 16:03	N2 on (drop to 0% DOT)		
14.10		Sat 09 Jul 2016 16:03	Sat 09 Jul 2016 16:08	Wait to reach DOT min		
14.11		Sat 09 Jul 2016 16:08	Sat 09 Jul 2016 16:08	Run #46 ii		
14.12		Sat 09 Jul 2016 16:08	Sat 09 Jul 2016 16:08	N2 off		
14.13		Sat 09 Jul 2016 16:08	Sat 09 Jul 2016 16:08	Gas flow (Air/mix) on		
14.14		Sat 09 Jul 2016 16:08	Sat 09 Jul 2016 16:13	Wait to reach DOT max		
14.15		Sat 09 Jul 2016 16:13	Sat 09 Jul 2016 16:13	Gas flow (Air/mix) off		
14.16		Sat 09 Jul 2016 16:13	Sat 09 Jul 2016 16:13	N2 on (drop to 0% DOT)		
14.17		Sat 09 Jul 2016 16:13	Sat 09 Jul 2016 16:17	Wait to reach DOT min		
14.18		Sat 09 Jul 2016 16:17	Sat 09 Jul 2016 16:17	Run #46 iii		
14.19		Sat 09 Jul 2016 16:17	Sat 09 Jul 2016 16:17	N2 off		
14.20		Sat 09 Jul 2016 16:17	Sat 09 Jul 2016 16:17	Gas flow (Air/mix) on		
14.21		Sat 09 Jul 2016 16:17	Sat 09 Jul 2016 16:23	Wait to reach DOT max		
14.22		Sat 09 Jul 2016 16:23	Sat 09 Jul 2016 16:23	End of Run #46		

Unload bioreactors

Appendix 5.1. Process design inputs and dependencies for consumables calculation in the ARC tool.

